مجله دامپزشکی ایران

صاحب امتیاز: دانشگاه شهید چمران اهواز
مدیرمسئول : دکتر منصور میاحی

سردبیر
دکتر محمدرحیم حاجی‌حاجیکلائی

کارشناس مجله
منا عباسی

آدرس پستی سردبیر
اهواز، دانشگاه شهید چمران اهواز، دانشکده دامپزشکی، سردبیر مجله علمی، کد پستی ۶۱۳۵۵، صندوق پستی ۱۴۵
تلفن و دورنگار: ۳۳۳۳۶۳۱۲ (۰۶۱)
E-mail: ivj@scu.ac.ir

- این مجله به استناد نامه شماره ۳/۲۹۱۰/۵۴۵ مورخ ۸۴/۵/۸ کمیسیون بررسی نشریات وزارت علوم، تحقیقات و فناوری دارای **درجه علمی ـ پژوهشی** می‌باشد.
- این مجله در فهرست نشریات علمی پژوهشی معتبر **ISC** که دارای ضریب تأثیر (**IF**) می‌باشند، قرار دارد. این اعتبار از سوی وزارت علوم، تحقیقات و فناوری تعیین شده است و در آئین‌نامه ارتقای مرتبه علمی دانشگاه‌ها و موسسات آموزشی مورد بهره‌برداری قرار می‌گیرد.
- متن کامل مقالات در پایگاه استنادی علوم جهان اسلام (**ISC**) قابل دسترسی می‌باشد.

چاپ و صحافی
مرکز منطقه‌ای اطلاع‌رسانی علوم و فناوری و پایگاه استنادی جهان اسلام

بسم اللّه الرحمن الرحیم

مجله دامپزشکی ایران

فهرست مطالب

Guide for Authors

Authors who are in the Farsi profile journal system do not need to create an English profile and should submit an article through their previous profile.

The aim of the publication of the ***Iranian Veterinary Journal*** is to publish research papers in various fields of veterinary medicine, medicine, biology and other sciences related to scientific and practical applications in veterinary and medical sciences. Articles will be published containing new findings in the specialized fields mentioned above. A case report is also available in this journal. Received papers will be published by the relevant experts and reviewed by the editorial board after initial review and arbitration. All or part of the submission should not have been published or has already been submitted to another journal. If the article has previously been submitted to the congress or scientific congress, please indicate the full details of the congress or relevant congress. This journal is published the annual quarterly form in four issues.

Essential files for submission

1) Main article file without the authors' names and containing all the parts of the article based on the base of the article.

2) Authors' Affiliation: For example First Name Last Name: Professor, Department of Clinical Sciences, Faculty of Veterinary Medicine, Shahid Chamran University of Ahvaz, Ahvaz, Iran

* No need to send tables and figures in separate files.

Types of Manuscripts

A. Original Article

The research paper is the result of the research work of the author or authors and has the title, abstract, keywords, introduction, materials and method, results, discussion, list of references and abstract of English, and **should not exceed 12 pages or less than 6 pages.**

B. Short Paper

This article is based on the type of work and the way of editing, as with the research paper. However, due to the importance and results of the research, the paper is presented in a compact and maximal format in **6 pages of the journal**. It is also necessary to have the title, abstract, keywords, introduction, materials and methods, results, discussion, bibliography and English.

C) Case Report

These reports contain rare and informative clinical and laboratory items and have the title, abstract, keywords, introduction, history, method of diagnosis, discussion and conclusion, bibliography and abstract in Persian, and should not be exceeded from **4 pages**.

Essentials for writing and submitting the article

1. **The title**

The title of the article is expressly and concisely brief and covers the whole article. The title of the article, the name of the author or authors, with the mention of a scientific or academic rank in both Farsi (for Persian speakers) and English with full postal address, mobile or fixed number, fax and e-mail address of the author on a separate page (page 1).

2. **Abstract**

The abstract considering that the referrers to the article first use the summary of the article for evaluation, and given that the summary is usually published by the centres and scientific information institutes, this part of the article should be accurate and fluent, and a maximum of 300 words represent the chief complaint, purpose,

method, overall conclusions and conclusions of that research. Persian (for Persian speakers) abstract should also be included.

3. **The keywords**
The keywords are considered to be introduced and guidelines of the article, at least 4 and maximums of 8 words.

4. **The introduction**
The introduction contains the importance of research and the scientific background of the work.

5. **Materials and methods**
Materials and methods of the work include a detailed and complete description of the consumables, the number, type and description of the specimens, the devices specifically designed for the research, with their full specifications and the method of execution. If the usual methods are used, they should refrain from mentioning them and mention the references, but if a new method is used, the full description of that method, together with the mention of the scientific names and sources of supplies, is essential. The statistical methods used should be presented in a comprehensible manner and based on valid references.

6. **The results**
The results of the research can be presented in the form of a table with all lines, diagrams and images with the necessary explanations. Figures and tables should be completely clear and easy to understand, and at the same time express the true results of the experiments. Make clear images and graphs and avoid sending a copy of them. The axes of the chart are fully defined and avoid any unnecessary explanations. Each of the tables, charts and images with the number in the specified text and captions of the tables at the top of the table and captions of the figures are presented below the figures. All images, tables and charts should be included in the text of the article. Data presented in tables or figures should not be discussed in this section. The results presented in the tables should not be repeated in the article, such as graphs or text.

7. **Discussion**
In the discussion, the presented results should be analyzed and interpreted, and it should attract the attention of the readers on the main subject of the research, the hypotheses in the introduction section and the results of the research. This section discusses the relationships between influential factors or shortcomings and proposes new ideas. Even if there is a consensus or difference between the results of this research and the research carried out in this field, the scientific and theoretical applications will emphasize the achievements of this research and the fundamental inference of this study and refrain from repeating the results.

8. The author/s can thank others which helped them to do research or prepare a paper. It should be noted that in the case of financial support and the use of laboratory equipment, the place of research and the name of the institution or persons concerned may be mentioned.

9. The list of references is limited to authoritative scientific books and articles and is not used in dissertations, articles presented at congresses and scientific congresses, and in internet sites.
English Font and size: Times New Roman, 12, 1.5space with 2 cm margins
Persian Font and Size: B lotus, 14, 1.5 space with 2 cm margins
It should be considered that the references excluded for page numbering.

How to cite the references in the manuscript?
All references used in the article should be used with the name of the author or authors as follows:

In the case of the references at the end of the paragraph, the method of referring to it at the end of the paragraph and in parentheses is as follows:

- If one is an author, (Mellor 2005), if there are two authors, (Arthur and Noakes 2011) and more than two authors, (Pearson et al., 2012).

If the reference is mentioned at the beginning of the relevant paragraph, the method of referring to it at the beginning of the paragraph without brackets is given by the following examples:

- If two authors: Arthur and Noakes in 2011, they reported that. . . And more than two authors: Pearson et al., in 2012 Reported that …

How to list the references?

All references which are used in the article should be included in the references list. Also, all references should be written in alphabetical order without mentioning the number. It should be noted that in the case of Persian references, the English equivalent is brought to its end in parentheses in Persian.

The use of theses, congresses, conferences, protocols, and sites in the references is not acceptable.

How to write references in the references list is as follows:

- Article: Herbert, R.; Nanney, J. and Spano, J.S. (1986). Erythrocyte distribution in ducks. American Journal of Veterinary Research, 50 (2): 958-960.

If the reference is part of a book, the surname of the author or authors of that book chapter with the initials, chapter title, title of the book, surname of the author or authors of the book, together with the first letters of the author's name, year of publication, publication number of the book, place release the book and number of pages, for example:

- Book: Arthur, G.H.; Noakes, D.E.; Pearson, H. and Parkinson, T.J. (1996). Veterinary Reproduction and Obstetrics. 7th ed. Saunders, London, Pp: 634-645.

Also, the name of the journals in the references section should be completely written and avoid abbreviated terms.

If the number of the authors of the article is more than 6, then added et al. after the sixth person.

Submission

The articles should be submitted through the electronic journal site to **http//www.ivj.ir.**

Article responsibility

The scientific and ethical responsibility of the article lies with the author or authors.

Submit a printed article (Reprint)

The published article is sent by the Islamic World Science Citation Center (ISC) for the corresponding authors of the article to distribute among the authors.

Copyright

Please **download** and complete the copyright form and submit it through the journal's electronic system.

Conflicts of Interest

Please **download** and complete Conflicts of Interest form and submit it through the journal's electronic system. Conflicts of interest comprise those which may not be fully apparent and which may influence the judgment of author, reviewers, and editors. They have been described as those which, when revealed later, would make a reasonable reader feel misled or deceived. They may be personal, commercial, political, academic or financial. “Financial” interests may include employment, research funding, stock or share ownership, payment for lectures or travel, consultancies and company support for staff. Authors must identify and declare any personal circumstances or interest that may be perceived as inappropriately influencing the

representation or interpretation of reported research results. If there is no conflict of interest, please state "The authors declare no conflict of interest." Any role of the funding sponsors in the design of the study; in the collection, analyses or interpretation of data; in the writing of the manuscript, or in the decision to publish the results must be declared in this section. If there is no role, please state “The founding sponsors had no role in the design of the study; in the collection, analyses, or interpretation of data; in the writing of the manuscript, and in the decision to publish the results”. Complete the Conflicts of Interest form and submit it through the journal's electronic system.

Publication Fee

Manuscripts that are accepted for publication in the Iranian Veterinary Journal are subjected to pay a mandatory charge of IRR 4,000,000 per Article. This charge covers expenses for peer review, journal publication, and online hosting and archiving. The charge form will be sent to the corresponding author on acceptance of an article for publication in the journal. Please be advised the publication of the accepted manuscripts is dependent upon payment of the charge. To facilitate the payment of paid articles, from July 26, 2020, the journal online system was equipped with an electronic payment gateway. Dear Authors, by referring to their profile in the journal online system and click the payment section, they can pay through the payment portal and send the image of the payment receipt.

Manuscripts that are accepted for publication in the Iranian Veterinary Journal are subjected to pay a mandatory charge of IRR 4,000,000 per Article. This charge covers expenses for peer review,

Vol. 22, No. 2, Summer, 2026, 05-14 *Original Article*
DOI: 10.22055/ivj.2025.535366.2819
Journal Homepage: http://www.ivj.ir/

Identification of antigenic proteins of *Setaria labiatopapillosa* in cattle (*Bos taurus*)

Alireza Alborzi[1*], Pedram Haddadmolayan[2], Masoud Ghorbanpoor[3] and Mohamadreza Tabandeh[4]

[1] Professor, Department of Pathobiology, Faculty of Veterinary Medicine, Shahid Chamran University of Ahvaz, Ahvaz, Iran
[2] PhD Student of Parasitology, Faculty of Veterinary Medicine, Shahid Chamran University of Ahvaz, Ahvaz, Iran
[3] Professor, Department of Pathobiology, Faculty of Veterinary Medicine, Sharekord University, Sharekord, Iran
[4] Professor, Department of Basic Sciences, Faculty of Veterinary Medicine, Shahid Chamran University of Ahvaz, Ahvaz, Iran

Received: 19.07.2025 Accepted: 14.12.2025

Abstract

Setaria labiatopapillosa is one of the parasitic nematodes found in bovines, which causes verminous encephalitis in non-specific hosts. This study aimed to determine the protein and antigenic profiles of *S. labiatopapillosa* in cattle using immunoblotting. The samples were taken from cattle at Ahvaz slaughterhouse. Somatic crude extracts of adult and microfilariae of the nematode (as S and MF proteins or antigens) were prepared separately by homogenization. Excretory secretory products (ES) were prepared by incubating the adult nematode in RPMI medium. Protein profiles and antigenic properties of ES, S, and MF samples of *S. labiatopapillosa* were determined by sodium dodecyl sulfate-polyacrylamide gel electrophoresis (SDS-PAGE). Immunogenic properties of the proteins were determined using immunoblotting and positive sera from cattle infected with the adult nematode. More than two, 8, and 15 predominant protein bands at 200 to 22 kDa were demonstrated in SDS-PAGE gels of ES, MF, and S samples. Consequently, in immunoblotting of ES, MF, and S, two, 14, and 4 predominant ES antigenic bands were demonstrated; among them, the 68- and 64-kDa proteins were the most common antigenic components. The results of immunoblotting of ES, MF, and S of *S. labiatopapillosa* showed that the 68- and 64-kDa proteins were the most common antigenic components, and can be potential candidates for future studies.

Key words: Antigens, Bovine, Immunoblotting, *Setaria labiatopapillosa,*

Introduction

The parasitic nematode *Setaria labiatopapillosa* is a causative agent of verminous encephalitis and an important member of the Onchocercidae family that inhabits the peritoneal cavity of bovids (Kuts et al, 2012; Singh et al, 2015).

Setaria worms have indirect life cycles that have not yet been fully elucidated. Various mosquito species (*Aedes* spp, *Anopheles* spp, *Culex* spp and *Armigeres* spp) are the main intermediate hosts. The adults are commonly found in the abdominal cavity of definitive hosts, domestic and wild animals (Anderson, 2000; Cancrini et al, 1997).

Generally, the presence of *Setaria* adult worms in the peritoneal cavity of infected hosts is not considered pathogenic, but their

* **Corresponding Author**: Alireza Alborzi, Professor, Department of Pathobiology, Faculty of Veterinary Medicine, Shahid Chamran University of Ahvaz, Ahvaz, Iran
E-mail: a.alborzi@scu.ac.ir

migration to various organs, particularly the eyes, liver, brain, heart, etc., can cause significant harm (Shin et al, 2017; Sunder et al, 2005).

Ocular Setariosis can cause blurred vision and even blindness in the host. The particular form of cerebrospinal infection is caused by migration of parasitic infective microfilariae (third stage larvae) in the nervous system of non-specific hosts (such as sheep, goats and horses) as well as non-infective microfilariae in specific hosts.

Due to serious threat of setariasis to livestock in endemic areas, it is of particular importance in veterinary medicine (Bazargani et al, 2008; Mahmoud et al, 2004; Tung et al, 2003; Wang et al, 1986).

Detection of the parasite infection is only concluded by microscopic observation of the parasite microfilariae on blood smears of infected animals.

However, most reports on the infection in animals have come from postmortem examinations or abattoir inspections, which have mostly isolated adult nematodes from thoracic or abdominal cavities of the host animals (Khedri et al, 2014; Kim et al, 2010; Mrifag et al, 2021; Nakano et al, 2007; Rodrigues et al, 2021).

The control of vector mosquitoes is an important part of preventing or at least reducing the infection of the hosts (cattle) although it is difficult due to the behavior and extent of their intermediate mosquito hosts (Cancrini et al, 1997; Laaksonen et al, 2009; Karunamoorthi and Sabesan, 2013).

A thorough understanding of pathogenic agents in the region is essential for diagnosis, control, and prevention.

A more practical and important measure for controlling the disease is to identify and treat infected animals.

In our previous study, using molecular and scanning electron microscopy techniques, *S. labiatopapillosa* was the only species of *Setaria* isolated from calves in southwestern Iran (Alborzi et al, 2019).

Identifying and assessing the antigenic properties of somatic and excretory-secretory proteins of parasites exposed to the host's immune response is crucial for serological diagnostic studies and the development of preventive vaccines.

Moreover, excretory-secretory products can be one of the targets of immune control against parasites due to their important role in parasite biology (Richer et al, 1992; Ring et al, 1993).

Considerable studies have been conducted on excretory-secretory and somatic antigens of various parasites (Alborzi et al, 2006; Alborzi et al, 2014; Alborzi et al, 2016; Alborzi et al, 2022; Razi Jalali et al, 2014; Rashidi et al, 2018; Virginio et al, 2012)

A greater number of studies have identified antigens in excretory-secretory products and somatic extracts of some *Setaria* species to detect human filariasis, but fewer have focused on the diagnosis of animal setariasis (Raj et al, 1997; Mohanty et al, 2006; Kaushal et al, 2009).

The present study aimed to characterize the antigens of *S. labiatopapillosa* so that its results could provide a clearer background for future research on the specific immunological diagnosis of setariasis in cattle.

Materials and Methods

Samplings

The samples were taken from animals at the Ahvaz slaughterhouse. The slaughterhouse of Ahvaz is a center for receiving animals from different areas of Khuzestan province. Following the marking of the cattle, two blood samples were collected from each animal, one with an anticoagulant (EDTA) for microfilaria observation and another for separating serum. Modified Knott's technique was used to detect microfilariae of the nematode in the blood (Watanabe et al, 2004).

The abdominal cavity of the slaughtered animal was carefully checked for worms; those that were found were transferred into containers containing phosphate buffered saline (PBS, pH=7.2). After three washes

with serum saline solution, the collected worms were used for culture, antigen preparation, and morphological identification.

Preparation of protein products/ extracts (antigens)

In order to prepare the excretory-secretory products (ES), *S.labiatopapillosa* adults collected from the peritoneal cavity of infected cattle were washed with physiological saline three times.

The nematodes were cultured in a 50 ml flask containing Roswell Park Memorial Institute medium (RPMI-1640, Bahar Afshan, Tehran, Iran) supplemented with penicillin (100 U/ml) and streptomycin (100 mcg/ml).

The culture medium (3 mL/nematode) was changed every 12 hours, and the survival of the worms was observed by examining and observing their movement.

The flask was incubated for 24 hours in 5.0% CO2 at 37°C. Media were collected, centrifuged at 4000g for 4 min, filtered through 0.22m filters, the filtrate (soluble proteins) was then added to sterile falcons as ES, and kept at -20°C for further analyses.

In order to prepare somatic crude extracts of adult and microfilariae collected from the uterine of adult females (as S and MF proteins or antigens), some nematode parts (without uterus) and microfilariae were homogenized separately. The homogenization was performed with a Bandelin homogenizer (Bandelin, Berlin, Germany) using 10 cycles lasting 15 seconds each at a voltage of 80 in 0.2 ml PBS (pH = 7.2). Homogenized solutions were centrifuged at 4000 rpm for 4 minutes at 4 °C, and the supernatants were filtered through 0.22 m filters (Biofil Syringe Filter, Shanghai, China). The refined liquids were collected as S and MF separately and stored at -20 ° C until use. The concentration of proteins in ES, S, and MF solutions was determined by the Bradford method (Bradford, 1976). Positive serum samples were obtained from animals with both adult worms in their peritoneal cavity and microfilariae in their blood.

Electrophoretic analysis

Proteins in ES, S, and MF samples of *S. labiatopapillosa* were separated by sodium dodecyl sulfate-polyacrylamide gel electrophoresis (SDS-PAGE). Based on the Laemmeli's method (Laemmeli,1970), it was performed in an electrophoresis apparatus (Paya Pajoohesh Pars, Tehran, Iran) with 12.0% separating gels (6 ml of 30% acryl amide + bis, 3.8 ml of 1M Tris-HCl pH 8.8, 150 µl of 10% (w/v) SDS, 150 µl of 10% Ammonium persulfate, 6 µl of TEMED [(Tetramethylethylenediamine) and 4.9 ml deionized water (DH2O)] and 5% stacking gels (1.3 ml of 30% acryl amide + bis, 1ml of 1M Tris-HCl pH 6.8, 80 µl of 10% SDS, 80 µl of 10% Ammonium persulfate, 8 µl of TEMED and 5.5 ml DH2O.

Before electrophoresis, 60 µl of each sample (ES, S, and MF) were mixed with 30 µl of non-reducing buffer (1 ml 1 M Tris-HCl (pH 6.8), 5 ml of ddH20, 2ml 10% SDS, 5 mg Bromophenol Blue, 1 ml 100% glycerol, 1 ml β-mercaptoethanol) and boiled for 5 min then centrifuged for 2 min. Unstained Protein Markers (AbCam) ranging from 254 to 17 kDa were used in 5 µl in 10 µl sample buffers as molecular weight standards.

Electrophoresis was run at 100 V for 5 hr. under reducing conditions. The gels were stained with Coomassie Brillant Blue R-250 according to the manufacturer's instructions and silver staining as follows: After electrophoresis, gels were fixed for 1 hr. in an appropriate volume of fixing solution (50 ml ethanol, 2 ml acetic acid and 448 ml DH2O).

After discarding the fixing solution, the gel was stained in silver staining solution (0.1% (w/v) silver nitrate) for 15 min. The gels were rinsed in deionized water twice for 30 sec. and then in the developing

solution (3% (w/v) sodium carbonate and 0.04% formalin).

Next, the gels were washed in deionized water. In the final step, the reactions terminated by adding 5% acetic acid.

Immunoblotting

For immunoblotting, proteins of ES, S, and MF samples of *S. labiatopapillosa* were first electrophoresed on 12 % SDS-polyacrylamide gel. Western blotting was carried out following established protocols (Towbin et al, 1979). Proteins were transferred onto a nitrocellulose membrane using Tris-glycine-methanol buffer for 3 hr. at 60 V.

The membrane was blocked in 5% skim milk in PBS for overnight at -4 ºC temperature (refrigerator).

After rinsing 3 times (each 5 min) in the washing buffer (PBS-T: PBS,0.05% Tween20) and once in PBS.

Sera (10 positive and 10 negative) were diluted (1:4, 1:5, 1:8, 1:10, 1:16, 1:20, 1:32, 1:40 and 1:80) in PBS-T buffer and the membranes incubated with stirring at room temperature (RT) for 1 hr. and again washed as above.

After 4 repetitions, 1:8 dilution of S, 1:10 dilution of MF, and 1:4 dilutions of ES were determined as the most proper dilutions.

the membrane was cut in strips and incubated with positive and negative sera and with stirring, for 1 hr. at 37 ºC and then washed as above.

The strips were then incubated with secondary antibody (anti-Bovine Anti-IgG horseradish peroxidase conjugated antibody Sigma- Aldrich, USA) diluted with PBS-T (1:1000) with stirring, for 1 hr. at 37 ºC, after washing, developed in a mixture of 4-cloronapthol and hydrogen peroxide for 15 min.

Results

Protein profiles of ES, S, and MF samples of *S. labiatopapillosa*

Excretory- secretory products of cultured adults of *S. labiatopapillosa* (ES), somatic extracts of adults (S) and microfilariae (MF) were analyzed by SDS-PAGE and the gels were stained with Coomassie Brillant Blue R-250 and a silver staining method. As shown in Figure 1, silver-stained gel of ES revealed the presence of more than six protein bands ranging in molecular weight from 250 to 17 kilodaltons (KDa). However, the predominant ES protein bands were at 74, 68, 64, 51, 38, and 22 KDa. In Coomassie –stained gel of S, there were more than 15 protein bands with weights of approximately 200, 133, 107, 91, 80, 74, 68, 64, 60, 51, 48, 40, 38, 22 and several bands above 245 kDa were more predominant (Figure 2). Protein dominants in gel of MF were 8 bands including 124, 107, 96, 68, 64, 48, 31 and 22 kDa (Figure 3).

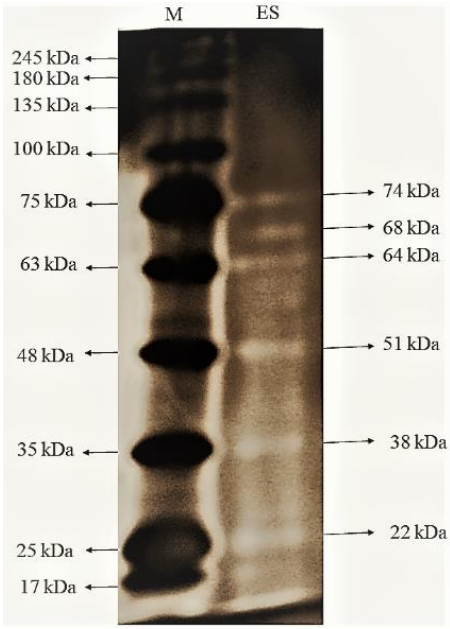

Figure 1: Protein profile on a silver-stained SDS-PAGE gel of excretory-secretory-products (ES) from *S. labiatopapillosa*, Molecular weight marker (M).

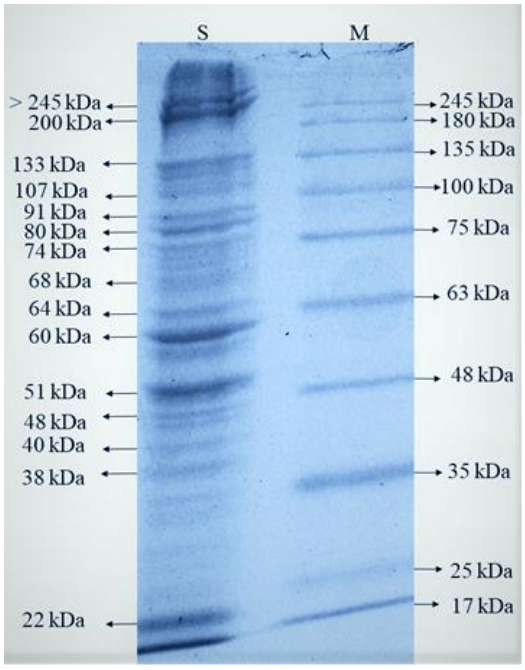

Figure 2: Protein profile on a Coomassie-stained SDS-PAGE gel of somatic extract (S) of *S. labiatopapillosa***, Molecular weight marker (M).**

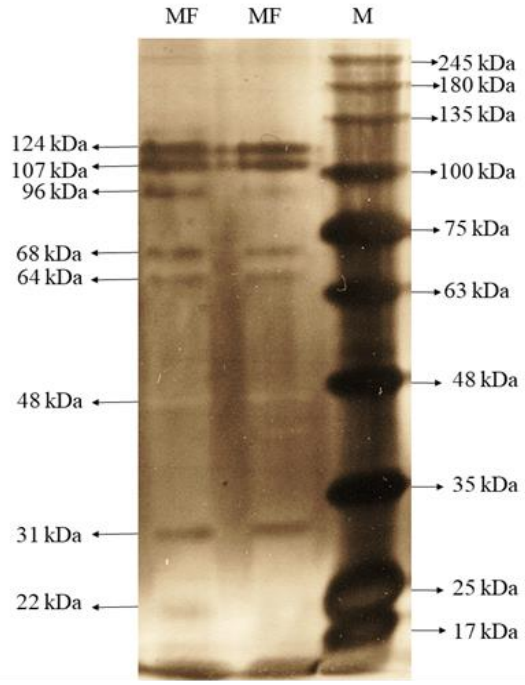

Figure 3: Protein profile on a silver-stained SDS-PAGE gel of somatic extract of microfilariae of *S. labiatopapillosa* **(MF), Molecular weight marker (M).**

Immunoblotting

Analysis of electrophoretic patterns in immunoblotting of *S. labiatopapillosa* ES, S, and MF with dilutions: 1:5, 1:8, and 1:10 of sera respectively of naturally infected and 1:1000 dilution of anti-bovine IgG conjugate, positive reactions (as visible bands) were obtained.

The results demonstrated that the predominant ES antigenic bands were two bands at 68 and 64 kDa (Figure 4). The somatic extracts (S) of 4 antigenic bands were recognized, including bands of 68, 64, 60, and 56 kDa (Figure 5). In somatic extracts of microfilariae(MF) 14 predominant antigenic bands including bands of 182, 157, 133, 124, 107, 102, 88, 74, 68, 64, 60, 51, 41, and 38 (Figure 6) were observed. Among the protein profiles, the 68 and 64 kDa protein was the most common antigenic component.

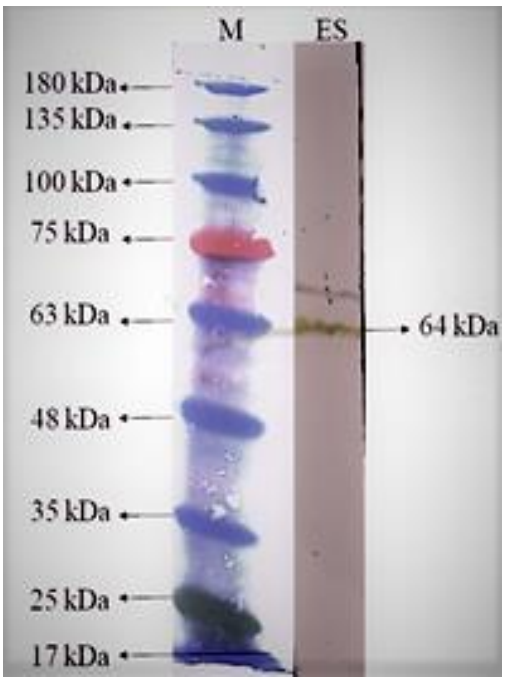

Figure 4: Immunoblotting of excretory-secretory antigens of *S. labiatopapillosa* **(ES), with sera of naturally infected cattle. Molecular weight marker (M).**

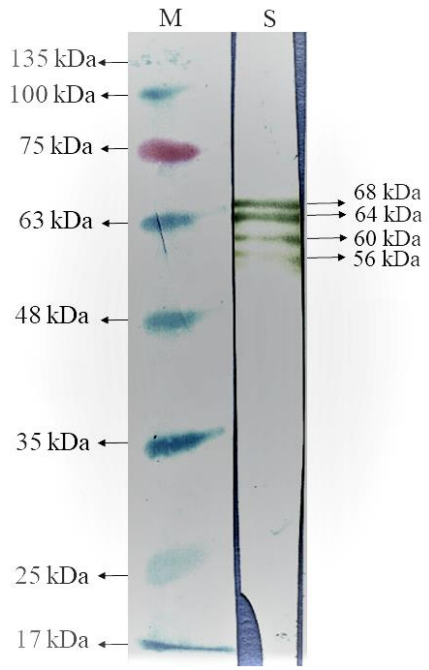

Figure 5: Immunoblotting of somatic antigens of *S. labiatopapillosa* (S), with sera of naturally infected cattle. Molecular weight marker (M).

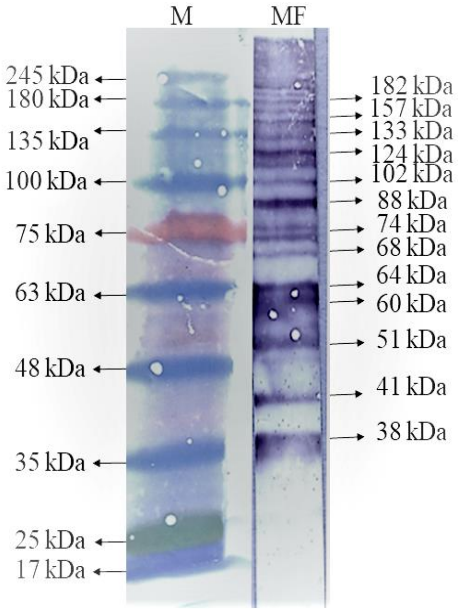

Figure 6: Immunoblotting of somatic antigens of *S. labiatopapillosa* microfilariae (MF), with sera of naturally infected cattle. Molecular weight marker (M).

Discussion

In this study, preparations of excretory products (ES) and crude somatic extracts from *S. labiatopapillosa* adults and microfilariae (as S and MF proteins), and positive serum samples from the nematode-infected animals were obtained.

The antigenic profile was determined in excretory-secretory, somatic extracts of adult and microfilariae of *S. labiatopapillosa* females using SDS-PAGE and immunoblot methods.

Immunoblotting of ES, MF and S proteins demonstrated two, 14 and 4 predominant ES antigenic bands.

The presence of immunogenic proteins indicates stimulation of the host immune system at different stages of the parasite infection and the production of humoral antibodies, especially systemic IgG.

Among the protein profiles, the 68 and 64 kDa protein was the most common antigenic component.

It appears that these proteins are expressed at all stages of the parasite development in the host.

Although, in the protein profiles, the number of adult *S. labiatopapillosa* proteins (bands) was much higher than that of microfilariae, in the immunoblotting results, more immunogenic proteins were observed with microfilaria extract (MF) than with adult ES and somatic extract(S).

It appears that the high number of immunogenic proteins found in microfilaria extracts results from their entry into the blood stream, possible death, and exposure of the released proteins to the immune system of the host, as well as their secretory excretory proteins.

While the mature worms are primarily present in the abdominal (peritoneal) cavity of their hosts, adult female worms release microfilariae in the abdominal cavity. These microfilariae get into the blood stream. Most studies on the protein and immunogenicity characteristics of some *Setaria* species, including *S. digitata*, have been conducted on its both specific host (cattle) and non-specific host (horse). These studies have shown that antigens from these animal nematodes can be used in the diagnosis of filarial nematode infections in animals and even in humans. However,

there are very few reports on *S. labiatopapillosa* (Mohanty et al, 2006; Takesue, et al, 2016).

Berezhko et al, (2016) demonstrated that *S. labiatopapillosa* can be used as an antigenic source for diagnosing dirofilariasis (*Dirofilaria immitis*) in dogs. According to Bright and Raj, (1991), SDS-PAGE analysis of adult *S digitata* surface antigen preparations (SAPs) revealed three major proteins with molecular weights 17, 29 and 36 KD, and all SAPs were antigenic. The release of 29 KD surface protein from in vitro culture of the adult and cross-reactivity between it and antisera to surface antigens revealed the possibility of natural surface shedding (Bright et al, 1991). The cross-reactivity of filarial species has made access to heteroantigens to detect infection in humans. Dissanayake and Ismail (1980) isolated several antigenic components from *Setaria digitata* extract, and then showed that they cross-reacted with surface antigens from microfilarae of *Wuchereria bancrofti*, a filarial nematode that is the main cause of lymphatic filariasis in human. Immunoelectrophoretic analysis of ES products of *Setaria cervi*, a bovine filarial parasite, in RPMI-1640 medium which revealed 11-15 antigens most of were common to somatic antigenic preparations from both adult worms and microfilariae (Malhotra et al, 1987).

Beuria and Das, (1995) isolated a serine protease of 30 kDa from the extract of *S. digitata* and investigated the immediate hypersensitivity reaction in lymphatic filariasis patients. Dalai, et al, (1998) showed that *S. digitata* adult 14- to 20-kDa antigens induce differential Th1 and Th2 cytokine responses in the lymphocytes of endemic normals and asymptomatic microfilariae carriers in bancroftian filariasis. Interestingly, Sharma, et al, (1998) found that *S. cervi* microfilariae secrete acetyl cholinesterase, which has antigenic cross-reactivity with *Wuchereria bancrofti*. A study by Subhachalat et al, (1999a) differentiated *S. digitata* and *Setaria marshali* based on their antigenic profiles and found that *S. marshali* contained a 69 kDa protein different from *S. digitata* (Subhachalat et al, 1999a). Further investigation of the protein by two-dimensional gel electrophoresis revealed a spot ranging from 64 to 73 kDa in *S. marshalli* (Subhachalat et al, 1997b). There is a high level of anti-*Setaria* antibodies in cattle infected with microfilariae or adult worms as well as apparently uninfected cattle. It may be indicative of the similarity between human and bovine anti-microfilaria immune responses.

Sasisekhar et al, (2005) identified two proteins of 34 and 64 kDa in the crude protein extract of *S. digitata*. It was found that these proteins were sheath proteins located in the parasite's hypodermal region. As a result of the investigation by Pokharel et al, (2006a, b) a collagenase and leucine aminopeptidase of 175 kDa have been isolated from *Setaria cervi* showing their potential to be used as vaccines or diagnostic markers for *Brugia malayi* infection, human lymphatic filariasis. Madathiparambil et al, (2009) isolated a 200 kDa glycoprotein from the surface pores of *S. digitata* male and female worms. In SDS-PAGE analysis, several proteins ranging from 11 to 66 kDa were identified in this glycoprotein. According to the findings of this study, the glycoprotein (200kDa) can be a strong candidate for antigen-based immunodiagnosis of filariasis in humans.

Due to the stimulation of the host immune system by different stages of the parasite and the presence of anti-nematode antibodies, especially IgG, in the serum of infected animals, antibody detection immunological methods can be used to detect infected animals.

Results of immunoblotting of ES, MF and S of *S. labiatopapillosa*, the 68 and 64 kDa proteins were the most common antigenic components that can be candidate to future studies.

Acknowledgment

The authors gratefully acknowledge the Research Councils of Shahid Chamran University of Ahvaz, Iran, for providing financial assistance.

Conflict of interest

The authors confirm that there is no conflict of interest.

Funding

Funding This work was supported by Shahid Chamran University of Ahvaz.

References

Alborzi, A. R., Bahrami, S., & Khajeh, F. (2022). A Preliminary Study on the Antigenic Proteins of *Linguatula serrata* Nymphal Stage in Sheep with Visceral Linguatulosis. *Archives of Razi Institute*, *77*(1), 13-18.

Alborzi, A. R., Seyfiabadshapouri, S. M., & Hoghoughirad, N. (2006). Identification of excretory-secretory products from larval stages of *Ostertagia circumcincta* cultured in vitro by SDS-PAGE and immunoblotting. *Iranian Journal of Veterinary Research, 7*(30),13-16.

Alborzi, A, R., Haddadmolayan, P., Tabandeh, M. R., & Ghorbanpoor, M. (2019). Ultrastructural and molecular characteristics of *Setaria* species based on sequence analysis of genomic and mitochondrial gene markers in cattle (*Bos taurus*) and buffaloes (*Bubalus bubalis*) from Iran. *Journal of the Hellenic Veterinary Medical Society*, *70*(4), 1777-1788.

Alborzi, A. R., Ghorbanpoor, M., Hamidinejat, H., Chamanara, S., & Noori, S. (2016). Seroprevalence of *Linguatula serrata* nymph infection in sheep from west of Iran by ELISA. *Iranian Veterinary Journal, 12*(2),11-17.

Alborzi, A., Jolodar, A., & Seyfiabadshapouri, M. S. A. (2014). Isolation and identification of excretory-secretory and somatic antigens from the *Oestrus ovis* larvae by SDS-PAGE and immunoblotting. In *Veterinary Research Forum* (Vol. 5, No. 4, p. 307).

Anderson, R. C. (2000). *Nematode parasites of vertebrates: their development and transmission*. Cabi, 479-482.

Bazargani, T., Esmaeili, A., Gholami, G. R., Moulaei, A., Ghafari, C. J., Davoudi, J., & Ashrafi, J. (2008). Cerebrospinal nematodiasis of cattle, sheep and goats in Iran. *Iranian Journal of Parasitology*, *3*(1):16-20.

Berezhko, V. K., Khaydarov, V. K., Napisanova, L. A., & Thakahova, A. A. (2016). Mature *Setaria labiatopapillosa* in cattle-a source for receiving antigens for diagnosis of dirofilariasis (*Dirofilaria immitis*). *Rossiĭskiĭ Parazitologicheskiĭ Zhurnal*, (2), 192-201.

Beuria, M. K., Bal, M., & Das, M. K. (1995). Allergic reactivity and IgG subclasses to a proteinase fraction of *Setaria digitata* in filariasis. *Journal of helminthology*, *69*(3), 181-185.

Bradford, M. M. (1976). A rapid and sensitive method for the quantitation of microgram quantities of protein utilizing the principle of protein-dye binding. *Analytical biochemistry*, *72*(1-2), 248-254.

Bright, J. J., & Raj, R. K. (1991). Isolation and analysis of surface antigens of filarial nematode *Setaria digitata*. *Indian Journal of Experimental Biology*, *29*(8), 725-729.

Cancrini, G., Pietrobelli, M. A. R. I. O., Di Regalbono, A. F., & Tampieri, M. P. (1997). Mosquitoes as vectors of *Setaria labiatopapillosa*. *International journal for parasitology*, *27*(9), 1061-1064.

Cancrini, G., Pietrobelli, M. A. R. I. O., Di Regalbono, A. F., & Tampieri, M. P. (1997). Mosquitoes as vectors of *Setaria labiatopapillosa*. *International journal for parasitology*, *27*(9), 1061-1064.

Dalai, S. K., Das, D., & Kar, S. K. (1998). *Setaria digitata* adult 14-to 20-kDa antigens induce differential Thl/Th2 cytokine responses in the lymphocytes of endemic normals and asymptomatic microfilariae carriers in bancroftian filariasis. *Journal of clinical immunology*, *18*(2), 114-123.

Dissanayake, S., & Ismail, M. M. (1980). Antigens of *Setaria digitata*: cross-reaction with surface antigens of *Wuchereria bancrofti* microfilariae and serum antibodies of *W. bancrofti*-infected subjects. *Bulletin of the World Health Organization*, *58*(4), 649.

Karunamoorthi, K., & Sabesan, S. (2013). Insecticide resistance in insect vectors of disease with special reference to mosquitoes: a potential threat to global public health. *Health Scope. 2*(1) 4-18.

Kaushal, N. A., Srivastava, N., Mustafa, H., Tandon, A., Singh, S. K., & Kaushal, D. C. (2009). Isolation of an antigen fraction from *Setaria cervi* adults having potential for immunodiagnosis of human filariasis. *Immunological Investigations*, *38*(8), 749-761.

Khedri, J., Radfar, M. H., Borji, H., & Azizzadeh, M. (2014). An epidemiological survey of *Setaria* in the abdominal cavities of Iranian Sistani and Brahman cattle in the southeastern of Iran. *Iranian Journal of Parasitology*, *9*(2), 249.

Kim, N. S., Kim, H. C., Sim, C., Ji, J. R., Kim, N. S., & Park, B. K. (2010). Congenital infection with *Setaria digitata* and *Setaria marshalli* in the thoracic cavity of a Korean calf: a case report. *Veterinární medicína*, *55*(6), 275-280.

Kutz, S. J., Ducrocq, J., Verocai, G. G., Hoar, B. M., Colwell, D. D., Beckmen, K. B., ... & Hoberg, E. P. (2012). Parasites in ungulates of Arctic North America and Greenland: a view of contemporary diversity, ecology, and impact in a world under change. *Advances in parasitology*, *79*, 99-252.

Laaksonen, S., Solismaa, M., Kortet, R., Kuusela, J., & Oksanen, A. (2009). Vectors and transmission dynamics for *Setaria tundra* (Filarioidea; Onchocercidae), a parasite of reindeer in Finland. *Parasites & Vectors*, *2*(1), 1-10.

Laemmli, U. K. (1970). Cleavage of structural proteins during the assembly of the head of bacteriophage T4. *nature*, *227*(5259), 680-685.

Madathiparambil, M. G., Kaleysa, K. N., & Raghavan, K. (2009). A diagnostically useful 200-kDa protein is secreted through the surface pores of the filarial parasite *Setaria digitata*. *Parasitology research*, *105*(4), 1099-1104.

Mahmoud, O. M., Haroun, E. M., & Omer, O. H. (2004). An outbreak of neurofilariosis in young goats. *Veterinary parasitology*, *120*(1-2), 151-156.

Malhotra, A. N. J. U., Kaushal, N. A., Kaushal, D. C., & Ghatak, S. (1987). Antigenic characterization of excretory-secretory products of *Setaria cervi*. *Tropical Medicine and Parasitology: Official Organ of Deutsche Tropenmedizinische Gesellschaft and of Deutsche Gesellschaft fur Technische Zusammenarbeit (GTZ)*, *38*(2), 106-110.

Mohanty, B. P., Dalai, S. K., & Kar, S. K. (2006). IgG4-reactive low molecular weight antigens from *Setaria digitata* adult parasites have immunodiagnostic potential in lymphatic filariasis. *Current Science*, 1221-1225.

Mohanty, B. P., Dalai, S. K., & Kar, S. K. (2006). IgG4-reactive low molecular weight antigens from *Setaria digitata* adult parasites have immunodiagnostic potential in lymphatic filariasis. *Current Science*, 1221-1225.

Mrifag, R., Lemrabott, M. A., El Kharrim, K., Belghyti, D., & Basco, L. K. (2021). *Setaria labiatopapillosa* (Filarioidea, Nematoda) in Moroccan cattle: atypical localization and morphological characterization of females and microfilariae by light and scanning electron microscopy. *Parasitology Research*, *120*(3), 911-918.

Nakano, H., Tozuka, M., Ikadai, H., Ishida, H., Goto, R., Kudo, N., ... & Oyamada, T. (2007). Morphological survey of bovine *Setaria* in the abdominal cavities of cattle in Aomori and Kumamoto Prefectures, Japan. *Journal of veterinary medical science*, *69*(4), 413-415.

Pokharel, D. R., Rai, R., Kodumudi, K. N., Reddy, M. V. R., & Rathaur, S. (2006 a). Vaccination with *Setaria cervi* 175 kDa collagenase induces high level of protection against *Brugia malayi* infection in jirds. *Vaccine*, *24*(37-39), 6208-6215.

Pokharel, D. R., Rai, R., Kumar, P., Chaturvedi, C. M., & Rathaur, S. (2006 b). Tissue localization of collagenase and leucine aminopeptidase in the bovine filarial parasite *Setaria cervi*. *Filaria journal*, *5*(1), 1-8.

Raj, R. K., Pradeep, C. G., Devi, C. M., John, L., Rekha, M. R., & Oommen, S. K. (1997). Immunomodulation of excretory secretory materials from the filarial parasite *Setaria digitata*. *Indian Journal of Clinical Biochemistry*, *12*(1), 32-34.

Rashidi, S., Kalantar, K., & Hatam, G. (2018). Using proteomics as a powerful tool to develop a vaccine against Mediterranean visceral leishmaniasis. *Journal of Parasitic Diseases*, *42*(2), 162-170.

Razi Jalali, M. H., Ghorbanpoor, M., Pourmahdi Borujeni., &Khodadadian, V. (2014). Evaluation of counterimmunoelectrophoresis method for detection of somatic circulating antigen of *Fasciola gigantica* in bovine sera. *Iranian Veterinary Journal*, *10*(1), 30-36.

Richer, J. K., Sakanari, J. A., Frank, G. R., & Grieve, R. B. (1992). *Dirofilaria immitis*: proteases produced by third-and fourth-stage larvae. *Experimental parasitology*, *75*(2), 213-222.

Ring, C. S., Sun, E., McKerrow, J. H., Lee, G. K., Rosenthal, P. J., Kuntz, I. D., & Cohen, F. E. (1993). Structure-based inhibitor design by using protein models for the development of antiparasitic agents. *Proceedings of the national academy of Sciences*, *90*(8), 3583-3587.

Rodrigues, R. A. R., Conga, D. M. F., Santos, J. N. D., Gonçalves, E. C., Pinheiro, R. H. D. S., & Giese, E. G. (2021). Morphological diagnosis of *Setaria labiatopapillosa* in domestic bovids from Marajó Island, Brazil. *Revista Brasileira de Parasitologia Veterinária*, *30*(3), e004321.

Sasisekhar, B., Suba, N., Sindhuja, S., Sofi, G. M. A., & Narayanan, R. B. (2005). *Setaria digitata*: identification and characterization of a hypodermally expressed SXP/RAL2 protein. *Experimental parasitology*, *111*(2), 121-125.

Sharma, S., Misra, S., & Rathaur, S. (1998). Secretory acetylcholinesterase of *Setaria cervi* microfilariae and its antigenic cross-reactivity with *Wuchereria bancrofti*. *Tropical Medicine & International Health*, *3*(1), 46-51.

Shin, J., Ahn, K. S., Suh, G. H., Kim, H. J., Jeong, H. S., Kim, B. S., ... & Shin, S. S. (2017). First blindness cases of horses infected with *Setaria digitata* (Nematoda: Filarioidea) in the Republic of Korea. *The Korean Journal of Parasitology*, *55*(6), 667.

Singh, H., Singh, N. K., Singh, N. D., Jyoti, & Rath, S. S. (2015). Occurrence of *Setaria labiatopapillosa* in peritoneal cavity of a crossbred cattle. *Journal of Parasitic Diseases*, *39*(2), 152-154.

Subhachalat, P., & Adachi, Y. (1997). Classification of *Setaria* worms from calves and adult cattle into *Setaria digitata* and *Setaria marshalli* by polyacrylamide gel electrophoresis. *Zentralblatt für Bakteriologie*, *286*(4), 527-533.

Subhachalat, P., Shirasaka, S., Nakajima, H., & Adachi, Y. (1999). *Setaria digitata* in cattle of Thailand identified by sodium dodecyl sulfate polyacrylamide gel electrophoresis. *Journal of veterinary medical science*, *61*(4), 443-445.

Sundar, S. B., D'souza, P. E., & Jagannath, M. S. (2005). Prevalence of setariosis in cattle and buffaloes in Karnataka. *Journal of Parasitic Diseases*, *29*, 147-149.

Takesue, M., Osaka, Y., Muranaka, M., Katayama, Y., & Ikadai, H. (2016). Identification of immunodiagnostic antigens for cerebrospinal filariasis in horses by western blot analysis. *Journal of Equine Science*, *27*(1), 17-18.

Towbin, H., Staehelin, T., & Gordon, J. (1979). Electrophoretic transfer of proteins from polyacrylamide gels to nitrocellulose sheets: procedure and some applications. *Proceedings of the national academy of sciences*, *76*(9), 4350-4354.

Tung, K. C., Lai, C. H., Ooi, H. K., Yang, C. H., & Wang, J. S. (2003). Cerebrospinal setariosis with *Setaria marshalli* and *Setaria digitata* infection in cattle. *Journal of Veterinary Medical Science*, *65*(9), 977-983.

Virginio, V. G., Monteiro, K. M., Drumond, F., de Carvalho, M. O., Vargas, D. M., Zaha, A., & Ferreira, H. B. (2012). Excretory/secretory products from in vitro-cultured Echinococcus granulosus protoscoleces. *Molecular and Biochemical Parasitology*, *183*(1), 15-22.

Wang, M. Z., Ye, K. X., & Hu, L. S. (1986). Study on etiology of" lumbar paralysis" in horses, sheep and goats. *In Proceedings of the 4th international symposium on veterinary epidemiology and economics Changchun Veterinary College, Changchun, Jilin, China., Singapore*, 283-284.

Watanabe, Y., Yang, C. H., Tung, K. C., & Ooi, H. K. (2004). Comparison of microfilaria concentration method for *Setaria digitata* infection in cattle and for *Dirofilaria immitis* infection in dogs. *Journal of veterinary medical science*, *66*(5), 543-545.

Received: 19.07.2025
Accepted: 14.12.2025

Vol. 22, No. 2, Summer, 2026, 15-24 *Original Article*
DOI: 10.22055/ivj.2026.566326.2875
Journal Homepage: http://www.ivj.ir/

Innovative semi-quantitative multiplex single primer pair PCR method for simultaneous detecting some obligate intracellular piroplasms

Zahra Alizadeh Sarabi[1], Sedighe Nabian[2], Parviz Shayan[2*], Said Bokaei[3] and Hamid Reza Shokrani[4]

[1] PhD Student of Parasitology, Research Center for Ticks and Tick-borne Diseases, Faculty of Veterinary Medicine, University of Tehran, Tehran, Iran
[2] Professor, Department of Parasitology, Research Center for Ticks and Tick-borne Diseases, Faculty of Veterinary Medicine, University of Tehran, Tehran, Iran
[3] Professor, Departeman of Food Hygiene and Quality Control, Faculty of Veterinary Medicine, University of Tehran, Tehran, Iran
[4] Associate Professor, Department of Pathobiology, Lorestan University, Khorramabad, Iran

Received: 15.12.2025 Accepted: 20.05.2026

Abstract

The causative agents of piroplasmosis, *Babesia* spp. and *Theileria* spp. infect ruminants in the livestock industry with high economical loses worldwide. The early diagnosis of the disease can help manage the successful treatment. Giemsa staining is a common method used worldwide for diagnosis of piroplasmosis which unfortunately can be accompanied with some serious problems like suitable blood smears and quality of staining and needs high experience. Serological methods like ELISA or IFAT was also used in some laboratories. The molecular methods based on DNA analysis preferably used in many laboratories are accurate and reliable. The aim of the present study was to introduce a simple and innovative semi-quantitative multiplex PCR method which can be helpful for simultaneously detection of *Babesia spp.* and *Theileria spp*. For this aim, we used primers derived from 18S rRNA genes which can amplify simultaneously the DNA from hosts (ruminants and ticks) and also from *Babesia* spp., and *Theileria* spp with different easily distinguishable PCR products. Our results showed that, as was expected, the different length of ampilicons generated from *Theileria spp*. and *Babesia spp*. make it possible to differentiate these parasites from each other on the same agarose gel. Interestingly, since the same primer pair can also amplify the 18S rRNA from host cells with larger amplicon compared to the parasites, this property can be used for semi-quantitative analysis of the parasite burden in the samples. It is necessary to mention that the introduced primer pair (VetUTPiro) can be used for differential diagnosis of babesiosis and theileriosis as well as for semi-quantitative multiplex PCR analysis of the parasite burden consequently for controlled therapy management.

Keywords: *Theileria spp., Babesia spp*., Semi-quantitative multiplex PCR, Therapy management, Sheep

Introduction

Piroplasmosis is a significant hemoparasitic disease that primarily affects livestock, particularly ruminants. This disease is predominantly caused by protozoan parasites from the genera *Babesia* and *Theileria*. The economic impact on the livestock industry is substantial, leading to considerable global losses due to reduced productivity, including weight loss, decreased milk yield,

[*] **Corresponding Author**: Parviz Shayan, Professor, Department of Parasitology, Research Center for Ticks and Tick-borne Diseases, Faculty of Veterinary Medicine, University of Tehran, Tehran, Iran
E-mail: pshayan@ut.ac.ir

increased susceptibility to secondary infections, and higher mortality rates among infected animals. The high costs associated with veterinary care and management further exacerbate this economic burden (Shayan et al, 2007; Hossein et al, 2024; Modirrousta et al, 2019).

The widespread prevalence of piroplasmosis poses serious implications for animal welfare and food security, particularly in regions with heavy tick infestations. In some areas, it has been reported that up to 20% of animals may carry *Babesia* or *Theileria*, often remaining asymptomatic (Onyiche et al, 2019; Onyiche, 2020; Jouglin, 2025). Therefore, early and accurate diagnosis is crucial for effective management of the disease. Traditional diagnostic methods, such as blood smears, frequently yield false negatives, particularly in carrier animals. This limitation highlights the necessity for more sensitive molecular techniques, such as polymerase chain reaction (PCR), which can detect low parasitic loads and improve early diagnosis and treatment outcomes (Tian et al, 2015; El-Ashker, 2015; Shayan et al, 2007). Accurate and early diagnosis of piroplasmosis is essential for effective treatment and management. Traditional diagnostic techniques, including Giemsa-stained blood smears, have been the standard practice in clinical settings; however, they present significant limitations. One major drawback is that these methods require highly trained personnel to correctly identify the parasites under a microscope, because some *Theileria sp.* and *Babesia sp.* resemble each other in stained blood smears. Additionally, the quality of blood smears and variability in staining can lead to inconsistent results, potentially resulting in misdiagnosis or delayed treatment, which can worsen the impact of the disease on livestock (Malekifard et al, 2014; Riaz et al, 2023).

Moreover, Giemsa staining exhibits low sensitivity, particularly in cases with low parasitic loads, and may fail to detect subclinical infections. This limitation is especially problematic in regions where the disease is endemic, as animals may serve as asymptomatic carriers. Misdiagnosis can result in unnecessary treatments, escalating costs and potentially contributing to drug resistance. Therefore, there is an increasing demand for more accurate and sensitive diagnostic techniques (Mendoza et al, 2024; Rosenblatt et al, 2009).

Serological techniques, such as enzyme-linked immunosorbent assay (ELISA) and the indirect fluorescent antibody test (IFAT), have emerged as valuable alternatives for diagnosing piroplasmosis. These methods detect antibodies against protozoan parasites like *Babesia* and *Theileria*, offering insights into the immune response of infected animals. Recent studies underscore the utility of these serological tests; however, they often face challenges related to specificity and sensitivity when compared to molecular methods like PCR (Jongejan et al, 2024; Jaffer et al, 2010; Tirosh-Levy et al, 2020). PCR has gained prominence in piroplasmosis diagnosis due to its high accuracy and reliability. It is capable of detecting low parasitic loads in blood samples, making it especially useful during the early stages of infection when antibody responses may not yet be detectable. For example, a comparative study demonstrated that PCR could identify piroplasm DNA in horses that were serologically negative, indicating that molecular methods can uncover active infections that serological tests might miss (Jaffer et al, 2010).

While serological methods effectively detect past infections and assess herd immunity, their inability to differentiate between active and passive infections can lead to misdiagnosis. Thus, the integration of PCR with serological techniques is increasingly recommended to enhance diagnostic accuracy and facilitate timely intervention (Jaffer et al, 2010).

In this study, we present a novel semi-quantitative multiplex PCR method

designed for the simultaneous detection of *Babesia spp*. and *Theileria spp*. This innovative approach employs primers derived from the highly conserved 18S rRNA genes, allowing for the amplification of DNA from both the target pathogens and their hosts (ruminants and ticks). The generated PCR products exhibit distinct fragment lengths, which can be effectively analyzed through agarose gel electrophoresis. This dual amplification capability facilitates the differential diagnosis of babesiosis and theileriosis, enabling prompt and accurate identification of the causative agents.

Furthermore, considering the semi-quantitative multiplex nature of this PCR method, it holds significant promise for therapeutic management. It allows veterinarians to monitor the effectiveness of treatment regimens and adjust strategies as necessary based on the parasitic load in the host. The development of this method represents a critical advancement in the diagnostic tool for managing piroplasmosis, with potential implications for enhancing livestock health and productivity.

Materials and methods

Morphologic characterization of ticks

Hard ticks were collected from sheep in different places of Tehran province. All specimens were stored in tubes containing 70% ethanol. All ticks were identified morphologically based on identification keys described by Walker et al. 2003 and Estrada-Penna et al. 2017, using stereomicroscope. Different characteristic factors such as: the length of capitulum, Basis capituli, presence or absence of eye, the number of festoons, leg coloration, were noticed for identification of genus and the other characteristicss like cornua length, the form of cocxae in different legs, lateral groove, the kind of punctuation distribution were used for species identification.

Isolation of salivary gland of ticks

In order to remove the tick's salivary glands for DNA extraction, ticks were first placed on a glass slide from the dorsal surface and their scutum was cut from the posterior margin and set aside.

Then the salivary glands of the ticks located on both sides of the tick's body under the mouthparts were taken out by forceps and kept in 70% ethanol, until used.

DNA extraction

Hyalomma anatolicum anatolicum, *Rhipicephalus turanicus* and blood from sheep infected with *Theileria spp.* were provided by National Parasitology Museum of Iran (Faculty of Veterinary Medicine, University of Tehran). DNA was extracted from the salivary glands of mentioned ticks and blood of sheep infected with *Theileria spp.* using DNA isolation kit (MBST, Iran) according to the manufacturer's protocol. In brief, the salivary gland or 100 µl of blood were first lysed in 180 µl of lysis buffer, and the proteins were digested by adding 20 µl of proteinase K and incubating for 10 minutes at 55°C. Afterward, 360 µl of binding buffer was added, followed by a 10-minute incubation at 70°C. Then, 270 µl of 100% ethanol (Merck, Germany) was added to the mixture. The solution was vortexed and transferred to the MBST column, which was centrifuged, and then washed twice with 500 µl of washing buffer. Finally, DNA was extracted from the column using 70 µl of elution buffer.

PCR and nested PCR

DNA extracted from salivary glands of ticks and blood sample was amplified using primer pair (All sense 5` CACAGGGAGGTAGTGACAAG 3`, All antisense 5` AAGAATTTCACCTCTGACAG 3`) derived from 18S rRNA gene of *Babesia spp*. and *Theileria spp*., which can simultaneously amplify the corresponding DNA region in both piroplasms. This primer pair cannot amplify the DNA

derived from ticks and ruminants (Shayan and Rahbari, 2005).

The same DNA probes were also amplified using primer pair (VetUTPiro-Forward primer 5` TGCAGTTAAAAAGCTCGTAG 3` and VetUTPiro-Reverse primer 5` GAGCACTCTAATTTTCTCAAAGTA 3`) which can amplify simultaneously not only *Babesia spp*. and *Theileria spp*., but also can amplify DNA from ticks and ruminants with different PCR products in length, to be used for semi-quantitative multiplex PCR analysis. The PCR reaction mixture consisted of 20 µM of each primer, 1 µl of extracted DNA, 9.5 µl of double distilled water, and 12.5 µl of Taq PCR Master Mix (SinaClon), for a final volume of 25 µl. In all experiments, DNA from *Theileria*-infected blood was used as positive control and H_2O as negative control. The PCR was performed in Thermo cycler (MWG/Germany) under following conditions: initial denaturation of 5 minutes at 95°C, 38 cycles of 45 seconds at 94 °C (denaturation), 45 seconds at 52 °C (annealing), 45 seconds at 72 °C (extension) and final 10 minutes at 72 °C. This condition was used for each primer pair. The amplified DNA was then analyzed on agarose gel under UV condition using Gel-Documentation-system (Pouiesh Teb Adak, Theran, Iran).

Results

Identification of ticks

The morphometric characterization of ticks was performed using identification keys described above. Among hard Ticks collected from sheep and goat, two different genera including Rhipicephalus *turanicus* (Figure 1 A1) and *Hyalomma anatolicum* (Figue 1A2) were detected. The *Hyalomma anatolicum* was characterized according to the length of capitulum, the presence of typical oval and darkness colour parma cell, separation of paracentral festoons and the presence of pale rings in leg coloration (Figure 1 A2). *Rhipicephalus turanicus* was characterized according to having hexagonal base of capitulum and festoons, narrow Adanal plates, spiracle plate arias having sparse setae and broad spiracle plate tails. Figure 1B showed the extracted mentioned tick's salivary glands. In order to extraction of pure salivary glands, it was noticed that they were without contaminated materials from midgut as can be seen in Figure 1B.

The Figure of the tick's salivary glands which were taken out, is shown in Figure 1. Regarding our experience, it should be mentioned that the color of infected salivary glands to *Babesia* and *Theileria* piroplasms usually is brown, while in the uninfected salivary glands, it turns transparent milky color (our observations).

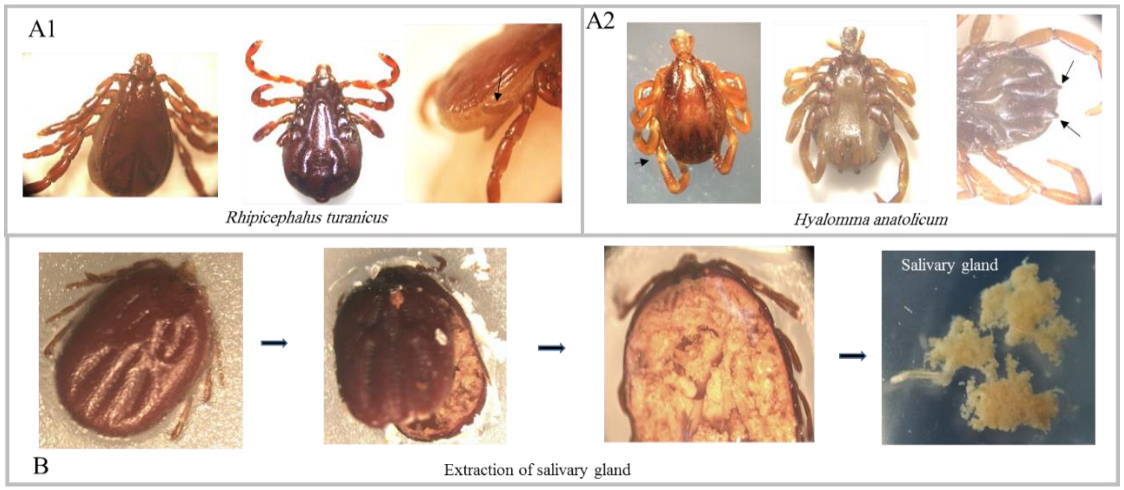

Figure 1: Upper figures are morphological characteristics of *Rhipicephalus turanicus* **and** *Hyalomma anatolicum* **and lower figures are the process of tick`s salivary glands extraction.**

DNA extraction from salivary gland and PCR

DNA was extracted from salivary glands of *Hyalomma anatolicum* and *Rhipicephalus turanicus* and amplified using common specific primer pair amplifying simultaneously *Babesia spp*. and *Theileria spp*. resulting in PCR product of approximately 426 bp for *Theileria spp*. and approximately 389 bp for *Babesia spp.* (Figure 2). Figure 2, shows that salivary glands of one *Hyalomma anatolicum* was negative (lane 1) and the second one was positive (lane 2) for *Theileria spp.* resulting PCR product of approximately 426 bp.. Figure 2 also showed the amplification of extracted DNA from salivary glands of *Rhipicephalus turanicus* resulting in PCR product of 389 bp in length, confirming infection with *Babesia spp*. (lane 3 and 4).

PCR using host-parasite common primer pair

Interestingly we could find a small region in 18S rRNA gene, which were found conserved from one site in homo sapiens, mammalians and ticks and from the other site in obligate intracellular protozoan parasites like *Theileria spp.* and *Babesia spp*. Figure 3 shows the analysis of DNA extracted from *Theileria* infected Blood samples using VetUTPiro primer pair by PCR. As it can be seen in Figure 3, lanes 2 and 3, two PCR products were visible. The PCR product with 157 bp in length belong to the host genomic DNA whereas the PCR products with 125-127 bp in length belong to the genomic DNA of *Theileria* species. The results to the amplification of regarding genomic DNA originated from *Babesia* and *Theileria* species with the mentioned primer pair can be confirmed in ticks infected with these piroplasms. Figure 4, lane 6 and 7 shows PCR product generated from host and parasite in ticks *Hyalomma anatolicum* and *Rhipicephalus turanicus*. Interestingly, lane 7 clearly shows the mix infection (*Babesia* and *Theileria*) in *Rhipicephalus turanicus,* since PCR product generated from *Babesia spp*. should be between 91-113 bp. Figure 4, lanes 4 and 5 shows PCR analysis with DNA sample extracted from uninfected salivary gland of *Hyalomma anatolicum* and *Rhipicephalus turanicus* respectively, in which only PCR product generated from salivery glands with 157 bp in length was visible. We believe that the ability to amplify the genomic DNA generated from host and parasite simultaneously can help to analyze the parasite burden while the treatment. For this aim, the ratio between intensity of PCR product of parasite to intensity of PCR product of host cell gives an index for parasite burden in the sample, which can be used for semi-quantitative multiplex analysis. Furthermore, the mentioned index can be also used for determination of drug efficacy.

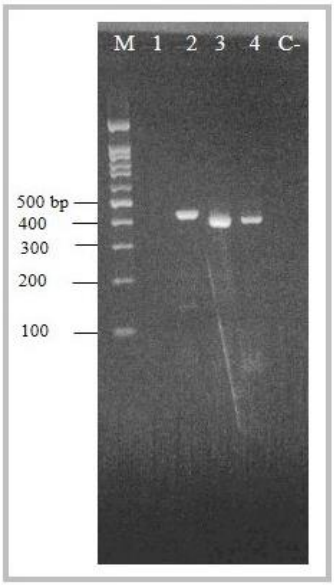

Figure 2: DNA was extracted from salivary glands of *Hyalomma anatolicum* **and** *Rhipicephalus turanicus* **and analyzed using common specific primer pair amplifying simultaneously** *Theileria* **and** *Babesia spp.* **Lane 1 and 2 (PCR analysis of DNA extracted from salivary glands of** *Hyalomma anatolicum***), Lane 3 and 4 (PCR analysis of DNA extracted from salivary glands of** *Rhipicephalus turanicus***). C- = negative control and M = 100 bp DNA marker.**

The VetUTPiro primers were checked by https://www.ncbi.nlm.nih.gov/guide/howto/design-pcr-primers program and could find that they can amplify also *Plasmodium falciparum, Plasmodium vivax, Plasmodium ovale* and

Plasmodium malariae generating PCR product of 198, 202, 207 and 236 bp respectively, which could be easily distinguished from the genomic DNA derived from human and other Mammalians (Table 1). It is also necessary to mention that the above introduced primers can also amplify *Toxoplasma gondii* producing PCR products of 86, 157 bp respectively. Interestingly, these primers cannot amplify genomic DNA generated from *Trypanosoma* or *Neospora* (Table 1).

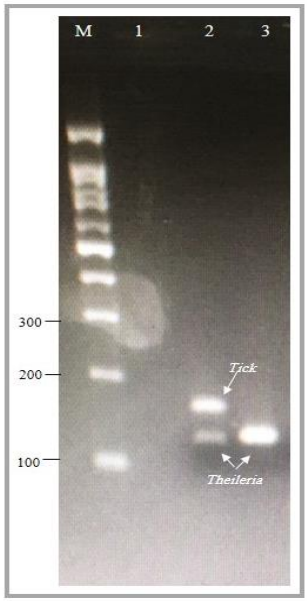

Figure 3: DNA was extracted from salivary glands of ticks, The DNA was amplified using VetUTPiro specific primer pair. Lane 2 was amplification of DNA from *Theileria* infected salivary gland using VetUTPiro primers. Lane 3: amplification of PCR product generated from DNA extracted from infected blood using the first primer pair shown in figure 2 with VetUTPiro primers (Lane 2) and Lane 1 was negative control and M = 100 bp DNA marker.

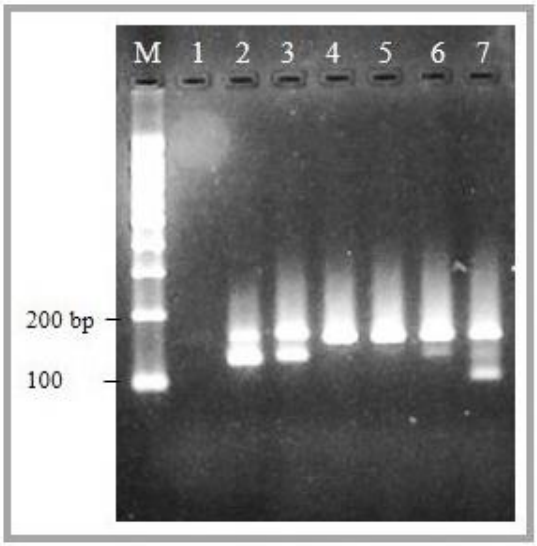

Figure 4: DNA was extracted from *Theileria* infected sheep blood, salivary gland of *Hyalomma anatolicum* and *Rhipicephalus turanicus* and analyzed using VetUTPiro specific primer pair amplifying simultaneously *Theileria* and *Babesia spp*. Lane 2 and 3 are PCR analysis of *Theileria* infected blood samples, Lane 4 and 5 were PCR analysis with DNA sample extracted from uninfected salivary gland of *Hyalomma anatolicum* and *Rhipicephalus turanicus* respectively, Lane 6 was PCR analysis with DNA sample extracted from salivary gland of *Theileria* infected *Hyalomma anatolicum*, Lane 7 was PCR analysis with DNA sample extracted from salivary gland of *Theileria/Babesia* mix infected *Rhipicephalus turanicus*. Lane 1 was negative control and M = 100 bp DNA marker (CinaClone, Iran).

Table 1: Alighnment of the genomic DNA of some hemoparasites and hosts with vetmedTUPiro-primers using https://www.ncbi.nlm.nih.gov/tools/primer-blast program

species	Accession no.	PCR product	species	Accession no.	PCR product
T. lestoquardi *T. ovis*	AF081135.1 AY533144.1	126	*H. anatolicum*, *H. asiaticus*, *Rh. sanguineous*, *Rh. turanicus*, *Rh. haemolyticus*, *Rh.Appendiculatus*, *Rh. bursa*, *D. andersoni*, *D. marginatus*, *D. niveus*, *D. nuttalli*, *I. ricinus*	JX051052.1, JX051026.1, L76342.1, JX987495.1, DQ839552.1, AF018653.1, AJ003816.1, L76340.1, Z74480.1, KR002680.1, KJ410657.1, GU074704.1	157
T. orientalis *T. annulata* *T. equi*	LC576821.1 KF429795.1 JQ390047.1	125			
T. parva *B. equi* (*T. equi*)	L02366.1 AB515315.1	127			
B. bovis *B. ovis*	KF928959.1 AY260178.1	91			
B. bigemina	JQ437261.1	95			
B. motasi	AY260180.1	96			
B. crassa	MK240324.1	102			
B. cabballi	XR_010957797.1	105	*Bos Taurus*, *Ovis aries*, *Equus asi*, *Equus caba*, *Camelus dr*, *Homo sapie*	DQ222453.1, KY129860.1, XR_006524340.1, XR_011434517.1, XR_010379165.1, XR_007090847.1	157
B. divergens *B. canis*	U16370.1 PP574310.1	113			
P. falciparum	CP101634.1	198			
P.vivax	LT635613.2	202			
P. ovale	MN515109.1	207			
P. malariae	XR_003751948.1	236			
Toxoplasma gondii	PQ894615.1 U03070.1	86 157			

Discussion

Among the hard Ticks collected from sheep and goat, two different genera including *Hyalomma anatolicum* and *Rhipicephalus turanicus* were detected based on characterization keys (Walker, 2003). *Hyalomma anatolicum* is an important three-host hard ticks which is distributed widely from North Africa to India and its more importance is for transmission of some hemoparasites (Walker, 2003). *Rhipicephalus turanicus* is also a three-host hard tick whose information about geographical distribution, ecology and genetic patterns and diversity is very contradictory and unreliable. So, its vectorial capacity is also under discussion. Therefore, its role as a vector of human pathogens, including *Rickettsia massiliae, R. conorii* and other microorganisms, needs confirmation based on molecular detection (Estrada-Peña et al, 2018).

It is worthy of mention that these tick species are distributed across various provinces of Iran, suggesting a high level of adaptability to the country`s diverse climatic and environmental conditions. Studies indicate that both tick species can be considered as potential vectors of hemoprotozoan such as *Babesia* and *Theileria*. In a study conducted by Abdallah et al, 2017. *Hyalomma anatolicum* was reported to be infected with protozoan parasites from both *Theileria* and *Babesia* genera, indicating the potential role of this tick species in the simultaneous transmission of these two pathogenic agents. Furthermore, findings from a study by Shayan et al, 2007, using PCR, confirmed infection in *Rhipicephalus turanicus* by *Babesia ovis*, highlighting the significant role of this species in the transmission of ovine babesiosis in Iran. In addition, a more recent study conducted in

2024 in the Xinjiang Autonomous Region of China identified *R. turanicus* and *H. anatolicum* among ticks collected from sheep and confirmed that they were infected with *Theileria* parasites.

Theileria and *Babesia* species play an important role in the animal and public health with economical losses. The early diagnosis of malignant piroplasmosis is of great importance for both disease control and controlling the economic losses worldwide. Shayan and Rahbari (2005), introduced an easy PCR method for simultaneous differential diagnosis of *Theileria* and *Babesia* infections on DNA extracted from stained blood smears. In that study, they showed that the amplification of the DNA generated from *Theileria* spp. using common primer pair by PCR resulting in PCR product of ca. 426-430 bp in length, whereas for *Babesia* genus the PCR product was 389-402 bp in length. Although the difference of PCR products between these two genera was approximately 30 bp, but on the 2% agarose gel was this difference distinguishable. Therefore, in lesser agarose gel concentration, the differentiation between both PCR products could be accompanied with some problems. To resolve this problem, a new innovative primer pair was designed, with which interestingly, the genomic DNA from *Theileria* or *Babesia spp*. as well as host (tick or mammalian) can be simultaneously amplified. Since the PCR products generated from genomic DNA of *Theileria, Babesia spp*. and host are 125-127 bp and 91-113 and 157 bp respectively, this extraordinary property of primers makes them useful for molecular semi-quantitative multiplex analysis and detection of mix-infections. Another method, in which the simultaneously detection of *Theileria* and *Babesia spp.* at genus and species level was previously described, was based on the species-specific probes linked to the sufficient membrane for detecting biotin marked PCR products by streptavidin-peroxidase in chemoluminescence (Gubbels et al, 1999; Ranjbar-Bahadori et al, 2012). This method is much expensive and time intensive and can be performed in special studies. For routine diagnosis, the mentioned method in the present study is recommended. Furthermore, since the introduced VetUTPiro-primers can amplify simultaneously the genomic DNA from parasite as well as host, the results achieved by PCR can be used for semi-quantitative multiplex analysis. This possibility can be useful for therapy management and additionally the mentioned method can be used for determination of the efficacy of the drugs. Interestingly, the above mentioned VetUTPiro-primers can also amplify simultaneously the genomic DNA generated from *Plasmodium falciparum, Plasmodium vivax, Plasmodium ovale, Plasmodium malariae* and *Toxoplasma gondii*. Data search in GenBank showed that for some small subunit of rRNA gene generate the mentioned primers 157 bp (accession no. U03070.1), whereas for some others 86 bp (accession no. PQ894615). We believe that the reason of this difference of 71 bp should be answered. Moreover, the genomic DNA derived from genomic DNA of other hemoparasites like *Trypanosoma spp* and *Neospora caninum* cannot be amplified. Since in the subtropical or tropical area, the obligate intracellular parasites can occur simultaneously, so the use of the primers can be performed for broad spectrum of parasite infection.

Acknowledgments

We thank the Research Institute Molecular Biological System Transfer for the financial and technical support. We also thank the Research Council of Faculty of Veterinary Medicine, University of Tehran.

Conflict of Interests

The authors declare no conflict of interest.

Funding

This study received financial support from University of Tehran.

References

Abdallah, M. O., Niu, Q., Yang, J., Hassan, M. A., Yu, P., Guan, G., ... & Yin, H. (2017). Identification of 12 piroplasms infecting ten tick species in China using reverse line blot hybridization. *The Journal of Parasitology*, *103*(3), 221-227.

El-Ashker, M., Hotzel, H., Gwida, M., El-Beskawy, M., Silaghi, C., & Tomaso, H. (2015). Molecular biological identification of Babesia, Theileria, and Anaplasma species in cattle in Egypt using PCR assays, gene sequence analysis and a novel DNA microarray. *Veterinary parasitology*, *207*(3-4), 329-334.

Estrada-Peña, A., Mihalca, A. D., & Petney, T. N. (Eds.). (2018). *Ticks of Europe and North Africa: a guide to species identification*. Springer.

Gubbels, J. M., De Vos, A. P., Van der Weide, M., Viseras, J., Schouls, L. M., De Vries, E., & Jongejan, F. (1999). Simultaneous detection of bovine Theileria and Babesia species by reverse line blot hybridization. *Journal of clinical microbiology*, *37*(6), 1782-1789.

Hussain, S., Hussain, A., Aziz, M. U., Song, B., Zeb, J., Moutailler, S., ... & Sparagano, O. (2024). Exploring the Coinfection and Genetic Diversity of Multiple Tick-Borne Pathogens in Livestock Population of Punjab, Pakistan. *Transboundary and emerging diseases*, *2024*(1), 9958535.

Jaffer, O., Abdishakur, F., Hakimuddin, F., Riya, A., Wernery, U., & Schuster, R. K. (2010). A comparative study of serological tests and PCR for the diagnosis of equine piroplasmosis. *Parasitology Research*, *106*(3), 709-713.

Jongejan, F., Du, C., Papadopoulos, E., Blanda, V., Di Bella, S., Cannella, V., ... & Wang, X. (2024). Diagnostic performance of a rapid immunochromatographic test for the simultaneous detection of antibodies to Theileria equi and Babesia caballi in horses and donkeys. *Parasites & vectors*, *17*(1), 160.

Jouglin, M., Bonsergent, C., de La Cotte, N., Mege, M., Bizon, C., Courouce, A., ... & Malandrin, L. (2025). Equine piroplasmosis in different geographical areas in France: Prevalence heterogeneity of asymptomatic carriers and low genetic diversity of Theileria equi and Babesia caballi. *Ticks and Tick-borne Diseases*, *16*(1), 102434.

Malekifard, F., Tavassoli, M., Yakhchali, M., & Darvishzadeh, R. (2014). Detection of Theileria equi and Babesia caballi using microscopic and molecular methods in horses in suburb of Urmia, Iran. In *Veterinary research forum: an international quarterly journal*, *5*(2), 129.

Mendoza, F. J., Pérez-Écija, A., Kappmeyer, L. S., Suarez, C. E., & Bastos, R. G. (2024). New insights in the diagnosis and treatment of equine piroplasmosis: pitfalls, idiosyncrasies, and myths. *Frontiers in Veterinary Science*, *11*, 1459989.

Modirrousta, H., Habibi, G., Shayan, P., Afshari, A., Mirjalili, A., & Abdigoudarzi, M. (2019). Determination of the Infectivity of Cryopreserved Theileria annulata Sporozoites in Tick Derived Stabilates Iran Ak-93 Strain, by in vivo and in vitro Methods. *Iranian Journal of Parasitology*, *14*(4), 572.

Onyiche, T. E., Suganuma, K., Igarashi, I., Yokoyama, N., Xuan, X., & Thekisoe, O. (2019). A review on equine piroplasmosis: epidemiology, vector ecology, risk factors, host immunity, diagnosis and control. *International journal of environmental research and public health*, *16*(10), 1736.

Onyiche, T. E., Taioe, M. O., Molefe, N. I., Biu, A. A., Luka, J., Omeh, I. J., ... & Thekisoe, O. (2020). Equine piroplasmosis: An insight into global exposure of equids from 1990 to 2019 by systematic review and meta-analysis. *Parasitology*, *147*(13), 1411-1424

Ranjbar-Bahadori, S., Eckert, B., Omidian, Z., Shirazi, N. S., & Shayan, P. (2012). Babesia ovis as the main causative agent of sheep babesiosis in Iran. *Parasitology Research*, *110*(4), 1531-1536.

Riaz, M., Nasreen, N., Khan, A., & Said, M. B. (2023). Differential diagnosis of theileriosis through blood smear examination and polymerase chain reaction in small ruminants from Pakistan. *Open Veterinary Journal*, *13*(6), 697-704.

Rosenblatt, J. E., Reller, L. B., & Weinstein, M. P. (2009). Laboratory diagnosis of infections due to blood and tissue parasites. *Clinical infectious diseases*, *49*(7), 1103-1108.

Shayan, P., & Rahbari, S. (2005). Simultaneous differentiation between Theileria spp. and Babesia spp. on stained blood smear using PCR. *Parasitology Research*, *97*(4), 281-286.

Shayan, P., Hooshmand, E., Rahbari, S., & Nabian, S. (2007). Determination of Rhipicephalus spp. as vectors for Babesia ovis in Iran. *Parasitology research*, *101*(4), 1029-1033.

Tian, Z., Du, J., Yang, J., Liu, A., Liu, X., Liu, G., & Yin, H. (2015). A PCR-RFLP Assay targeting RPS8 gene for the discrimination between bovine Babesia and Theileria species in China. *Parasites & Vectors*, *8*(1), 475.

Tirosh-Levy, S., Gottlieb, Y., Fry, L. M., Knowles, D. P., & Steinman, A. (2020). Twenty years of equine piroplasmosis research: Global distribution, molecular diagnosis, and phylogeny. *Pathogens*, *9*(11), 926.

Walker, A. R. (2003). *Ticks of domestic animals in Africa: a guide to identification of species* (Vol. 74). Edinburgh: Bioscience Reports.

Received: 15.12.2025
Accepted: 20.05.2026

Vol. 22, No. 2, Summer, 2026, 25-32 *Original Article*
DOI: 10.22055/ivj.2025.556919.2864
Journal Homepage: http://www.ivj.ir/

Histological and Ultrastructural Identification of Telocytes in Canine Uterine Tissue

Hadis Amirian[1], Tayebeh Mohammadi[2*] and Mehrdad Pooyanmehr[2]

[1] DVM Graduated, Faculty of Veterinary Medicine, Razi University, Kermanshah, Iran
[2] Assistant Professor, Department of Basic Sciences and Pathobiology, Faculty of Veterinary Medicine, Razi University, Kermanshah, Iran

Received: 02.11.2025 Accepted: 14.12.2025

Abstract

Telocytes, characterized by slender cell bodies and elongated cytoplasmic processes known as telopodes, are distinct interstitial cells identified in various mammalian organs, including the heart, lung, fallopian tube, and kidney. This study investigated the presence, morphology and ultrastructure of telocytes in the uterine tissue of the dog. Samples from the uterine horn of adult Spitz dogs were collected and processed for histological, histochemical, and transmission electron microscopic examinations. Under light microscopy, telocytes were observed as elongated cells possessing a slender nucleus and numerous thin cytoplasmic processes extending from the cell body. They were in proximity to secretory units of uterine glands, blood vessels, collagen bundles of the connective tissue, and, smooth muscle cells throughout all layers of the uterine wall. The complete morphology of telocytes and telopodes, including their close associations with glandular, smooth muscle, and endothelial cells, as well as collagen fibers, was clearly visualized by transmission electron microscopy. Collectively, the findings of this study provide the first evidence of telocyte presence in the canine uterus and describe their morphology.

Key words: Telocyte, Uterus, Dog, Histology, Cell structure

Introduction

Telocytes are mesenchymal-derived cells characterized by their exceptionally long and thin cellular processes. They are distinct from neurons, fibroblasts, and smooth muscle cells, yet they possess the remarkable ability to interact with all these cell types. Telocytes are consistently found in close proximity to nerve endings, smooth muscle cells, blood vessels, and other interstitial cells (Awad and Ghanem, 2018; Dolbnya et al, 2025).

Despite their identification in numerous tissues, a universally accepted consensus on the defining characteristics of telocytes remains elusive. Their morphology and protein composition exhibit considerable variability across different tissues, which can pose challenges for their precise immunohistochemical identification (Cretoiu, 2016; Hanan et al, 2025).

Telocytes engage in intricate interactions with various cell types, playing a pivotal role in regulating tissue functions through intercellular communication, immune response modulation, and the maintenance of homeostasis (Creţoiu, et al, 2012; Kondo and Kaestner, 2019). Serving as master regulators, telocytes maintain tissue homeostasis and guide stem cells toward proliferation and differentiation, thereby

* **Corresponding Author**: Tayebeh Mohammadi, Assistant Professor, Department of Basic Sciences and Pathobiology, Faculty of Veterinary Medicine, Razi University, Kermanshah, Iran
E-mail: tymhd@razi.ac.ir

facilitating tissue repair (Popescu and Faussone-Pellegrini, 2010; Shoshkes-Carmel, et al, 2018). Furthermore, these cells actively modulate the immune response by providing essential information that enables the immune system to efficiently combat pathogens (Aleksandrovych et al, 2022; Sanches et al, 2024).

As specialized cells dispersed throughout uterine tissue, telocytes are subject to changes in response to the extensive hormonal fluctuations that occur during the estrous cycle and pregnancy. Numerous studies have investigated these changes in telocytes across various reproductive stages to better understand their role in regulating uterine function (Salama, 2013). Telocytes appear to interact with virtually all cell types within an organ. This arrangement suggests a vast array of potential integrative and regulatory roles, akin to a rudimentary yet crucial neuronal network at the cellular level, implying a surveillance function (Smythies and Edelstein, 2014). Given the significant role of telocytes in tissue repair and regeneration, a comprehensive understanding of their function in organ regeneration will soon become a major challenge, ultimately leading to potential advancements in clinical applications (Bei, et al, 2015).

The study of telocytes not only enhances our understanding of the physiology of various tissues but can also lead to the discovery of novel therapeutic approaches. Identifying telocytes in different body tissues and examining their functions can significantly improve our comprehension of diseases and facilitate the development of new treatments, particularly in the context of uterine pathologies (Kondo and Kaestner, 2019). To the best of our knowledge, no existing studies have examined the presence, structural and ultrastructural characteristics of telocytes within canine uterine tissue. Additionally, research on uterine tissue in other animal species is quite limited. Therefore, this study was conducted with the aim of identifying telocytes in canine uterine tissue, describing their structural and ultrastructural characteristics within the canine uterus.

Materials and Methods

Light Microscopy

Uteri from three adult female Spitz dogs, of defined and homogeneous mean age, were immediately removed following ovariohysterectomy at a small animal clinic. The owners of the dogs provided informed consent for this procedure. The uterine horns were divided into three parts, and the middle portion was further subdivided into smaller pieces. Uterine samples (5 mm × 5 mm) were immersed in 10% buffered formalin for histological and histochemical studies. The samples were then processed using standard histological techniques for light microscopic examination. After fixation and washing, tissues were dehydrated, cleared, and embedded in paraffin wax using an automated processor. Subsequently, thin (5 um) and semi-thin (1 um) sections were cut from the paraffin blocks and stained with hematoxylin-eosin (HandE), periodic acid-Schiff (PAS), Giemsa, Masson's trichrome (MT), methylene blue (MB), and toluidine blue (TB) (Bancroft and Gamble, 2008). The sections were observed under light microscope (Olympus CX23, Japan) and images were captured using a digital camera (KEView, China).

Transmission Electron Microscopy (TEM)

A 1 mm^3 piece from the mid-section of the uterine horn was excised and fixed in 2.5% glutaraldehyde in phosphate buffer (pH 7.4, 0.1 M) for 48 hours. The samples were then post-fixed in 1% osmium tetroxide for one hour and subsequently dehydrated in ascending concentrations of ethanol (50%, 70%, 90%, and 100%). Finally, the samples were embedded in Epon resin. Semi-thin sections (0.5–1 µm) were prepared from the resulting blocks and

stained with toluidine blue. A light microscope was used to select the area of interest. In the next step, ultrathin sections (60 nm) were obtained and stained with saturated uranyl acetate and lead citrate. The sections were examined using a Philips CM10 transmission electron microscope (Eindhoven, The Netherlands) at an accelerating voltage of 80 kV in Aria Rastak company TEM laboratory (Tehran, Iran).

Results

Histological Study

Based on HandE and MT staining results, the canine uterine tissue, when viewed in cross-section, exhibited three distinct layers. The innermost layer, the endometrium, comprised a single layer of columnar cells lining a thick bed of connective tissue. Embedded within this connective tissue were uterine glands. The middle layer, the myometrium, displayed a dual muscular arrangement with an inner circular layer and an outer longitudinal layer. Sandwiched between these muscular layers was a layer rich in blood vessels. The outermost layer, the perimetrium, comprised a thin layer of loose connective tissue (Figure 1).

Light microscopic examination of uterine tissue sections stained with Giemsa, MT, and PAS unveiled small, elongated cells within the uterine wall. These cells, possessing spindle or oval-shaped nuclei, were characterized by the presence of two prominent, thread-like extensions at each end. Their distribution was notable, with a predilection for locations surrounding endometrial glands, blood vessels, and within the interstitial spaces between stromal and smooth muscle cells. These morphological features led to the identification of these cells as telocytes. A distinguishing characteristic of telocytes is their limited cytoplasmic volume, which tapers into the aforementioned thread-like extensions, aptly termed telopodes (Figures 2 and 3).

Semi-thin sections of the uterus stained with TB and MB clearly demonstrated the typical characteristics of these cells, including an elongated oval body and long, thin cytoplasmic processes. These cells were particularly abundant around endometrial glands and blood vessels. Within the myometrium, small cell bodies with distinct telopodes were observed interspersed among smooth muscle cells (Figure 4).

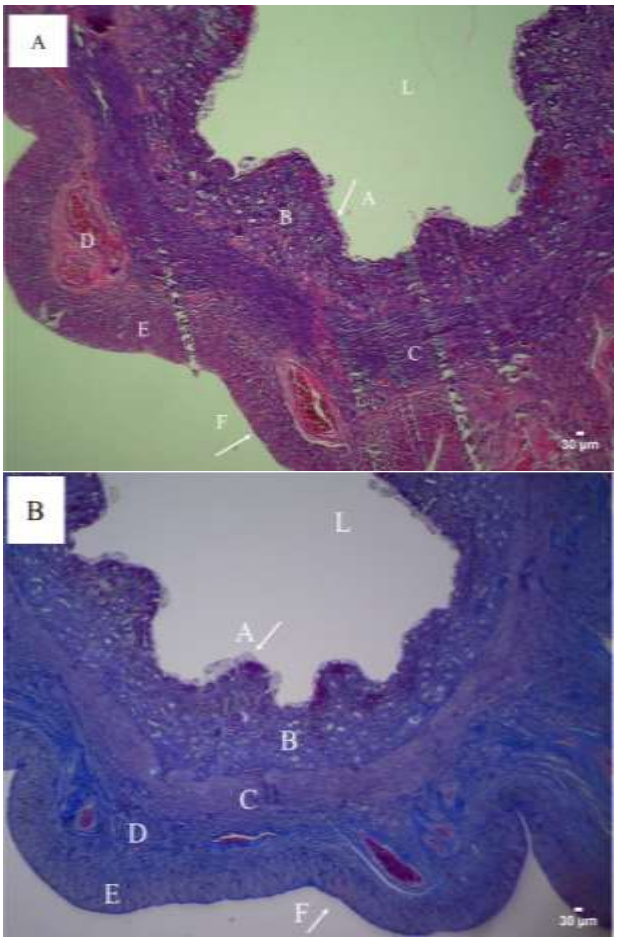

Figure 1: Cross section of uterine tissue representatives general histology of the Spitz's uterus; Uterine lumen (L), Endometrial epithelium (A), Endometrial propria-submucosa connective tissue (B), Myometrium inner muscle layer(C), Vascular layer(D), Myometrium outer muscle layer (E), Epimetrium(F), (**A**: **HE staining, and B: MT staining).**

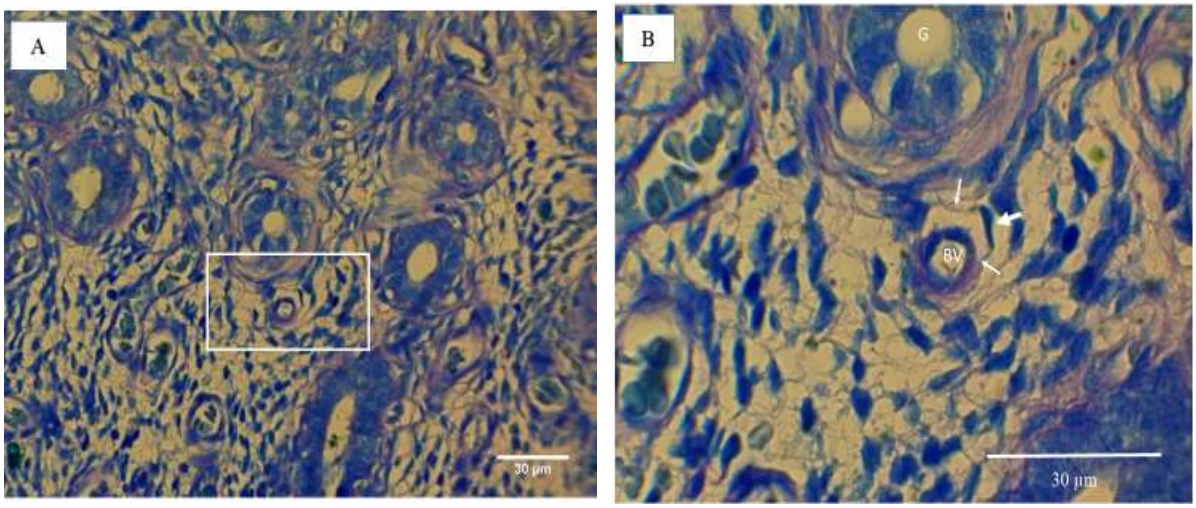

Figure 2: Light micrographs of the endometrium, (A) representatives photomicrograph of Geimsa -stained endometial tissue sections, (B) representatives a higher magnification of the box area in (A) to indicate telocyte with a large nucleus and very small cytoplasm (thick arrow) and telopodes as moniliform cytoplasmic processes (thin arrows). Telocyte are particularly in the vicinity of blood vessels (BV) and endometrial glands (G).

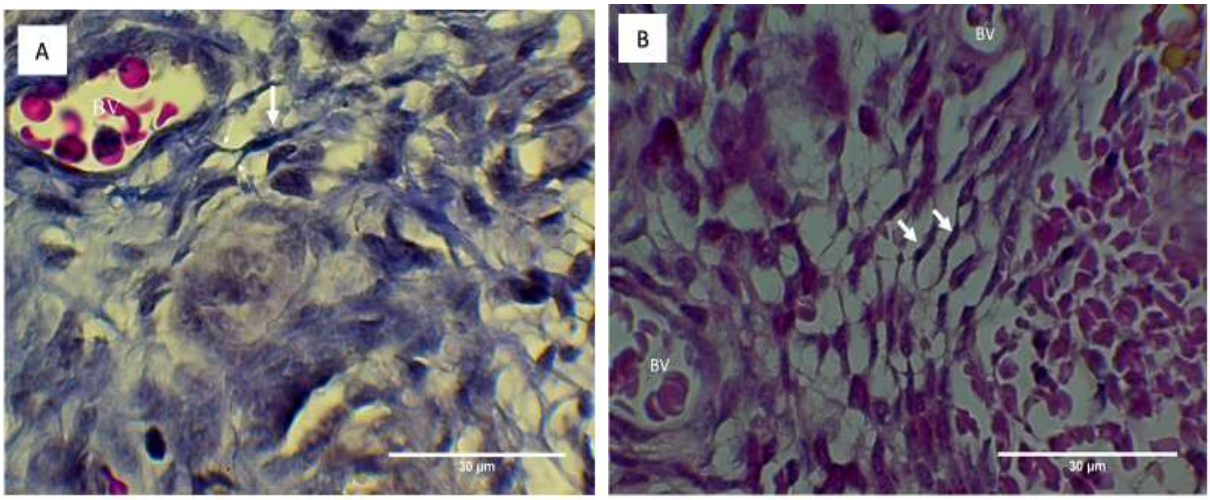

Figure 3: Light micrographs of the endometrium representatives photomicrograph of MT (A) and PAS (B)-stained endometial tissue sections to indicate telocyte with a large nucleus and very small cytoplasm (thick arrows) and telopodes as moniliform cytoplasmic processes (thin arrows).

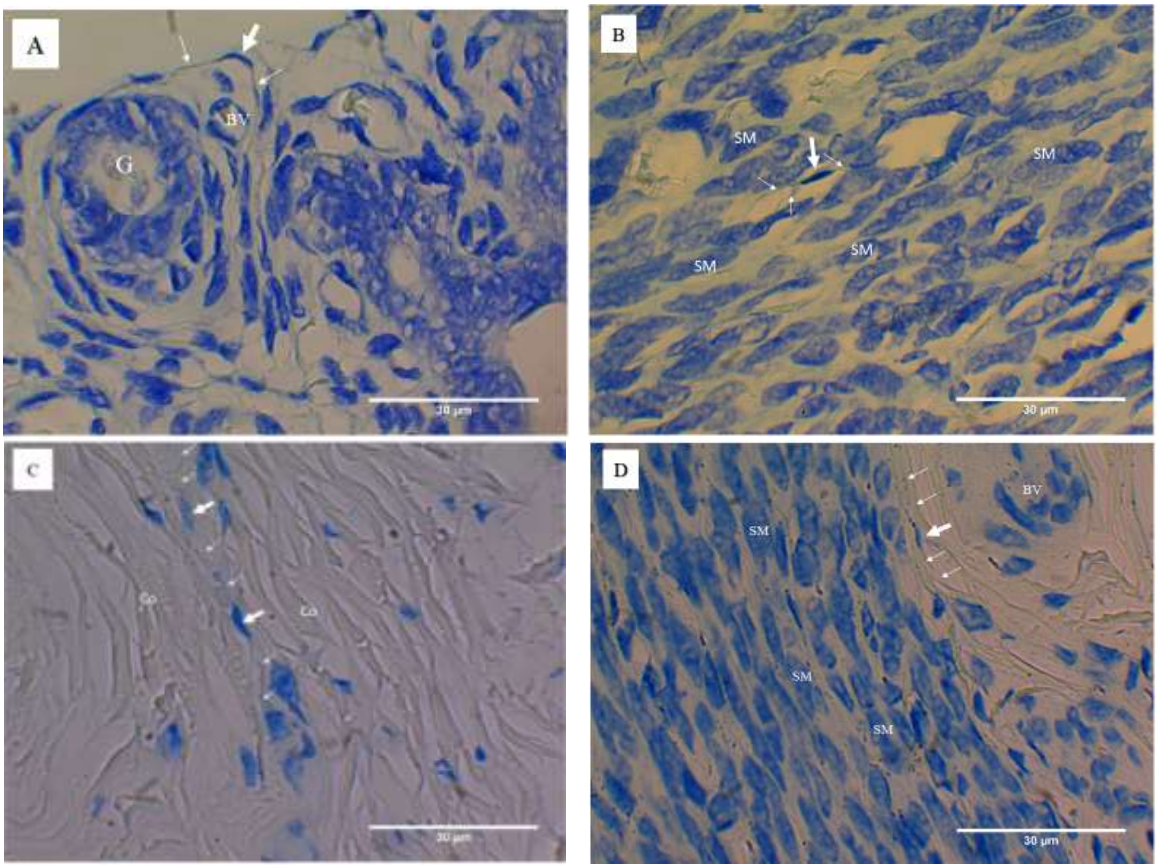

Figure 4: Light micrographs of the endometrium representatives photomicrograph of TB and MB-stained endometial tissue semi thin sections to indicate telocyte with a large nucleus and very small cytoplasm (thick arrows) and telopodes as moniliform cytoplasmic processes (thin arrows). (A), (B), (C): (TB staining) and (D): (MB staining). Telocytes are particularly in the vicinity of blood vessels (BV) and endometrial glands (G). SM shows smooth muscle cells and Co shows collagen fibers.

Telocyte Ultrastructure (Transmission Electron Microscopy)

Transmission electron microscopy images of canine uterine tissue in this study revealed that telocytes exhibited a small, spindle-shaped or pyramidal cell body surrounded by a scant amount of cytoplasm. Notably, they were smaller than their neighboring cells. Several extremely long cytoplasmic processes (telopodes) extended from the cell body as thin cytoplasmic protrusions. A basal lamina was not observed in telocytes. Exosomes were found in the vicinity of the telopodes; specifically, exosomes detached from the telopodes were also observed. The cell body contained a centrally located nucleus, organelles such as mitochondria and rough endoplasmic reticulum, polyribosome aggregates or glycogen granules, and other electron-dense bodies. Telocytes were identified in the paracrine region surrounding endometrial glands and in the myometrium. Telocytes were often found between collagen fibers and were in close contact with them. A close association between telopodes and longitudinal and transverse sections of collagen fibers was observed along their course. Telopodes were in very close proximity to each other and were in close contact with neighboring cells. The nucleus of telocytes was indented and conformed to the general outline of the cell body. Electron-dense heterochromatin masses were observed attached to the nuclear membrane (Figure 5).

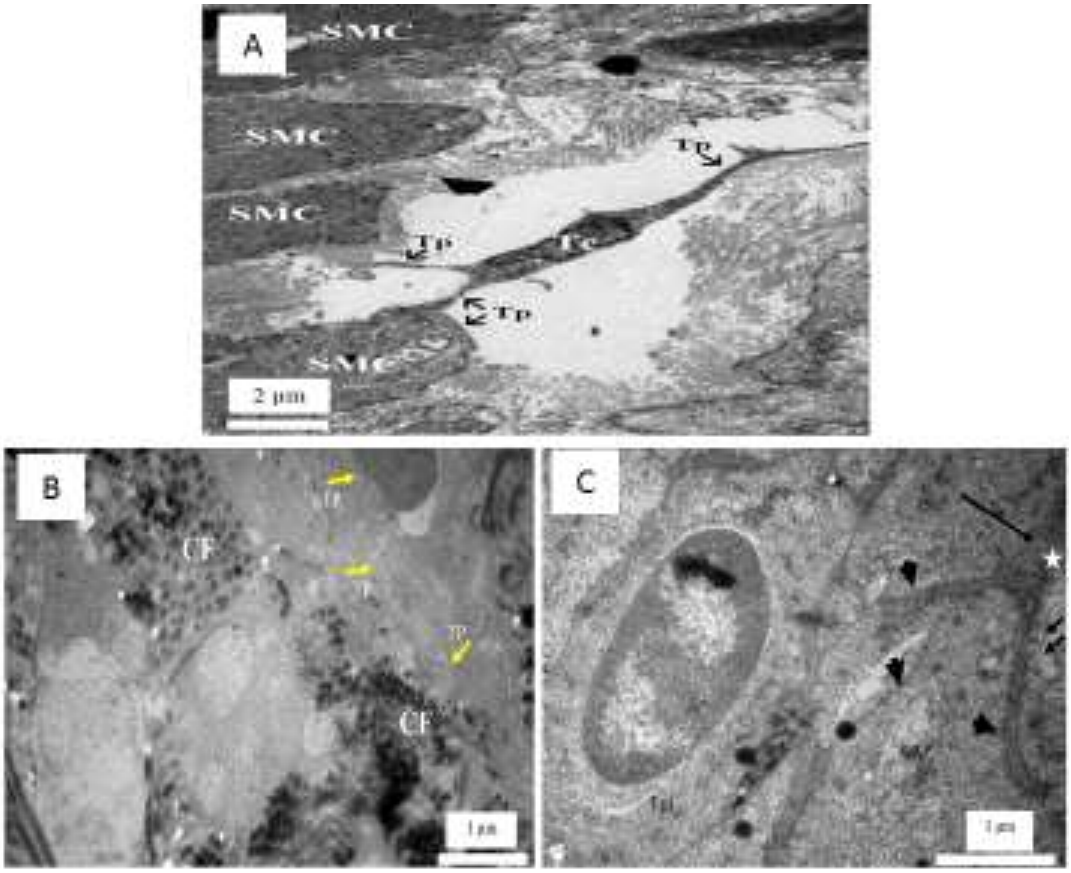

Figure 5: TEM micrograph of uterine tissue, (A) A telocyte (TC) is situated adjacent to a smooth muscle cell (SMC). The telocyte's telopodes (TP) extend to make close contact with the SMC. (B) shows telopodes (TP) as long, thin processes in contact with the cross-section of collagen fibrils (CF), (C) A telocyte is shown, with its cell body indicated by a long arrow. Three slender telopodes (arrowheads) extend from the cell body, one of which contacts a neighboring cell. Short arrows highlight exosomes budding from a telopode. The telocyte nucleus is marked with an asterisk, and a blood capillary (Cap) is also visible.

Discussion

This study investigated the morphology and distribution of telocytes in the uterus of the Spitz dog, providing detailed information on their light and electron microscopic features and their distribution within the organ. Using light microscopy and various staining techniques, we identified telocytes as long, thread-like cells with a small, spindle-shaped cell body containing a nucleus. These cells possess very long, thin processes, termed telopodes, which form an extensive network-like structure in the endometrial connective tissue and the vascular layer of the uterus. They were also present, albeit in smaller numbers, among the smooth muscle cells of the myometrium. Telocytes frequently formed close associations with capillaries, nerve endings, and immune cells. Similar to telocytes found in other tubular organs in mammals, telocytes in the canine uterus exhibited a strong affinity for PAS staining. Since this staining highlights neutral polysaccharides, this indicates the presence of this carbohydrate group within these cells (Soliman, 2021). Additionally, telocytes in semi-thin sections of uterine tissue demonstrated a strong affinity for MB and TB staining techniques, which target cellular proteins, including cytoskeletal proteins (Zheng et al, 2014).

Semi-thin sections of tissue specimens stained with TB and MB are generally useful for determining the overall distribution of telocytes within a tissue. The observation of a small cell body with a few

thin cytoplasmic processes is often considered sufficient for defining a telocyte. However, the most accurate method for identifying telocytes remains transmission electron microscopy (TEM) (Etcharren et al, 2023).

Despite limitations in accessing samples preserved in epoxy resin, which hindered a comprehensive electron microscopic analysis of all telocytes within the entire uterine wall, we successfully confirmed their presence. We employed ultrastructural criteria specific to telocytes for this confirmation. Our observations revealed that uterine telocytes exhibit a distinctive ultrastructure characterized by a prominent nucleus occupying a significant portion of the cell, while the cytoplasm remains relatively limited. Long, slender, and intricately branched cytoplasmic extensions, known as telopodes, extended abruptly from the cell body. Electron micrographs further demonstrated close interactions between these telopodes and surrounding structures, including collagen fibers, glandular epithelial cells, and smooth muscle cells. While the sample size in this study restricted a thorough examination of all uterine wall regions, we conclusively identified cells possessing the characteristic structural features of telocytes within a subset of the analyzed tissue. In the present study, telocytes were more frequently observed in the endometrium and vascular layer, which is consistent with the findings of Hatta and colleagues (2012) who hypothesized that telocytes are often found in tissues with low cell density and significant space between neighboring cells (Hatta et al, 2012). As previously reported for telocytes in the human exocrine pancreas, parotid gland, and sublingual salivary glands, we observed, in this study, that telocytes surrounded the secretory units of the uterine glands. This finding may indicate their involvement in regulating glandular function along with the adjacent myoepithelial cells in the walls of the secretory units (Nicolescu et al, 2011; Nicolescu et al, 2012; Alunno et al, 2015). Research on the distribution of telocytes in the uterine myometrium is likely to have practical or clinical value. The various functions of uterine telocytes, such as the coordination of myometrial contractility, have been discussed (Hutchings et al, 2006).

Based on histological, histochemical, and ultrastructural features, telocytes were definitively present in the canine uterine tissue. Although ultrastructural characteristics provide the most reliable method for identifying telocytes, by conducting more extensive research, especially immunohistochemical analyses, and performing in-depth ultrastructural studies of cells in various regions of the uterine wall, we can expect to gain a more comprehensive understanding of the distribution, potential roles of telocytes, and their intricate interactions within the uterine tissue of dog.

Acknowledgments

We sincerely appreciate and acknowledge the valuable assistance and support of all individuals who contributed in any way to the successful completion of this research.

Conflict of Interest

The authors declare that they have no conflict of interest.

Funding

This research received no specific grant from any funding agency in the public, commercial, or not-for-profit sectors.

References

Abd-Elhafeez, H. H., Abou-Elhamd, A. S., Ismail, H., Abdel-Raheem, S. M., Meligy, A. M. A., and Soha, A. (2025). Perichondral telocytes and their role in cartilage development and regeneration: Insights from histochemistry, immunohistochemistry, and TEM. *Research in Veterinary Science, 193*, 105780.

Aleksandrovych, V., Bereza, T., Ulatowska-Białas, M., Pasternak, A., Walocha, J. A., Pityński, K., and Gil, K. (2022). Identification of PDGFRα+ cells in uterine fibroids–link between angiogenesis and uterine telocytes. *Archives of Medical Science, 18*(5), 1329–1339.

Alunno, A., Ibba-Manneschi, L., Bistoni, O., Rosa, I., Caterbi, S., Gerli, R., and Manetti, M. (2015). Telocytes in minor salivary glands of primary Sjögren's syndrome: Association with the extent of inflammation and ectopic lymphoid neogenesis. *Journal of Cellular and Molecular Medicine, 19*(7), 1689–1696.

Awad, M., and Ghanem, M. E. (2018). Localization of telocytes in rabbit testis: Histological and immunohistochemical approach. *Microscopy Research and Technique, 81*(11), 1268–1274.

Bancroft, J. D., and Gamble, M. (Eds.). (2008). *Theory and practice of histological techniques*. Elsevier, 126-135.

Bei, Y., Zhou, Q., Fu, S., Lv, D., Chen, P., Chen, Y., and Xiao, J. (2015). Cardiac telocytes and fibroblasts in primary culture: Different morphologies and immunophenotypes. *PLoS ONE, 10*(2), e0115991.

Dolbnya, A., Ivanova, V., and Serebryakova, O. (2025). Telocytes: History, origin, identification, structure, distribution, and functions. *Histochemistry and Cell Biology, 163*, 86.

Etcharren, V., Mouguelar, H., and Aguilar Valenciano, J. J. (2023). Identification of telocytes in the oviduct of the mare. *Theriogenology, 205*, 18–26.

Hatta, K., Huang, M. L., Weisel, R. D., and Li, R. K. (2012). Culture of rat endometrial telocytes. *Journal of Cellular and Molecular Medicine, 16*(7), 1392–1396.

Hutchings, G., Williams, O., Cretoiu, D., and Ciontea, S. M. (2009). Myometrial interstitial cells and the coordination of myometrial contractility. *Journal of Cellular and Molecular Medicine, 13*(10), 4268–4282.

Kondo, A., and Kaestner, K. H. (2019). Emerging diverse roles of telocytes. *Development, 146*(14), 1-9.

Nicolescu, M. I., and Popescu, L. M. (2012). Telocytes in the interstitium of human exocrine pancreas: Ultrastructural evidence. *Pancreas, 41*(6), 949–956.

Nicolescu, M. I., Bucur, A., Dinca, O., Rusu, M. C., and Popescu, L. M. (2012). Telocytes in parotid glands. *The Anatomical Record: Advances in Integrative Anatomy and Evolutionary Biology, 295*(3), 378–385.

Popescu, L. M., Ciontea, S. M., and Cretoiu, D. (2007). Interstitial Cajal-like cells in human uterus and fallopian tube. *Annals of the New York Academy of Sciences, 1101*(1), 139–165.

Salama, N. M. (2013). Immunohistochemical characterization of telocytes in rat uterus in ﻑdifferent reproductive states. *Egyptian Journal of Histology, 36*(1), 185–194.

Sanches, B. D. A., Rocha, L. C., Neto, J. P., Beguelini, M. R., Ciena, A. P., and Carvalho, H. F. (2024). Telocytes of the male reproductive system: Dynamic tissue organizers. *Frontiers in Cell and Developmental Biology, 12*, 1444156.

Shoshkes-Carmel, M., Wang, Y. J., Wangensteen, K. J., Tóth, B., Kondo, A., Massasa, E. E., and Kaestner, K. H. (2018). Author correction: Subepithelial telocytes are an important source of Wnts that supports intestinal crypts. *Nature, 560*(7718), E29.

Smythies, J., and Edelstein, L. (2014). Telocytes, exosomes, gap junctions and the cytoskeleton: The makings of a primitive nervous system? *Frontiers in Cellular Neuroscience, 7*, 278.

Soliman, S. A. (2021). Telocytes are major constituents of the angiogenic apparatus. *Scientific Reports, 11*, 5775.

Zheng, Y., Cretoiu, D., Yan, G., Cretoiu, S. M., Popescu, L. M., and Wang, X. (2014). Comparative proteomic analysis of human lung telocytes with fibroblasts. *Journal of Cellular and Molecular Medicine, 18*(4), 568–589.

Received: 02.11.2025
Accepted: 14.12.2025

Vol. 22, No. 2, Summer, 2026, 33-46
DOI: 10.22055/ivj.2026.556170.2862
Journal Homepage: http://www.ivj.ir/

Original Article

Dimethyl itaconate attenuates ovarian histological changes and apoptosis, and improves sex hormone production in doxorubicin-treated 4T1 breast cancer mice

Azam Asad-Saftjani[1], Shima Hosseinifar[2*] and Mohammad Reza Tabandeh[3]

[1] PhD Student of Histology, Faculty of Veterinary Medicine, Shahid Chamran University of Ahvaz, Ahvaz, Iran
[2] Associate Professor, Department of Basic Sciences, Faculty of Veterinary Medicine, Shahid Chamran University of Ahvaz, Ahvaz, Iran
[3] Professor, Department of Basic Sciences, Faculty of Veterinary Medicine, Shahid Chamran University of Ahvaz, Ahvaz, Iran and Professor, Stem Cells and Transgenic Technology Research Center, Shahid Chamran University of Ahvaz, Ahvaz, Iran

Received: 29.10.2025 Accepted: 16.02.2026

Abstract

Ovarian toxicity induced by Doxorubicin (DOX) is a common side effect treatment in breast cancer, leading to apoptosis, impaired folliculogenesis and reduced ovarian steroid hormone levels. Dimethyl itaconate (DMI) is an immunometabolite with anti-inflammatory and antioxidant properties that could play a protective role, although data are limited. This study evaluated the potential protective effects of DMI on ovarian histology, apoptosis, and ovarian hormone production in a 4T1 breast cancer mouse model treated with DOX. In this study, 30 adult female BALB/c mice were randomly divided into five groups: healthy control, cancer control (cancer induction by injection of 4T1 cells), cancer - DMI (50 mg/kg; daily; IP, 28 days), cancer - DOX (5 mg/kg; once a week; IP, 4 weeks) and DMI + DOX cancer. Serum estrogen and progesterone levels, ovarian apoptotic gene expression (Bax and Bcl2), and histological changes were evaluated. Statistical analysis was performed by GraphPad Prism software (10) and data were presented as mean ± standard deviation. DOX significantly decreased estradiol (E2; 37.23 ± 4.43 pg/ml) and progesterone (P4; 3.4 ± 0.2 ng/ml) levels, reduced Bcl2 (0.31 ± 0.1) expression and increased Bax expression (4.04 ± 0.39) in ovarian tissue compared to cancer control group (54.10 ± 2.8 pg/ml, 5.1 ± 0.2 ng/ml; 0.72 ± 0.09; 1.81 ± 0.35, respectively). Co-treatment with DMI and DOX led to a significant decrease in Bax expression (2.59 ± 0.45) and a significant increase in Bcl-2 (0.61 ± 0.03) expression compared to the only DOX treated cancer group. DOX caused notable ovarian damage, including increased follicular atresia, reduced follicle size, and absence of corpus luteum. DMI treatment mitigated these effects by preserving ovarian architecture, thinning the surface epithelium, and normalizing hormone levels and expression of apoptosis-related genes. Co-administration of DMI and DOX was particularly effective in reducing DOX-induced histological damage. These findings suggest that DMI may serve as a potential protective compound for reducing DOX-induced ovarian toxicity during chemotherapy.

Key words: Dimethyl Itaconate, Doxorubicin, Ovarian histology, Apoptosis, Breast cancer

Introduction

Breast cancer is one of the most common malignancies among women, and with advancements in therapeutic strategies, patient survival rates have significantly improved. One major challenge in this context is the occurrence of premature ovarian failure (POF), resulting from chemotherapy-induced gonadotoxicity; a

[*] **Corresponding Author**: Shima Hosseinifar, Associate Professor, Department of Basic Sciences, Faculty of Veterinary Medicine, Shahid Chamran University of Ahvaz, Ahvaz, Iran
E-mail: sh.hosseinifar@suc.ac.ir

process that impairs folliculogenesis and depletes the ovarian reserve (Yildiz et al, 2023). Among chemotherapeutic agents, doxorubicin (DOX) is widely used in the treatment of breast cancer. However, its high toxicity to healthy tissues, especially the ovaries, remains a significant concern (Bedoschi et al, 2016). DOX induces oxidative stress, DNA damage, lipid peroxidation, calcium imbalance, and activation of p53-dependent pathways, ultimately leading to apoptosis (Bedoschi et al, 2016; Nguyen et al, 2025; Markowska et al, 2024; Guo et al, 2021; Rad et al, 2021). DOX also damages granulosa cells, promotes follicular atresia, triggers premature activation of primordial follicles, and disrupts the hypothalamic–pituitary–gonadal axis by reducing levels of estradiol, progesterone, FSH, and LH hormones (Markowska et al, 2024; Rad et al, 2021). Doxorubicin treatment induces apoptosis in ovarian tissue by upregulating pro-apoptotic gene Bax and downregulating the anti-apoptotic gene Bcl-2, leading to follicular cell death, ovarian dysfunction and impaired steroidogenesis (Cai et al, 2019; Saleh et al, 2020; Zhang et al, 2017). DOX induces significant histopathological alterations in the ovary including follicular atresia, which is characterized with a marked reduction in the number of primordial and secondary follicles (Gao et al, 2023, Nishi et al, 2018). DOX therapy induces vascular damage and fibrosis of the ovarian stroma, resulting in the onset of premature ovarian failure (POF) (Soleimani et al, 2011).

Given the toxic effects of DOX on the ovaries, there is increasing interest in identifying protective agents that can mitigate chemotherapy-induced gonadotoxicity. Itaconate, an immunometabolite produced by macrophages through ACOD1 enzyme activation in response to inflammatory stimuli such as LPS, has demonstrated anti-inflammatory and antioxidant properties in various pathological conditions (Hosseinkhani et al, 2024; Khadem et al, 2022; Azari et al, 2024). Dimethyl itaconate (DMI) and 4-octyl itaconate (4-OI) are the most studied cell permeable derivatives of itaconic acid. These derivatives exert anti-inflammatory effects primarily through activation of the Nrf2 pathway and inhibition of the Keap1–Nrf2 complex (Ferreira et al, 2023). They also suppress key pro-inflammatory pathways, including NF-κB and NLRP3 inflammasome activation (Azari et al, 2024). In addition, they reduce reactive oxygen species (ROS) production and upregulate antioxidant enzymes such as HO-1 and NQO1. By modulating cellular metabolism and enhancing immunity, itaconate derivatives help maintain redox balance and protect against inflammation-induced tissue damage (Zhan et al, 2022). Limited data are available regarding the role of itaconic acid in regulating ovarian function. Recently, it was found that in bovine granulosa cells, DMI suppresses LPS-induced inflammation by downregulating NLRP3 and TLR4 pathways and inhibiting NF-κB and JNK signaling pathways, thereby reducing the expression of pro-inflammatory cytokines (Tabandeh et al, 2022). It has been also reported that DMI alleviates ovarian dysfunction in a rat model of PCOS by reducing oxidative stress, inflammation, and insulin resistance. Recently, He et al, (2023) showed that growth hormone co-treatment in women with diminished ovarian reserve significantly altered follicular fluid metabolism. Notably, itaconic acid was elevated alongside glutathione, and its levels positively correlated with the number of oocytes retrieved. Recent evidence showed that DMI has protecting role against chemotherapy-induced toxicity in non-reproductive organs. Shan et al, (2019) demonstrated that *DMI* alleviated acute DOX-induced heart injury in mice by activating the Nrf2/HO-1 antioxidant pathway. Daneshmandi et al, (2024) found that *4-OI* protected both monocytic and

polymorphonuclear cells from DOX-induced apoptosis and mitochondrial ROS accumulation. However, no data are available about the possible protective effects of DMI against ovarian toxicity induced by chemotherapy.

Therefore, the present study aims to evaluate the protective effects of DMI against DOX-induced ovarian toxicity in a 4T1 murine model of breast cancer. Specifically, this study focuses on assessing histological changes, apoptosis-related gene expression, and alterations in sex hormone production to determine whether DMI can mitigate gonadotoxicity and preserve ovarian function during chemotherapy.

Materials and Methods

Experimental Animals

A total of 30 adult female BALB/c mice with breast cancer (average weight 20 ± 2 g) were obtained from AvinStemGene Biohealth laboratory. The animals were housed in standard cages under controlled temperature (25±2°C), relative humidity (55% ±15%), and a 12-hour light/12-hour dark cycle. Food and water were provided ad libitum using standard laboratory chow (Pars Feed, Iran). All procedures were approved by the Ethics Committee of Shahid Chamran University of Ahvaz (EE/1404.085/scu.ac.ir).

4T1 breast cancer mouse model

A total of 24 adult female BALB/c mice were used to develop the 4T1 breast cancer mouse model. 4T1 cell line was obtained from the AvinStemGene Biohealth laboratory (Iran, Ahvaz). Cells were cultured in a DMEM-HG medium (Bioidea, Iran), supplemented with 10% fetal bovine serum (FBS, Biosera, France) and 100 unit/ml penicillin/streptomycin (Bioidea, Iran). Cells were incubated at 37°C with 5% CO2 and 95% humidity for 36 h. Approximately, 100 µL of 1×10^5 4T1 cells were isolated and introduced subcutaneously at the 3rd mammary fat pad of the BALB/c mice as described earlier (Laftah et al, 2025). The appearance of tumors was checked once a week.

Experimental design

When tumors became palpable and the tumor size reached the 10 mm, tumor-bearing mice were randomly assigned to five groups (n=6 per group):

Group 1: Normal (Healthy Control): Healthy mice maintained under identical environmental and dietary conditions as the other groups.

Group 2: Cancer (Cancer Control): Mice bearing breast tumor that received no anticancer treatment during the study.

Group 3: Cancer + DOX: Tumor-bearing mice treated with DOX (5 mg/kg; once a week; IP) for four consecutive weeks (Ramezani et al, 2024).

Group 4: Cancer + DMI: Tumor-bearing mice treated with DMI (50 mg/kg; daily; IP) for four weeks (Hosseinkhani et al, 2024).

Group 5: Cancer + DOX + DMI: Tumor-bearing mice simultaneously treated with both DOX (5 mg/kg; once a week; IP) and DMI (50 mg/kg; daily; IP,) for four weeks.

Sample Collection

At the end of the experiment, the animals were anesthetized with ketamine hydrochloride (100 mg/kg) and xylazine (10 mg/kg). Blood samples were obtained via cardiac puncture. Serum samples were collected by centrifuging at *5000 × RPM for 10 min and stored at -20*°C for serum biochemical analysis. The ovaries were removed and fixed in Bouin's solution for histological evaluation. The ovary was also collected and stored at -70 °C for gene expression analysis (Figure 1).

Histological Analysis

Ovarian tissues were fixed in Bouin's solution for 72 h. After fixation, the tissues were dehydrated, embedded in paraffin, and sectioned at 5–7 µm thickness. Sections were mounted on glass slides and dried

overnight at 37°C. After deparaffinization, the sections were stained with hematoxylin and eosin (H&E) and periodic acid–Schiff (PAS). Folliculogenesis was evaluated by assessing atretic follicles, corpora lutea, and granulosa cell layers. Five sections per ovary were examined using a light microscope (Olympus PX 50 F3, Japan) Histological images were captured using a Dino-Lite digital (FDP2, Taiwan) microscope camera and analyzed with DinoCapture 2.0 software.

Hormonal assay

The serum estradiol (E2) and progesterone (P4) concentrations were determined by using ELISA Kits (Diametra, Italy) according to the manufacturer's instructions. All samples were run in one assay to avoid inter-assay variation. The limits of detection of P4 and E2 were 0.05 ng/ml and 5 pg/ml, respectively. The intra-assay coefficients of variation of both hormones were less than 10%. All assays were carried out in duplicate.

RNA extraction and cDNA synthesis

Total RNA was extracted using the Total RNA Extraction Kit (Pars Tous, Iran), following the manufacturer's instructions. The purity of RNA at 260/280 OD ratio and the RNA integrity was evaluated using an Eppendorf µCuvette G1.0 microvolume measuring cell (Eppendorf, Germany). High-purity RNA with an OD of 260/280 ratio above 1.8 was used for cDNA synthesis. The cDNA was synthesized using 1 µg of RNA by Easy™ cDNA Synthesis Kit (ParsTous, Iran) and random hexamer according to the manufacturer's instructions.

Real-Time PCR analysis

To assess the expression levels of Bax and Bcl2 genes in ovary, real-time PCR (qRT-PCR) analysis was performed. The qRT-PCR primers were designed using the Primer3 software version 4.1.1 based on the sequences ofBax, Bcl2 and GAPDH genes available in NCBI Genebank (Table 1). The SYBR® Green Real Time PCR Master mix (ParsTous, Iran) was used to perform qRT-PCR on the Lava96T^{M} Real-Time PCR detection System (DaanGene, Co, Ldt, China). The thermal cycling conditions were as follows: initial denaturation at 94°C for 5 min; 45 cycles of: 94°C for 15 s and 60°C for 25 s. Two control reactions including a negative control without cDNA and a control containing RNA instead of DNA were considered. The relative expression of the genes compared to the calibrator gene was analyzed using the comparative $2^{-\Delta\Delta Ct}$ method. Evaluation of the amplification efficiency of the target genes compared to the reference gene (GAPDH) was done by preparing different dilutions of cDNA and drawing the efficiency graph as described previously (Tabandeh et al, 2022).

Table 1: Characteristics of primers that used in the current study

Gene	Forward Primer (5'→3')	Reverse Primer (5'→3')	Product Size (bp)	Accession No.
GAPDH	AGCCTTCTCCATGGTGGTGA	TGAAGTCGCAGGAGACAACC	116	NM_001289726.2
BAX	TGGAGCTGCAGAGGATGATT	CAGTTGAAGTTGCCATCAGCA	110	NM_017059.2
BCL-2	ATGGAGCTGCAGAGGATGAT	AGTTGAAGTTGCCATCAGCA	100	NM_007527.4

Statistical analysis

Statistical analysis was performed using GraphPad Prism software version 10 (Graph Pad Software, Inc., San Diego, CA). For evaluating the statistical significance of differences between groups, one-way analysis of variance (ANOVA) with Tukey's post hoc test was performed. Data are expressed as mean ± standard deviation (SD). Statistically significance difference between different experimental groups was represented as follows: #, *p< 0.05, ##, **p< 0.01, ###, *** p< 0.001, #### **** p<0.0001.

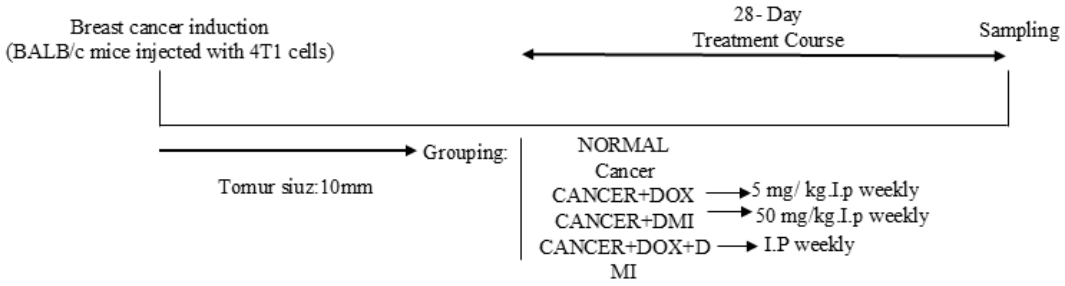

Figure 1: Overview of 5-week experimental protocol.

Results

Effects of DMI on histological alterations in the ovaries of DOX treated mice bearing breast cancer

In the healthy control (normal) group, the ovaries showed normal histological architecture. This included an intact stromal matrix, a regular surface epithelium, and follicles at various developmental stages such as primordial, primary, secondary, preantral, antral, and atretic follicles characterized by signs of apoptosis and pyknosis. The corpus luteum structures, normal blood vessels and vascular networks, and occasionally follicles containing two oocytes were also observed (Figure 2-A). In the cancer control group, the ovarian stroma showed increased cellular density compared to the normal group. The surface epithelium appeared thickened in areas containing developing primordial and primary follicles, with epithelial cells showing enlargement and notable morphological alterations. A prominent vascular network composed of dilated and congested blood vessels was observed in the central region of the ovary and beneath the surface epithelium. Numerous atretic follicles, mainly at the secondary to preantral stages, were identified. These atretic follicles were often elongated in shape. The corpus luteum was either rarely seen or entirely absent (Figure 2-B). In the cancer group treated with DOX (Cancer + DOX group), the ovarian stroma displayed a lower cellular density compared to the cancer control group. A broad vascular network remained present in the central ovarian region and beneath the surface epithelium, although it was less prominent than in the cancer control group. Follicles were generally smaller in size compared to those in the cancer control group, and the surface epithelium remained thickened. Various types of atretic follicles were observed, and their numbers were higher than in the cancer control group. No corpus luteum structures were detected in this group. Notably, the number of primordial and primary follicles was considerably higher than in both the healthy and cancer control groups (Figure 2-C). In the cancer mice group treated with DMI (Cancer + DMI group), the ovarian stroma showed a lower cellular density compared to the cancer control group. A vascular network was observed within the stromal region of the ovarian cortex and beneath the surface epithelium. The number of atretic follicles in this group was lower than in the group treated with DOX. These atretic follicles included various follicular types and mainly involved isolated granulosa cells, with the zona pellucida being less affected. The number of primordial and primary follicles was higher in this group than in the healthy control, cancer control, and Cancer + DOX + DMI groups, but lower than in the Cancer + DOX group. Secondary follicles in this group typically appeared round and spherical. The ovarian surface epithelium was thinner compared to that in the DOX-treated group. No corpus

luteum was observed (Figure 2-D). In the cancer + DOX + DMI group, the cellular density of the ovarian stroma was lower than that in the Cancer + DOX group. The corpus luteum was either rarely observed or completely absent. A vascular network was present in the central region of the ovary, but it was less extensive compared to the Cancer + DOX group. Although there was no marked increase in the thickness of the surface epithelium, the epithelial cells appeared larger than those observed in the Cancer + DOX group. The number of atretic follicles in this group was lower than in the group treated with DOX (Figure 2-E).

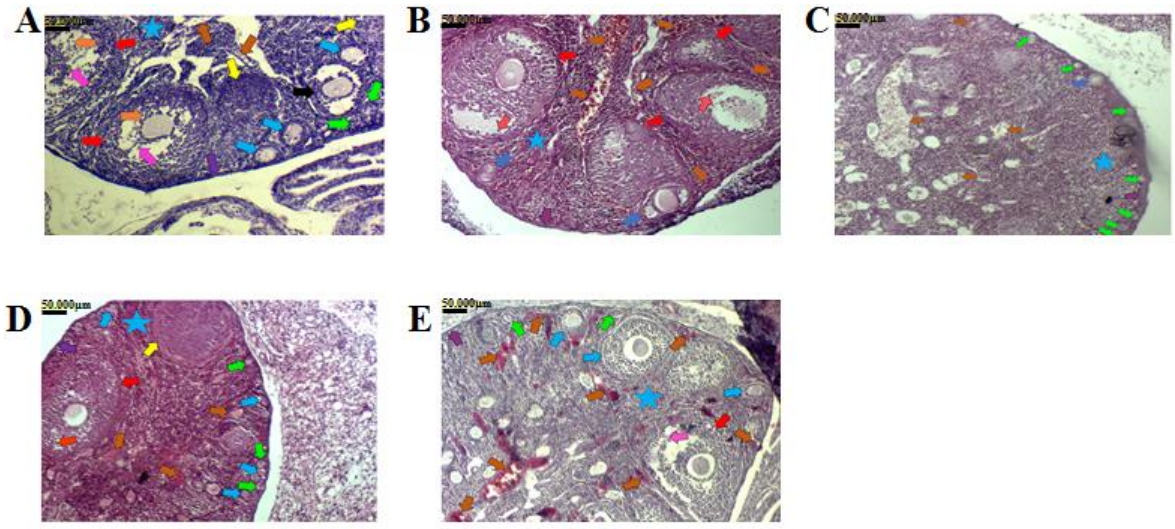

Figure 2: Sections of ovarian tissue from different experimental groups (A) Healthy control, (B) Cancer control, (C) Cancer + DOX, (D) Cancer + DMI, (E) Cancer + DOX + DMI (H&E, 10X). Yellow arrowhead: corpus luteum, green arrow: primary follicle, blue arrow: secondary follicle, black arrow: antral follicle, red arrow: atretic follicle, purple arrow: ovarian surface epithelium, brown arrow: blood vessels, orange arrow: pyknotic nucleus, pink arrow: apoptotic bodies within atretic follicles, blue asterisk indicates the stromal matrix.

Evaluation of Zona Pellucida Uniformity

To evaluate the structural integrity of the zona pellucida, PAS staining was conducted on ovarian sections from all experimental groups. In the healthy control group, the zona pellucida showed its structural continuity and showed minimal signs of atresia (Figure 3-A). In contrast, the cancer control group exhibited disrupted zona pellucida morphology in many atretic follicles, characterized by irregular thickness. In certain regions, the zona pellucida appeared markedly thinned, detached, and freely floating within the antrum, displaying an undulating pattern (Figure 3-B). In DOX group, the zona pellucida exhibited irregular thickness and a wavy morphology. Areas of disrupted continuity and compromised structural integrity were more frequently observed compared to the cancer control group. These alterations were notably more severe than those in the cancer control group (Figure 3-C). In the Cancer + DMI group, the zona pellucida showed a pattern similar to the Cancer + DOX group, characterized by uneven thickness, a wavy appearance, and increased fragmentation and discontinuities compared to the cancer control group (Figure 3-D). In the Cancer + DOX + DMI group, the zona pellucida thickness in many atretic follicles was more uniform compared to the Cancer + DOX group (Figure 3-E).

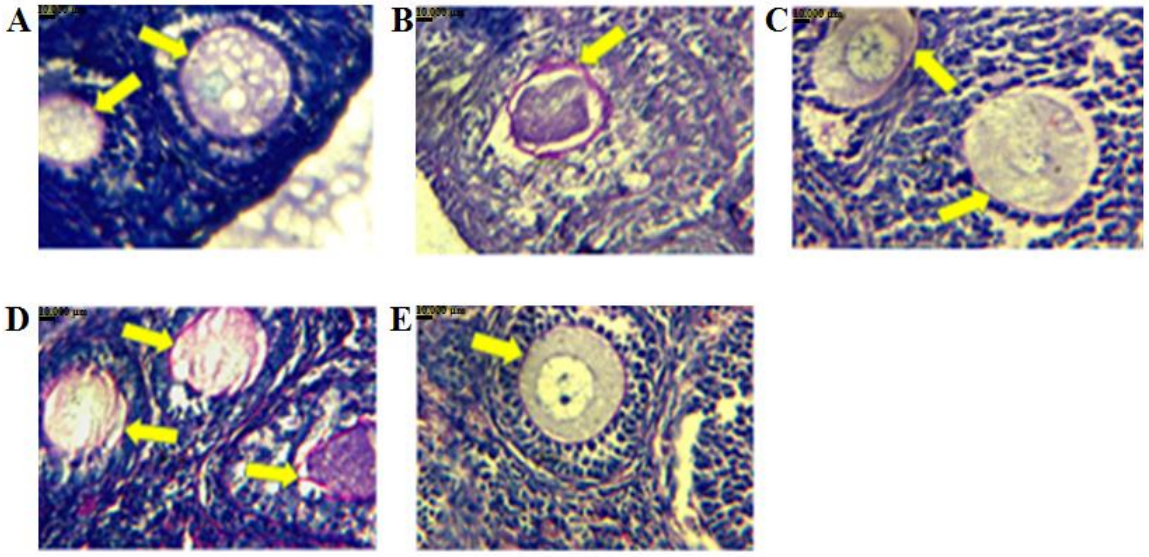

Figure 3: Ovarian tissue sections examined from five experimental groups, focusing on the zona pellucid. Groups: (A) Healthy control, (B) Cancer control, (C) Cancer + DOX, (D) Cancer + DMI, (E) Cancer + DOX + DMI (PAS, 40X). Yellow arrow: zona pellucid.

Effect of DMI on serum estradiol and progesterone concentrations in DOX-treated mice bearing breast cancer

Serum estradiol level was significantly reduced in the cancer group compared to the normal (control) group ($P<0.01$). This reduction was even more pronounced in the cancer + DOX group, which showed a further significant decrease compared to the cancer group ($P<0.01$). Treatment of cancer-bearing mice with DMI alone had no significant effect on serum estradiol concentration when compared to untreated cancer mice ($P>0.05$). However, in DOX-treated mice, co-administration of DMI significantly elevated serum estradiol level compared to those receiving DOX alone ($P<0.05$) (Figure 4-A). Serum progesterone level was significantly reduced in the cancer group compared to the normal control group ($P<0.0001$). The Cancer + DOX group exhibited a greater decrease in serum progesterone level compared to the cancer group ($P<0.0001$). Treatment of cancer-bearing mice with DMI had no significant effect on serum progesterone concentration compared to untreated cancer mice ($P>0.05$). However, in DOX-treated mice, DMI significantly increased serum progesterone level compared to untreated animals ($P<0.01$) (Figure 4-B).

Effect of DMI on ovarian expression of apoptosis related genes in DOX-treated mice bearing breast cancer

There was no significant difference in the relative expression level of the Bax gene between the cancer group and the normal group ($P>0.05$). DMI administraion in cancer mice had no significant effect on Bax gene expression compared to untreated mice. The Bax expression level was increased in the cancer + DOX group compared to the cancer group ($P<0.0001$). DMI could reduce the expression of Bax gene in ovary of DOX-treated mice compared to the un treated mice ($P<0.01$) (Figure 5-A). There was a significant decrease in the relative expression level of the Bcl2 gene in the cancer group compared to the normal group ($P<0.01$). Administration of DMI in cancer-bearing mice significantly increased Bcl2 gene expression compared to untreated cancer mice ($P<0.05$). However, BCL2 expression was reduced in the cancer + DOX group compared to the cancer group ($P<0.01$). DMI was able to increase Bcl2 gene expression in the ovaries of DOX-treated mice compared to those treated with DOX alone ($P<0.05$) (Figure 5-B).

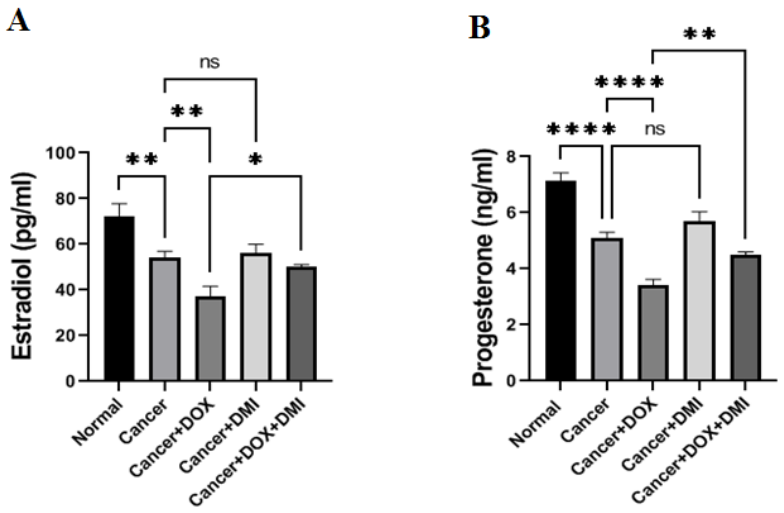

Figure 4: Serum concentrations of estradiol (A) and progesterone (B) in healthy mice (normal), 4T1 breast cancer-bearing mice (cancer), cancer-bearing mice treated with DOX (cancer + DOX), cancer-bearing mice treated with DMI (cancer + DMI), and cancer-bearing mice treated with both DOX and DMI (cancer + DOX + DMI). Data are presented as mean ± SD (n = 6 per group). Statistical significance is indicated as follows: ns, not significant; *p < 0.05; **p < 0.01; ****p < 0.0001

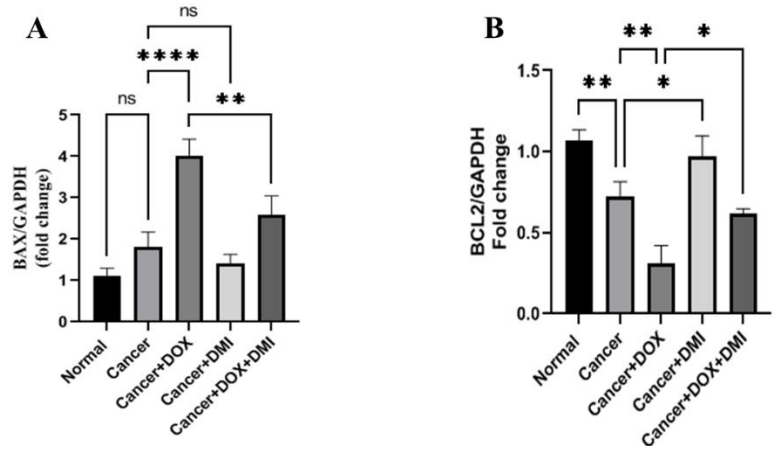

Figure 5: Ovarian expression levels of Bax (A) and Bcl2 (B) genes in different experimental groups. healthy mice (normal), 4T1 breast cancer mice (cancer), breast cancer mice treated with DOX (cancer + DOX), breast cancer mice treated with DMI (cancer +DMI), and breast cancer mice treated with both DOX and DMI (cancer +DOX + DMI). The GAPDH was used as a housekeeping gene. Relative quantification was performed according to the comparative $2^{-\Delta\Delta Ct}$ method. Data represent mean ± SD for 6 animals in each group. Statistical significance is denoted as follows: *p < 0.05; **p < 0.01; ***p < 0.001; ns indicates not significant.

Discussion

DOX is one of the most common drugs widely used in breast cancer treatment. However, although effective against tumor, it can adversely affect ovarian function and fertility in women of reproductive age. Damage to growing follicles, increased apoptosis of granulosa cells, and disruptions in sex hormone production are well-documented side effects of DOX. Consequently, the combination of protective agents with DOX therapy has emerged as a promising strategy to mitigate

DOX-induced toxicity and preserve fertility in patients undergoing treatment. DMI, a metabolite derived from macrophage metabolic pathways, is considered a potential cytoprotective agent because it can activate the Nrf2 pathway and reduce oxidative stress and inflammation. This study aimed to explore the effects of DMI on apoptosis, folliculogenesis, and serum sex hormone production in a mouse model of breast cancer receiving DOX treatment. The results provide new insights into protecting the ovaries during cancer treatment through the use of DMI.

Results indicated that mice bearing breast tumors had reduced serum estradiol and progesterone levels, and DOX treatment further exacerbated this reduction. Additionally, tumor-bearing mice exhibited increased expression of the pro-apoptotic gene Bax and decreased expression of the anti-apoptotic gene Bcl-2, effects that were further potentiated by DOX treatment. Histological evaluations revealed impaired normal folliculogenesis in the ovaries of cancer-bearing mice as well as in those treated with DOX. In the ovary of cancer control group, many degenerating atretic follicles, especially at early developmental stages, were observed, and corpus luteum formation was minimal or absent. Treatment with DOX reduced stromal cellular density and vascular prominence but increased the number of early-stage (primordial and primary) follicles. These results suggest that DOX treatment alters ovarian structure by reducing cellular density and vascularization while preserving or even increasing the early follicle pool, potentially impacting ovarian function differently than untreated cancer. In the untreated cancer group, reduced serum estradiol and progesterone closely corresponded with increased follicular atresia and decreased secondary and antral follicles, highlighting the dependency of folliculogenesis on steroid hormones. Doxorubicin exacerbated these effects through granulosa cell apoptosis (Bax↑, Bcl-2↓) and loss of growing follicles, resulting in impaired steroidogenesis. In contrast, DMI treatment, alone or combined with DOX, preserved granulosa cell survival, maintained secondary follicles, and reduced atresia, thereby supporting follicular growth and steroid hormone production. Changes in steroid hormone levels are directly associated with folliculogenesis in the ovary; reduced estradiol and progesterone correlate with increased follicular atresia and loss of growing follicles, whereas preservation of granulosa cell survival supports follicle maintenance and steroid hormone production (Chauvin et al., 2022). Although most studies on cancer-related gonadotoxicity have focused on chemotherapy, our results indicated that tumor itself can disrupt reproductive function. The previous studies have indicated that systemic tumors may exert distant effects on the ovary through inflammatory cytokines, metabolic modukators, or hormonal feedback dysregulation. Supporting it, studies in tumor-bearing rodents have shown alterations in the hypothalamic-pituitary-gonadal axis, which can impair gonadotropin release and disrupt folliculogenesis. Inflammation and oxidative stress induced by tumor burden may also contribute to granulosa cell dysfunction and apoptosis. Wang et al (2017) reported that tumor-bearing mice showed loss of both primordial and growing follicles, alongside abnormal steroid hormone levels and elevated ROS in ovarian tissue. They linked tumor-induced ovarian damage to mitochondrial dysfunction in oocytes and granulosa cells via the PI3K–Akt–mTOR pathway (Wu et al, 2023). These mechanisms align with our observed increase in Bax expression and reduction in Bcl-2, markers of mitochondrial-mediated apoptosis in ovary of mice bearing cancer showed impaired follicular development. Further, supporting this interpretation, inflammation-associated

cytokines such as IL-6 and TNF-α—known to be elevated in tumor-bearing mice and breast cancer patients—can directly inhibit granulosa cell steroidogenesis and promote apoptotic signaling (Ojo et al, 2023). Furthermore, breast cancer is known to be hormonally responsive, and its metabolic activity may affect systemic estrogen levels or feedback regulation on the ovary. Reduced levels of E2 and P4 in our cancer-induced mice are consistent with findings from stress or toxin-induced ovarian dysfunction models, where hormonal imbalances are typically accompanied by granulosa cell apoptosis and follicle depletion. Moreover, ovarian cachexia models showed that cancer-induced dysregulation of ovarian hormones often precedes overt weight loss and systemic symptoms (Guo et al, 2024). This highlights that tumor presence disrupts the hypothalamic–pituitary–gonadal axis early on, consistent with our observations of reduced E_2/P_4 and declining follicle counts (Hetzler et al, 2017). Taken together, our data support the hypothesis that breast tumor presence alone is sufficient to induce ovarian damage, potentially through endocrine, inflammatory, and apoptotic pathways. This underlines the importance of considering tumor-related effects on fertility even before the initiation of chemotherapy and suggests a need for early fertility assessment and intervention in cancer patients.

In accordance with our findings Ben-Aharon et al, (2010) indicated that DOX treatment caused a significant reduction in ovarian weight, increasing follicular atresia, particularly secondary and antral follicles and a marked depletion of the ovarian follicle reserve and granulosa cell apoptosis one month after treatment with DOX. Additionally, serum estradiol levels were significantly decreased following DOX exposure, reflecting impaired steroidogenesis. At the molecular level, DOX induced upregulation of pro-apoptotic genes such as Bax and downregulation of anti-apoptotic genes like Bcl-2, alongside increased caspase-3 activation, confirming activation of the apoptotic pathway. Wang et al, (2017) showed that DOX depletes the ovarian reserve through a dual mechanism involving both direct oocyte apoptosis and indirect overactivation of primordial follicles. Their study demonstrated that DOX causes DNA double-strand breaks, particularly in granulosa cells and oocytes of growing follicles, triggering apoptosis via the TAp63α–caspase-3 pathway. These findings collectively demonstrate that DOX induces ovarian toxicity by promoting granulosa cell apoptosis, follicular atresia, and hormonal disruption, thereby compromising ovarian reserve and function.

Researchers showed that administration of DMI significantly reversed ovarian pathological and molecular changes induced by DOX therapy. DMI treatment restored the number of growing follicles, improved the morphology of ovarian tissue, and supported the reappearance of corpus luteum structures. In addition, DMI improved the serum levels of E_2 and P_4 and balanced the expression of Bax and Bcl-2, indicating a reduction in DOX and tumor-induced apoptotic signaling. These results suggest that DMI exerts a protective effect on the ovary under conditions of oxidative and apoptotic stress associated with cancer and chemotherapy.

The observed variations in serum E2 and P4 levels across the groups suggest differential impacts on ovarian follicular development and luteal function. Estradiol production during the follicular phase primarily depends on the activity of growing antral follicles, while progesterone secretion during the luteal phase is contingent upon the presence of a functional corpus luteum. In the cancer and cancer + DOX groups, reductions in both E2 and P4 levels reflect disrupted folliculogenesis, increased follicular atresia, and regression or loss of the corpus luteum. These changes can be attributed to the combined effects of

tumor-induced systemic stress and the cytotoxicity of DOX, both of which are known to induce oxidative damage, impaired granulosa and luteal cell function, and accelerate ovarian follicle depletion (Markowska et al , 2024; Rad et al, 2021; Guo et al, 2024). In contrast, the restoration of E2 and P4 levels in the cancer + DOX + DMI and cancer + DMI groups suggests that DMI may exert a protective role in ovarian physiology. DMI's antioxidant and anti-inflammatory properties may contribute to an improved ovarian microenvironment, preserving granulosa and luteal cell viability, sustaining steroidogenic enzymes activity, and facilitating the development of a functional corpus luteum. This can support both estradiol biosynthesis and progesterone production. Taken together, the recovery of serum estradiol and progesterone levels in the DMI-treated group underscores DMI's potential to mitigate chemotherapy- and cancer-induced ovarian dysfunction. By enhancing follicular survival and preserving luteal activity, DMI may contribute to the maintenance of endocrine function and reproductive health under conditions of oncogenic and chemotherapeutic stress. These findings highlight the therapeutic potential of DMI in protecting ovarian integrity and function during cancer treatment.

Several mechanisms may be related to improvement of ovarian dysfunctions in DOX-treated mice following DMI treatment. One of the primary mechanisms by which DMI exerts its protective effect against ovarian dysfunctions is via activation of the Nrf2 (nuclear factor erythroid 2–related factor 2) pathway. DMI alkylates specific cysteine residues on KEAP1, the cytoplasmic repressor of Nrf2, thereby disrupting KEAP1-mediated degradation of Nrf2. Stabilized Nrf2 translocates to the nucleus, where it binds to antioxidant response elements (AREs) in the promoters of target genes involved in redox homeostasis, including HO-1, NQO1, and glutathione biosynthesis enzymes (Mills et al, 2018). This leads to upregulation of cellular antioxidant defenses and a corresponding reduction in ROS. In addition to its antioxidant effects, DMI also exerts anti-inflammatory activity through suppression of the NF-κB signaling pathway. It interferes with the phosphorylation and degradation of IκBα, thereby preventing nuclear translocation of the p65/p50 NF-κB complex. Furthermore, DMI may directly alkylate cysteine residues on upstream kinases such as IKKβ, leading to broad inhibition of NF-κB–dependent transcription of proinflammatory cytokines, including TNF-α, IL-1β, and IL-6 (Williams et al, 2018; O'Neill et al, 2019). Another important target of DMI is succinate dehydrogenase (SDH), a key mitochondrial enzyme whose inhibition reduces succinate oxidation and downstream ROS production, further contributing to redox balance and inhibition of HIF-1α–mediated proinflammatory gene expression. Collectively, these mechanisms demonstrate how DMI modulates both inflammatory and oxidative stress responses, highlighting its potential therapeutic application in protecting granulosa cells and ovarian tissue under pathological conditions such as DOX-induced gonadotoxicity.

To support this hypothesis, DMI has been shown to restore steroidogenesis and improve granulosa cell viability under inflammatory conditions. In a recent study, Tabandeh et al, (2022) reported that DMI significantly improved E2 and P4 production in lipopolysaccharide treated bovine ovarian granulosa cells, a well-established model of inflammation-induced ovarian dysfunction. LPS exposure activated key inflammatory signaling pathways, including TLR4/NF-κB, NLRP3 inflammasome, and JNK, leading to impaired cell viability, suppressed steroidogenesis, and increased production of proinflammatory cytokines such as IL-1β and TNF-α. Treatment with DMI

effectively countered these effects by downregulating the expression and activation of TLR4, NF-κB, NLRP3, and phosphorylated JNK. This was accompanied by a reduction in inflammatory cytokine release and restoration of steroidogenic function, suggesting that DMI exerts its protective effects by modulating inflammatory signaling and preserving granulosa cell function. Recently, Hosseinkhani et al (2024), indicated that DMI ameliorated ovarian dysfunction in a rat model of testosterone-induced PCOS. Their findings demonstrated that DMI exhibited strong anti-inflammatory effects by decreasing ovarian levels of pro-inflammatory cytokines, including TNF-α and IL-1β. It also reduced oxidative stress, as evidenced by a lower ovarian oxidative stress index (OSI). Histological evaluations revealed that DMI improved folliculogenesis, decreased the number of cystic follicles, and restored normal ovarian tissue architecture. Additionally, it enhanced ovarian steroidogenic function. Zhou et al (2020), also showed that itaconic acid, through its endogenous enzyme IRG1, exerted a protective effect against endoplasmic reticulum (ER) stress–induced necroptosis in bovine granulosa cells. They demonstrated that itaconic acid attenuated tunicamycin-induced ER stress by inhibiting the PERK–ATF4 signaling pathway and reducing acetylcholinesterase (AChE) expression, which in turn suppressed necroptosis and preserved cell viability and ultrastructure. These findings highlight a novel role of itaconate in maintaining granulosa cell function under stress conditions (Yang et al, 2025).

This study demonstrated that breast tumor induction and DOX chemotherapy significantly disrupt ovarian hormone levels, gene expression related to apoptosis, and ovarian follicular development. DOX treatments further exacerbate tumor-induced ovarian damage by altering ovarian structure, reducing cellular density and vascularization, and increasing follicular atresia. Importantly, DMI administration effectively mitigates these detrimental effects by restoring normal ovarian morphology, hormone balance, and apoptotic gene expression. These findings suggest that DMI has a protective role against cancer and chemotherapy-induced ovarian dysfunction, highlighting its potential as a therapeutic agent to preserve ovarian health during breast cancer treatment.

Ethical statement

All protocols and procedures were in compliance with international guidelines for care and use of laboratory animals, and they were approved by Shahid Chamran University of Ahvaz (SCU.VB1404.085/scu.ac.ir).

Acknowledgment

The authors would like to appreciate the Research Council of Shahid Chamran University of Ahvaz for funding this study.

Conflict of interest

The authors declare that they have no known competing financial interests or personal relationships that could have appeared to influence the work reported in this paper.

Funding

This study was supported by a grant (no SCU.VB1404.158) from the Shahid Chamran University of Ahvaz, Iran.

References

Azari, N., Rezaee, M., Dayer, D., & Tabandeh, M. R. (2024). Dimethyl itaconate modulates neuroprotective effect on primary rat astrocytes under inflammatory condition by regulating the expression of neurotrophic factors and TrkA/B-P75 receptors. *Neurological Research*, *46*(12), 1137–1148.

Bedoschi, G., Navarro, P. A., & Oktay, K. (2016). Chemotherapy-induced damage to ovary: Mechanisms and clinical impact. *Future Oncology*, *12*(20), 2333–2344.

Ben-Aharon, I., Bar-Joseph, H., Tzarfaty, G., Kuchinsky, L., Rizel, S., Stemmer, S. M., & Shalgi, R. (2010). Doxorubicin-induced ovarian toxicity. *Reproductive Biology and Endocrinology*, *8*, 1–7.

Cai, G., Si, M., Li, X., Zou, H., Gu, J., Yuan, Y., ... & Bian, J. (2019). Zearalenone induces apoptosis of rat Sertoli cells through Fas-Fas ligand and mitochondrial pathway. *Environmental Toxicology*, *34*(4), 424–433.

Chauvin, S., Cohen-Tannoudji, J., & Guigon, C. J. (2022). Estradiol signaling at the heart of folliculogenesis: Its potential deregulation in human ovarian pathologies. *International Journal of Molecular Sciences*, *23*(1), 512.

Daneshmandi, S., Choi, J. E., Yan, Q., MacDonald, C. R., Pandey, M., Goruganthu, M., ... & Mohammadpour, H. (2024). Myeloid-derived suppressor cell mitochondrial fitness governs chemotherapeutic efficacy in hematologic malignancies. *Nature Communications*, *15*(1), 2803.

Ferreira, A. V., Kostidis, S., Groh, L. A., Koeken, V. A., Bruno, M., Baydemir, I., ... & Netea, M. G. (2023). Dimethyl itaconate induces long-term innate immune responses and confers protection against infection. *Cell Reports*, *42*(6), Article 112558.

Gao, Y., Wu, T., Tang, X., Wen, J., Zhang, Y., Zhang, J., & Wang, S. (2023). Increased cellular senescence in doxorubicin-induced murine ovarian injury: Effect of senolytics. *Geroscience*, *45*(3), 1775–1790.

Guo, S., Quan, S., & Zou, S. (2021). Roles of the notch signaling pathway in ovarian functioning. *Reproductive Sciences*, *28*(10), 2770–2778.

Guo, Y., Xue, L., Tang, W., Xiong, J., Chen, D., Dai, Y., ... & Wang, S. (2024). Ovarian microenvironment: Challenges and opportunities in protecting against chemotherapy-associated ovarian damage. *Human Reproduction Update*, *30*(5), 614–647.

He, F., Wang, F., Yang, Y., Yuan, Z., Sun, C., Zou, H., ... & Han, T. L. (2023). The effect of growth hormone on the metabolome of follicular fluid in patients with diminished ovarian reserve. *Reproductive Biology and Endocrinology*, *21*(1), 21.

Hetzler, K. L., Hardee, J. P., LaVoie, H. A., Murphy, E. A., & Carson, J. A. (2017). Ovarian function's role during cancer cachexia progression in the female mouse. *American Journal of Physiology-Endocrinology and Metabolism*, *312*(5), E447–E459.

Hosseinkhani, F., Hosseinifar, S., & Tabandeh, M. R. (2024). Dimethyl itaconate mitigates histological distortions, inflammation, and oxidative stress in the rat model of polycystic ovary syndrome. *The Journal of Steroid Biochemistry and Molecular Biology*, *243*, Article 106546.

Khadem, M. D., Tabandeh, M. R., Haschemi, A., Kheirollah, A., & Shahriari, A. (2022). Dimethyl itaconate reprograms neurotoxic to neuroprotective primary astrocytes through the regulation of NLRP3 inflammasome and NRF2/HO-1 pathways. *Molecular and Cellular Neuroscience*, *122*, Article 103758.

Laftah, A. H., Alhelfi, N., Al Salait, S. K., Altemimi, A. B., Tabandeh, M. R., Tsakali, E., ... & Abedelmaksoud, T. G. (2025). Mitigation of doxorubicin-induced liver toxicity in mice breast cancer model by green tea and Moringa oleifera combination: Targeting apoptosis, inflammation, and oxidative stress. *Journal of Functional Foods*, *124*, Article 106626.

Markowska, A., Antoszczak, M., Markowska, J., & Huczyński, A. (2024). Gynotoxic effects of chemotherapy and potential protective mechanisms. *Cancers*, *16*(12), 2288.

Mills, E. L., Ryan, D. G., Prag, H. A., Dikovskaya, D., Menon, D., Zaslona, Z., ... & O'Neill, L. A. (2018). Itaconate is an anti-inflammatory metabolite that activates Nrf2 via alkylation of KEAP1. *Nature*, *556*(7699), 113–117.

Nguyen, N. M. P., Chang, E. M., Chauvin, M., Sicher, N., Kashiwagi, A., Nagykery, N., ... & Oktay, K. (2025). AMH protects the ovary from doxorubicin by regulating cell fate and the response to DNA damage. *Proceedings of the National Academy of Sciences*, *122*(5), e2414734122.

Nishi, K., Gunasekaran, V. P., Arunachalam, J., & Ganeshan, M. (2018). Doxorubicin-induced female reproductive toxicity: An assessment of ovarian follicular apoptosis, cyclicity and reproductive tissue histology in Wistar rats. *Drug and Chemical Toxicology*, *41*(1), 72–81.

Ojo, O. A., Nwafor-Ezeh, P. I., Rotimi, D. E., Iyobhebhe, M., Ogunlakin, A. D., & Ojo, A. B. (2023). Apoptosis, inflammation, and oxidative stress in infertility: A mini review. *Toxicology Reports*, *10*, 448–462.

O'Neill, L. A., & Artyomov, M. N. (2019). Itaconate: The poster child of metabolic reprogramming in macrophage function. *Nature Reviews Immunology*, *19*(5), 273–281.

Rad, P., Safari, F., Mohammadi, J., & Delaviz, H. (2021). Preserved ovarian function following toxicity with doxorubicin in rats: Protective effect of nasturtium officinale extract. *Iranian Journal of Toxicology*, *15*(1), 57–64.

Ramezani-Aliakbari, K., Jalali, S. A., Alinejad, M., Jeddi-Tehrani, M., & Shabani, M. (2024). 5-Fluorouracil effectively depletes tumor induced myeloid derived suppressor cells in 4T1 mammary carcinoma model. *Avicenna Journal of Medical Biotechnology*, *16*(4), 244–250.

Saleh, D., Abdelbaset, M., Hassan, A., Sharaf, O., Mahmoud, S., & Hegazy, R. (2020). Omega-3 fatty acids ameliorate doxorubicin-induced cardiorenal toxicity: In-vivo regulation of oxidative stress, apoptosis and renal Nox4, and in-vitro preservation of the cytotoxic efficacy. *PLoS ONE*, *15*(11), e0242175.

Shan, Q., Li, X., Zheng, M., Lin, X., Lu, G., Su, D., & Lu, X. (2019). Protective effects of dimethyl itaconate in mice acute cardiotoxicity induced by doxorubicin. *Biochemical and Biophysical Research Communications*, *517*(3), 538–544.

Soleimani, R., Heytens, E., Darzynkiewicz, Z., & Oktay, K. (2011). Mechanisms of chemotherapy-induced human ovarian aging: Double strand DNA breaks and microvascular compromise. *Aging (Albany NY)*, *3*(8), 782–793.

Tabandeh, M. R., Jozaie, S., Ghotbedin, Z., & Gorani, S. (2022). Dimethyl itaconic acid improves viability and steroidogenesis and suppresses cytokine production in LPS-treated bovine ovarian granulosa cells by regulating TLR4/nfkβ, NLRP3, JNK signaling pathways. *Research in Veterinary Science*, *152*, 89–98.

Wang, L., Wang, Y., Wang, Z., Qi, Y., Zong, B., Liu, M., ... & Ma, Y. (2018). Growth differentiation factor 11 ameliorates experimental colitis by inhibiting NLRP3 inflammasome activation. *American Journal of Physiology-Gastrointestinal and Liver Physiology*, *315*(6), G909–G920.

Williams, N. C., & O'Neill, L. A. (2018). A role for the Krebs cycle intermediate citrate in metabolic reprogramming in innate immunity and inflammation. *Frontiers in Immunology*, *9*, 141.

Wu, Y., Huang, J., Chen, H., Tao, H., He, Y., Yang, G., ... & Li, P. (2023). Tumor-derived oxidative stress triggers ovarian follicle loss in breast cancer. *The American Journal of Pathology*, *193*(5), 608–623.

Yang, X., Chen, Y., Wang, X., Xu, G., Wang, H., Shu, X., ... & Lu, W. (2025). Ameliorative effect of itaconic acid/IRG1 against endoplasmic reticulum stress-induced necroptosis in granulosa cells via PERK-ATF4-AChE pathway in bovine. *Cells*, *14*(6), 419.

Yildiz, S., Bildik, G., Benlioglu, C., Turan, V., Dilege, E., Ozel, M., ... & Oktay, K. (2023). Breast cancer treatment and ovarian function. *Reproductive BioMedicine Online*, *46*(2), 313–331.

Zhan, Z., Wang, Z., Bao, Y., Liu, W., & Hong, L. (2022). OI inhibits development of ovarian cancer by blocking crosstalk between cancer cells and macrophages via HIF-1α pathway. *Biochemical and Biophysical Research Communications*, *606*, 142–148.

Zhang, T., He, W. H., Feng, L. L., & Huang, H. G. (2017). Effect of doxorubicin-induced ovarian toxicity on mouse ovarian granulosa cells. *Regulatory Toxicology and Pharmacology*, *86*, 1–10.

Zhou, S., Xi, Y., Chen, Y., Zhang, Z., Wu, C., Yan, W., ... & Wang, S. (2020). Ovarian dysfunction induced by chronic whole-body PM2.5 exposures. *Small*, *16*(33), 2000845.

Received: 29.10.2025
Accepted: 16.02.2026

Vol. 22, No. 2, Summer, 2026, 47-55 *Original Article*
DOI: 10.22055/ivj.2026.536372.2821
Journal Homepage: http://www.ivj.ir/

The prevalence of *Cryptosporidium spp.* in sheep and goats in Urmia, Iran

Behnam Ghorbani[1], Vahid Najarnezhad[2*] and Farnaz Malekifard[3]

[1] DVM Graduated, Faculty of Veterinary Medicine, Urmia University, Urmia, Iran
[2] Associated Professor, Department of Internal Medicine, Faculty of Veterinary Medicine, Urmia University, Urmia, Iran
[3] Associated Professor, Department of Pathobiology, Faculty of Veterinary Medicine, Urmia University, Urmia, Iran

Received: 22.07.2025 Accepted: 02.06.2026

Abstract

Cryptosporidiosis, a zoonotic disease caused by *Cryptosporidium spp*., affects both domestic animals and humans. In newborn ruminants, it often manifests as outbreaks of diarrhea, leading to significant morbidity and economic losses. This study aimed to determine the prevalence of *Cryptosporidium spp*. infection in small ruminants in Urmia, Iran. A total of 560 small ruminants from seven farms located in seven villages around Urmia were examined across four seasons. *Cryptosporidium* oocysts were concentrated using formalin-ether sedimentation method, and oocysts were identified through a modified Ziehl-Neelsen staining procedure. Of the 560 animals, 67 (11.96%) tested positive for *Cryptosporidium spp*. Sheep exhibited a higher prevalence (17.86%) compared to goats (6.07%). Statistical analysis revealed significant associations between infection prevalence and factors such as fecal consistency, age, sex, and season. These findings underscore the potential zoonotic threat of *Cryptosporidium spp*. in the region, indicating the need for public health awareness and effective management strategies in small ruminant farming.

Key words: *Cryptosporidium*, Prevalence, Small ruminants, Urmia, Iran

Introduction

Cryptosporidiosis, caused by protozoan parasites of the genus *Cryptosporidium*, is a globally important zoonotic disease affecting humans and a wide range of vertebrate hosts, including mammals, birds, and reptiles (Roellig and Xiao 2020). These apicomplexan parasites are responsible for gastrointestinal illness characterized by diarrhea, which can be particularly severe in immunocompromised individuals such as those with HIV/AIDS (Gerace, Presti et al, 2019).

Molecular studies have identified nearly 40 *Cryptosporidium* species and more than 50 genotypes, with *C. hominis* and *C. parvum* being the primary etiologic agents of human infection (Kabira, et al, 2020; Roellig and Xiao, 2020). *C. parvum* is also a major pathogen in livestock, commonly associated with neonatal diarrhea in ruminants such as calves, lambs, and goat kids (Constable, Hinchcliff et al, 2017; Mammeri, et al, 2019). Infected animals shed large numbers of environmentally resistant oocysts, which contaminate water, food, and soil, facilitating transmission between animals and humans (Santin, 2020).

[*] **Corresponding Author**: Vahid Najarnezhad, Associated Professor, Department of Internal Medicine, Faculty of Veterinary Medicine, Urmia University, Urmia, Iran
E-mail: v.najarnezhad@urmia.ac.ir

Small ruminants, including sheep and goats, are increasingly recognized as important reservoirs of zoonotic *Cryptosporidium* species (Robertson, 2009; Mi, et al, 2014), particularly in rural and peri-urban areas where close contact with humans enhances the risk of cross-species transmission. In these hosts, infection is primarily associated with neonatal diarrhea, leading to dehydration, poor growth, and sometimes death, thereby causing substantial economic losses through reduced productivity and increased treatment costs (Constable, et al, 2017; Mammeri, et al, 2019).

The persistence of oocysts in the environment perpetuates the infection cycle and underscores the significance of *Cryptosporidium* as a continuing threat to both animal and public health, warranting further investigation. Despite the importance of cryptosporidiosis in small ruminants, there remains a significant gap in knowledge regarding the prevalence and distribution of *Cryptosporidium spp*. infections in sheep and goats, particularly in regions like the northwest of Iran. Urmia, the capital of West Azerbaijan province, has a large population of small ruminants, but limited studies have investigated the prevalence of *Cryptosporidium* infections in these animals in this region. Therefore, the present study was undertaken to determine the prevalence of *Cryptosporidium spp.* infections in sheep and goats in Urmia and its surrounding areas. Additionally, the study sought to identify potential risk factors associated with infection, such as the presence of diarrhea, age, sex, and seasonality.

Materials and Methods

Ethical Approval

The study protocol was reviewed and approved by the Bioethics and Animal Welfare Commission of the Faculty of Veterinary Medicine, Urmia University, Iran (IR-UU-AEC-33/75). All animal handling and sample collection procedures adhered to ethical guidelines for the humane treatment of animals.

Study Design

This cross-sectional study was conducted in Urmia and its surrounding rural areas, located in the northwest of Iran, from January 2022 to 2023. Urmia, with a population of over 600,000 people, is the capital of West Azerbaijan province and lies at an altitude of 1368 meters above sea level. The region experiences a semi-arid climate, characterized by hot, dry summers and cold winters, with an Annual humidity ranges from 52% to 64%, average annual temperature of 8.9°C and average annual precipitation of 238.2 mm (Sima, et al, 2013; Mousavi, et al, 2024). The study area is predominantly rural, with small ruminant farming being a key agricultural activity. Sheep and goats are raised in various smallholder farms, often in close contact with humans and other animals.

Sample Collection

A total of 560 small ruminants, consisting of 280 sheep and 280 goats, were included in the study. The animals were selected from seven farms in the rural outskirts of Urmia, distributed across three geographical areas: (1) Northern villages, including Nazloo, Anzal, and Somay; (2) Central (nearby) villages, including Tape-Ghalee and Barandaz; and (3) Southern villages, including Margvar and Silvane. Ten sheep and ten goats were randomly selected from each of the villages during each of the four seasons—spring, summer, autumn, and winter—resulting in a total of 560 fecal samples.

Fresh fecal samples (5–10 grams) were collected directly from the rectum of each animal. Prior to sample collection, general data were recorded, including the presence of diarrhea, the animal's age (classified as ≤1 year or >1 year), and sex (male or female). The collected fecal samples were immediately placed in disposable containers and transported to the

parasitology laboratory at the Faculty of Veterinary Medicine, Urmia University, for analysis.

Laboratory Analysis

Upon arrival at the laboratory, fecal samples were processed using the Clayton-Lane flotation method to isolate and identify *Cryptosporidium* oocysts. For each sample, 3 grams of feces were suspended in 42 ml of distilled water and left to settle for approximately one hour at room temperature. Afterward, 15 ml of the strained fecal suspension was transferred to a test tube and left to stand for 30 minutes to allow for sedimentation of larger particles. The supernatant was discarded, and a saturated sugar solution was added to the precipitate. The mixture was then centrifuged at 2000 rpm for 10 minutes to separate the oocysts from the remaining debris. The oocyst-rich supernatant was examined under a microscope for the presence of *Cryptosporidium* oocysts. Positive samples were then treated with a 2.5% potassium dichromate solution (Merk, Germany) and incubated at 28°C for 48 hours, with the suspension aerated three times daily to encourage oocyst sporulation (Hendrix and Robinson, 2016).

The oocysts were examined daily for sporocyst formation under a light microscope. The morphological characteristics of the oocysts, including shape, wall structure, color, and sporocyst residue, were recorded. Additionally, micrometry (oocyst length, width, and shape index) was performed using Image Focus software to assist in species identification, following Soulsby's (1986) identification key (Soulsby, 1986).

Statistical Analysis

Data were analyzed using SPSS version 17 (SPSS Inc., Chicago, IL, USA). The Chi-square test was used to determine the association between *Cryptosporidium* infection and various factors, including fecal consistency (diarrhea or no diarrhea), age, sex, and season. A significance level of ($P<0.05$) was considered statistically significant.

Results

Prevalence of *Cryptosporidium* Infection

Of the 560 small ruminants sampled, 67 animals (11.96%) were found to be infected with *Cryptosporidium spp*. The infection rate was significantly ($P<0.05$) higher in sheep (50/280, 17.86%) compared to goats (17/280, 6.07%).

Factors Associated with Infection

The prevalence of *Cryptosporidium* infection varied significantly according to several factors, including fecal consistency, age, sex, and season. As shown in (Table 1), the prevalence of infection was significantly higher in animals with diarrhea (22.63%) compared to those without diarrhea (8.51%) ($P<0.05$).

Table 1: The prevalence of *Cryptosporidium spp.* infection in sheep and goats in Urmia according to feces status, sex, and age

Animals	Feces status		Age (year)		Sex	
	Normal	Diarrhea	≤1	>1	Female	Male
No. of examined sheep	193	87	132	148	134	146
No. of infected sheep (%)	26(13.47)[a]	24(27.59)[b]	36(27.27)[a]	14(9.46)[b]	11(8.21)[a]	39(26.71)[b]
No. of examined goats	230	50	144	136	113	167
No. of infected goats (%)	10(4.35)[a]	7(14.00)[b]	14(9.72)[a]	3(2.21)[b]	3(2.65)[a]	14(8.38)[b]
No. of total examined	423	137	276	284	247	313
No. of total infected (%)	36(8.51)[a]	31(22.63)[b]	50(18.12)[a]	17(5.99)[b]	14(5.67)[a]	53(16.93)[b]

[a] and [b] Statistically significant ($P<0.05$)

Age was another significant factor influencing the prevalence of *Cryptosporidium* infection. Infection was more common in animals ≤1 year old (18.12%) than in older animals (>1 year) (5.99%) (P<0.05).

Sex also played a role in infection rates. Male animals had a significantly higher prevalence of *Cryptosporidium* infection (16.93%) than females (5.67%) (P<0.05).

Seasonality was another important factor influencing infection rates. According to (Table 2) the highest prevalence of *Cryptosporidium* was observed in the spring (23.57%) and summer (15.00%), while the lowest prevalence occurred in autumn (6.43%) and winter (2.86%) (P<0.05).

Table 2: The prevalence of *Cryptosporidium spp.* infection in sheep and goats in Urmia according to season

Animals	Season			
	spring	summer	autumn	winter
No. of examined sheep	70	70	70	70
No. of infected sheep (%)	23(32.86)[a]	16(22.86)[a]	7(10.00)[b]	4(5.71)[b]
No. of examined goats	70	70	70	70
No. of infected goats (%)	10(14.29)[a]	5(7.14)[b]	2(2.86)[c]	0(0.00)[c]
Total examined	140	140	140	140
Total infected (%)	33(23.57)[a]	21(15.00)[b]	9(6.43)[c]	4(2.86)[c]

[a, b] and [c] Statistically significant (P<0.05)

Discussion

Cryptosporidium is a significant parasitic protozoan responsible for cryptosporidiosis in both humans and a wide range of animal species. This protozoan, has demonstrated remarkable adaptability and resilience in various environmental conditions. Over the past few years, numerous studies have been conducted on *Cryptosporidium* across different regions globally (Young, et al, 2014; Ali Ahmed, et al, 2025). However, information regarding the prevalence of *Cryptosporidium* infection in small ruminants, as compared to cattle, remains scarce in Iran (Firoozi, et al, 2019; Haghi, et al, 2020). This represents the first reported evidence of *Cryptosporidium spp.* infection in small ruminants in Urmia, Iran.

The results of this study reveal that cryptosporidiosis is prevalent in sheep and goats in Urmia city, with infection rates of 11.42% and 2.50%, respectively. This demonstrates the widespread presence of *Cryptosporidium* in the region and underscores the potential public health risk associated with animal-to-human transmission. To accurately identify the strain of *Cryptosporidium* involved, molecular characterization using polymerase chain reaction (PCR) is required. Differences in *Cryptosporidium* prevalence between sheep and goats are quite common in epidemiological studies. Greater host susceptibility, flock management practices, and grazing behaviors can be the resions (Hatam-Nahavandi, et al, 2019; Chen, et al, 2022).

The prevalence of *Cryptosporidium* infection in sheep has been reported to vary considerably in both Iran and other regions worldwide, with rates ranging from 1.7% to 85% (Gharekhani, et al, 2014; Sadeghi Dehkordi, et al, 2016; Dalimi and Tahvildar, 2017; Yang, et al, 2021; Chen, et al, 2022; Papanikolopoulou, et al, 2022; Cheng, et al, 2024). In comparison to the previous studies, the prevalence of *Cryptosporidium* infection in sheep reported in this study is lower than that observed in Hamadan (43.04%) and Esfahan (19%), but higher than in Kerman (13.8%), Yazd (12.5%), Tehran (1.7%), Kurdestan (1.6%), Lorestan (5.8%), Mazandaran (4.1%), Fars (6.3%), Mashad (11%), and Bushehr (3.7%) (Fasihi Harandi and Fotouhi, 2008; Vahedi, et al, 2009; Heidari, 2011; Gharekhani, et al, 2014;

Sadeghi Dehkordi, et al, 2016; Shafieyan, et al, 2016; Dalimi and Tahvildar, 2017; Ghorbanzadeh, et al, 2024). A summary of the prevalence of *Cryptosporidium* infection in sheep from other countries is provided in Table 3.

While there is limited data on the prevalence of *Cryptosporidium* infection in goats across different regions of Iran, global reports indicate infection rates ranging from 0.00% to 72.5% (Romero-Salas, et al, 2016; Papanikolopoulou, et al, 2022; Cheng, et al, 2024). In this study, the prevalence of *Cryptosporidium* infection in goats was lower than that reported in Kerman (17.6%) (Fasihi Harandi and Fotouhi, 2008) and Kurdestan (18.86%) (Khezri and Khezri, 2013), but higher than that in Yazd (2%) (Firoozi, et al, 2019). A summary of the prevalence of *Cryptosporidium* infection in goats from other countries is presented in Table 3.

Table 3: The prevalence of *Cryptosporidium* infection in sheep and goats

Country	Sheep	N	Goats	N	Reference
Poland	10.1%	159	0.00%	91	(Majewska, et al, 2000)
Egypt	2.5%	120	-	-	(Mahfouz, et al, 2014)
Iraq	13.3%	45	17.7%	45	(Mahdi and Ali, 2002)
Tunisia	11.2%	89	0.00%	184	(Soltane, et al, 2007)
India	1.8%	55	-	-	(Maurya, et al, 2013)
New Guinea	2.2%	276	4.4%	228	(Koinari, et al, 2014)
Poland	19.2%	234	37.1%	105	(Kaupke, et al, 2017)
Algeria	14.5%	62	8.7%	92	(Baroudi, et al, 2018)
Turkey	-	-	67.9%	112	(Sayin ipek, 2017)
China	-	-	11.4%	604	(Mi, et al, 2014)
Mexico	67.5%	80	72.5%	80	(Romero-Salas, et al, 2016)
Spain	30%	673	30%	184	(Castro-Hermida, et al, 2007)

The variability in the prevalence of cryptosporidiosis across different studies can be attributed to a range of factors, including regional climate conditions, breed differences, the immune status of the animals, environmental factors (e.g., humidity, temperature, rainfall), seasonal variations, laboratory methods and the sanitary conditions of livestock management (Constable, et al, 2017; Ghorbanzadeh, et al, 2024). Therefore, comparisons of prevalence rates of *Cryptosporidium* infection across different regions should be interpreted with caution, as aligning animal characteristics and management conditions across studies is inherently challenging.

To assess the relationship between animal's risk factors and *Cryptosporidium* infection, the prevalence of infection was evaluated in relation to fecal status, age, sex, and season.

In this study, a history of diarrhea in the animals was significantly associated with *Cryptosporidium* infection. This suggests that diarrhea is a common clinical manifestation of *Cryptosporidium* infection in small ruminants and is likely a key indicator for diagnosis. This finding is consistent with the previous studies conducted on sheep and goats by Fasihi Harandi and Fotouhi (2008), Sayin Ipek (2017), Firoozi et al. (2019), Papanikolopoulou et al. (2022), and Ghorbanzadeh et al. (2024). *Cryptosporidium* is a well-established cause of neonatal diarrhea in small ruminants (Constable, et al, 2017). The higher the concentration of *Cryptosporidium* oocysts in the environment, the greater the risk of infection to animals. It is likely that the persistence of diarrhea in newborns, which can last up to two weeks, combined with the large number of oocysts shed into the environment by infected animals, contributes to the spread of *Cryptosporidium*. This infection can rapidly disseminate through direct contact between

animals or through environmental contamination. Preventative measures such as avoiding overcrowding, isolating sick animals during diarrheal outbreaks, disinfecting facilities, and administering anti-protozoal treatments such as Halofuginone lactate and Paromomycin are essential for controlling the spread of infection and minimizing both morbidity and mortality rates in affected herds (Constable, et al, 2017; Thomson, et al, 2017).

Age was another significant factor in this study. Statistical analysis revealed that *Cryptosporidium* infection was more prevalent in animals under 1 year of age. This finding is consistent with the previous research (Fotouhi Ardakani, et al, 2008; Papanikolopoulou, et al, 2022; Ghorbanzadeh, et al, 2024). Younger animals are more susceptible to infection, while older animals develop immunity through repeated exposure, resulting in increased resistance to *Cryptosporidium* (Thomson, et al, 2017).

The higher number of positive cases among male animals may be attributed to their younger age, as males are typically kept for slaughter at a younger age.

In this study, the prevalence of infection in sheep and goats was higher during the spring and summer months. This finding aligns with that of Fasihi Harandi and Fotouhi (2008) and is likely linked to the lambing season, when newborn animals with cryptosporidial diarrhea are show a higher prevalence of cryptosporidial diarrhea, further contributing to the environmental contamination and transmission of *Cryptosporidium* (Fasihi Harandi and Fotouhi, 2008). Additionally, warmer temperatures and higher humidity during the spring and summer months in this region favor the survival and transmission of *Cryptosporidium* oocysts in the environment (King and Monis, 2007; Yang, et al, 2022).

In conclusion, this study provides important insights into the prevalence of *Cryptosporidium* infection in small ruminants in Urmia, Iran. The findings highlight the need for improved control measures to mitigate the spread of cryptosporidiosis, particularly in regions where small ruminant farming is prevalent. Management practices such as improved sanitation, and isolation and treatment of infected animals could help reduce the environmental load of oocysts and limit the transmission of *Cryptosporidium* to both animals and humans. Further studies are needed to explore the molecular epidemiology of *Cryptosporidium* in small ruminants and to identify potential interventions for controlling the disease.

Acknowledgements

The authors wish to express their gratitude to the Research Council of Urmia University, for financial support.

Competing Interests

The authors declare that there is no conflict of interest.

Funding

This study was supported by a grant from the Urmia University, Urmia, Iran.

References

Ali Ahmed, S.A., Boughattas, S., Mahmoudi, M.R., Khan, H., Mamedova, S., Namboodiri, A., Masangkay, F.R., and Karanis, P. (2025). *Cryptosporidium* and cryptosporidiosis: An update of Asian perspectives in humans, water and food, 2015–2025. *CRPVBD*, 8, 1-18.

Baroudi, D., Hakem, A., Adamu, H., Amer, S., Khelef, D., Adjou, K., Dahmani, H., Chen, X., Roellig, D., Feng, Y., and Xiao, L. (2018). Zoonotic *Cryptosporidium* species and subtypes in lambs and goat kids in Algeria. *Parasites and Vectors*, *6*(11), 1-8.

Castro-Hermida, J. A., González-Warleta, M., and Mezo, M. (2007). Natural infection with *Cryptosporidium parvum* and *Giardia duodenalis* in sheep and goats in Galicia (NW, Spain). *Small Ruminant Research*, 72, 96-100.

Chen, Y., Qin, H., Huang, J., Li, J., and Zhang, L. (2022). The global prevalence of *Cryptosporidium* in sheep: a systematic review and meta-analysis. *Parasitology*, *149*(12), 1652-1665.

Cheng, C., Fan, Z., Cheng, D., and Tao, J. (2024). Prevalence of *Cryptosporidium spp.* in Sheep and Goats in Jiangsu, China. *Veterinary Sciences*, *11*(4), 1-8.

Constable, P.D., Hinchcliff, K.W., Done, S.H., and Grunberg, W. (2017). *Veterinary Medicine, A textbook of the diseases of Cattle, Horses, Sheep, Pigs, and Goats.* 11th ed. Philadelphia, Saunders Elsevier, 397-400.

Dalimi, A., and F. Tahvildar (2017). Molecular study on *Cryptosporidium andersoni* strains isolated from sheep based on 18S rRNA gene. *Infection Epidemiology and Microbiology*, *3*(3), 100-103.

Fasihi Harandi, M., and A. R. Fotouhi (2008). *Cryptosporidium* infection of sheep and goats in Kerman: epidemiology and risk factor analysis. *Journal of Veterinary Research*, *63*(1), 47-51.

Firoozi, Z., Sazmand, A., Zahedi, A., Astani, A., Fattahi-Bafghi, A., Kiani-Salmi, N., Ebrahimi, B., Dehghani-Tafti, A., Ryan, U., and Akrami-Mohajeri, F. (2019). Prevalence and genotyping identification of *Cryptosporidium* in adult ruminants in central Iran. *Parasites and Vectors*, *12*(510), 1-6.

Fotouhi Ardakani, R., Fasihi Harandi, M., Solayman Banai, S., Kamyabi, H., Atapour, M., and Sharifi, I. (2008). Epidemiology of *Cryptosporidium* Infection of Cattle in Kerman/Iran and Molecular Genotyping of some Isolates. *Journal of Kerman University of Medical Sciences*, *15*(4), 313-320.

Gerace, E., Presti, V. D. M. L., and Biondo, C. (2019). *Cryptosporidium* Infection: Epidemiology, Pathogenesis, and Differential Diagnosis. *European Journal of Microbiology and Immunology*, 9, 119-123.

Gharekhani, J., Heidari, H., and Youssefi, M. (2014). Prevalence of *Cryptosporidium* infection in sheep in Iran. *Türkiye Parazitoloji Dergisi*, 38, 22-25.

Ghorbanzadeh, M. B., Ebrahimzadeh,E., Azizzadeh,M., and Mohammadi, G. (2023). *Cryptosporidium* infection in lambs: prevalence and potential risk factors in villages of Mashhad city, eastern Iran. *Journal of Zoonotic Diseases*, *8*(1), 436-444.

Haghi, M.M., Khorshidvand, Z., Khazaei,S., Foroughi-Parvar, F., Sarmadian, H., Barati, N., Etemadifar, F., and Ghasemikhah, R. (2020). *Cryptosporidium* animal species in Iran: a systematic review and meta-analysis. *Tropical Medicine and Health*, *48*(97), 1-15.

Hatam-Nahavandi, K., Ahmadpour, E., Carmena, D., Spotin, A., Bangoura, B., and Xiao, L. (2019). *Cryptosporidium* infections in terrestrial ungulates with focus on livestock: a systematic review and meta-analysis. *Parasites and Vectors*, *12*(453): 1-23.

Heidari, H. (2011). Identification of Eimeria species in sheep of Hamadan surburb. *Journal of Veterinary Research*, *66*(2), 165-167.

Hendrix, C. M., and Robinson, E. D. (2016). *Diagnostic Parasitology for Veterinary Technicians*. 5th ed. USA, Mosby Publication, 121-124.

Kabira, M. H. B., Ceylanc, O., Ceylanc, C., Shehatad, A. A., Bandod, H., Essae, M. I., Xuana, X., Sevincc, F., and Katoa, K. (2020). Molecular investigations have identified nearly 40 species and over 50 genotypes, of which *Cryptosporidium hominis* and *Cryptosporidium parvum* are the most prevalent in humans, causing asymptomatic or mild-to-severe gastrointestinal diseases. *Parasitology International*, 79, 1-6.

Kaupke, A., Michalski, M. M., and Rzeżutka, A. (2017). Diversity of *Cryptosporidium* species occurring in sheep and goat breeds reared in Poland. *Parasitology Research*, *116*(3), 871-879.

Khezri, M., and Khezri, O. (2013). The prevalence of *Cryptosporidium spp.* in lambs and goat kids in Kurdistan, Iran. *Veterinary World*, 6, 974-977.

King, B. J., and Monis, P. T. (2007). Critical processes affecting *Cryptosporidium* oocyst survival in the environment. *Parasitology, 134*(3): 309-323.

Koinari, M., Lymbery, A. J., and Ryan, U. M. (2014). *Cryptosporidium* species in sheep and goats from Papua New Guinea. *Experimental Parasitology*, 141, 134-137.

Mahdi, N. K., and Ali, N. H. (2002). Cryptosporidiosis among animal handlers and their livestock in Basrah, Iraq. *East African Medical Journal*, 79, 550-553.

Mahfouz, M. E., Mira, N., and Amer, S. (2014). Prevalence and genotyping of *Cryptosporidium spp*. in farm animals in Egypt. *The Journal of Veterinary Medical Science*, 76, 1569-1575.

Majewska, A. C., Werner, A., Sulima, P., and Luty, T. (2000). Prevalence of *Cryptosporidium* in sheep and goats bred on five farms in west-central region of Poland. *Veterinary Parasitology, 89*(4), 269-275.

Mammeri, M., Cartou, L., Chevillot, A., Thomas, M., Julien, C., Vallée, I., Polack, B., Follet, J., and Adjou, K. T. (2019). First identification of *Cryptosporidium parvum* zoonotic subtype IIaA15G2R1 in diarrheal lambs in France. *Veterinary Parasitology: Regional Studies and Reports*, 18, 1-4.

Maurya, P. S., Rakesh, R. L., Pradeep, B., Kumar, S., Kundu, K., Garg, R., Ram, H., Kumar, A., and Banerjee, P. S. (2013). Prevalence and risk factors associated with *Cryptosporidium spp.* infection in young domestic livestock in India. *Tropical Animal Health and Production*, 45, 941-946.

Mi, R., Wang, X., Huang, Y., Zhou, P., Liu, Y., Chen, Y., Chen, J., Zhu, W., and Chen, Z. (2014). Prevalence, molecular characterization and zoonotic potential of *Cryptosporidium spp*. in goats in Henan and Chongqing, China. *Experimental Parasitology*, 142, 11-16.

Mousavi, H., Dehghanipour, A. H., Ferreira, C. S. S., and Kalantari, Z. (2024). Investigating the Impact of Large Lakes on Local Precipitation: Case Study of Lake Urmia, Iran. *Water, 16(*9): 1-19.

Papanikolopoulou, V., Lafi, S. Q., Papadopoulos, E., Diakou, A., Xiao, L., and Giadinis, N. D. (2022). Risk factors for *Cryptosporidium* infection in small ruminants in northern Greece. *Veterinary Parasitology*, 309, 1-6.

Robertson, L. J. (2009). Giardia and *Cryptosporidium* infections in sheep and goats: a review of the potential for transmission to humans via environmental contamination. *Epidemiology and Infection, 137*(7), 913-921.

Roellig, D. M., and Xiao, L. (2020). *Cryptosporidium* genotyping for epidemiologytracking. *Methods in Molecular Biology*, 2052, 103-116.

Romero-Salas, D., Alvarado-Esquivel, C., Cruz-Romero, A., Aguilar-Domínguez, M., Ibarra-Priego, N., Merino-Charrez, J. O., Pérez de León, A. A., and Hernández-Tinoco, J. (2016). Prevalence of *Cryptosporidium* in small ruminants from Veracruz, Mexico. *BMC Veterinary Research, 12*(14), 1-6.

Sadeghi Dehkordi, Z., Partoandazan, A., and Abdolmaleki, N. (2016). Epidemiology of cryptosporidiosis in sheep of Sanandaj city. *Zoonoses Research, 2*(1), 25-29.

Santin, M. (2020). *Cryptosporidium* and *Giardia* in ruminants. *Veterinary Clinics of North America: Food Animal Practice, 36*(1), 223-238.

Sayin ipek, D. N. (2017). Prevalence and molecular characterisation of *Cryptosporidium spp*. in diarrhoeic pre-weaned goat kids reared under traditional farming system in Diyarbakır, Southeastern Anatolia City, Turkey. *Revue de Medecine Veterinaire*, 168, 229-234.

Shafieyan, H., Alborzi, A., Hamidinejat, H., Tabandeh, M. R., and Hajikolaei, M. R. H. (2016). Prevalence of *cryptosporidium spp.* in ruminants of Lorestan Province, Iran. *Journal of Parasitic Diseases, 40*(4), 1165-1169.

Sima, S., A. Ahmadalipour, A., and Tajrishy, M. (2013). Mapping surface temperature in a hyper-saline lake and investigating the effect of temperature distribution on the lake evaporation. *Remote Sensing of Environment*, 136, 374–385.

Soltane, R., Guyot, K., Dei-Cas, E., and Ayadi, A. (2007). Prevalence of *Cryptosporidium spp.* (Eucoccidiorida: Cryptosporiidae) in seven species of farm animals in Tunisia. *Parasite*, 14, 335-338.

Soulsby, E. J. L. (1986). *Helminthes, Arthropods and Protozoa of Domesticated Animals.* 7th ed. London.UK. Ballier, 808-810.

Thomson, S., Hamilton, A., Hope, J.C., Katzer, F., Mabbott, N.A., Morrison, L., and Innes, E.A. (2017). Bovine cryptosporidiosis: impact, host-parasite interaction and control strategies. *Vet Res*, *48*(42): 1-16.

Vahedi, N., Asl, A., and Saadat, M. (2009). Primary research on gastro-intestinal *cryptosporidium* incidence rate in lambs and calves in Amol city. *Iranian Journal of Veterinary Research, 64*(2), 101-103.

Yang, F., Ma, L., Gou, J., Yao, H., Ren, M., Yang, B., and Lin, Q. (2022). Seasonal distribution of *Cryptosporidium spp.*, Giardia duodenalis and Enterocytozoon bieneusi in Tibetan sheep in Qinghai, China. *Parasit Vectors*, *15*(394): 1-9.

Yang, R., Jacobson, C., Gordon, C., and Ryan, U. (2021). Prevalence of *Cryptosporidium* Infection in Sheep and Goat Flocks in China During 2010-2019: A Systematic Review and Meta-Analysis. *Vector-Borne and Zoonotic Diseases*, *21*(9), 692-706.

Young, I., Smith, B., and Fazil, A.M. (2014). A systematic review and meta-analysis of the effects of extreme weather events and other weather-related variables on *Cryptosporidium* and *Giardia* in fresh surface waters. *Journal of Water and Health*, *13*(1): 1-17.

Received: 22.07.2025
Accepted: 02.06.2026

Vol. 22, No. 2, Summer, 2026, 56-67 *Original Article*
DOI: 10.22055/ivj.2026.579063.2889
Journal Homepage: http://www.ivj.ir/

Molecular Prevalence and Epidemiological Risk Factors of *Bartonella henselae* Infection in Owned and Non-Owned Cats in Ahvaz district, Iran

Sara Hajizadeh[1], Bahman Mosallanejad[2*], Darioush Gharibi[3], Mohammad Razi Jalali[2] and Mahdi Pourmahdi Borujeni[4]

[1] DVSc Student of Small Animal Internal Medicine, Faculty of Veterinary Medicine, Shahid Chamran University of Ahvaz, Ahvaz, Iran
[2] Professor, Department of Clinical Sciences, Faculty of Veterinary Medicine, Shahid Chamran University of Ahvaz, Ahvaz, Iran
[3] Professor, Department of Pathobiology, Faculty of Veterinary Medicine, Shahid Chamran University of Ahvaz, Ahvaz, Iran
[4] Professor, Department of Food Hygiene, Section of Epidemiology, Faculty of Veterinary Medicine, Shahid Chamran University of Ahvaz, Ahvaz, Iran

Received: 19.04.2026 Accepted: 15.06.2026

Abstract

Bartonella henselae (*B. henselae*) is a zoonotic bacterium for which domestic cats serve as the primary reservoir host, maintaining persistent bacteremia and facilitating transmission mainly through the cat flea, *Ctenocephalides felis*. Given the public health significance of feline infection and the limited molecular epidemiological data available from southwestern Iran, this study aimed to determine the molecular prevalence of *B. henselae* and identify independent epidemiological risk factors associated with infection in owned and non-owned cats in Ahvaz, Iran. A cross-sectional study was conducted involving 160 cats, equally distributed between owned and non-owned populations. Adult cats constituted 65% of the study population, whereas juveniles accounted for 35%; 55% were male and 45% were female. Domestic Shorthair cats represented the predominant breed type (51.9%). Whole-blood, oral-swab, and nail samples were collected and analyzed using conventional polymerase chain reaction (PCR) targeting a 414-bp fragment of the htrA , followed by sequencing confirmation of representative amplicons. Associations between potential risk factors and infection were assessed using univariable and multivariable logistic regression analyses, and population attributable fractions (PAFs) were estimated. *B. henselae* DNA was detected in 16.9% of cats (95% CI: 11.4–23.7). The prevalence of infection was significantly higher in non-owned cats (26.3%) than in owned cats (7.5%) (OR = 4.39, 95% CI: 1.66–11.58; $p = 0.002$). Population attributable fraction analysis indicated that 67% and 36% of infections were attributable to outdoor exposure and flea infestation, respectively. These findings demonstrate that environmental exposure and ectoparasite infestation are major determinants of *B. henselae* infection, highlighting the importance of effective flea control and restricting outdoor access to reduce the burden of infection and mitigate zoonotic risk.

Key words: *Bartonella henselae*; Cats; Molecular prevalence; Epidemiology; Zoonosis

Introduction

Bartonella henselae (*B. henselae*) is a globally distributed zoonotic bacterium of considerable veterinary and public health importance. It is a small, fastidious, Gram-negative, facultative intracellular bacterium belonging to the genus *Bartonella* within the family *Bartonellaceae*. Members of this genus are vector-borne pathogens that

* **Corresponding Author**: Bahman Mosallanejad, Professor, Department of Clinical Sciences, Faculty of Veterinary Medicine, Shahid Chamran University of Ahvaz, Ahvaz, Iran
E-mail: bmosallanejad@scu.ac.ir

infect a wide range of mammalian hosts and are characterized by their ability to invade erythrocytes and endothelial cells, resulting in persistent bloodstream infections (Osikowicz et al, 2021).

Domestic cats serve as the primary reservoir host, maintaining long-term intraerythrocytic bacteremia with limited or no clinical manifestations. Transmission among cats occurs primarily through hematophagous arthropods, particularly the cat flea, *Ctenocephalides felis*, which plays a central role in maintaining the bacterium within feline populations (Mazurek et al, 2020). Human infection may result in cat scratch disease and, in susceptible individuals, more severe systemic manifestations (Yakubovsky et al, 2026). The close association between cats and humans, particularly in urban environments, underscores the need to better understand infection dynamics within feline reservoirs.

The reported prevalence of *B. henselae* infection in cats varies widely across geographic regions, reflecting differences in climate, vector ecology, population structure, and management practices (Zarea et al, 2023). Studies conducted in Europe, Asia, and the Americas have identified several epidemiological factors associated with an increased risk of infection. Outdoor access has consistently been linked to higher infection rates because of increased exposure to vectors and contact with infected cats (Stepanić et al, 2024; Lopes et al, 2026). Stray or free-roaming status is frequently associated with greater environmental exposure and reduced access to preventive care (Sepúlveda-García et al, 2023). Flea infestation remains the most biologically plausible and consistently reported risk factor (Kokkinaki et al., 2022). Age has also been implicated, with adult cats often exhibiting higher prevalence, likely reflecting cumulative exposure over time (Álvarez-Fernández et al, 2022; Ebani et al, 2021). Additional studies from Europe and North America have further documented the circulation of *Bartonella* spp. in domestic cat populations (Mazurek et al, 2020; Osikowicz et al, 2021).

In the Middle East, molecular evidence of *B. henselae* infection has been reported in cats and humans in Egypt (Sayed et al, 2022). In Iran, data on feline bartonellosis remain limited. An earlier investigation conducted in Tehran confirmed the presence of *B. henselae* among domestic cats (Oskoueizadeh et al, 2008). Furthermore, a study conducted in Ahvaz identified *B. henselae* infection in dogs, suggesting the possibility of shared transmission cycles within the region (Oskoueizadeh et al, 2013). However, information from southwestern Iran remains scarce. Ahvaz is characterized by a hot climate and prolonged warm seasons that may favor vector survival and reproduction. Urban expansion, a substantial stray cat population, and variable standards of preventive veterinary care may further influence transmission dynamics. Molecular epidemiological studies investigating infection prevalence and associated risk factors in this region are therefore warranted.

This study aimed to determine the molecular prevalence of *B. henselae* infection in owned and non-owned cats in Ahvaz, Iran, and to identify independent epidemiological risk factors associated with infection. By focusing on molecular detection and the analytical assessment of demographic and management-related variables, this investigation sought to clarify the epidemiological drivers of infection within an urban feline population in southwestern Iran.

Materials and Methods

Study Design, Population, and Ethical Approval

This cross-sectional study was conducted between March 2024 and March 2025 in Ahvaz, Khuzestan Province, Iran. A total of 160 domestic cats were enrolled. The sampling framework was designed to

ensure equal representation of owned and non-owned animals, comprising 80 owned cats presented to the Veterinary Teaching Hospital of Shahid Chamran University of Ahvaz and 80 non-owned cats. The non-owned group included 60 free-roaming stray cats captured humanely within urban districts and 20 cats housed in municipal shelters.

Owned cats were defined as animals living under direct human care with an identifiable caretaker. These were further categorized according to management conditions as indoor-only, referring to cats permanently confined within the household environment, and indoor-outdoor, referring to cats with regular or intermittent access to external environments. Non-owned cats were classified as stray when free-roaming without permanent human guardianship and as shelter-housed when maintained in organized municipal or private shelter facilities.

All animals underwent a complete physical examination prior to sampling. Cats showed no clinical signs suggestive of severe systemic or acute infectious disease and were considered clinically stable at the time of sampling. Inclusion criteria required apparent clinical stability and the absence of severe systemic disease requiring emergency intervention. No animals were excluded based on sex, breed, or age.

All procedures were conducted in accordance with institutional guidelines for animal care and use. The study protocol was reviewed and approved by the Institutional Animal Care and Use Committee of Shahid Chamran University of Ahvaz. Written informed consent was obtained from owners prior to enrollment of privately owned cats. Sampling of stray and shelter cats was performed under the supervision of municipal veterinary authorities, ensuring minimal stress and humane handling.

For each cat, demographic and management data were recorded using a standardized questionnaire designed by the research team. For owned cats, information was obtained through structured owner interviews. For non-owned cats, data were obtained through direct assessment and shelter records when available.

Age was categorized as juvenile (younger than 12 months) and adult (12 months of age or older), based on dental examination and available history. Sex was recorded as male or female. Breed was classified as Domestic Shorthair, Domestic Longhair, or purebred according to phenotypic characteristics and owner reports when available.

Outdoor access was coded as a binary variable and defined as present when a cat had any degree of access to outdoor environments and absent when it was permanently confined indoors. Flea infestation was assessed through direct visual inspection and combing using a fine-toothed flea comb (Hauptner Herberholz, Solingen, Germany). The presence of live fleas or flea dirt was recorded as positive. Tick infestation was evaluated by systematic palpation and visual examination of the entire body surface and coded as positive when at least one tick was detected.

Dietary regimen was categorized into three groups: commercial dry food, home-cooked food, and raw diet or active hunting behavior. History of systemic illness within the previous six months was recorded as present or absent based on owner reports or shelter documentation. Antibiotic administration during the preceding three months was documented and coded as yes or no.

All categorical variables were numerically coded prior to statistical analysis. Binary variables were coded as 1 for presence and 0 for absence. Multilevel categorical variables were transformed into dummy variables for inclusion in regression modeling where appropriate.

From each enrolled cat, three biological samples were collected under aseptic conditions, resulting in a total of 480 samples. Whole blood was obtained via

cephalic or saphenous venipuncture using sterile disposable needles and syringes and collected into ethylenediaminetetraacetic acid (EDTA) anticoagulant tubes (Teif Azma Tajhiz Company, Tehran, Iran). These peripheral veins were selected to minimize invasiveness and animal discomfort, particularly in non-owned and stray cats where restraint is challenging. Approximately 1.5–2.0 mL of blood was collected from each animal.

Oral samples were collected using sterile nylon flocked swabs (Zist Fanavaran Mehr Company, Tehran, Iran). The swab was gently rotated along the gingival margin and buccal mucosa for approximately 10 seconds and then placed into sterile transport tubes.

Nail samples consisted of freshly clipped distal claw tips obtained using sterile stainless-steel nail clippers (Rahpooyan Dampezeshki Company, Tehran, Iran). Each clipping was transferred into a sterile 1.5-mL microcentrifuge tube (Arvin Tajhiz Azma Company, Tehran, Iran).

All samples were transported to the Molecular Microbiology Laboratory within two hours of collection in insulated containers and stored at −20 °C until DNA extraction.

Genomic DNA was extracted from whole blood, oral swab, and nail samples using a silica membrane based commercial DNA extraction kit (Sinacolon, Tehran, Iran) according to the manufacturer's standard instructions. Because of the different physical and biological characteristics of the sample types, sample specific pretreatment protocols were applied as follows before proceeding with the main extraction procedure.

For whole blood samples (100 microL), samples were mixed directly with lysis buffer and Proteinase K according to the standard kit protocol without any additional pretreatment.

For oral swab samples, each swab was first immersed in 200 microL of sterile distilled water and incubated at 55 degrees Celsius for 30 minutes with vortexing every 5 minutes to facilitate detachment of cellular material. Thereafter, 100 microL of the resulting suspension was used for DNA extraction according to the same kit protocol.

For nail samples, nail clippings (approximately 10 to 20 mg) were first pulverized using a sterile mortar and pestle under liquid nitrogen to obtain a fine powder. The powdered tissue was then incubated with 40 microL of Proteinase K instead of the standard 20 microL, along with 200 microL of lysis buffer, at 56 degrees Celsius for 1 hour with intermittent shaking before proceeding with the standard kit protocol.

After these pretreatment steps, the extraction protocol continued according to the manufacturer's instructions. Briefly, samples were lysed using lysis buffer and Proteinase K, followed by incubation and binding of DNA to a silica membrane column. After sequential washing steps to remove impurities, purified DNA was eluted using 50 microL of elution buffer.

DNA concentration and purity were assessed spectrophotometrically using a microvolume spectrophotometer (Parto Tandis Company, Tehran, Iran). Extracted DNA was stored at minus 20 degrees Celsius until amplification.

Detection of Bartonella henselae DNA was performed by conventional polymerase chain reaction (PCR) targeting a 414 bp fragment of the htrA , as previously described (Diniz et al, 2007; Anderson and Neuman, 2000). All extraction kits used in this study were obtained from Sinacolon Company (Tehran, Iran).

Oligonucleotide primers were synthesized commercially by Sinacolon Company (Tehran, Iran). The primer sequences were as follows: forward primer BartF (5' to 3'): GATTCAATTGGTTTGAAGGAGGCT and reverse primer BartR (5' to 3'): TCACATCACCAGGACGTATTC.

Each reaction was carried out in a total volume of 25 microL containing 12.5 microL of 2 times PCR Master Mix (BioTeb Company, Tehran, Iran), 0.5 microM of each primer, 5 microL of template DNA, and nuclease free water (Parto Tandis Company, Tehran, Iran). Amplification was performed in a thermal cycler (BIO RAD T100, Bio Rad Laboratories, USA). Cycling conditions consisted of an initial denaturation at 95 degrees Celsius for 5 minutes, followed by 35 cycles of denaturation at 94 degrees Celsius for 30 seconds, annealing at 58 degrees Celsius for 30 seconds, and extension at 72 degrees Celsius for 45 seconds, with a final extension step at 72 degrees Celsius for 7 minutes.

A reference strain of B. henselae (ATCC 49793) was obtained from the Faculty of Veterinary Medicine, University of Tehran, Tehran, Iran, and served as a positive control in each run. Sterile nuclease free water was used as a negative control. Amplified products were separated by electrophoresis on 1.5 percent agarose gels stained with GelRed and visualized under ultraviolet illumination using a gel documentation system (Ariya Mabna Tajhiz Company, Tehran, Iran).

Five representative positive amplicons exhibiting clear and distinct bands were selected for sequencing (Figure 1). PCR products were purified using a commercial purification kit (Codon Genetics Company, Tehran, Iran). Bidirectional Sanger sequencing was performed by a commercial sequencing provider (Codon Genetics Company, Tehran, Iran).

Raw chromatograms were examined and edited using sequence analysis software (Technelysium Pty Ltd, South Brisbane, Australia). Consensus sequences were generated and compared with reference sequences available in the National Center for Biotechnology Information (NCBI) database using the BLASTn algorithm. All analyzed sequences demonstrated 99–100% nucleotide identity to reference *B. henselae* sequences, confirming species-level identification. The validated sequences were submitted to GenBank, and accession numbers were obtained.

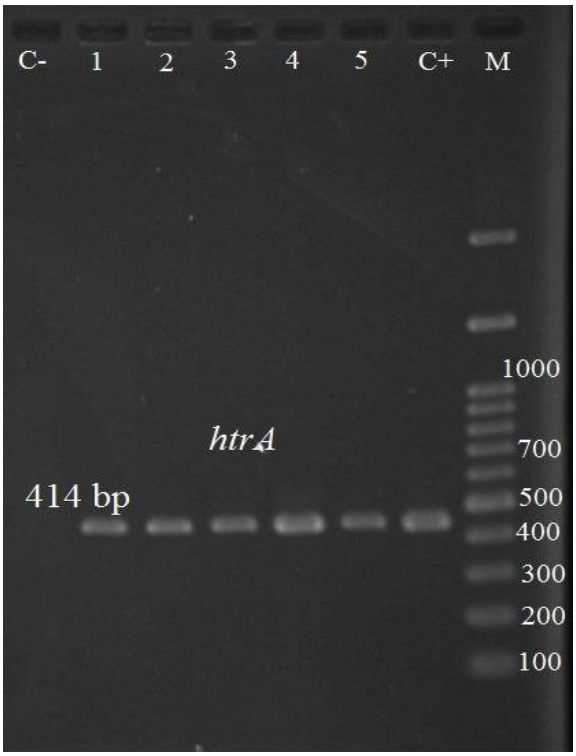

Figure 1: Representative agarose gel electrophoresis of PCR products showing the expected 414-bp amplicon. M: 100-bp DNA ladder; C−: negative control; C+: positive control; lanes 1–5: representative positive clinical samples.

Statistical analyses were performed using IBM SPSS Statistics version 26. Molecular prevalence was calculated as the proportion of PCR-positive animals among the total examined population, and exact binomial 95% confidence intervals were computed. Associations between categorical variables and PCR status were initially evaluated using the chi-square and Fisher's exact test when expected cell counts were less than five, and crude odds ratios with corresponding 95% confidence intervals were calculated.

Variables with *p*-values < 0.10 in univariable analyses were considered eligible for inclusion in the multivariable logistic regression model, and a backward stepwise procedure was applied to construct

the final model while maintaining an appropriate events-per-variable ratio. Multicollinearity was assessed using variance inflation factor and tolerance statistics, and highly correlated variables were not entered simultaneously into the model. Adjusted odds ratios with 95% confidence intervals were reported.

Model calibration was evaluated using the Hosmer–Lemeshow goodness-of-fit test, and explanatory performance was assessed using Nagelkerke R^2. Population attributable fractions (PAFs) were calculated for significant independent risk factors according to the formula PAF = Pe (AOR − 1) / [Pe (AOR − 1) + 1], where Pe represents the prevalence of exposure in the study population. Statistical significance was defined at a two-sided alpha level of 0.05.

Results

Population Characteristics

A total of 160 cats were included in the study, comprising 80 owned and 80 non-owned animals. The demographic and management characteristics of the study population are presented in Table 1. Adult cats represented 65.0% (104/160) of the population, whereas 35.0% (56/160) were classified as juveniles. The sex distribution was balanced, with 55.0% males (88/160) and 45.0% females (72/160). Domestic Shorthair cats were the most common breed type, accounting for 51.9% (83/160) of the study population, followed by purebred cats (31.2%; 50/160) and Domestic Longhair cats (16.9%; 27/160).

With respect to housing conditions, 32.5% (52/160) of cats were kept exclusively indoors, 17.5% (28/160) were classified as indoor-outdoor, 12.5% (20/160) were shelter-housed, and 37.5% (60/160) were classified as stray. Overall, 67.5% (108/160) of cats had some degree of outdoor access. Flea infestation was detected in 28.7% (46/160) of animals, whereas tick infestation was uncommon, occurring in only 1.9% (3/160) of cats. Approximately 27.5% (44/160) of cats were reported to consume a raw diet or engage in hunting behavior.

Molecular Prevalence of *B. henselae*

Molecular analysis identified 27 PCR-positive animals among the 160 cats examined, resulting in an overall prevalence of 16.9% (27/160; 95% CI: 11.4–23.7) (Table 2).

Table 1: Baseline Characteristics of the Study Population (n = 160)

Variable	Category	n (%)
Age	Juvenile (<12 months)	56 (35.0)
	Adult (≥12 months)	104 (65.0)
Sex	Male	88 (55.0)
	Female	72 (45.0)
Breed	Domestic Shorthair	83 (51.9)
	Domestic Longhair	27 (16.9)
	Purebred	50 (31.2)
Ownership status	Owned	80 (50.0)
	Non-owned	80 (50.0)
Housing category	Indoor-only	52 (32.5)
	Indoor–outdoor	28 (17.5)
	Shelter-housed	20 (12.5)
	Stray	60 (37.5)
Outdoor access	Yes	108 (67.5)
	No	52 (32.5)
Flea infestation	Positive	46 (28.7)
	Negative	114 (71.3)
Tick infestation	Positive	3 (1.9)
	Negative	157 (98.1)
Diet	Commercial dry food	74 (46.3)
	Home-cooked food	42 (26.2)
	Raw/hunting	44 (27.5)
Recent illness (6 months)	Yes	38 (23.7)
	No	122 (76.3)
Antibiotic use (3 months)	Yes	29 (18.1)
	No	131 (81.9)

Note: Values are presented as number and percentage of total population. Flea infestation was defined as detection of live fleas or flea dirt during clinical examination.

Table 2: Molecular Detection of *Bartonella henselae* by PCR

A. Animal-Level Prevalence

PCR Status	n	%	95% CI
Positive	27	16.9	11.4–23.7
Negative	133	83.1	—
Total	160	100	—

B. PCR Positivity by Sample Type

Sample Type	Positive (n)	Total (n)	% Positive
Blood	27	160	16.9
Saliva	0	160	0
Nail	3	160	1.9

Note: PCR targeted a 414 bp fragment of the htrA. Confidence intervals were calculated using the exact binomial method. All PCR-positive animals yielded detectable *Bartonella henselae* DNA in whole blood samples.

When evaluated by sample type, all positive animals were detected in whole-blood samples, corresponding to a blood positivity rate of 16.9% (27/160). No cat tested positive exclusively in oral-swab samples without concurrent blood positivity. Specifically, none of the 160 oral-swab samples were PCR-positive. Three nail samples (3/160; 1.9%) tested positive; however, all corresponding animals were also positive in blood samples. These findings indicate that whole blood was the most sensitive sample type for molecular detection in this study (Table 2).

Stratified prevalence according to housing category is illustrated in Figure 2. The highest prevalence was observed among stray cats (31.7%; 19/60), followed by indoor-outdoor cats (17.9%; 5/28) and shelter-housed cats (10.0%; 2/20). Indoor-only cats exhibited the lowest prevalence (1.9%; 1/52). When stratified by ownership status, infection prevalence was significantly higher in non-owned cats than in owned cats. Among owned cats, 6 of 80 animals (7.5%) were PCR-positive, whereas 21 of 80 non-owned cats (26.3%) tested positive. This difference was statistically significant (OR = 4.39, 95% CI: 1.66–11.58; p = 0.002).

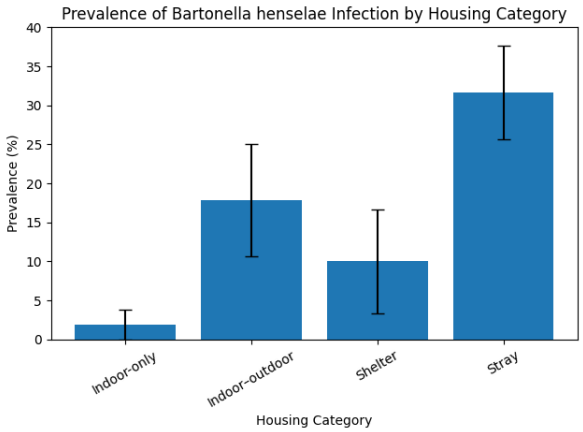

Figure 2: Prevalence of molecularly confirmed *Bartonella henselae* infection among cats according to housing category in Ahvaz, Iran. Bars represent the proportion of PCR-positive animals within each group. Error bars indicate the standard error of the proportion. The highest prevalence was observed in stray cats, followed by indoor–outdoor and shelter-housed cats, whereas indoor-only cats showed the lowest prevalence.

Univariable Analysis of Risk Factors

The results of the univariable analysis are presented in Table 3. Adult cats exhibited a significantly higher prevalence of infection than juveniles (21.2%; 22/104 versus 8.9%; 5/56), corresponding to a crude odds ratio of 2.75 (95% CI: 1.01–7.46; p = 0.048). Sex was not significantly associated with infection status.

Table 3: Univariate Analysis of Risk Factors Associated with PCR Positivity (n = 160)

Variable	Category	Positive/Total	Prevalence (%)	Crude OR	95% CI	p-value
Ownership status	Owned	6/80	7.5	1 (Ref)	—	—
	Non-owned	21/80	26.3	4.39	1.66–11.58	0.002
Age	Juvenile	5/56	8.9	1 (Ref)	—	—
	Adult	22/104	21.2	2.75	1.01–7.46	0.048
Sex	Female	11/72	15.3	1 (Ref)	—	—
	Male	16/88	18.2	1.23	0.53–2.87	0.52
Flea infestation	Negative	6/114	5.3	1 (Ref)	—	—
	Positive	21/46	45.7	15.12	5.38–42.47	<0.001
Tick infestation	Negative	26/157	16.6	1 (Ref)	—	—
	Positive	1/3	33.3	2.53	0.21–29.9	0.34
Outdoor access	No	1/52	1.9	1 (Ref)	—	—
	Yes	26/108	24.1	16.17	2.11–123.8	<0.001
Diet	Commercial dry	8/74	10.8	1 (Ref)	—	—
	Home-cooked	5/42	11.9	1.12	0.34–3.70	0.85
	Raw/hunting	14/44	31.8	3.83	1.48–9.94	0.018

Note: Crude odds ratios were calculated using binary logistic regression. Chi-square or Fisher exact tests were applied as appropriate. Ref indicates reference category.

Outdoor access was strongly associated with PCR positivity. Cats with outdoor access had a prevalence of 24.1% (26/108), compared with 1.9% (1/52) among indoor-confined cats, yielding a crude odds ratio of 16.17 (95% CI: 2.11–123.8; $p < 0.001$).

Flea infestation was also strongly associated with infection. Cats infested with fleas had a prevalence of 45.7% (21/46), compared with 5.3% (6/114) among flea-negative animals, corresponding to a crude odds ratio of 15.12 (95% CI: 5.38–42.47; $p < 0.001$).

Dietary regimen was significantly associated with infection status. Cats consuming a raw diet or engaging in hunting behavior showed a prevalence of 31.8% (14/44), which was significantly higher than that observed in cats fed commercial dry food (10.8%; 8/74), corresponding to a crude odds ratio of 3.83 (95% CI: 1.48–9.94; $p = 0.018$). Tick infestation (1/3; 33.3%) and recent antibiotic administration were not significantly associated with PCR positivity.

Multivariable Logistic Regression

Variables with p-values < 0.10 in the univariable analysis were entered into the multivariable logistic regression model. In the final model, outdoor access and flea infestation remained independently associated with *B. henselae* infection (Table 4).

Table 4: Multivariable Logistic Regression Model for Independent Risk Factors

Variable	Adjusted OR	95% CI	p-value
Outdoor access	4.05	1.37–11.98	0.011
Flea infestation	2.94	1.04–8.28	0.042
Adult age	2.18	0.90–5.26	0.082

Note: Model fit was acceptable, as indicated by a non-significant Hosmer–Lemeshow test ($p = 0.73$). The model showed moderate explanatory power with a Nagelkerke R^2 of 0.34, and the −2 log likelihood was 78.6. Variables with $p < 0.10$ in univariate analysis were entered into the multivariable model using backward stepwise elimination, and multicollinearity was assessed prior to model construction.

Outdoor access was the strongest independent predictor of infection, with an adjusted odds ratio of 4.05 (95% CI: 1.37–11.98; $p = 0.011$). Flea infestation was also independently associated with PCR positivity (AOR = 2.94, 95% CI: 1.04–8.28; $p = 0.042$). Although adult age was associated with increased odds of infection, the association did not reach statistical significance in the multivariable model (AOR = 2.18, 95% CI: 0.90–5.26; $p = 0.082$).

Model fit was acceptable, as indicated by a non-significant Hosmer–Lemeshow goodness-of-fit test (p = 0.73). The model demonstrated moderate explanatory power, with a Nagelkerke R^2 value of 0.34. The −2 log-likelihood value was 78.6.

Population Attributable Fractions

Population attributable fractions (PAFs) for the independent risk factors are presented in Table 5. Based on the adjusted odds ratios and exposure prevalence, 67% of infections, corresponding to approximately 18 of the 27 identified cases, were attributable to outdoor access. Flea infestation accounted for an estimated 36% of infections, corresponding to approximately 10 cases. Because these exposures partially overlapped within the study population, the estimated PAFs are not additive and should not be interpreted as representing independent or mutually exclusive proportions of the total infection burden.

Table 5: Population Attributable Fraction for Independent Risk Factors

Risk Factor	Adjusted OR	Exposure Prevalence (Pe)	PAF	Attributable (%)
Outdoor access	4.05	0.675	0.67	67
Flea infestation	2.94	0.287	0.36	36

Note: Population attributable fraction was calculated using the formula PAF = Pe (AOR − 1) / [Pe (AOR − 1) + 1], where Pe represents exposure prevalence in the total study population. Values indicate the proportion of infection cases theoretically preventable if the exposure were eliminated, assuming a causal relationship.

Discussion

The present study identified a molecular prevalence of *Bartonella henselae* infection of 16.9% among cats in Ahvaz, Iran, with significantly higher prevalence observed in non-owned cats than in owned animals. This prevalence can be considered moderate to high within the global spectrum of feline bartonellosis (Zarea et al, 2023). Outdoor access emerged as the strongest independent predictor of infection, followed by flea infestation, whereas adult age showed a borderline association after adjustment. These findings indicate that environmental exposure and vector contact are the principal epidemiological drivers of infection in this urban feline population, consistent with the previous epidemiological observations in domestic cats (Kokkinaki et al, 2022; Sepúlveda-García et al, 2023).

Comparable findings have been reported in the previous studies conducted in Iran. Oskoueizadeh et al, (2008) investigated the prevalence of *B. henselae* infection in domestic cats from Tehran and reported a seroprevalence of 23% (23/100 cats) using indirect fluorescent antibody testing, although *B. henselae* was not isolated by blood culture. Their study also demonstrated significantly higher seropositivity in outdoor cats (21/50, 42%) than in indoor cats (2/50, 4%). Although the epidemiological context differed from that of the present investigation because serology and molecular detection measure different aspects of infection, their findings similarly highlighted the circulation of *B. henselae* among cats in Iranian metropolitan areas. In comparison, the molecular prevalence observed in the present study (16.9%) appears consistent with the exposure level reported in Tehran, considering that molecular detection identifies active bacteremia whereas serology reflects previous exposure. The observed differences may also reflect regional ecological variation, including climatic conditions, flea abundance, and the larger proportion of free-roaming cats included in the samples of Ahvaz population.

Furthermore, the potential role of dogs in the transmission cycle of *B. henselae* in Ahvaz merits consideration. A previous cross-sectional study conducted in Ahvaz reported the presence of *B. henselae* DNA in dogs using PCR (Oskoueizadeh et al, 2013), indicating that dogs in this region can also become infected. Although dogs are not considered primary reservoirs of *B.*

henselae and are generally regarded as incidental hosts (Mazurek et al., 2020; Osikowicz et al, 2021), their possible role in maintaining the bacterium within urban environments, particularly through shared arthropod vectors such as fleas and ticks, cannot be excluded. Given that stray dogs and cats often occupy overlapping ecological niches and may be exposed to the same flea populations, cross-species transmission remains biologically plausible. However, further studies incorporating molecular characterization of isolates and investigations of vector-borne transmission dynamics are required to clarify whether dogs contribute meaningfully to the epidemiology of feline bartonellosis in this region.

Compared with the recent European studies, the prevalence observed in Ahvaz exceeds several reported estimates. Stepanić et al, (2024) in Croatia documented a molecular prevalence of approximately 12%, with outdoor lifestyle and stray status identified as significant risk factors. Similarly, Lopes et al, (2026) in Portugal reported prevalence estimates ranging from 8% to 11% among apparently healthy cats. In both settings, outdoor exposure was associated with infection, although the overall prevalence was lower than that observed in the present study. Additional European investigations have reported similar epidemiological patterns linking environmental exposure and ectoparasite infestation with infection risk (Álvarez-Fernández et al, 2022; Ebani et al, 2021; Mazurek et al, 2020). These differences may reflect climatic variation, as Mediterranean and Central European regions experience shorter periods of vector activity than the prolonged warm conditions characteristic of southwestern Iran.

Globally, the meta-analysis conducted by Zarea et al, (2023) estimated a pooled molecular prevalence of approximately 12% among cats, with higher rates reported in free-roaming populations. The prevalence of 16.9% observed in Ahvaz exceeds the pooled global estimate and approaches the upper range reported for stray cat populations worldwide. In the Middle East, Sayed et al, (2022) reported a molecular prevalence of 10.8% in Egypt, which is lower than that observed in the present study, although similar associations with outdoor exposure were identified. In South America, Sepúlveda-García et al, (2023) reported prevalence estimates ranging from 14% to 18% in Chile, closely approximating the findings reported here. Collectively, these comparisons suggest that the infection burden in Ahvaz is comparable to that of high-transmission regions but exceeds that reported in many recent European studies, potentially because of climatic conditions that favor flea survival and sustained transmission cycles.

The biological plausibility of the identified risk factors further strengthens the validity of these findings. Outdoor access increases opportunities for contact with infected conspecifics and exposure to flea vectors. Free-roaming cats are more likely to encounter ectoparasites and engage in aggressive interactions that may facilitate transmission. Flea infestation, which remained independently associated with infection after adjustment, reflects the established role of *Ctenocephalides felis* as the principal vector of *B. henselae* (Osikowicz et al, 2021). Adult age was associated with increased odds of infection, consistent with cumulative exposure over time, although this association did not retain statistical significance in the multivariable model. Similar age-related patterns have been reported in Croatia and Chile, suggesting that repeated environmental exposure, rather than intrinsic susceptibility, accounts for this effect (Stepanić et al, 2024; Sepúlveda-García et al, 2023).

From a public health perspective, these findings highlight the importance of the stray cat population as a potential urban reservoir of infection. The markedly higher

prevalence observed among free-roaming animals suggests that uncontrolled outdoor populations may sustain transmission within urban environments. Given the zoonotic nature of *B. henselae*, close contact with infected cats, particularly those lacking routine ectoparasite control, may increase the risk of cat scratch disease and other clinical manifestations associated with this pathogen (Yakubovsky et al, 2026). Population attributable fraction analysis indicated that 67% of infections could theoretically be attributed to outdoor exposure and 36% to flea infestation, underscoring the potential impact of targeted preventive interventions. Routine flea control programs, responsible ownership practices, and restriction of uncontrolled outdoor access may substantially reduce infection burden, consistent with recent molecular evidence of vector-borne pathogens in free-roaming companion animals in Iran (Hatooth et al., 2025).

Several limitations should be acknowledged. First, the cross-sectional design precludes causal inference and does not permit assessment of temporal relationships between exposure and infection. Second, the study was conducted in a single metropolitan area, which may limit the generalizability of the findings to other ecological settings within Iran. Third, molecular detection identifies active bacteremia but does not capture previous exposure or serological status. In addition, co-infections with other vector-borne pathogens were not investigated and therefore cannot be excluded. Furthermore, although the sample size was adequate for multivariable analysis, the number of positive animals was relatively modest, which may have reduced the precision of certain estimates. Despite these limitations, the study provides robust molecular and epidemiological evidence that environmental exposure and vector infestation are central determinants of *B. henselae* infection in this urban feline population.

In conclusion, this study demonstrates that *Bartonella henselae* infection occurs at a moderate to high molecular prevalence among owned and non-owned cats in Ahvaz, Iran, with environmental exposure emerging as the principal determinant of infection. Outdoor access and flea infestation were independently associated with bacteremia and accounted for a substantial proportion of the population-level infection burden. These findings reinforce the central role of vector-mediated transmission and unrestricted roaming behavior in sustaining urban transmission cycles. Implementation of routine ectoparasite control measures and reduction of uncontrolled outdoor exposure may substantially decrease infection prevalence and mitigate potential zoonotic risk.

Ethics Approval and Consent to Participate

All procedures involving animals were conducted in accordance with institutional guidelines for animal care and use. The study protocol was reviewed and approved by the Institutional Animal Care and Use Committee of Shahid Chamran University of Ahvaz.Written informed consent was obtained from owners prior to enrollment of privately owned cats.

Acknowledgments

The authors thank the staff of the Veterinary Teaching Hospital of Shahid Chamran University of Ahvaz and the municipal veterinary authorities for their assistance with sampling and data collection.

Conflict of Interest

The authors declare that they have no competing interests.

Funding

This research received no external funding.

References

Álvarez-Fernández, A., Maggi, R., Martín-Valls, G. E., Baxarias, M., Breitschwerdt, E. B., & Solano-Gallego, L. (2022). Prospective serological and molecular cross-sectional study focusing on *Bartonella* and other blood-borne organisms in cats from Catalonia (Spain). *Parasites & Vectors*, *15*(1), 6.

Anderson, B. E., & Neuman, M. A. (1997). *Bartonella* spp. as emerging human pathogens. *Clinical Microbiology Reviews*, *10*(2), 203–219.

Diniz, P. P. V. P., Maggi, R. G., Schwartz, D. S., Cadenas, M. B., Bradley, J. M., Hegarty, B., & Breitschwerdt, E. B. (2007). Canine bartonellosis: serological and molecular prevalence in Brazil and evidence of co-infection with *Bartonella henselae* and *Bartonella vinsonii* subsp. *berkhoffii*. *Veterinary Research*, *38*(5), 697–710.

Ebani, V. V., Nardoni, S., Maestrini, M., Perrucci, S., & Mancianti, F. (2021). Serological survey on the occurrence of *Rickettsia* spp., *Neospora caninum*, *Bartonella henselae* and *Toxoplasma gondii* in cats from Tuscany (Central Italy). *Animals*, *11*(6), 1842.

Hatooth, A. H., Tavassoli, M., Yakhchali, M., & Al-Abedi, G. J. K. (2025). Molecular detection of tick-borne blood parasites (Theileria, Babesia, and Anaplasma) in stray dogs using Nested PCR. *Iranian Veterinary Journal*, *21*(3), 22-29.

Kokkinaki, K. C. G., Saridomichelakis, M. N., Skampardonis, V., Mataragka, A., Ikonomopoulos, J., Leontides, L., & Xenoulis, P. G. (2022). Prevalence and risk factors for *Bartonella* spp. and haemoplasma infections in cats from Greece. *Veterinary Sciences*, *9*(7), 337.

Lopes, R., Carvalho, H. L., Sampaio, F., Fernandes, C., Santos, C. C., Sousa, C., Silva, A. R., Sousa, R., Silva, H., Lopes, A. P., Duarte, E. L., Cardoso, L., & Coelho, A. C. (2026). Molecular detection of *Bartonella henselae* in healthy cats from Portugal (2015–2025): One Health context and implications for transfusion medicine. *Pathogens*, *15*(2), 131.

Mazurek, Ł., Carbonero, A., Skrzypczak, M., Winiarczyk, S., & Adaszek, Ł. (2020). Epizootic situation of feline *Bartonella* infection in eastern Poland. *Journal of Veterinary Research*, *64*(1), 79–84.

Oskoueizadeh, K., Mosallanejad, B., Seyfiabad Shapouri, M. R., & Sanaei, K. (2013). A cross sectional study on *Bartonella henselae* infection in dogs in Ahvaz district by PCR. *Iranian Veterinary Journal*, *9*(3), 5–12.

Oskoueizadeh, K., Zahraei, S. M., Ale, D. S., Majlesi, B., Ghafari, H., Eshrafi, T. I., & Ali, Y. A. (2008). Study on the prevalence of *Bartonella henselae* infection in domestic cats from Tehran. *Journal of Veterinary Research*, *63*(4), 183–189.

Osikowicz, L. M., Horiuchi, K., Goodrich, I., Breitschwerdt, E. B., Chomel, B., Biggerstaff, B. J., & Kosoy, M. (2021). Exposure of domestic cats to three zoonotic *Bartonella* species in the United States. *Pathogens*, *10*(3), 354.

Sayed, A. S. M., Alsaadawy, R. M., Ali, M. M., Abd El-Hamid, R. F., Baty, R. S., & Elmahallawy, E. K. (2022). Serological and molecular detection of *Bartonella henselae* in cats and humans from Egypt: Current status and zoonotic implications. *Frontiers in Veterinary Science*, 9, 859104.

Sepúlveda-García, P., Alabi, A., Álvarez, K., Rojas, L., Mella, A., Gonçalves, L. R., & Monti, G. (2023). *Bartonella* spp. in households with cats: Risk factors for infection in cats and human exposure. *One Health*, 16, 100545.

Stepanić, M., Duvnjak, S., Reil, I., et al. (2024). Epidemiology of *Bartonella henselae* infection in pet and stray cats in Croatia with risk factors analysis. *Parasites & Vectors*, 17, 48.

Yakubovsky, M., Kadar, L., Katchman, E., Regev, A., Atamna, A., Yelin, D., & Giladi, M. (2026). Cat scratch disease encephalitis: New insights into rate, clinical features, and long-term outcomes. *International Journal of Infectious Diseases*. Advance online publication.

Zarea, A. A. K., Tempesta, M., Odigie, A. E., Mrenoshki, D., Fanelli, A., Martella, V., & Greco, G. (2023). The global molecular prevalence of *Bartonella* spp. in cats and dogs: A systematic review and meta-analysis. *Transboundary and Emerging Diseases*, 2023, 2437445.

Received: 19.04.2026
Accepted: 15.06.2026

Vol. 22, No. 2, Summer, 2026, 68-79 *Original Article*
DOI: 10.22055/ivj.2025.536829.2823
Journal Homepage: http://www.ivj.ir/

Characterization and phylogenetic analysis of a cDNA encoding an EF-hand domain-containing calumenin-like protein in *Strongyloides ratti*

Abbas Jolodar[1*]

[1] Associate Professor, Department of Basic Sciences, Faculty of Veterinary Medicine, Shahid Chamran University of Ahvaz, Ahvaz, Iran

Received: 24.07.2025 Accepted: 16.10.2025

Abstract

Strongyloides ratti serves as an experimental model for diagnosing strongyloidiasis in humans. The secretory EF-hand-containing calumenin-like protein functions as calcium signaling molecule from rat was characterized. An 849-nucleotide cDNA fragment was amplified using RT-PCR, and a GenBank search revealed that the amplified product shared 98.54% identity with an incomplete mRNA sequence for *S. ratti*. Using this fragment as a probe, a search was conducted in the Expressed Sequence Tags (EST) database, identifying a 998 bp cDNA fragment through overlapping regions designated as *Sr*CAL. The encoded protein consists of 314 amino acids and has a molecular weight of 36.74 kDa, and an isoelectric point (pI) of 4.61. The sequence includes a signal peptide, which has a cleavage site located between amino acids 21 and 22. A protein domain database search identified five highly conserved EF-hand calcium-binding motifs (cd16226), classifying *Sr*CAL within the Efh_CREC_Calumenin-like protein superfamily, spanning amino acids 29 to 296. Structural prediction revealed that *Sr*CAL is composed of 39.18% alpha-helices, 18.21% beta-strands, and 42.61% loops. Three dimensional (3D) structural modeling focused on 232 amino acids, covering 74% of the total coding sequence, with 99.8% confidence, showing strong structural resemblance to the crystal structure of an EF-hand protein from *Danio rerio*. Genetic distance and phylogenetic analysis revealed that *Sr*CAL shares the lowest genetic distance (0.19%) with the only known protein sequence isolated from *S. ratti* (XP_024499492.1). *Sr*CLA plays a crucial role in calcium signaling and may serve as a housekeeping gene with strong potential as a nematode-specific drug target.

Key words: Nematodes, EF-hand domain, *Strongyloides ratti*, RT-PCR, Calumenin-like proteins

Introduction

Strongyloides ratti is a soil-transmitted gastrointestinal nematode that primarily infects rodents. This parasite exhibits a unique life cycle, alternating between free-living non-parasitic and obligatory parasitic generations (Buonfrate, et al, 2020). During infection, infective L3 larvae (iL3) penetrate the host's skin, migrate to the lungs, and eventually reach the small intestine, where they mature into parthenogenetic adult female worms that produce eggs. Due to its biological similarities, S. ratti is maintained in laboratories as a model organism for *S. stercoralis*, a human-infecting nematode responsible for strongyloidiasis, a neglected tropical disease ranked among the most widespread human infections (Viney and Kikuchi, 2017; Hotez et al, 2008). Despite belonging to different phylogenetic clades, nematodes such as *Ascaris*, *Toxocara*, *Necator*, and *Strongyloides* follow similar

[*] **Corresponding Author**: Abbas Jolodar, Associate Professor, Department of Basic Sciences, Faculty of Veterinary Medicine, Shahid Chamran University of Ahvaz, Ahvaz, Iran
E-mail: jolodara@scu.ac.ir

migration patterns and elicit comparable immune responses in their hosts (Maizels et al, 2009; Finkelman et al, 2004).

The EF-hand calcium-binding loop motif is a structural domain found in various calcium-binding proteins, including calumenin. Also known as crocalbin or CBP-50, calumenin plays a critical role in protein folding and trafficking within the endoplasmic reticulum (ER). Similarly, RCN-1 and RCN-3 are involved in calcium-dependent processes, influencing cell signaling and protein interactions (Grabarek, 2006). The calumenin-like protein family contains five EF-hand motifs in *Caenorhabditis elegans* and six in Homo sapiens, exhibiting a relatively low affinity for Ca^{2+} (Cho et al, 2009; Yabe et al, 1997). These proteins play essential roles in intracellular calcium regulation, contributing to various cellular functions.

The EF-hand protein family has been identified in a diverse range of organisms, including bacteria, protozoa, helminths, arthropods, and mammals (Nagamune et al, 2008; Orans et al, 2010; Chazin, 2011). Genomic analysis estimates that 250 EF-hand genes exist in plant species such as Arabidopsis (Day et al, 2002). Several secretory acidic and rich in cysteine (SPARC) Ca^{2+}-binding proteins have been cloned from cDNA libraries of parasitic nematodes *Strongyloides ratti* (Anandarajah et al, 2016) and *Necator americanus* (Mason et al, 2014), as well as trematodes (Ruiz de Eguino et al, 1999) and *Clonorchis sinensis* (Zhou et al, 2013). These proteins are involved in host-parasite interactions. In Caenorhabditis elegans, calumenin plays a role in Ca^{2+}-regulated behaviors, including pharyngeal pumping and defecation (Cho et al, 2009). Experimental studies have demonstrated that CaM-null individuals of *Drosophila melanogaster* survive embryogenesis but die within two days of hatching as first-instar larvae (Heiman et al, 1996). Furthermore, the previous research using RNA interference (RNAi) to deplete the single nematode CaM gene (cmd-1) resulted in lethal embryos, exhibiting abnormalities in morphogenesis, cell migration, apoptosis, cell proliferation, and cytokinesis (Karabinos et al, 2015).

In this study, we successfully identified a full-length cDNA sequence from *S. ratti*, encoding an EF-hand calcium-binding protein. This highlights the functional significance of EF-hand calcium-binding proteins, particularly calumenin-like proteins, in mediating host-parasite interactions and regulating calcium-dependent cellular processes

Materials and Methods

Total RNA isolation and cDNA Synthesis

Total RNA was extracted from approximately 100,000 infective larvae (iL3) of *S. ratti* (Anandarajah et al, 2016) using RNX Plus solution (Cinnagen, Iran), following the manufacturer's protocol. A 12 µL aliquot, containing 2 µg of total RNA, was incubated with 0.5 µg of oligo(dT) primer at 70°C for 10 minutes, followed by brief centrifugation. The reaction was then placed on ice before adding 1 µL of RNasin (Cinnagen, Iran), 1 µL of a 120 mM dNTP mixture, 2.5 µL of 5X enzyme buffer, and 1 µL (200 units) of Moloney Murine Leukemia Virus (M-MuLV) reverse transcriptase. The mixture was subsequently incubated at 42°C for 1 hour, followed by heat inactivation at 70°C.

RT-PCR amplification

The selected coding region was amplified using specific primers: CAL-F (5´-GAACATGGACATGGAAGTGAACA) and CAL-R (5´-ATCATGTTTTTGAAGTTGCTCACC), designed based on a partial mRNA sequence encoding the EF-hand domain (XM_024643085) using the Primer3Plus program. The PCR reaction contained 5 µL of the reverse transcription product, 0.2 µM of each primer, 250 µM of each dNTP, and

1 U of *Taq* DNA polymerase in a standard PCR buffer. Amplification conditions included an initial denaturation at 94°C for 3 minutes, followed by 30 cycles of 94°C for 30 seconds, 56°C for 30 seconds, and 72°C for 1 minute, with a final extension at 72°C for 7 minutes. The resulting PCR products were analyzed using electrophoresis on a 1% (w/v) agarose gel to assess amplification efficiency.

DNA sequence analysis

The amplified cDNA fragments were sequenced using a BigDye Terminator v3.1 Cycle Sequencing Kit (Applied Biosystems, Foster City, CA, USA). Homology searches were conducted using the NCBI BLAST program available at NCBI. The complete cDNA sequences were assembled from overlapping fragments. Primers were designed using the Primer3Plus program (www.primer3plus.com). For sequence analysis, multiple alignments were performed using CLUSTAL_W (Thompson et al, 1994) and refined using BOXSHADE software (www.ch.embnet.org/software/BOX_form.html). The theoretical molecular weight (MW) and isoelectric point (pI) was calculated using ExPASy-Compute pI/Mw tool (web.expasy.org/compute_pi/). Protein domain predictions were performed using ExPASy Prosite (prosite.expasy.org/scanprosite), and DeepLoc 2.0 (services.healthtech.dtu.dk/services/DeepLoc-2.0/) was used to determine subcellular localization of eukaryotic proteins. Phylogenetic analysis and genetic distance estimations were carried out using the neighbor-joining method (Saitou, 1987) with 1,000 bootstrap replicates in MEGA11 software (Tamura et al, 2021). Three-dimensional structure predictions were generated using the Phyre2 program (Kelley and Sternberg, 2009).

Results

RT-PCR amplification and sequence analysis

RT-PCR amplification was performed using aliquots of *S. ratti* cDNA as the template, yielding an 849 bp amplified fragment (Figure 1). The resulting product was consistent with the expected sequence, as predicted through manual calculation, confirming the accuracy of the amplification process.

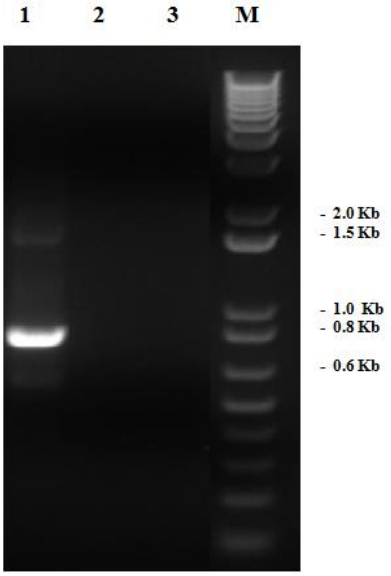

Figure 1: Agarose gel electrophoresis of RT-PCR products for the SrCLA transcript from infective *S. ratti* larvae. Lanes: M, 1 Kb plus DNA ladder; 1, RT-PCR amplification products; 2. No-template negative control; 3-empty.

To compare the amplified cDNA fragment with existing sequences, the BLASTn program available on the NCBI website was used with the Highly Similar Sequences (Megablast) algorithm. Sequence analysis revealed that the amplified fragment exhibited 99.06% identity to the only available *S. ratti* sequence, consisting of a 945 bp partial mRNA encoding an EF-hand domain (XM_024643085). Additionally, the amplified sequence showed identity to the *S. papillosus* genome assembly (LM525584) and a partial mRNA sequence from *Brugia malayi* (XM_043073392) encoding an EF hand family protein (Bma-

calu-1) at 90.26% and 76.03 %, respectively. Furthermore, a search of the Expressed Sequence Tags (EST) database using the amplified sequence as a probe identified four overlapping sequences: FC821077 (919 bp), FC821696 (832 bp), BI450405.1 (515 bp), and BI142485.1 (521 bp). The complete nucleotide sequence of *Sr*CAL was assembled from overlapping cDNA fragments. Sequence analysis revealed that the full-length *Sr*CAL sequence consists of 998 bp, encompassing the complete coding region along with 9 bp and 44 bp non-coding regions at the 5´ and 3´ ends, respectively (Figure 2). The start codon (nucleotides 10-12) and stop codon (952-954) were identified within the sequence. The open reading frame (ORF) spans 942 nucleotides, encoding a 314-amino acid protein with a molecular mass of 36.74 kDa and an isoelectric point (pI) of 4.61. The protein sequence contains a complete ORF of 291 amino acids, categorized into aliphatic (84, 26.75%), aromatic (28, 8.92%), basic (54, 17.2%), and acidic (98, 31.21%) side groups. Among these, glutamate is the most abundant amino acid (40, 12.74%), whereas cysteine is the least represented (2, 0.64%). The total number of negatively charged residues (Asp + Glu) is 78, while positively charged residues (Arg + Lys) amount to 40.

```
ccagttgagA TGCGTTTTTT AATTTTAATA TCTCTTTTAC TTATTGGCAT TACATTAGCT      60
GAACATCATA CTGATCCATT ATCTGATAAA GAACATGGAC ATGGAAGTGA ACATAATAAA     120
CAATATGATC ATGAAGCTTT CTTAGGTAAG GATACTGCTG CTGAATTTGA TGAATTAACA     180
CCTGAAAAAT CTAAAGAAAA ACTTGCTTCA CTTATTCCAA AAATGGATAG TAATGGTGAT     240
GGATTTGTTG AAGAGGATGA ACTTAGAAAT CATATTAATT TTATGCAACA AAGATATGTT     300
AATAATGATG TTGAACGTAC ATGGAAAAAT TATAAAGCTG AAGAGATAGC TGATGGTAAA     360
TTGTCATGGG CTGATTATAG AGAAATTGTT TATAGACATC CAACAGGTGA AGGACAAGAT     420
TTATCTGATG AGTATAAAAA AATGATTACT AGAGATGAAC GTAGATGGAA AGTTGCTGAT     480
TATGATTCAG ATGAAAAATT AGATAGAACT GAGTATGGAT GTTTTATGCA CCCTGAAGAT     540
TGTGAATCAA TGAGAGATGT TGTTGCTACA GAAACTATTG AAGATATTGA TAAAAATAAG     600
GATGGATTTG TTGATATTAA TGAATATATT AGTGATATGT ATAGACCAGA AGATTATCCT     660
GAATTAAATG GTAAAGAACC AGAATGGGTT GAATCTGAAA GAGAACTTTT CAAAGAACAT     720
CGTGATAAGA ATAATGATGG TAAATTAGAT CGTGATGAGA TGCGTGATTG GATTATGCCA     780
ATTGGTTTTG ATCATGCTGA TGCTGAGGCA AAGCATTTAA TTGGAATTGC TGATGAAAAT     840
AAGGATGGAA AACTTTCACC AGAAGAGATT ATCCAACATT ATGATACATT TGTTGGATCA     900
CAAGCAACTG ATTATGGTGA GCAACTTTCA AAACATGATC CATCTGAATT ATAAaaaaaa     960
aaaaaaaaaa ctcgagacta gttctctctt tctctctc                            998
```

Figure 2: Nucleotide sequence of *Sr*CLA. Non-coding sequences are in lowercase, start and stop codons are bolded, and primer binding sites are underlined.

A protein domain database search identified a highly conserved domain containing the EF-hand calcium-binding motif (cd16226), with an e-value of 4.23e-124, classifying it within the Efh_CREC_Calumenin-like protein superfamily spanning amino acids 29 to 296. Further domain analysis predicted the presence of five EF-hand Ca^{2+}-binding domains at residues 6-95, 144-179, 181-216, 239-261, and 262-297 in *Sr*CAL (Figure 3). This domain superfamily consists of five EF-hand structural units, each composed of two helices connected by a twelve-residue calcium-binding loop, essential for calcium coordination and protein function.

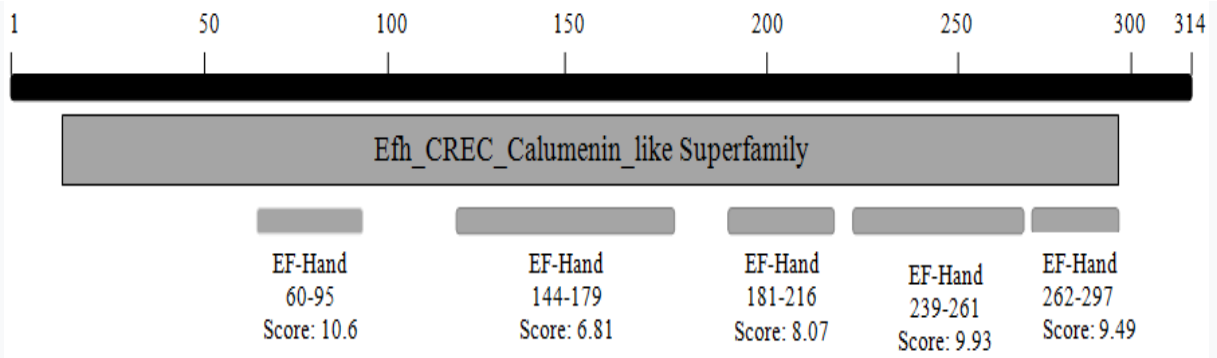

Figure 3: Schematic representation of the *Sr*CLA domain, highlighting its structural organization, key functional elements, and defining features essential for its biological role.

Taxonomic analysis of *Sr*CLA at the nucleotide level revealed similarities with three sequences within the *Rhabditida* order, two of which specifically belong to the genus *Strongyloides*. Among these, *S. ratti* exhibited the highest similarity, while the third sequence corresponded to *S. papillosus*. At the protein level, *Sr*CAL displayed homology with 126 sequences within the Nematode phylum, of which 105 were classified under the *Rhabditida* order. Within this subset, only three sequences were assigned to the *Strongyloidoidea* family, with two sequences specifically matching *S. ratti*.

Multiple alignments

The amino acid sequence identity of *Sr*CLA in aligned regions with *Mesorhabditis belari* (CAJ0935108.1), *Steinernema hermaphroditum* (KAK0423442.1), *Ostertagia ostertagi* (KAK6033036.1), *Ancylostoma caninum* (RCN51010.1), *Nippostrongylus brasiliensis* (WKY16943.1), and *Necator americanus* (XP_064070443.1) was 75.32%, 74.80%, 75.39%, 75.15%, 75.07%, and 75.20%, respectively (Figure 4). Sequence analysis using SignalP predicted that SrCAL contains a signal peptide, which is cleaved at Ala17-Glu18. Additionally, DeepLoc-2.0, a program for eukaryotic protein subcellular localization, determined that *Sr*CLA is primarily localized in the endoplasmic reticulum (ER) and is considered non-cytoplasmic with a probability of 0.8562. Further analysis revealed the presence of a C-terminal ER retention signal sequence (PSEL) at positions 311-314, consistent with the previous findings (Honore and Vorum 2000). The critical C-terminal residues (EL) are conserved, aligning with observations in other homologs (Yabe et al. 1997).

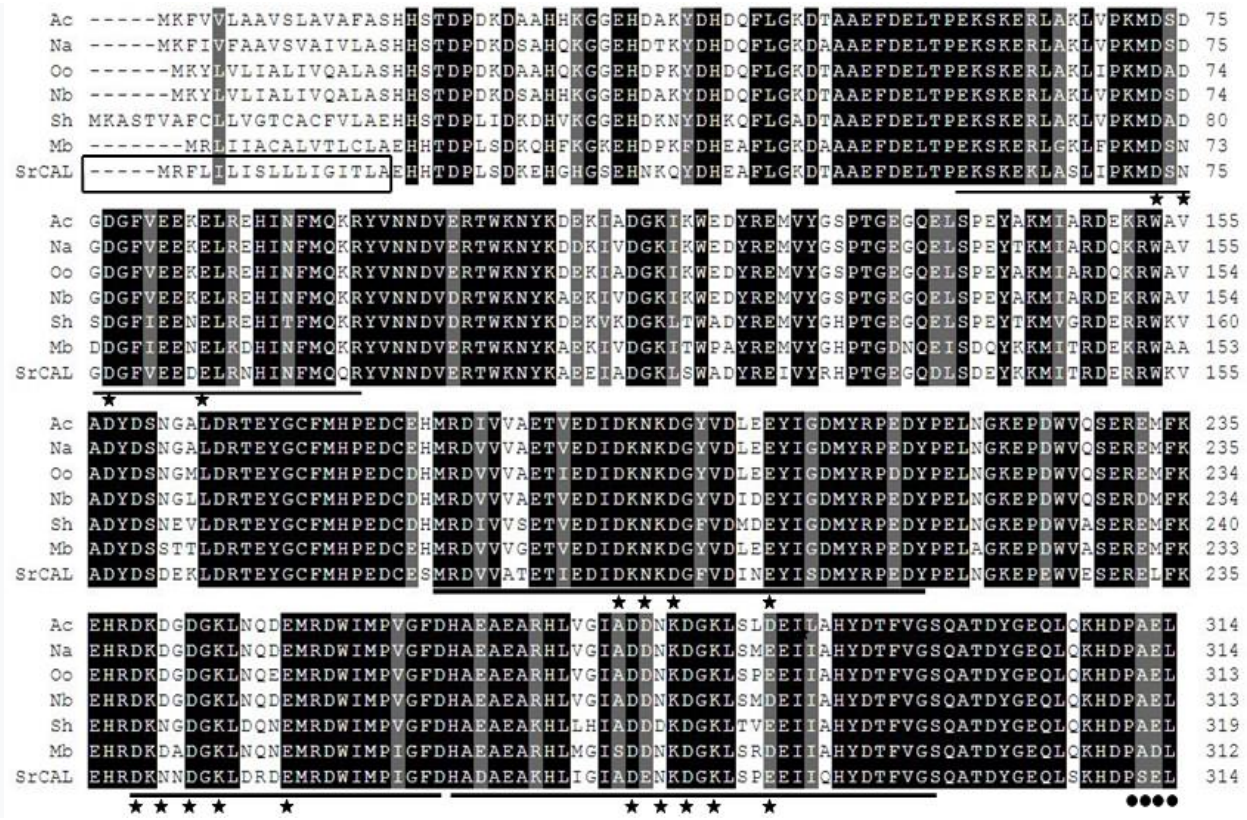

Figure 4: Multiple sequence alignment of the *Sr*CAL sequence with its homologous counterparts. The aligned sequences include *Ancylostoma caninum* (Ac), *Necator americanus* (Na), *Ostertagia ostertagi* (Oo), *Nippostrongylus brasiliensis* (Nb), *Steinernema hermaphroditum* (Sh), and *Mesorhabditis belari* (Mb). Identical residues are shaded black, while conservative substitutions are highlighted gray. The EF-hand domain is underlined, active sites are marked with stars, and the signal peptide is enclosed within a box. C-terminal tetra-peptides associated with endoplasmic reticulum (ER) retention are indicated by black circles.

Molecular characterization and secondary structure

The secondary structure of *Sr*CAL protein was predicted using the PSIPRED protein sequence analysis method, where each amino acid was assigned values for alpha-helix, beta-sheet, and loops within a 7-amino acid window (Figure 4). By applying these parameters and calculating the probability for each residue, the protein structure was predicted with high confidence. Further PSIPRED analysis determined that the *Sr*CAL sequence consists of 39.18% alpha-helices, 18.21% beta-sheets, and 42.61% loops, highlighting its structural composition (Figure 5A). Structurally, the EF-hand domain is arranged in a characteristic helix-loop-helix conformation, facilitating calcium-binding interactions. For 3D structural modeling, the analysis focused on 232 amino acids, covering 74% of the total coding sequence, with 99.8% confidence, revealing a strong resemblance to the crystal structure of an EF-hand protein from *Danio rerio* dr.36843 (Figure 5B).

A)

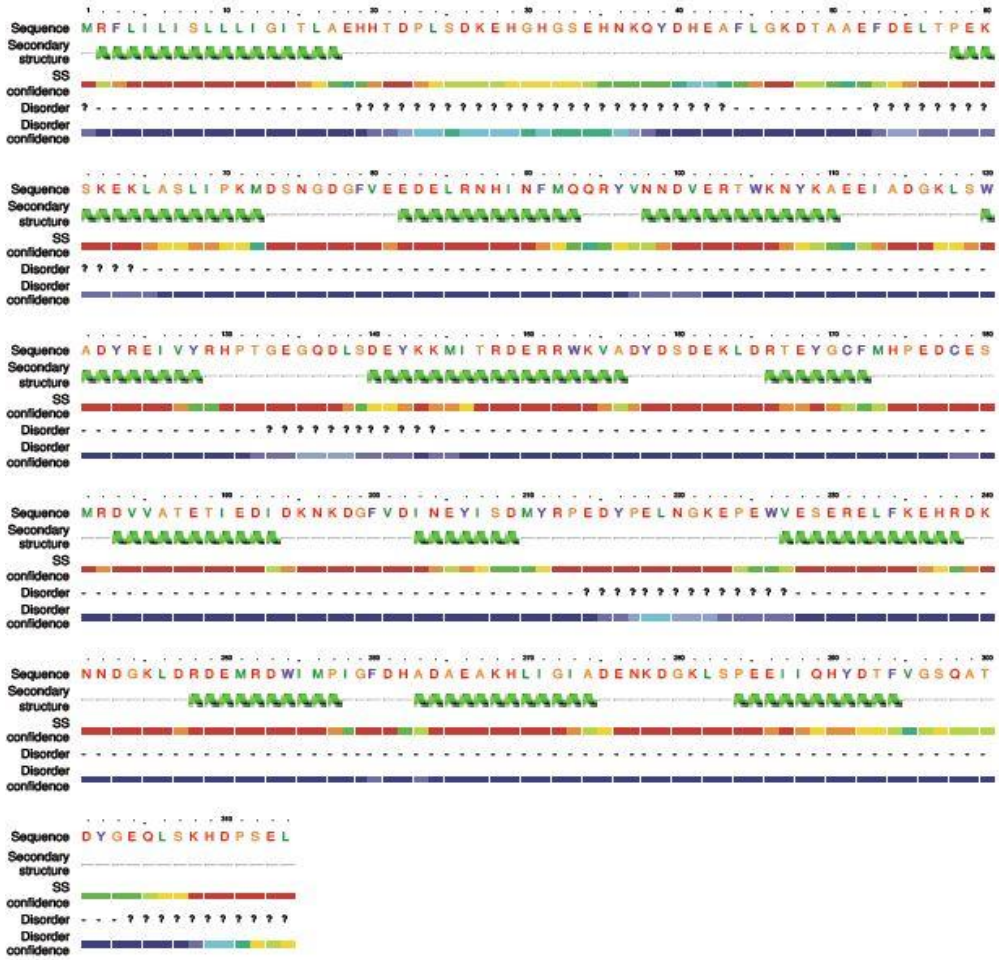

B)

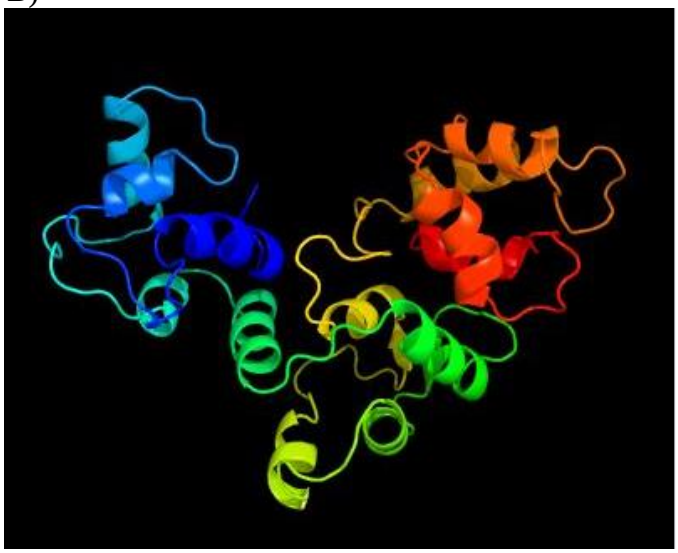

Figure 5: Structural visualization of *Sr*CAL, showcasing its secondary structure (A) alongside its three-dimensional (3D) molecular model (B).

Phylogenetic analysis and genetic distances

To examine *Sr*CLA within the broader context of EF-hand domain-containing proteins, a phylogenetic tree of the *Sr*CAL protein sequence was generated using the Neighbor-Joining method in MEGA11 software, incorporating 16 homologous sequences from the parasitic nematode family. As illustrated in Figure 6, the constructed phylogram reveals two distinct clusters. In the major cluster, *Sr*CAL is positioned alongside other nematode parasite sequences, forming a sub-cluster that groups exclusively with the only available *S. ratti* sequence (XP_024499492.1), supported by a moderate bootstrap value of 49%. Meanwhile, all filarial nematode parasites are categorized into a separate cluster, which is strongly supported by a bootstrap value of 96%, indicating a high degree of confidence in their phylogenetic grouping. To ensure accurate phylogenetic placement, *Trichinella papuae* (KRZ78707.1) was included as an out-group sequence, providing a reference point for evolutionary divergence.

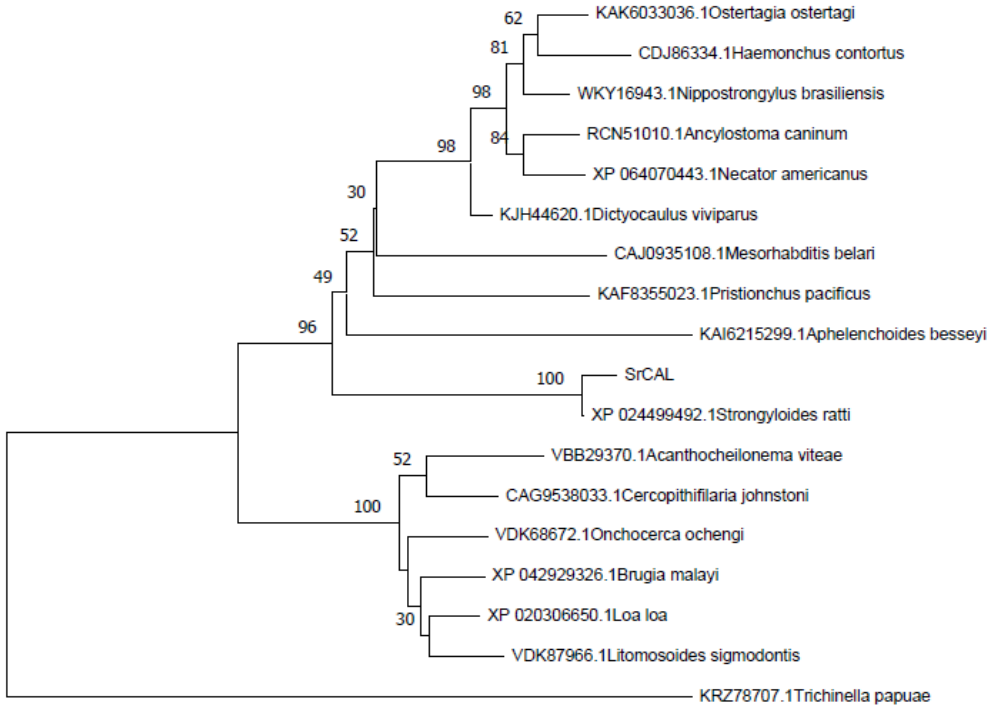

Figure 6: Phylogenetic analysis of *Sr*CLA amino acid sequences and their parasite homologs, constructed using the Neighbor-Joining method. Bootstrap values, derived from 1,000 replicates, indicate the reliability of branching patterns. Numbers preceding species names represent GenBank accession numbers corresponding to related gene variants, while the numbers above the branches depict phylogenetic relationships between groups.

As presented in Table 1, the genetic distance of *Sr*CLA from related EF-hand-containing calumenin-like protein sequences was calculated using MEGA11 software. Among the 14 homologous sequences available in GenBank, *Sr*CAL exhibited the lowest genetic distance (0.19%) with the only known protein sequence isolated from Strongyloides ratti (XP_024499492.1). In contrast, the genetic distance between *Sr*CAL and other related nematode species ranged from 23.5% to 33.6%, highlighting significant sequence divergence within this family.

Table 1: Genetic pairwise distances of *Sr*CAL, comparing its sequence similarity to related S. ratti protein sequences

	1	2	3	4	5	6	7	8	9	10	11	12	13
1-SrCAL													
2-XP 024499492.1 S. ratti	0.019												
3-CAJ0935108.1 M. belari	0.275	0.262											
4-KAK0423442.1 S. hermaphroditum	0.274	0.257	0.271										
5-RCN51010.1 A. caninum	0.282	0.261	0.222	0.208									
6-KAK6033036.1 O. ostertagi	0.258	0.238	0.226	0.209	0.073								
7-WKY16943.1N. brasiliensis	0.262	0.242	0.218	0.201	0.066	0.059							
8-XP_064070443.1 N. americanus	0.282	0.261	0.206	0.208	0.059	0.076	0.076						
9-KAI1725696.1 D. destructor	0.267	0.255	0.251	0.239	0.205	0.222	0.226	0.217					
10-KAF8355023.1 P. pacificus	0.274	0.252	0.228	0.252	0.215	0.220	0.216	0.219	0.228				
11-CDJ86334.1 H. contortus	0.301	0.279	0.254	0.213	0.108	0.073	0.073	0.108	0.251	0.241			
12-KAI6215299.1 A. besseyi	0.336	0.318	0.306	0.331	0.301	0.297	0.302	0.292	0.284	0.292	0.333		
13-KJH44620.1 D. viviparus	0.235	0.210	0.186	0.186	0.071	0.067	0.058	0.071	0.193	0.172	0.093	0.230	
14-KRZ78707.1 T. papuae	0.645	0.627	0.693	0.636	0.649	0.645	0.652	0.649	0.664	0.663	0.671	0.693	0.529

Discussion

Parasitic worms have evolved elaborate strategies to thrive within diverse host environments. To improve their chances of survival, they secrete excretory/secretory proteins that effectively suppress the host's immune response. Recent advancements in *Strongyloides ratti* genome analysis have provided researchers with a vast dataset of Expressed Sequence Tags (ESTs), enabling deeper molecular investigations. A targeted approach to anti-parasitic drug development focuses on exploiting metabolic differences between parasites and hosts to design enzyme inhibitors, paving the way for effective therapeutic solutions.

Calumenin-like proteins appear to be conserved across a diverse range of nematode species. Homologs have been identified in both animal parasitic nematodes, including *Ascaris sum, Brugia malayi*, and *Trichinella spiralis*, as well as plant parasitic nematodes such as *Meloidogyne hapla* and *Bursaphelenchus xylophilus*. Additionally, calumenin homologs are present in free-living nematodes like *Caenorhabditis elegans* and *C. briggsae*. The broad distribution of these orthologs, including *C. elegans* protein (CAA96655.1), which has been linked to embryo development (Jantsch-Plunger and Glotzer, 1999), suggests that *Sr*CLA homologs may serve a fundamental housekeeping function in nematodes. However, the exact biological roles and mechanisms of these proteins remain to be fully elucidated.

Calumenin is an endoplasmic reticulum (ER)-resident protein that contains five EF-hand motifs in *Caenorhabditis elegans* and six in humans, exhibiting a relatively low affinity for Ca^{2+}. Calcium-binding proteins generally contain two to eight EF-hand motifs, each consisting of a paired EF-hand structure that facilitates Ca^{2+} ion coordination, emphasizing their functional importance (Nakayama *et al.*, 2000). Multiple sequence alignment and phylogenetic analysis of *Sr*Cal confirm that it encodes an EF-hand domain-containing protein. The findings indicate that *Sr*Cal belongs to the Calumenin-like protein subfamily, with a high degree of conservation in both soil-transmitted gastrointestinal nematodes and parasitic filarial nematodes. Given its strong evolutionary preservation, developing calumenin-targeting drugs could represent a promising strategy for treating lymphatic filariasis and gastrointestinal nematode infections, including *Strongyloides*.

The presence of the signal peptide in the N-terminal region of *Sr*CLA indicates that this protein is secreted from the cell as an extracellular protein. The results indicate that *Sr*CLA contains a signal peptide, a short amino acid sequence located at the N-

terminus of the protein, which directs it to the endoplasmic reticulum (ER) during translation. Also, the retention signal (PSEL) at the C-terminus part of *Sr*CLA sequence ensures its ER localization, preventing its unrestricted distribution in the cytoplasm (Yabe et al, 1997).

Procollagen biosynthesis involves chaperones and folding-modifying enzymes, which continue to function after secretion from the endoplasmic reticulum (ER) (Lamande and Bateman, 1999). ER-resident enzymes such as protein disulfide isomerase (PDI) and peptidyl prolyl cis-trans isomerase (PPIase) play essential roles in procollagen modification, and their activity has been reported to be regulated by Ca^{2+} (Primm et al, 1996). Given this, it is plausible that *Sr*CLA may contribute to maintaining ER Ca^{2+} levels, thereby influencing the enzymatic processes required for proper procollagen modification. Additionally, studies have shown that calumenin mutants in *Caenorhabditis elegans* exhibit reduced fertility and severe cuticle defects (Cho et al, 2009). Due to its involvement in cuticle formation, *C. elegans* calumenin has been proposed as a potential drug target for human-infective nematodes, particularly filarial worms (Choi et al, 2018). It is also possible that *Sr*CLA plays a possible role in various cuticle development processes.

In conclusion, Calumenin-like proteins are gaining increasing research interest due to their involvement in various cellular functions as calcium signaling molecules. However, their physiological and pathological mechanisms are not yet fully understood. Due to their essential role as housekeeping genes in related nematodes and their high conservation across soil-transmitted gastrointestinal, the proteins in this parasite are considered as potential candidates for nematode-specific drug targets.

Acknowledgments

This study was financially supported by a research grant from the Vice President of Research Affairs Office at Shahid Chamran University of Ahvaz, Ahvaz, Iran.

Conflict of interest

The authors declare no conflicts of interest.

Funding

The authors declare that no funding was received from any private or commercial organization.

References

Anandarajah, E. M., Ditgen, D., Hansmann, J., Erttmann, K. D., Liebau, E. (2016). SPARC (secreted protein acidic and rich in cysteine) of the intestinal nematode Strongyloides ratti is involved in mucosa-associated parasite-host interaction. *Molecular and Biochemical Parasitology*, 207(2), 75-83.

Buonfrate, D., Bisanzio, D., Giorli, G., Odermatt, P., Fürst T (2020). Greenaway C, French M, Reithinger R, Gobbi F, Montresor A, Bisoffi Z. The Global Prevalence of *Strongyloides stercoralis* Infection. *Pathogens*, 9(6), 468.

Chazin, W. J. (2011). Relating form and function of EF-hand calcium binding proteins. *Accounts of chemical research*, 44(3), 171-9.

Cho, J. H., Song, H. O., Singaravelu, G., Sung, H., Oh, W. C. (2009). Pleiotropic roles of calumenin (calu-1), a calcium-binding ER luminal protein, in *Caenorhabditis elegans*. *FEBS Letters*, 583(18), 3050-6.

Cho, J. H., Song, H. O., Singaravelu, G., Sung, H., Oh, W. C. (2009). Pleiotropic roles of calumenin (*calu-1*), a calcium-binding ER luminal protein. Caenorhabditis elegans. *FEBS Letters*, 583(18), 3050-3056.

Cho, J. H., Song, H. O., Singaravelu, G., Sung, H., Oh, W.C. (2009). Pleiotropic roles of calumenin (calu-1), a calcium-binding ER luminal protein, in Caenorhabditis elegans. *FEBS Letters*, 583(18), 3050-6.

Choi, T. W., Cho, J. H., Ahnn, J., Song, H. O. (2018) Novel Findings of Anti-Filarial Drug Target and Structure-Based Virtual Screening for Drug Discovery. *International Journal of Molecular Sciences*, 19(11), 3579.

Day, I. S., Reddy, V. S., Shad Ali, G. (2002). Analysis of EF-hand-containing proteins in *Arabidopsis*. *Genome Biology*, 3(10), RESEARCH0056.

Finkelman, F. D., Shea-Donohue, T., Morris, S. C, Gildea, L., Strait, R., Madden K. B., Schopf, L., Urban, J. F. (2004). Interleukin-4- and interleukin-13-mediated host protection against intestinal nematode parasites. *Immunological Review*, 201, 139-55.

Grabarek, Z. (2006). Structural basis for diversity of the EF-hand calcium-binding proteins. *Journal of molecular biology*, 359(3), 509-25.

Heiman, R. G., Atkinson, R.C., Andruss, B. F., Bolduc, C., Kovalick, G. E. (1996). Spontaneous avoidance behavior in Drosophila null for calmodulin expression. *Proceedings of the National Academy of Sciences of the United States of America*, 93(6), 2420-5.

Honore, B., Vorum, H. (2000). The CREC family, a novel family of multiple EF-hand, low-affinity Ca(2+)-binding proteins localized to the secretory pathway of mammalian cells. *FEBS Letters*, 466(1), 11-8.

Hotez, P. J., Brindley, P. J., Bethony. J. M., King, C. H., Pearce, E. J. (2008). Helminth infections: the great neglected tropical diseases. *The Journal of Clinical Investigation*, 118(4), 1311-21.

Jantsch-Plunger, V., Glotzer, M. (1999). Depletion of syntaxins in the early Caenorhabditis elegans embryo reveals a role for membrane fusion events in cytokinesis. *Current Biology*, 9(14), 738-45.

Karabinos, A. (2015). RNA interference and protein expression of the four calmodulin-like genes in Caenorhabditis elegans. *Biologia*, 70(6), 826-830.

Kelley, L. A., Sternberg, M. J. (2009). Protein structure prediction on the Web: a case study using the Phyre server. *Nature Protocols*, 4(3), 363-71.

Lamande, S. R., Bateman, J. F. (1999). Procollagen folding and assembly: the role of endoplasmic reticulum enzymes and molecular chaperones. *Seminars in Cell and Developmental Biology*, 10(5), 455-64.

Maizels, R. M., Pearce E. J., Artis, D., Yazdanbakhsh, M., Wynn, T. A. (2009). Regulation of pathogenesis and immunity in helminth infections. *Journal of Experimental Medicine*, 206(10), 2059-66.

Mason, L., Tribolet, L., Simon, A., von Gnielinski, N., Nienaber, L. (2014). Probing the equatorial groove of the hookworm protein and vaccine candidate antigen, Na-ASP-2. *International Journal of Biochemistry & Cell Biology*, 50, 146-55.

Nakayama, S., Kawasaki, H., Kretsinger, R. (2000). Evolution of EF-Hand Proteins. In: Carafoli, E., Krebs, J. (eds). Calcium Homeostasis. Topics in Biological Inorganic Chemistry, Springer, Berlin, Heidelberg. 3, 29-58.

Nagamune, K., Moreno, S. N., Chini, E. N., Sibley, L. D. (2008). Calcium Regulation and Signaling in Apicomplexan Parasites. In: Burleigh, B.A., Soldati-Favre, D. (eds) Molecular Mechanisms of Parasite Invasion. *Subcellular Biochemistry*, Springer, New York, NY. 47, 70-81.

Orans, J., Johnson, M. D., Coggan, K. A., Sperlazza, J. R., Heiniger, R. W., Wolfgang, M. C., Redinbo, M. R. (2010). Crystal structure analysis reveals Pseudomonas PilY1 as an essential calcium-dependent regulator of bacterial surface motility. *Proc Natl Acad Sci U S A*, 107(3), 1065-70.

Primm, T. P., Walker, K. W., Gilbert, H. F. (1996) Facilitated protein aggregation. Effects of calcium on the chaperone and anti-chaperone activity of protein disulfide-isomerase. *Journal of Biological Chemistry*, 271(52), 33664-9.

Ruiz de Eguino, A. D., Machín, A., Casais, R., Castro, A. M., Boga, J. A. (1999). Cloning and expression in Escherichia coli of a Fasciola hepatica gene encoding a calcium-binding protein. *Molecular and Biochemical Parasitology* 101(1-2), 13-21.

Saitou, N., Nei, M. (1987). The neighbor-joining method: A new method for reconstructing phylogenetic trees. *Molecular Biology and Evolution*, 4, 406-425.

Tamura, K., Stecher, G., Kumar, S. (2021). MEGA 11: Molecular Evolutionary Genetics Analysis Version 11. *Molecular Biology Evolution*, 38(7), 3022-3027.

Thompson, J. D., Higgins, D. G., Gibson, T. J. (1994). CLUSTAL W: improving the sensitivity of progressive multiple sequence alignment through sequence weighting, position-specific gap penalties and weight matrix choice. *Nucleic Acids Research*, 22, 4673-4680.

Viney, M., Kikuchi, T. (2017). Strongyloides ratti and S. venezuelensis - rodent models of Strongyloides infection. *Parasitology*, 144(3), 285-294.

Yabe, D., Nakamura, T., Kanazawa, N., Tashiro, K., Honjo, T. (1997). Calumenin, a Ca2+- binding protein retained in the endoplasmic reticulum with a novel carboxyl-terminal sequence HDEF. *Journal of Biological Chemical*, 272(29), 18232-18239.

Zhou, J., Sun, J., Huang, Y., Zhou, C., Liang, P. (2013). Molecular identification, immunolocalization, and characterization of Clonorchis sinensis calmodulin. *Parasitology Research*, 112(4), 1709-17.

Received: 24.07.2025
Accepted: 16.10.2025

Vol. 22, No. 2, Summer, 2026, 80-88 *Original Article*
DOI: 10.22055/ivj.2026.579925.2890
Journal Homepage: http://www.ivj.ir/

Effects of Intraperitoneal Administration of Flunixin Meglumine, Metamizole Sodium, Diclofenac Sodium, and Carprofen on Experimentally Induced Intra-Abdominal Adhesion Formation in Rats

Serdar Köklü[1] and Nuh Kılıç[2*]

[1] MSc, Department of Surgery, Faculty of Veterinary Medicine, Adnan Menderes University, 09016 Isikli, Aydin, Turkey
[2] Professor, Department of Surgery, Faculty of Veterinary Medicine, Adnan Menderes University, 09016 Isikli, Aydin, Turkey

Received: 29.04.2026 Accepted: 08.07.2026

Abstract

Postoperative intra-abdominal adhesions remain a major complication following abdominal surgery and may lead to intestinal obstruction, infertility, chronic abdominal pain, and difficulties during repeat surgical procedures. This experimental study investigated the effects of intraperitoneally administered flunixin meglumine, metamizole sodium, diclofenac sodium, and carprofen on postoperative adhesion formation in a rat cecal abrasion model. Sixty female Sprague–Dawley rats were randomly allocated into six groups including sham, control, flunixin meglumine, metamizole sodium, diclofenac sodium, and carprofen groups (n=10 each). Following standardized cecal abrasion, the treatment agents were administered intraperitoneally immediately after induction of peritoneal injury. Adhesion formation was evaluated macroscopically on postoperative day 10 using the Nair adhesion scoring system. Hematological and biochemical parameters together with tissue hydroxyproline concentrations were also analyzed. All treatment groups demonstrated significantly lower adhesion scores compared with the control group. Metamizole sodium and carprofen produced the most pronounced reduction in adhesion severity. Hydroxyproline concentrations were significantly lower in the carprofen group compared with the flunixin meglumine, metamizole sodium, and diclofenac sodium groups. The findings suggest that intraperitoneal administration of selected NSAIDs may reduce postoperative intra-abdominal adhesion formation and may represent a supportive pharmacological strategy for adhesion prevention.

Key words: Intra-abdominal adhesion, NSAID, Hydroxyproline, Rat, Peritoneal adhesion

Introduction

Postoperative intra-abdominal adhesions are among the most common complications following abdominal surgery and represent a major clinical problem in both human and veterinary medicine. Adhesion formation has been associated with serious consequences such as intestinal obstruction, chronic abdominal pain, infertility and increased difficulty during subsequent surgical interventions (Ellis, 1971; Menzies and Ellis, 1990). Despite improvements in surgical techniques and perioperative management, adhesion development remains a frequent postoperative outcome.

Adhesions are formed as a result of peritoneal injury that initiates a complex inflammatory cascade involving fibrin deposition, leukocyte migration and

[*] **Corresponding Author**: Nuh Kılıç, Professor, Department of Clinical Science, Department of Surgery, Faculty of Veterinary Medicine, Adnan Menderes University, 09016 Isikli, Aydin, Turkey
E-mail: nkilic@adu.edu.tr

fibroblast activation. Under normal physiological conditions, fibrinolytic activity removes temporary fibrin bridges formed between injured peritoneal surfaces; however, impairment of this mechanism leads to persistent fibrotic connections and permanent adhesion formation (Hellebrekers et al., 2000). Several cytokines, including interleukin-1, interleukin-6 and tumor necrosis factor-alpha, have been shown to play important regulatory roles during adhesion development following peritoneal trauma (Hershlag et al., 1991; Saba et al., 1996).

Various strategies have been investigated to prevent postoperative adhesion formation, including mechanical barrier materials, fibrinolytic agents and pharmacological approaches targeting inflammatory pathways (Treutner and Schumpelick, 2000). Recent advances in adhesion prevention research have highlighted the importance of biomaterial-based barriers and targeted pharmacological delivery systems designed to modulate inflammatory signaling at the site of injury (Rodgers et al., 1998). In addition, several standardized experimental animal models have been developed to evaluate the mechanisms of adhesion formation and to test preventive strategies under controlled conditions (Cofer et al., 1994).

Among pharmacological agents, non-steroidal anti-inflammatory drugs (NSAIDs) have received considerable attention because of their inhibitory effects on cyclooxygenase activity and prostaglandin synthesis during the early stages of adhesion formation (Siegler et al., 1980). Experimental studies have demonstrated that several NSAIDs, including ibuprofen and meclofenamate, reduce adhesion severity by modulating inflammatory mediator release and fibroblast proliferation during peritoneal healing (Muscara et al., 2000).

In veterinary medicine, commonly used NSAIDs such as flunixin meglumine, diclofenac sodium, metamizole sodium and carprofen are widely administered for their analgesic and anti-inflammatory effects. However, comparative evaluation of their potential roles in preventing postoperative intra-abdominal adhesion formation following local intraperitoneal administration remains limited. Since these agents differ in their pharmacological properties, anti-inflammatory potency and cytokine-modulating effects, evaluation of their relative influence on adhesion severity may contribute to identifying more effective pharmacological strategies for postoperative adhesion prevention.

Although several experimental studies have evaluated the effects of individual NSAIDs on adhesion formation, direct comparative investigations assessing the relative effectiveness of these commonly used veterinary agents within the same experimental adhesion model remain scarce. Therefore, the aim of the present study was to investigate the effects of intraperitoneal administration of flunixin meglumine, metamizole sodium, diclofenac sodium and carprofen on postoperative adhesion formation using a standardized rat cecal abrasion model.

Materials and methods

Ethics Statement

This study was approved by the Institutional Animal Experimentation Ethics Committee. All the experimental procedures were conducted in accordance with national and institutional guidelines for the care and use of laboratory animals.

Animals and experimental design

The study was conducted at the Experimental Animal Research Laboratory of the Faculty of Veterinary Medicine, Adnan Menderes University. A total of sixty healthy adult female Sprague-Dawley rats weighing approximately 236±17 g were used. The animals were housed in standard laboratory cages under controlled environmental conditions and had free access to commercial pellet feed and

drinking water throughout the experimental period.

Following overnight fasting, the animals were randomly allocated into six equal groups (n=10 per group): sham group, control group, flunixin meglumine group, metamizole sodium group, diclofenac sodium group and carprofen group.

Surgical Procedure and Drug Administration

General anesthesia was induced by intraperitoneal administration of ketamine hydrochloride (75 mg/kg) and xylazine hydrochloride (10 mg/kg). Following shaving and aseptic preparation of the abdominal region, a 3 cm ventral midline laparotomy was performed.

The cecum was exteriorized gently, and a standardized abrasion model was created by applying repeated strokes to the anterior cecal serosa using a sterile toothbrush until petechial hemorrhage became visible.

Immediately after induction of the adhesion model, treatment solutions were administered intraperitoneally in equal final volumes of 2 mL/kg in all experimental groups in order to standardize intraperitoneal exposure.

The treatment groups received:

- Flunixin meglumine: 2.5 mg/kg
- Metamizole sodium: 50 mg/kg
- Diclofenac sodium: 2.5 mg/kg
- Carprofen: 2.5 mg/kg

The control group received sterile 0.9% NaCl solution in the same final intraperitoneal volume. The abdominal wall was closed routinely in two layers using absorbable suture material for the muscle layer and non-absorbable suture material for the skin.

Postoperative monitoring and sample collection

Following recovery from anesthesia, animals were returned to their cages and maintained under standard laboratory conditions. Ten days after surgery, all animals were euthanized with an overdose of ketamine anesthesia.

The abdominal cavity was reopened through a reverse U-shaped incision to allow complete visualization of intra-abdominal organs. Adhesion formation between the cecum and surrounding tissues was evaluated macroscopically.

Blood samples were collected by cardiac puncture for hematological and biochemical analyses. Hemoglobin concentration and leukocyte counts were determined using an automated blood analyzer. Serum albumin levels were measured using standardized laboratory procedures.

Evaluation of adhesion formation

Adhesion severity was evaluated macroscopically on postoperative day 10 according to the Nair (1974) adhesion scoring system:

Grade	Description
0	No adhesions
1	Single thin adhesion
2	Two thin adhesions
3	More than two adhesions or localized dense adhesions
4	Generalized dense adhesions involving viscera and abdominal wall

All evaluations were performed independently by two blinded observers.

Determination of hydroxyproline levels

Adhesion tissue samples were collected on postoperative day 10 and stored at −85 °C until analysis. Hydroxyproline concentrations were determined spectrophotometrically according to the modified method previously described by Muscara et al. (2000). Results were expressed as µg/g tissue.

Statistical analysis

Adhesion scores were analyzed using the Kruskal–Wallis test. Hematological and biochemical parameters were evaluated by one-way analysis of variance (ANOVA), followed by Duncan's multiple comparison test when appropriate. Statistical analyses were performed using SPSS software, and

differences were considered statistically significant at $P<0.05$.

Results

Macroscopic evaluation of adhesion formation

Macroscopic examination performed on postoperative day 10 demonstrated that intra-abdominal adhesions were mainly located between the cecum and adjacent abdominal wall structures in animals subjected to the abrasion procedure. Adhesion severity differed among the experimental groups (Figure 1).

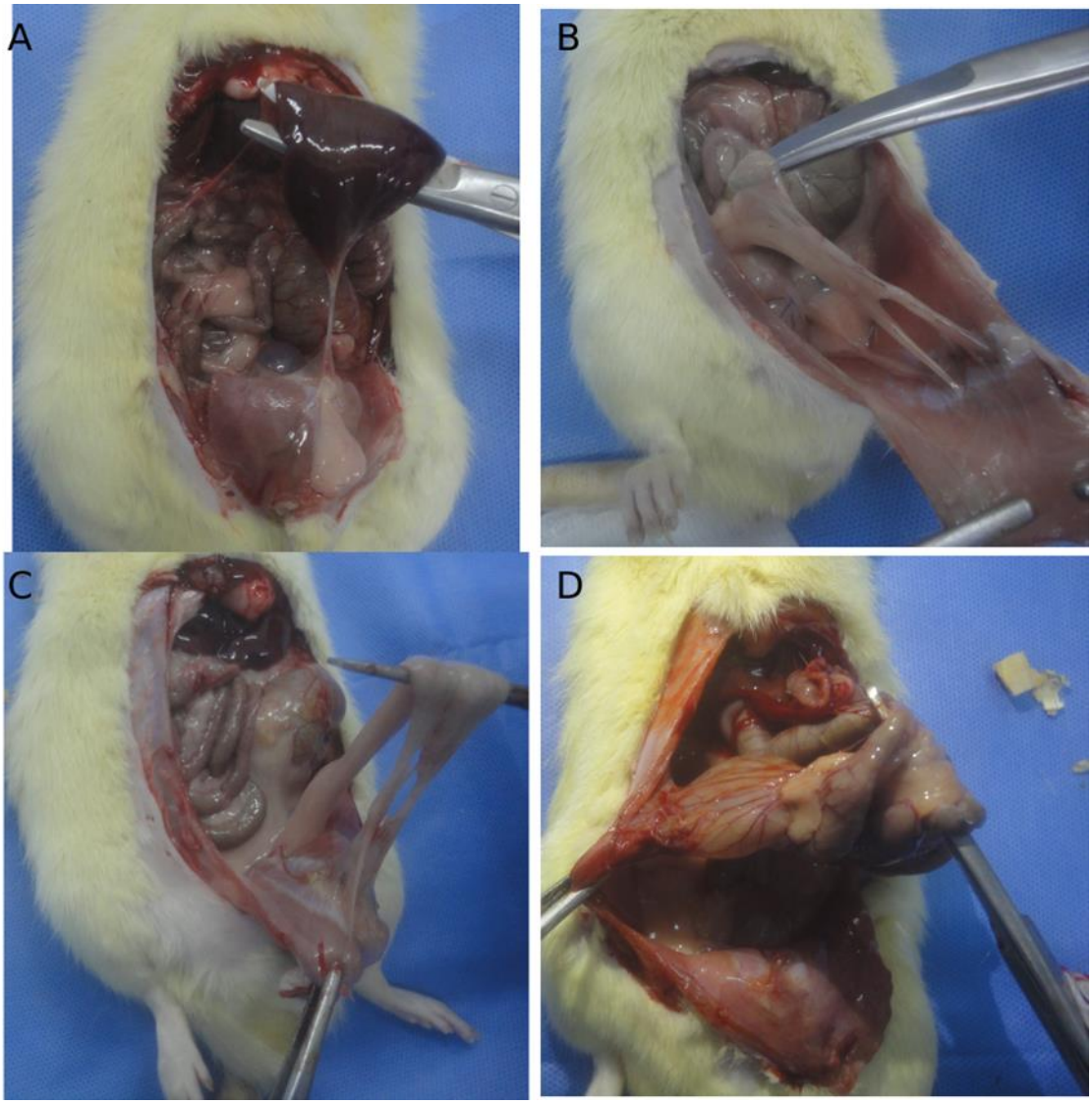

Figure 1: Representative intra-abdominal adhesion formations observed in rats (A) Grade 1 mild adhesion formation from control group. (B) Grade 2 moderate adhesion formation from flunixine group (C). Grade 3 marked adhesion formation from control group and (D) Grade 4 severe adhesion formation from control group.

The highest adhesion scores were observed in the control group, whereas all treatment groups showed reduced adhesion formation compared with controls. Among the evaluated agents, metamizole sodium and carprofen produced the most pronounced reduction in adhesion severity. The distribution of individual adhesion grades and mean adhesion scores for each group are presented in Table 1.

Statistical analysis revealed that adhesion scores in the flunixin meglumine, metamizole sodium, diclofenac sodium and carprofen groups were significantly lower

than those of the control group (P<0.05) (Table 1).

Hematological and biochemical findings

Mean erythrocyte counts, leukocyte counts, packed cell volume values and serum albumin concentrations were similar among experimental groups and did not show statistically significant differences. Detailed hematological and biochemical findings are summarized in Table 2.

However, eosinophil counts were significantly lower in the metamizole sodium group compared with the flunixin meglumine group (P<0.05). In addition, eosinophil values in the carprofen group were significantly reduced compared with the control group (P<0.05) (Table 2). No statistically significant differences were detected in other differential leukocyte parameters.

Table 1: Individual and mean (±SEM) adhesion scores of the rats from the sham, control and treatment groups

Groups	n	Grade					Average [a]
		0	1	2	3	4	
Sham	10	0	2	2	1	3	2.10+0.37
Control	10	0	1	2	4	1	2.20+0.42
Flunixin Meglumine	10**	4	3	1	0	1	0.90+0.18
Metamizol	10*	8	2	0	0	0	0.20+0.05
Diclofenac	10**	5	4	1	0	0	0.60+0.24
Carprofen	10*	7	2	1	0	0	0.30+0.11

* Statistically different from control (P<0.005).
** Statistically different from control (P<0.01).
[a] The data were expressed as means ± standard errors (SEM).

Table 2: Albumin, erythrocyte and total and differential leucocyte counts in the all groups (mean ± SE)

Parameters	Sham (*n* = 10)	Control (*n* = 10)	Flunixin Meglumine (*n* = 10)	Metamizol (*n* = 10)	Diclofenac (*n* = 10)	Carprofen (*n* = 10)
RBC (10^6/µl)	7.90 ± 0.73	7.53 ± 0.21	7.42 ± 0.60	7.81 ± 0.86	7.92 ± 0.60	7.85 ± 0.66
WBC (10^3/µl)	7.70 ± 1.02	7.44 ± 0.42	8.08 ± 0.97	7.83 ± 0.19	7.91 ± 1.93	7.47 ± 0.52
PCV(%)	40.80 ± 1.07	39.70 ± 0.84	39.00 ± 1.46	39.80 ± 0.94	40.77 ± 0.46	39.95 ± 0.74
Neu (%)	39.50 ± 4.52	36.20 ± 4.95	37.87 ± 3.40	40.80 ± 2.30	36.47 ± 0.40	41.00 ± 4.30
Eos (%)	3.16 ± 0.56	3.60 ± 0.72	3.88 ± 0.60	2.71 ± 0.88*	3.08 ± 0.20	3.71 ± 0.18
Baso (%)	0.56 ± 0.23	0.50 ± 0.26	0.87 ± 0.32	0.57 ± 0.20	0.77 ± 0.22	0.47 ± 0.20**
Lym (%)	55.20 ± 1.78	59.60 ± 1.96	54.45 ± 0.67	60.28 ± 0.92	61.85 ± 0.76	58.28 ± 0.52
Monocyte(%)	2.60 ± 0.10	2.78 ± 0.41	3.00 ± 1.43	2.82 ± 0.20	2.00 ± 0.23	2.52 ± 0.40
Albumin	3.76 ± 0.5	3.70 ± 0.2	3.88 ± 0.60	3.61 ± 0.58	3.98 ± 0.30	3.71 ± 0.18

* Statistically different from control groups (P<0.05).
** Statistically different from flunixin group (P<0.05).

Hydroxyproline analysis

Hydroxyproline concentrations measured in adhesion tissue samples varied between groups and reflected differences in collagen deposition within adhesion areas.

The lowest hydroxyproline levels were detected in the carprofen-treated group. This reduction was statistically significant compared with the flunixin meglumine, metamizole sodium and diclofenac sodium groups ($P<0.05$). Quantitative hydroxyproline values obtained from each experimental group are presented in Table 3.

Table 3: Effect of flunixin meglumine, metamizole, diclofenac and carprofen on hydroxyproline content (pg/mg protein) of adhesion tissue (Values are mean±SE).

Parameter	Control	Sham	F.meglumine	Metamizol	Diclofenac	Carprofen
Hidroxyproline (µg/g tissue)	13.1±3.6	15.2±3.3	29.9±6.4	22.1±7.0	21.6±5.1	6.1±0.7*

*Statistically different from flunixin, metamizol and diclofenac group, P<0,05; ± SE (Standart error).

Discussion

Postoperative intra-abdominal adhesions remain one of the most important complications following abdominal surgery and continue to represent a significant clinical challenge in both human and veterinary practice. Adhesion formation results from a cascade of inflammatory responses triggered by peritoneal injury, leading to fibrin deposition, fibroblast proliferation and extracellular matrix remodeling (Hellebrekers et al., 2000). In the present study, intraperitoneal administration of flunixin meglumine, metamizole sodium, diclofenac sodium and carprofen significantly reduced adhesion severity compared with the control group (Table 1). These findings are consistent the with previous experimental studies demonstrating that modulation of early inflammatory mediators plays a critical role in limiting postoperative adhesion formation (Siegler et al., 1980; Baykal et al., 1997).

Peritoneal healing depends on the balance between fibrin deposition and fibrinolytic activity following tissue injury. Disruption of this balance results in persistent fibrotic adhesions between adjacent tissues (Ellis, 1971). Cyclooxygenase-mediated prostaglandin synthesis contributes to inflammatory cell recruitment and fibroblast activation during early wound healing. Therefore, inhibition of cyclooxygenase activity by NSAIDs may reduce adhesion formation through suppression of inflammatory signaling pathways (Muscara et al., 2000). The significantly lower adhesion scores observed in treatment groups compared with controls (Table 1), support this proposed mechanism.

Among the evaluated agents, metamizole sodium and carprofen demonstrated particularly pronounced reductions in adhesion severity. Similar reductions in adhesion formation have been reported in recent experimental studies evaluating pharmacological agents targeting inflammatory and fibrotic pathways in rat adhesion models (Kakanezhadi et al., 2022; Bayhan et al., 2016). These effects may be associated with inhibition of cytokines such as interleukin-6 and tumor necrosis factor-alpha, which are known to play important roles during adhesion development (Saba et al., 1996; Hershlag et al., 1991).

Evaluation of hematological parameters revealed no marked systemic alterations among experimental groups (Table 2), suggesting that intraperitoneal administration of the investigated NSAIDs did not produce significant systemic adverse effects. Similar safety profiles have been reported in the previous experimental adhesion prevention studies evaluating locally administered anti-inflammatory agents (Siegler et al., 1980).

Hydroxyproline concentration is widely accepted as a biochemical indicator of collagen accumulation and fibrosis in healing tissues (Muscara et al., 2000). Reduced hydroxyproline levels observed particularly in the carprofen-treated group (Table 3) suggest decreased collagen deposition within adhesion tissues. Similar findings have been reported in experimental adhesion prevention studies evaluating antifibrotic strategies targeting extracellular matrix remodeling (Baykal et al., 1997). The lower hydroxyproline concentrations observed particularly in the carprofen-treated group may reflect reduced collagen deposition and attenuation of excessive fibrotic tissue remodeling during the healing process. Hydroxyproline is widely accepted as an indirect biochemical marker of collagen synthesis and extracellular matrix accumulation within adhesion tissues. Therefore, reduced hydroxyproline levels may indicate suppression of fibroblast activity and limitation of pathological fibrosis rather than impaired tissue healing. Similar reductions in hydroxyproline concentration have been associated with decreased adhesion severity in the previous experimental anti-adhesion studies.

In addition, the observed differences among sham, control, and treatment groups may be explained by variations in the degree of peritoneal injury and inflammatory response. The sham group underwent laparotomy without severe peritoneal abrasion and therefore exhibited minimal inflammatory stimulation and limited adhesion formation. In contrast, the control group developed pronounced inflammatory reactions and extensive fibrin deposition following standardized cecal abrasion, resulting in higher adhesion scores. Treatment groups demonstrated reduced adhesion severity, likely due to the anti-inflammatory and antifibrotic effects of the administered NSAIDs, which may have modulated cytokine release, fibroblast proliferation, and extracellular matrix remodeling during peritoneal healing.

Recent systematic reviews have emphasized that although several pharmacological and biomaterial-based strategies show promising results in experimental adhesion prevention models, no single intervention has completely eliminated adhesion formation in clinical practice (Fatehi Hassanabad et al., 2021; Schaefer et al., 2024). Therefore, identification of safe and accessible pharmacological alternatives remains an important research objective. The results obtained in the present study suggest that locally administered NSAIDs may represent a useful supportive strategy for reducing postoperative adhesion severity.

Another important aspect of the present study is the use of intraperitoneal administration immediately after induction of peritoneal injury. Local drug delivery may allow higher concentrations at the site of injury while minimizing systemic exposure, which may enhance anti-adhesive efficacy. Similar advantages of localized pharmacological strategies have been highlighted in recent adhesion prevention research (Cofer et al., 1994, Pu et al.,).

Despite these promising findings, further experimental studies including longer observation periods, histopathological evaluation and cytokine profiling are required to better clarify the molecular mechanisms underlying the observed anti-adhesive effects. In addition, controlled clinical investigations will be necessary to determine whether similar outcomes can be achieved under clinical surgical conditions.

In conclusion, intraperitoneal administration of flunixin meglumine, metamizole sodium, diclofenac sodium, and carprofen reduced postoperative intra-abdominal adhesion formation in the experimental rat model.

Among the evaluated agents, metamizole sodium and carprofen demonstrated the most pronounced anti-adhesive effects. Reduced hydroxyproline concentrations in

the carprofen group further supported decreased collagen deposition and fibrosis within adhesion tissues.

The findings suggest that local intraperitoneal administration of selected NSAIDs may represent a useful supportive pharmacological strategy for reducing postoperative adhesion formation.

Further studies involving histopathological evaluation, cytokine analysis, and longer observation periods are warranted to better clarify the underlying molecular mechanisms and potential clinical applicability of these findings.

Acknowledgment

The authors respectfully dedicate this study to the memory of Serdar Köklü.

Conflict of interest

The authors declare that they have no financial or non-financial conflict of interest regarding authorship and publication of this article

Funding

This study was supported by the Adnan Menderes University Research Fund (Project No: VTF-07014), as part of the MSc thesis conducted by the late Serdar Köklü.

References

Akhlaghi, S., Ebrahimnia, M., Niaki, D. S., Solhi, M., Rabbani, S., & Haeri, A. (2023). Recent advances in preventative strategies for postoperative adhesions using biomaterial-based membranes and micro/nano drug delivery systems. *Journal of Drug Delivery Science and Technology, 85*, 104539.

Avsar, F. M., Sahin, M., Aksoy, F., Avsar, F. A., Akoz, M., & Hengirmen, S. (2001). Effects of diphenhydramine HCl and methylprednisolone in prevention of abdominal adhesions. *American Journal of Surgery, 181*, 512–515.

Bayhan, Z., Zeren, S., Kocak, F. E., Kocak, C., Akcılar, R., Kargı, E., Tiryaki, C., Yaylak, F., & Akcılar, A. (2016). Antiadhesive and anti-inflammatory effects of pirfenidone in postoperative intra-abdominal adhesion in an experimental rat model. *The Journal of surgical research, 201*(2), 348–355.

Baykal, A., Onat, D., Rasa, K., Renda, N., & Sayek, I. (1997). Effects of polyglycolic acid and polypropylene meshes on postoperative adhesion formation in mice. *World journal of surgery, 21*(6), 579–583.

Cofer, K. F., Himebaugh, K. S., Gauvin, J. M., & Hurd, W. W. (1994). Inhibition of adhesion reformation in the rabbit model by meclofenamate: an inhibitor of both prostaglandin and leukotriene production. *Fertility and sterility, 62*(6), 1262–1265.

Dunn, R. C., Steinleitner, A. J., & Lambert, H. (1991). Synergistic effect of intraperitoneally administered calcium channel blockade and recombinant tissue plasminogen activator to prevent adhesion formation in an animal model. *American journal of obstetrics and gynecology, 164*(5 Pt 1), 1327–1330.

Ellis, H. (1971). The cause and prevention of postoperative intraperitoneal adhesions. *Surgery, Gynecology & Obstetrics, 133*, 497–511.

Fatehi Hassanabad, A., Zarzycki, A. N., Jeon, K., Deniset, J. F., & Fedak, P. W. M. (2021). Prevention of postoperative adhesions: A comprehensive review of present and emerging strategies. *Biomolecules, 11*, 1027.

Hellebrekers, B. W., Trimbos-Kemper, T. C., Trimbos, J. B., Emeis, J. J., & Kooistra, T. (2000). Use of fibrinolytic agents in the prevention of postoperative adhesion formation. *Fertility and sterility, 74*(2), 203–212.

Hershlag, A., Otterness, I. G., Bliven, M. L., Diamond, M. P., & Polan, M. L. (1991). The Effect of Interleukin-1 on Adhesion Formation in the Rat. *American Journal of Obstetrics and Gynecology, 165*(3), 771–774.

Kakanezhadi, A., Rezaei, M., Raisi, A., Dezfoulian, O., Davoodi, F., & Ahmadvand, H. (2022). Rosmarinic acid prevents postoperative abdominal adhesions in a rat model. *Scientific Reports, 12*, 18593.

Menzies, D., & Ellis, H. (1990). Intestinal obstruction from adhesions: How big is the problem? *Annals of the Royal College of Surgeons of England, 72*, 60–63.

Muscará, M. N., McKnight, W., Asfaha, S., & Wallace, J. L. (2000). Wound collagen deposition in rats: effects of an NO-NSAID and a selective COX-2 inhibitor. *British Journal of Pharmacology*, *129*(4), 681–686.

Nair, S. K., Bhat, I. K., & Aurora, A. L. (1974). Role of proteolytic enzyme in the prevention of postoperative intraperitoneal adhesions. *Archives of Surgery*, *108*, 849.

Nishimura, K., Nakamura, R. M., & Dizerega, G. S. (1984). Ibuprofen inhibition of postsurgical adhesion formation: Biochemical evaluation in rabbits. *Journal of Surgical Research, 36*, 115–124.

Pu, Z., Nian, H., Li, Z., Zhong, P., Ma, S., & Li, J. (2025). Research progress on animal models of peritoneal adhesion. Surgery, 178, 108929.

Rodgers, K. E., Girgis, W., St Amand, K., Campeau, J. D., & diZerega, G. S. (1998). Reduction of adhesion formation by intraperitoneal administration of various anti-inflammatory agents. Journal of investigative surgery: *the official Journal of the Academy of Surgical Research*, *11*(5), 327–339.

Saba, A. A., Kaidi, A. A., Godziachvili, V., Dombi, G. W., Dawe, E. J., Libcke, J. H., & Silva, Y. J. (1996). Effects of interleukin-6 and its neutralizing antibodies on peritoneal adhesion formation and wound healing. *The American surgeon*, *62*(7), 569–572.

Schaefer, S. D., Alkatout, I., Dornhoefer, N., Herrmann, J., Klapdor, R., Meinhold-Heerlein, I., Meszaros, J., Mustea, A., Oppelt, P., Wallwiener, M., & Kraemer, B. (2024). Prevention of peritoneal adhesions after gynecological surgery: a systematic review. *Archives of Gynecology and Obstetrics*, *310*(2), 655–672.

Siegler, A. M., Kontopoulos, V., & Wang, C. F. (1980). Prevention of postoperative adhesions in rabbits with ibuprofen, a nonsteroidal anti-inflammatory agent. *Fertility and sterility*, *34*(1), 46–49.

Treutner, K. H., & Schumpelick, V. (2000). Adhäsionsprophylaxe. Wunsch und Wirklichkeit [Prevention of adhesions. Wish and reality]. Der Chirurg; Zeitschrift fur alle Gebiete der operativen Medizen, 71(5), 510–517.

Received: 29.04.2026
Accepted: 08.07.2026

Vol. 22, No. 2, Summer, 2026, 89-98 *Original Article*
DOI: 10.22055/ivj.2026.557381.2866
Journal Homepage: http://www.ivj.ir/

In Vitro Evaluation of the Synergistic Antibacterial and Antibiofilm Activities of *Parietaria muralis* Extract and Chitosan Nanoparticles

Afshin Salehi[1], Masoud Ghorbanpoor[2*], Ali Nazari Alam[3] and Amin Nematollahi[4]

[1] PhD Student of Bacteriology, Faculty of Veterinary Medicine, Shahrekord University, Shahrekord, Iran
[2] Professor, Department of Pathobiology, Faculty of Veterinary Medicine, Shahrekord University, Shahrekord, Iran
[3] Associate Professor, Department of Microbiology and Immunology, Faculty of Medicine, Kashan University of Medical Sciences, Kashan, Iran
[4] Associate Professor, Department of Food Hygiene and Quality Control, Faculty of Veterinary Medicine, School of Veterinary Medicine, Shahrekord University, Shahrekord, Iran

Received: 04.11.2025 Accepted: 25.06.2026

Abstract

Herbal medicines incorporated with nanomaterials have garnered considerable attention in biomedicine; however, the antibacterial potential of combining chitosan with *Protoparmeliopsis muralis* (*P. muralis*) extract has not yet been investigated. The present study aimed to evaluate the synergistic effect of *P. muralis* and chitosan nanoparticles (CS/NPs) against selected pathogenic bacteria. Antibacterial activity was assessed using the minimum inhibitory concentration (MIC) assay, while antibiofilm effects were determined by the crystal violet assay. A mixture containing 10% *P. muralis* extract and 0.5% CS/NPs was prepared, and the synergistic interaction was further examined by the checkerboard titration method. The results revealed that CS/NPs exhibited stronger antibacterial activity than *P. muralis* extract alone. Furthermore, the checkerboard assay confirmed a synergistic effect between *P. muralis* and CS/NPs. The combined treatment also significantly enhanced antibiofilm activity, highlighting its potential as a promising strategy for controlling bacterial growth and biofilm-associated infections. In conclusion, these findings indicate that the combination of *P. muralis* extract and chitosan nanoparticles may serve as a potential candidate for further studies focused on the identification and development of novel antibacterial and antibiofilm compounds. Future research, including mechanistic studies and in vivo evaluations, is necessary to better understand and validate the observed effects.

Key words: Chitosan, Lichen, Antibacterial, Antibiofilm

Introduction

Over the past decades, the prevention and treatment of infectious diseases have remained major public health challenges. These infections are associated with prolonged hospital stays, increased healthcare costs, and high mortality rates (Sydnor and Perl, 2011). One of the major obstacles in the treatment of bacterial infections is antibiotic resistance (Kolář, 2022). Antibiotic resistance arises through multiple mechanisms and is often associated with a variety of virulence factors, among which biofilm formation plays a key role by contributing to both resistance to antibiotics and evasion of host immune responses (Schroeder et al, 2017). Biofilm formation is an important survival strategy that enables bacteria to persist in

* **Corresponding Author**: Masoud Ghorbanpoor, Professor, Department of Pathobiology, Faculty of Veterinary Medicine, Shahrekord University, Shahrekord, Iran
E-mail: ghorbanpoor-m@sku.ac.ir

the presence of antibiotics. Biofilms are estimated to account for approximately 60% to 85% of bacterial infections in humans (Abebe, 2020). These infections are particularly difficult to treat because the biofilm matrix restricts the penetration of antimicrobial agents (Singh et al, 2022). Therefore, the discovery and development of novel antibiofilm and antibacterial agents capable of preventing biofilm formation, disrupting established biofilms, and treating biofilm-associated infections are urgently needed. New strategies for combating multidrug-resistant (MDR) bacterial strains include the use of nanoparticles, phage therapy, and secondary metabolites. Among these, secondary metabolites from medicinal plants have attracted considerable attention due to their antibacterial, antifungal, anticancer, anti-inflammatory, and antioxidant properties, and they may represent a promising and innovative approach against pathogenic bacteria (Bhatti et al, 2022).

Lichens have long been used in traditional medicine and are known for their potential in treating bacterial infections (Shrestha and Clair, 2013). In this context, *Protoparmeliopsis muralis*, a member of the lichen family, has shown promising biomedical applications due to its favorable physicochemical properties, including biocompatibility, biodegradability, and non-toxicity (Rashki et al, 2021). Moreover, this lichen contains a variety of bioactive compounds such as flavonoids, phenolics, phenolic acids, terpenoids, alkaloids, tannins, and quinones, which exhibit a wide range of biological activities, including antioxidant, antibacterial, antitumor, antiviral, and antifungal effects (Shrestha and Clair, 2013; Bhatti et al, 2022).

Chitosan (CS), a biodegradable polysaccharide, is widely used in nanotechnology due to its broad range of applications (Rashki and Valadbeigi, 2017).

CS is a naturally occurring biopolymer with promising biomedical potential, attributed to its physicochemical properties such as biocompatibility, biodegradability, and non-toxicity. Studies have demonstrated its therapeutic activities, including antibacterial, antiviral, and antioxidant effects, as well as its ability to inhibit biofilm formation (Gao and Wu, 2022; Varma and Vasudevan, 2020). Furthermore, several studies suggest that the integration of herbal medicines with nanotechnology provides a promising strategy to enhance their thermal stability, bioavailability, biological activity, and mechanical properties (Rashki et al, 2021).

Based on these encouraging results, the present study focused on the synergistic antimicrobial activity of chitosan–lichen extract against pathogenic bacteria. To the best of our knowledge, this is among the first studies to investigate the potential effects of this combination. Therefore, the aim of this work was to evaluate the antibacterial and antibiofilm activities of chitosan nanoparticles combined with *P. muralis* extract against pathogenic bacteria.

Materials and Methods

Preparation of Chitosan Nanoparticles

Chitosan nanoparticles were synthesized by the ionotropic gelation method (Algharib et al, 2022; Huang et al, 2016). Briefly, 10 mg of chitosan powder (degree of deacetylation 95%, molecular weight 100–300 kDa; Acros Organics, USA) was dissolved in 1% (v/v) glacial acetic acid (Merck, Germany, pH 5) and stirred at 25 °C for 24 h. A Sodium tripolyphosphate (TPP, Merck, Germany) solution (1 mg/mL in deionized water, pH 4) was then added dropwise under continuous stirring at 25 °C for 4 h. The suspension was centrifuged at 14,000 rpm for 40 min, the pellet was washed with deionized water, and the product was freeze-dried for 24 h.

Preparation of Methanolic Extract of *P. muralis*

The lichen *P. muralis* was collected from Ilam Province, Iran. Dried material (50 g) was extracted with 500 mL of methanol

using a Soxhlet apparatus for 48 h. The extract was concentrated by evaporation at 70 °C for 8 h, dried, and subsequently dissolved in 5% dimethyl sulfoxide (Merck, Germany) for experimental use (Aydın et al, 2013).

Characterization of Chitosan Nanoparticles

The structural features of CS, TPP, and the prepared CS/NPs were analyzed using Fourier Transform Infrared (FTIR) spectroscopy. FTIR spectra of the samples were recorded in the 400–4000 cm^{-1} range using a Nicolet™ Magana 550 FT-IR spectrometer. The morphology and dispersion of the nanoparticles (NPs) were examined by scanning electron microscopy (SEM). The particle size distribution and zeta potential of the synthesized chitosan nanoparticles were determined using dynamic light scattering (DLS) and electrophoretic light scattering techniques with a Zeta sizer instrument at 25°C (Hoang et al, 2022).

Bacterial Isolates

To evaluate the antibacterial activity of the aforementioned compounds, four bacterial clinical isolates from urine samples including *Staphylococcus aureus*, *Enterococcus faecalis*, *Escherichia coli*, and *Pseudomonas aeruginosa* were employed.

Biofilm Detection

Biofilm formation was assessed using the microtiter plate assay. Bacterial suspensions (200µL, 0.5 McFarland standard) were inoculated into 96-well plates and incubated at 37°C for 24 h. Wells were washed twice with PBS, fixed with 200µL methanol (Merck, Germany) for 20 min, and air-dried. Cells were stained with crystal violet (Merck, Germany), washed with PBS, and absorbance was measured at 630 nm using an ELISA reader. Isolates were classified according to the criteria described by O'Toole (2011), in which an OD630 value of ≤ 0.38 indicated weak biofilm formation, values between 0.38 and 0.70 indicated moderate biofilm formation, and values ≥ 0.70 indicated strong biofilm formation.

Antimicrobial Activity Assay

Minimum inhibitory concentrations (MICs) of CS/NPs and *P. muralis* extract were determined by the broth microdilution method according to CLSI guidelines (CLSI, 2018). Serial dilutions of the test samples (2500–4.9µg/mL) were prepared in 96-well plates containing Mueller Hinton Broth (Merck, Germany). Each well was inoculated with 10µL of bacterial suspension (1.5×10^5 CFU/mL) and incubated at 37 °C for 18–24 h. MIC was defined as the lowest concentration that inhibited visible bacterial growth (Aydın et al., 2013; Meletiadis et al, 2009).

Inhibitory Effect on Biofilm Formation

The effect of CS/NPs and *P. muralis* extract on biofilm inhibition was evaluated using the microtiter plate technique (Aydın et al, 2013; O'Toole, 2011). Bacterial suspensions were inoculated into 96-well plates, followed by the addition of CS/NPs and *P. muralis* extract at concentrations of 250 and 500µg/mL. Plates were incubated at 37 °C for 24 h, then washed with PBS. Wells were fixed with 200µL methanol for 20 min, air-dried, stained with crystal violet, and washed with PBS. Absorbance was recorded at 630 nm.

Synergistic Effect of CS/NPs and *P. muralis* Extract

The combined antibacterial effects of CS/NPs and *P. muralis* extract were assessed using the checkerboard titration method (Meletiadis et al, 2009). Fractional inhibitory concentration (FIC) indices were calculated, where the FIC of CS-NPs was defined as the MIC of CS-NPs in the presence of *P. muralis* divided by the MIC of CS-NPs alone, and the FIC of *P. muralis* was defined as the MIC of P. muralis in the presence of CS-NPs divided by the MIC of P. muralis alone. The overall FIC index was

obtained by summing these two values, and the interaction was interpreted as synergistic when the FIC index was < 1, additive when it was equal to 1, and antagonistic when it was > 1.

Statistical Analysis

All experiments were performed in triplicate, and the results are expressed as mean ± standard error of mean (SEM). Statistical analyses were carried out using GraphPad InStat 3 (GraphPad Software, San Diego, CA, USA). The normality of data distribution was evaluated using the Shapiro–Wilk test.

Differences among multiple groups, including antimicrobial and antibiofilm activities of chitosan nanoparticles (CS/NPs), *P. muralis* extract, and their combinations against different bacterial isolates, were analyzed using one-way analysis of variance (ANOVA) followed by Tukey's multiple comparison post hoc test. Comparisons between two groups were analyzed using the independent Student's t-test.

Results

FTIR Analysis of CS/NPs

The FTIR spectrum of the fabricated CS/NPs (Figure 1) exhibited a broad peak at ~3422 cm^{-1}, more pronounced than that of chitosan, corresponding to O–H and N–H stretching vibrations. The bands at ~2922 and 2896 cm^{-1} can be attributed to asymmetric C–H stretching of $–CH_3$ and $–CH_2$ groups (Jayakumar et al., 2011). In CS/NPs, the splitting of the 1630 cm^{-1} peak into two distinct bands suggests NH_2 bending vibrations and deacetylation, consistent with other FTIR analyses. Additionally, bands at ~1092 and 1087 cm^{-1} correspond to C–O stretching, while the appearance of signals near ~1100 cm^{-1} in TPP-containing samples aligns with phosphate group vibrations (Cushnie et al, 2014).

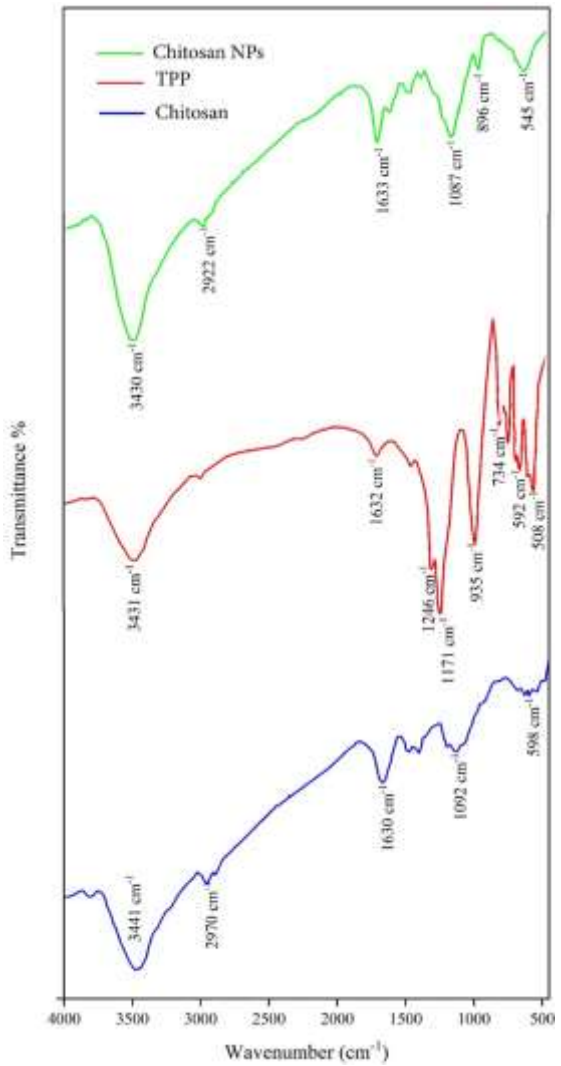

Figure 1: FTIR spectra of chitosan (CS), sodium tripolyphosphate (TPP), and the prepared chitosan nanoparticles (CS-NPs).

Characterization of CS/NPs

SEM imaging demonstrated that the prepared nanoparticles exhibited a uniform spherical morphology with smooth surfaces and narrow size distribution (Figure 2), which is advantageous for biomedical applications (Hoang et al, 2022). The particle size and zeta potential of chitosan nanoparticles in the current study using the ionotropic gelation method was in the range of 100–300 nm and +30 to +50 mV, respectively.

Antibacterial Activity of CS/NPs

CS/NPs exhibited significantly (P≤0.05) higher antibacterial activity than *P. muralis* extract against all tested isolates. Gram-positive bacteria (*S. aureus* and *E. faecalis*) were more susceptible than Gram-negative bacteria. MIC values of CS/NPs were 78.125, 156.25, 625, and 1250 µg/mL for *S. aureus*, *E. faecalis*, *E. coli*, and *P. aeruginosa*, respectively. Corresponding MICs for *P. muralis* extract were 156.25, 312.5, 2500, and 1250 µg/mL, respectively (Table 1).

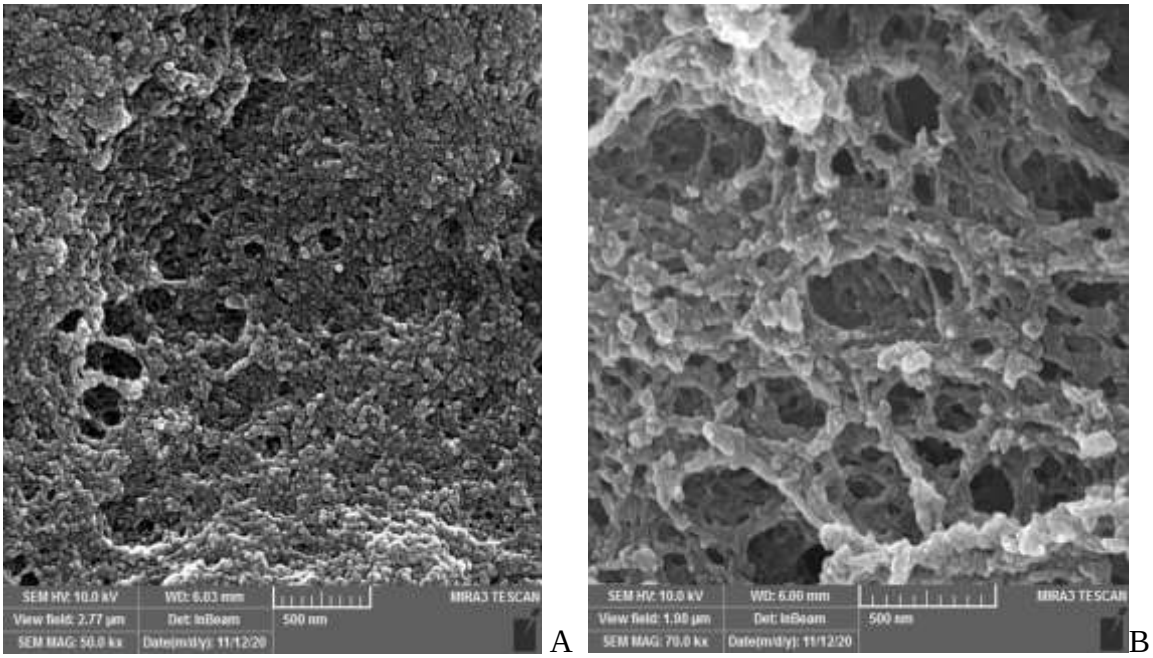

A B

Figure 2: Representative scanning electron microscopy (SEM) images of the synthesized chitosan nanoparticles (CS-NPs) showing the morphology of the particles at magnifications of (A) 50,000× and (B) 70,000×.

Table 1: Antibacterial activity of chitosan nanoparticles (CS/NPs) and *P. muralis extract* against *S. aureus, E. faecalis, E. coli*, and *P. aeruginosa* local clinical isolates

Bacteria	CS/NPs		*P. muralis*	
	MIC µg/ml	MBC µg/ml	MIC µg/ml	MBC µg/ml
S. aureus	78.125	78.125	156.25	625
E. feacalis	156.25	625	312.5	1250
E. coli	312.5	625	2500	2500
P. aeroginosa	1250	1250	1250	2500

Antibiofilm Activity of CS/NPs

The antibiofilm potential of CS/NPs and *P. muralis* extract is presented in table 2. The results demonstrated that these compounds were able to reduce biofilm formation at various concentrations, although the degree of inhibition varied depending on the bacterial species and the specific compound. Generally, the compounds at lower concentrations (0.5MIC) significantly decreased the initial adhesion of bacterial cells to surfaces, while higher concentrations (1MIC) exhibited a stronger antibiofilm effect. These findings suggest that the studied compounds not only possess antibacterial activity but also can inhibit the development of stable biofilms, which is crucial for preventing drug resistance and enhancing the efficacy of antibacterial treatments.

Table 2: Inhibitory effects of chitosan nanoparticles (CS/NPs) and *P. muralis* extract on *S. aureus*, *E. faecalis*, *E. coli*, and *P. aeruginosa* local clinical isolates biofilm formation. MIC: minimum inhibitory concentration; 0.5 MIC: half of the MIC value. Data are presented as mean ± SEM. Means with different letters within the same row are significantly different (P≤0.05)

Bacteria	CS/NPs		*P. muralis*	
	1 MIC	0.5 MIC	1 MIC	0.5 MIC
S. aureus	$^{A}65 \pm 2.6$	$^{B}55 \pm 2.9$	$^{C}51.3 \pm 1.8$	$^{D}46 \pm 1.5$
E. feacalis	$^{A}60 \pm 2.1$	$^{B}57.7 \pm 1.4$	$^{C}49.3 \pm 0.9$	$^{D}45.3 \pm 1.4$
E. coli	$^{B}48 \pm 1.5$	$^{B}44.3 \pm 1.2$	$^{C}37.3 \pm 1.4$	$^{D}27.3 \pm 1.4$
P. aeroginosa	$^{B}43 \pm 0.9$	B40.3 ± 0.9	$^{C}32.3 \pm 1.4$	$^{D}26.6 \pm 0.9$

CS/NPs markedly suppressed biofilm formation by 65±2.6% in *S. aureus*, 60±2.1% % in *E. faecalis*, 48±1.5% % in *E. coli*, and 43±0.9% in *P. aeruginosa*, whereas *P. muralis* extract showed significantly (P≤0.05) lower inhibition.

Notably, a comparison between Gram-positive and Gram-negative bacteria indicated that Gram-positive strains were relatively more sensitive to the antibiofilm effects of the compounds, which may be related to differences in cell wall structure and adhesion mechanisms.

Synergistic Effect of CS/NPs

FIC index values for the combination of CS/NPs and *P. muralis* extract were 0.39, 0.41, 0.64, and 0.75 for *S. aureus, E. faecalis, E. coli,* and *P. aeruginosa*, respectively, indicating synergism.

Discussion

The physicochemical analysis confirmed the successful fabrication of chitosan nanoparticles (CS/NPs) through ionic gelation with sodium tripolyphosphate (TPP). FTIR spectra revealed a characteristic broad peak at 3422 cm^{-1}, corresponding to stretching vibrations of hydroxyl, water, and amine groups, which is in agreement with earlier findings on chitosan-based nanoparticles (Varma and Vasudevan, 2020). The shift of the amide peak from 1630 cm^{-1} to two distinct bands in the CS/NPs spectrum further indicated strong electrostatic interactions between amino groups of chitosan and phosphate groups of TPP, signifying successful crosslinking and partial deacetylation. The appearance of phosphate-related signals provided additional confirmation of the crosslinking process.

SEM imaging demonstrated that the prepared nanoparticles exhibited a uniform spherical morphology with smooth surfaces and narrow size distribution. Such morphological consistency is considered advantageous for biomedical applications, as uniform particle size can enhance stability, reproducibility, and bioavailability. In particular, nanoscale dimensions increase surface area-to-volume ratio, facilitating stronger interactions with bacterial membranes and improved drug or metabolite loading capacity (Xie et al, 2015).

Methanolic extracts of *P. muralis* demonstrated concentration-dependent antibacterial activity against all tested bacterial isolates. Gram-positive bacteria were more sensitive than Gram-negative isolates, likely due to differences in cell wall structure. Gram-negative bacteria possess a lipopolysaccharide-rich outer membrane that acts as a selective barrier, restricting the entry of many hydrophobic compounds. By contrast, Gram-positive bacteria, which lack this outer membrane, are more susceptible to direct interactions with phytochemicals (Xie et al, 2015; Okoth et al, 2013).

The antibacterial potential of *P. muralis* has been documented in several reports. Valadbeigi et al. demonstrated stronger activity of methanolic extracts compared to aqueous fractions, particularly against *S. aureus* and *S. epidermidis* (Valadbeigi et al, 2020). Almola et al. also reported higher

inhibitory activity against Gram-positive than Gram-negative strains, supporting our observations (Almola et al, 2021). The bioactivity of *P. muralis* is largely attributed to secondary metabolites, including flavonoids, phenolic acids, terpenoids, alkaloids, tannins, and quinones (Bhatti et al, 2022; Shrestha and Clair, 2013; Xie et al, 2015; Okoth et al, 2013). These compounds exert diverse pharmacological effects such as antioxidant, antiviral, antibacterial, antifungal, and antitumor activities.

The antibacterial mechanisms of these metabolites have been widely studied. Alkaloids can intercalate into DNA or disrupt bacterial cell walls, leading to impaired replication and structural instability. Flavonoids interfere with nucleic acid synthesis, inhibit energy metabolism, and alter membrane permeability (Okoth et al, 2013). Phenolic compounds and terpenoids destabilize bacterial membranes by inserting into lipid bilayers and causing leakage of intracellular contents (Valadbeigi et al, 2020). Anthraquinones, on the other hand, can promote the generation of reactive oxygen species, leading to oxidative damage and bacterial cell death (Almola et al, 2021). The synergistic presence of these metabolites in *P. muralis* extract likely accounts for its broad-spectrum but moderate antibacterial effect.

Our findings revealed that CS/NPs inhibited the growth of *S. aureus*, *E. faecalis*, *E. coli*, and *P. aeruginosa* at MIC values of 78.125, 156.25, 625, and 1250 µg/mL, respectively. These results are consistent with the previous reports, although MIC values vary depending on bacterial strains and nanoparticle properties. For example, Valian et al. reported an MIC of 0.625 µg/mL against *S. mutans* (Valian et al, 2020), while Divya et al. demonstrated activity against *E. coli*, *K. pneumoniae*, *P. aeruginosa*, and *S. aureus* with MICs ranging from 64–512 µg/mL (Divya et al, 2017). Vimal et al. reported values of 128–512 µg/mL against different Gram-negative and Gram-positive pathogens (Vimal et al, 2013). Collectively, these studies highlight the consistent antibacterial efficacy of CS/NPs, although variability can be expected due to nanoparticle size, degree of deacetylation, and preparation method.

The antibacterial mechanism of CS/NPs is primarily attributed to their cationic amino groups, which enable electrostatic interaction with negatively charged bacterial cell surfaces. This disrupts membrane integrity, increases permeability, and results in leakage of intracellular contents such as proteins, nucleotides, and electrolytes. This disruption is typically more pronounced in Gram-positive bacteria due to their relatively permeable peptidoglycan layer, whereas Gram-negative bacteria are partially protected by their outer membrane barrier (Godoy-Gallardo et al., 2017; Kong et al., 2010). In addition to membrane disruption, CS/NPs have been reported to bind to bacterial DNA, thereby inhibiting replication and transcription, or chelate essential trace metals required for bacterial growth (Varma and Vasudevan, 2020).

Both *P. muralis* extract and CS/NPs demonstrated inhibitory effects on biofilm formation, with CS/NPs showing superior activity. At MIC concentrations, CS/NPs reduced biofilm formation by up to 65% in *S. aureus*. This is consistent with the previous studies showing that chitosan nanoparticles disrupt extracellular polymeric substances (EPS), prevent bacterial adhesion, and impair quorum sensing pathways (Varma and Vasudevan, 2020; Divya et al, 2017). Interestingly, we observed more pronounced inhibition in Gram-negative isolates, which may be due to differences in biofilm matrix density and nanoparticle penetration efficiency. The ability to inhibit biofilm formation is of particular clinical relevance, as biofilm-associated infections are notoriously

resistant to conventional antibiotics and represent a major therapeutic challenge.

The most significant finding of our study was the synergistic antibacterial and antibiofilm effect observed when CS/NPs were combined with *P. muralis* extract. The FIC index values confirmed synergy against all tested isolates. This effect likely arises from complementary mechanisms: CS/NPs enhance adhesion to bacterial surfaces and disrupt cell membranes, facilitating increased uptake of phytochemicals from *P. muralis*. The metabolites, in turn, may interfere with metabolic processes or generate oxidative stress, leading to enhanced bacterial killing.

Synergistic combinations of chitosan with plant extracts have been documented in earlier studies. Etemadi et al. (2019) reported that chitosan combined with turmeric aqueous extract showed enhanced activity against MRSA strains. Aldayel et al. demonstrated synergy between chitosan and *Capsicum annuum* extract against *S. aureus*, *S. typhimurium*, and *P. aeruginosa* (Aldayel et al, 2020). Tantala et al. found that chitosan films containing fingerroot and holy basil essential oils could reduce *Listeria monocytogenes* to undetectable levels within 12 hours (Tantala et al, 2019). Collectively, these findings reinforce the concept that nanotechnology-based systems can augment the antimicrobial efficacy of natural bioactive compounds.

The growing prevalence of antibiotic-resistant pathogens and biofilm-associated infections underscores the urgent need for alternative antimicrobial strategies. The results of the present study demonstrate that CS/NPs and *P. muralis* extract, individually and in combination, offer promising antibacterial and antibiofilm activities against clinically important bacteria. Importantly, the observed synergy suggests that lower doses of each agent may be sufficient when used in combination, thereby potentially reducing toxicity and minimizing the risk of resistance development (Varma and Vasudevan, 2020).

Given the biocompatibility and biodegradability of chitosan, CS/NPs have high translational potential in biomedical applications such as wound dressings, coatings for medical devices, and drug delivery systems. Similarly, the use of *P. muralis* extract, which is derived from a natural and sustainable source, aligns with the global movement toward eco-friendly and plant-based therapeutics. However, further investigations, particularly in vivo studies and molecular assays, are required to fully elucidate the mechanisms of action and to confirm safety and efficacy in clinical settings.

In summary, the current study demonstrated that CS/NPs exhibit potent antibacterial and antibiofilm activity, *P. muralis* extract shows moderate but notable antibacterial effects, and their combination results in synergistic enhancement. The underlying mechanisms involve complementary interactions between nanoparticle-mediated membrane disruption and phytochemical-driven metabolic interference. These findings highlight the potential of integrating nanotechnology with plant-derived compounds to develop innovative antimicrobial strategies against resistant and biofilm-associated infections. Future studies should focus on optimizing nanoparticle formulations, evaluating cytotoxicity, and conducting in vivo efficacy testing to pave the way for clinical translation.

Acknowledgment

The authors wish to express their sincere gratitude to Sharekord University and the Kashan University of Medical Sciences for their financial and technical support throughout this research.

Conflict of interest

The authors report no competing financial or personal interests that could have biased this work.

Funding

The authors received financial and technical support from Sharekord University for this research.

References

Sydnor, E. R., & Perl, T. M. (2011). Hospital epidemiology and infection control in acute-care settings. *Clinical Microbiology Reviews, 24*(1), 141–173.

Kolář, M. (2022). *Bacterial infections, antimicrobial resistance and antibiotic therapy* (p. 468). MDPI.

Schroeder, M., Brooks, B. D., & Brooks, A. E. (2017). The complex relationship between virulence and antibiotic resistance. *Genes, 8*(1), 39.

Abebe, G. M. (2020). The role of bacterial biofilm in antibiotic resistance and food contamination. *International Journal of Microbiology*, Article ID 1705814.

Singh, A., Amod, A., Pandey, P., Bose, P., Pingali, M. S., Shivalkar, S., *et al.* (2022). Bacterial biofilm infections, their resistance to antibiotics therapy and current treatment strategies. *Biomedical Materials, 17*(2), 022003.

Bhatti, M. Z., Ismail, H., & Kayani, W. K. (2022). Plant secondary metabolites: Therapeutic potential and pharmacological properties. In *Secondary metabolites – trends and reviews*. London: IntechOpen.

Shrestha, G., & St. Clair, L. L. (2013). Lichens: A promising source of antibiotic and anticancer drugs. *Phytochemistry Reviews, 12*, 229–244.

Rashki, S., Alshamsi, H. A., Amiri, O., Safardoust-Hojaghan, H., Salavati-Niasari, M., Nazari-Alam, A., *et al.* (2021). Eco-friendly green synthesis of ZnO/GQD nanocomposites using *Protoparmeliopsis muralis* extract for their antibacterial and antibiofilm activity. *Journal of Molecular Liquids, 335*, 116195.

Rashki, S., & Valadbeigi, T. (2017). In vivo screening antifungal activity of methanolic extract of *Protoparmeliopsis muralis* against *Aspergillus flavus*. *Journal of Advanced Biomedical Sciences, 7*(1), 53–59.

Gao, Y., & Wu, Y. (2022). Recent advances of chitosan-based nanoparticles for biomedical and biotechnological applications. *International Journal of Biological Macromolecules, 203*, 379–388.

Varma, R., & Vasudevan, S. (2020). Extraction, characterization, and antimicrobial activity of chitosan from shrimp shell waste. *Environmental Science and Pollution Research, 27*(15), 17369–17380.

Algharib, S. A., Elzoghby, A. O., El-Badawy, H., & Elkasabgy, N. A. (2022). Preparation of chitosan nanoparticles by ionotropic gelation: Characterization and applications. *Journal of Molecular Structure, 1252*, 132123.

Huang, M., Yin, Y., Li, D., Wang, D., & Zhang, X. (2016). Preparation and characterization of chitosan nanoparticles by ionic gelation. *International Journal of Biological Macromolecules, 88*, 111–117.

Aydın, M., Kocabaş, F., Yıldız, S., & Öztürk, S. (2013). Antimicrobial activity of methanolic extracts of lichens from Turkey. *Journal of Applied Pharmaceutical Science, 3*(10), 65–70.

Hoang, V. T., Ngo, H. T., Nguyen, T. T., & Tran, H. T. (2022). Characterization techniques for chitosan nanoparticles: A review. *International Journal of Biological Macromolecules, 216*, 703–717.

O'Toole, G. A. (2011). Microtiter dish biofilm formation assay. *Journal of Visualized Experiments, 47*, 2437.

Clinical and Laboratory Standards Institute (CLSI). (2018). *Methods for dilution antimicrobial susceptibility tests for bacteria that grow aerobically; approved standard* (11th ed., CLSI document M07). Wayne, PA: CLSI.

Meletiadis, J., Pournaras, S., Roilides, E., & Walsh, T. J. (2009). Defining fractional inhibitory concentration index cutoffs for additive, synergistic, and antagonistic interactions: A systematic review and meta-analysis of in vitro studies. *Antimicrobial Agents and Chemotherapy, 53*(8), 3435–3443.

Jayakumar, R., Prabaharan, M., Sudheesh Kumar, P. T., Nair, S. V., & Tamura, H. (2011). Biomaterials based on chitin and chitosan in wound dressing applications. *Biotechnology Advances, 29*(3), 322–337.

Cushnie, T. P., Cushnie, B., & Lamb, A. J. (2014). Alkaloids: An overview of their antibacterial, antibiotic-enhancing and antivirulence activities. *International Journal of Antimicrobial Agents, 44*(5), 377–386.

Xie, Y., Yang, W., Tang, F., Chen, X., & Ren, L. (2015). Antibacterial activities of flavonoids: Structure–activity relationship and mechanism. *Current Medicinal Chemistry, 22*(1), 132–149.

Okoth, D. A., Chenia, H. Y., & Koorbanally, N. A. (2013). Antibacterial and antioxidant activities of flavonoids from *Lannea alata*. *South African Journal of Botany, 86*, 131–136.

Valadbeigi, T., Mahmoudvand, H., Sharififar, F., Ezatpour, B., & Kheirandish, F. (2020). Antibacterial activities of selected Iranian medicinal plants against multidrug-resistant Gram-negative bacteria. *Iranian Journal of Basic Medical Sciences, 23*(9), 1163–1170.

Almola, N. A., Alghamdi, A. A., Alharbi, W. A., Alshahrani, M. Y., Alhakamy, N. A., & Al Sadoun, H. (2021). Phytochemical analysis and antibacterial activity of *Parietaria judaica* and *Parietaria muralis*. *Saudi Journal of Biological Sciences, 28*(9), 5130–5136.

Valian, A., Ramezanpour, S. S., Pourmahdi, M., Yazdian, F., & Navaee, M. (2020). Antibacterial activity of chitosan nanoparticles against *Streptococcus mutans*. *Nanomedicine Journal, 7*(3), 189–196.

Divya, K., Vijayan, S., George, T. K., & Jisha, M. S. (2017). Antimicrobial properties of chitosan nanoparticles: Mode of action and factors affecting activity. *International Journal of Biological Macromolecules, 104*(Pt B), 1372–1382.

Vimal, S., Abdul Majeed, S., Taju, G., Nambi, K. S., Raj, N. S., Madan, N., *et al.* (2013). Chitosan tripolyphosphate nanoparticles: Preparation, characterization and application for gene delivery in fish. *Acta Tropica, 128*(3), 486–493.

Godoy-Gallardo, M., Eckhard, U., Delgado, L. M., de Roo Puente, Y. J., Hoyos-Nogués, M., Gil, F. J., *et al.* (2017). Antibacterial properties of chitosan nanoparticles incorporated in dental resins. *Dental Materials, 33*(4), 465–474.

Kong, M., Chen, X. G., Xing, K., & Park, H. J. (2010). Antimicrobial properties of chitosan and mode of action: A state of the art review. *International Journal of Food Microbiology, 144*(1), 51–64.

Etemadi, F., Abdi-Ali, A., Rezaee, M. A., & Tahmasebi, R. (2019). Synergistic effect of chitosan and turmeric aqueous extract on methicillin-resistant *Staphylococcus aureus*. *Iranian Journal of Microbiology, 11*(2), 119–126.

Aldayel, T. S., Alqahtani, F. Y., Alshehri, S., Alzahrani, A. R., & Alshahrani, M. Y. (2020). Synergistic antibacterial activity of chitosan with *Capsicum annuum* extract. *Journal of Applied Microbiology, 128*(4), 1065–1073.

Tantala, K., Chanthong, S., Boonsong, W., Intaraksa, P., Pongtharangkul, T., Tadtong, S., *et al.* (2019). Antimicrobial activity of chitosan films containing fingerroot and holy basil essential oils against *Listeria monocytogenes*. *International Journal of Biological Macromolecules, 125*, 1289–1295.

Received: 14.11.2025
Accepted: 25.06.2026

Vol. 22, No. 2, Summer, 2026, 99-107
DOI: 10.22055/ivj.2025.505300.2775
Journal Homepage: http://www.ivj.ir/

Original Article

A Simple Method for the Production of anti-Fish IgM Monoclonal Antibodies

Masoud Reza Seyfi Abad Shapouri[1*], Roya Rahnama[2], Rahim Peyghan[3], Anahita Rezaie[1] and Nastaran Shahbazian[4]

[1] Professor, Department of Pathobiology, Faculty of Veterinary Medicine, Shahid Chamran University of Ahvaz, Ahvaz, Iran
[2] PhD Graduated of Aquatic Animal Health, Faculty of Veterinary Medicine, Shahid Chamran University of Ahvaz, Ahvaz, Iran
[3] Professor, Department of Livestock Animal, Poultry and Fish Health, Faculty of Veterinary Medicine, Shahid Chamran University of Ahvaz, Ahvaz, Iran and Member of Excellence Center of Warm Water Fish Health, Shahid Chamran University of Ahvaz, Ahvaz, Iran
[4] Assistant Professor, Department of Aquaculture Sector, Iranian Veterinary Organization, Tehran, Iran

Received: 18.02.2025 Accepted: 13.11.2025

Abstract

Immunoglobulin M (IgM) is the predominant antibody isotype in the serum of teleost fish and plays a central role in systemic immune responses. Monoclonal antibodies (mAbs) targeting fish IgM are essential tools for immunological research and disease management in aquaculture. However, conventional mAb production protocols require purified IgM, which is difficult to obtain due to the complexity of purification procedures in teleost species. This study introduces a simplified method for generating anti-IgM mAbs by immunizing mice with whole serum from rainbow trout (*Oncorhynchus mykiss*), thereby eliminating the need for IgM purification. To do this, hybridomas were screened using an indirect ELISA based on an unrelated antigen (e.g., maltose-binding protein) and trout sera containing antibodies against this antigen. This approach led to the identification of five stable hybridoma clones (1D4, 3D3, 3E3, 4B3, and 7F6). The resulting mAbs effectively recognized trout antibodies against *Infectious pancreatic necrosis virus, Lactococcus garvieae* bacterium and sheep red blood cells. Immunoblotting under reducing and non-reducing conditions confirmed the specificity of these mAbs for trout IgM. This method provides a practical and efficient alternative for producing functional monoclonal antibodies against fish IgM.

Key words: Monoclonal antibody, Trout, IgM, ELISA, Immunoblotting

Introduction

Immunoglobulins (Igs) are integral elements of the adaptive immune system in fish, with diverse roles in pathogen recognition and immune defense. In teleost fishes, three major immunoglobulin isotypes have been characterized: IgM, IgD, and IgT (Hikima et al, 2011). Among them, IgM exhibits substantial structural resemblance to mammalian IgM in terms of molecular size, glycosylation profile, and polymeric configuration (Coscia and Oreste, 1998). Functionally, IgM is the predominant isotype present in teleost serum and is central to systemic immune

[*] **Corresponding Author**: Masoud Reza Seyfi Abad Shapouri, Professor, Department of Pathobiology, Faculty of Veterinary Medicine, Shahid Chamran University of Ahvaz, Ahvaz, Iran
E-mail: masoudrs@scu.ac.ir

responses of fish. However, teleost IgM may also play a role in mucosal protection (Parra et al, 2013).

IgT, a teleost-specific immunoglobulin isotype, is predominantly localized at mucosal surfaces and functionally resembles mammalian IgA, indicating an evolutionary adaptation for mucosal immunity (Mashoof et al, 2014; Ji et al, 2020). Studies utilizing polyclonal antibodies raised against IgT have demonstrated no detectable antigenic cross-reactivity between IgT and IgM in rainbow trout (Zhang et al, 2010).

In contrast to mammalian IgD, the heavy chain of teleost IgD exhibits a chimeric structure composed of a Cμ1 domain followed by multiple Cδ regions (Salinas et al, 2021). Given this structural overlap, antigenic cross-reactivity between IgM and IgD in teleosts is plausible. The precise immunological role of IgD in teleosts remains to be conclusively defined. Nonetheless, it has been postulated that IgD may serve as a surface receptor on B lymphocytes, participating in cellular activation, maturation, and differentiation (Edholm et al, 2010; Ji et al, 2020).

Production of monoclonal antibodies against fish immunoglobulins, particularly IgM, is a growing field with significant implications for aquaculture, fish health management and research. Anti-fish IgM monoclonal antibodies can facilitate immunodiagnostic assays and vaccine efficacy studies within the aquaculture sector. These antibodies are instrumental in identifying IgM-expressing cells, quantifying serum immunoglobulin levels, and characterizing immune responses against specific antigens.

Although novel methodologies such as phage display and recombinant antibody technologies are emerging, hybridoma technology remains the most widely utilized for mAb generation. This technique entails the immunization of a laboratory animal—typically mice—followed by fusion of B cells with immortalized myeloma cells to produce hybridomas. These hybridomas possess the dual capacity to secrete antibody and proliferate indefinitely. Subsequent screening and cloning facilitate the establishment of stable cell lines capable of sustained mAb production (Ausubel, 1992).

Conventional immunization protocols to produce anti-fish IgM mAbs, typically have been relied on the use of purified fish IgM as the immunogen (DeLuca et al, 1983; Thuvander et al, 1990; Sanchez et al, 1991; Sanchez et al, 1993; Estevez et al, 1994; Pettersen et al, 1995; Magnadottir et al, 1996; Vasely et al, 2006; Shin et al, 2006; Zhang et al, 2017; Yang et al, 2018; Huang et al, 2019; Jones et al, 2022; Oliver et al, 2023). However, the isolation of IgM from fish serum presents considerable technical challenges (Sanchez et al, 1991), especially in species such as those belonging to the Salmonidae family, wherein IgM concentrations are relatively low (Uchida et al, 2000). Given these constraints, the present investigation aimed to evaluate an alternative and simplified strategy for mAb production against rainbow trout IgM (as a model). Specifically, whole serum from rainbow trout was employed as the immunogen without prior purification of IgM. The proposed approach demonstrates promising applicability for the generation of anti-IgM monoclonal antibodies across various teleost species.

Materials and methods

Immunization of Balb/c mice with trout whole serum

Female Balb/c mice, six weeks of age, were immunized with trout whole serum emulsified in an equal volume of incomplete Freund's adjuvant (Sigma, USA). A total of six mice received 200 µl of the emulsion via intraperitoneal injection on days 0, 14, and 35. One week following the final immunization, blood samples were collected, and the sera were used to develop an indirect ELISA for hybridoma screening.

Immunization of rainbow trout with Maltose-Binding Protein (MBP)

Ten rainbow trout (average weight: 300 g) were housed in two glass aquaria (five fish per tank) maintained at 15–17°C. After acclimatization, five fish were immunized with MBP (Mahmoodi et al, 2015) emulsified in ISA 70 oil-based adjuvant (SEPPIC, France). Each fish received 100 µl of the emulsion containing 50 µg of MBP via intraperitoneal injection on days 0 and 14. The control group received PBS-adjuvant emulsion. Blood samples were collected on day 28, and the sera were used for indirect ELISA development.

Indirect ELISA for hybridoma screening

ELISA plates were coated with 0.1 µg of MBP per well and blocked with 5% skim milk in PBS containing 0.05% Tween 20 (PBST) for 3 hours at 37°C. After washing, 50 µl of serial dilutions (1:200 to 1:1600) of trout sera (from immunized and control fish) diluted in blocking buffer were added to the wells and incubated for 45 minutes at room temperature. Subsequently, 50 µl of mouse serum (1:2000 dilution) from a trout-serum-immunized mouse was added and incubated for another 45 minutes. After washing, 50 µl of peroxidase-conjugated anti-mouse IgG (Komabiotech, Korea; 1:4000 dilution) was added and incubated for 30 minutes. Plates were washed and developed using 50 µl of TMB-H_2O_2 substrate. After 10 minutes, the reaction was stopped, and absorbance was measured at 450 nm (Dynatec, Netherlands). A 1:200 dilution of trout sera was found to effectively differentiate immunized from control samples.

Production of monoclonal antibodies against trout IgM

To generate monoclonal antibodies against trout IgM, spleen cells from a trout-serum-immunized mouse were fused with Sp2/0 myeloma cells using polyethylene glycol (Roche, Germany). A total of 10^7 myeloma cells in logarithmic growth phase were fused with 10^8 spleen cells. The fused cells were cultured in 96-well plates containing feeder cells (harvested from the peritoneal cavity of a mouse) in RPMI medium completed with 10% fetal bovine serum and hypoxanthine-aminopterin-thymidine supplement (Sigma, USA) (Ausubel, 1992). Hybridoma supernatants were screened for anti-trout IgM antibodies using the previously described ELISA protocol, substituting hybridoma culture supernatants for mouse serum.

Evaluation of mAbs for detecting antigen-specific trout antibodies

To assess the utility of the mAbs in detecting antigen-specific rainbow trout antibodies, ELISA plates were coated with antigens from *Infectious pancreatic necrosis virus* (IPNV), *Lactococcus garvieae* bacterium and sheep red blood cells. Corresponding positive rainbow trout sera (prepared in-house) were used at a 1:100 dilution. The ELISA protocol was like the hybridoma screening assay, with the substitution of respective antigens for the MBP and the use of positive rainbow trout sera instead of MBP-immunized fish serum.

Immunoblotting to assess mAbs specificity

The specificity of the mAbs for trout IgM was evaluated by immunoblotting under reducing and non-reducing conditions. The whole trout serum was mixed with SDS-PAGE sample buffer containing β-mercaptoethanol (reducing) or without it (non-reducing) (Ausubel, 1992). Reduced samples were boiled for 10 minutes; non-reduced samples were incubated at room temperature. Proteins were separated by SDS-PAGE (10% and 6% gels for reducing and non-reducing conditions, respectively) and transferred to nitrocellulose membranes. Membranes were blocked with 5% skim milk in PBST, cut into strips, and incubated with each mAb for 1 hour. After washing, strips were incubated with peroxidase-conjugated anti-mouse IgG for 1 hour, washed again, and developed using 4-chloro-1-naphthol and H_2O_2.

Results

Production and screening of hybridoma cells

Following the fusion of splenocytes from immunized mice with Sp2/0 myeloma cells, approximately 150 hybridoma colonies were generated and screened for the production of monoclonal antibodies specific to rainbow trout antibody using an indirect ELISA. In the initial screening, eight hybridoma supernatants exhibited optical density (OD) values ranging from 0.8 to 1.8, indicating positive reactivity compared to the remaining clones. After three rounds of subcloning, five hybridoma clones—designated 1D4, 3D3, 3E3, 4B3, and 7F6—demonstrated stable and high-level antibody production, with OD values exceeding 1.7. One subclone from each of these five clones was selected for further analysis.

Evaluation of mAbs for detection of antigen-specific trout antibodies

To determine the specificity and utility of the generated mAbs for detection of rainbow trout serum antibodies, an indirect ELISA was conducted using antigens derived from *Infectious pancreatic necrosis virus* (IPNV), *Lactococcus garvieae* bacterium and sheep red blood cells. Corresponding positive and negative rainbow trout sera were included for each antigen. The mAbs were employed as secondary antibodies prior to incubation with a peroxidase-conjugated anti-mouse IgG. As illustrated in Figure 1, the mAbs consistently yielded higher optical density (OD) values with positive sera compared to negative controls, confirming their capacity to selectively recognize antigen-specific trout antibodies.

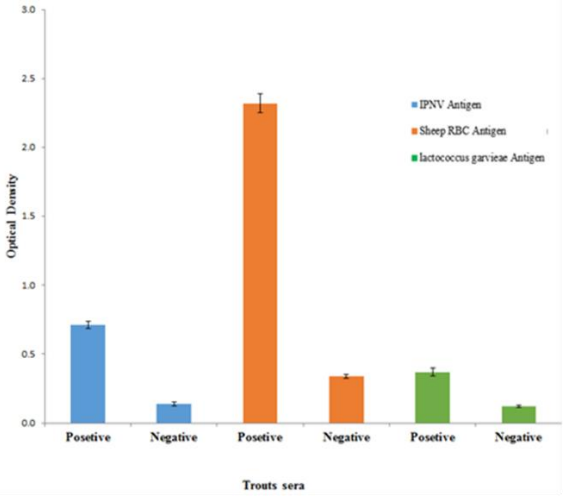

Figure 2: Evaluation of the applicability of the mAbs for detecting antigen-specific antibodies in positive and negative rainbow trout sera. This figure presents the mean optical density (OD) values obtained from the five mAbs in ELISA, targeting serum antibodies specific to antigens derived from *Infectious Pancreatic Necrosis Virus* (IPNV), *Lactococcus garvieae* bacterium, and sheep red blood cells (SRBCs). Each column represents the average OD response of all five mAbs, reflecting their collective ability to recognize antigen-specific immunoglobulins in rainbow trout sera.

Specificity of mAbs for trout IgM assessed by immunoblotting

To determine the specificity of the selected monoclonal antibodies for trout IgM, immunoblotting was performed using rainbow trout whole serum under both reducing and non-reducing conditions. Under reducing conditions, all five mAbs recognized a protein band in rainbow trout serum with an approximate molecular weight of 75 kDa (Figure 2A). Under non-reducing conditions, the antibodies reacted with serum proteins in the range of approximately 180 kDa, as well as with high-molecular-weight proteins that remained at the top of the nitrocellulose membrane, beyond the detectable range of the molecular weight marker (Figure 2B).

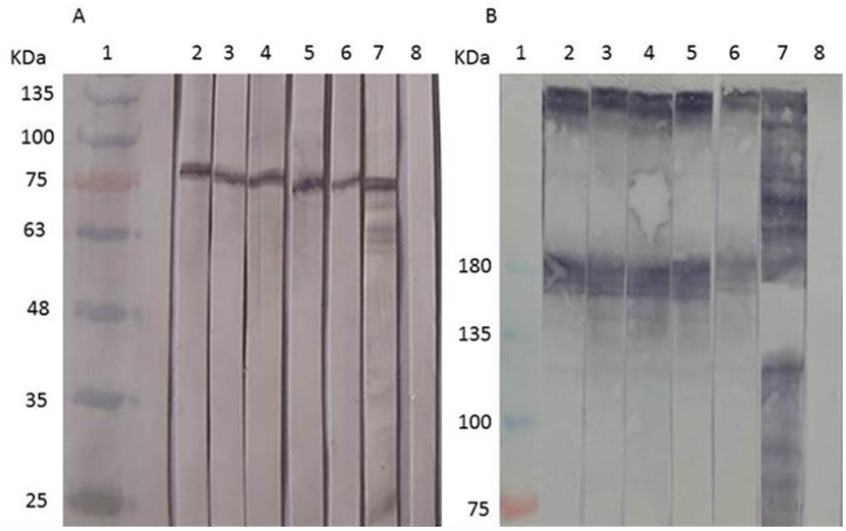

Figure 1: Immunoblot analysis under reducing and non-reducing conditions. (A) Reducing conditions: Strip 1 represents the molecular weight marker. Strips 2 through 6 show the reactivity of mAbs 1D4, 3D3, 3E3, 4B3, and 7F6 with a ~75 kDa protein present in the serum of rainbow trout. Strips 7 and 8 correspond to the positive control (serum from a mouse immunized with rainbow trout serum) and the negative control (RPMI medium supplemented with 10% fetal bovine serum), respectively. (B) Non-reducing conditions: Strip 1 indicates the molecular weight marker. Strips 2 through 6 demonstrate the binding of the same panel of mAbs to proteins of approximately 180 kDa and higher molecular weights in rainbow trout serum. Strips 7 and 8 represent the positive and negative controls, respectively.

Discussion

Effective disease control and prevention in aquaculture require the implementation of routine monitoring programs, complemented by eradication strategies or vaccination protocols. Within this context, serological assays play a critical role in both surveillance and diagnostic efforts (Morrison and Nowak, 2002). As in terrestrial animals, reliable serological testing in fish depends on the availability of species-specific anti-immunoglobulin antibodies, particularly monoclonal antibodies targeting IgM.

In recent years, considerable research efforts have been directed toward the development of monoclonal antibodies against IgM in a variety of freshwater and marine fish species. Conventionally, this process involves purifying IgM from fish serum and using it to immunize mice. However, the purification of fish IgM is notably time-consuming, labour-intensive and usually results in only partial purification (Sanchez et al, 1991). In order to overcome this challenge, researchers aiming to generate monoclonal antibodies against fish IgM have employed a range of purification techniques including ammonium sulfate precipitation (Al-Harbi et al, 2000), gel filtration (DeLuca et al, 1983; Magnadottir et al, 1996; Vasely et al, 2006), ion exchange chromatography (Sanchez et al, 1993; Pettersen et al, 1995), and various affinity chromatography methods (Thuvander et al, 1990; Sanchez et al, 1991; Estevez et al 1994, Al-Harbi et al, 2000; Shin et al, 2006; Zhang et al, 2017; Yang et al, 2018; Huang et al, 2019; Jones et al, 2022; Oliver et al, 2023), as well as combinations thereof.

To circumvent the difficulties associated with IgM purification, some studies have adopted molecular approaches. For instance, the expression of a truncated IgM heavy chain sequence in *Escherichia coli* has enabled the production of a recombinant protein suitable for immunization (Jingzhuang et al, 2014; Rahnama et al, 2018). Additionally, synthetic peptides derived from conserved regions of the IgM heavy chain have been successfully used to generate monoclonal antibodies for species

such as tilapia (Velázquez et al, 2021) and sea bass (Uchuwittayakul et al, 2025).

In the present study, whole serum from rainbow trout was employed for mouse immunization to facilitate the production of monoclonal antibodies targeting rainbow trout IgM. A review of the existing literature indicates that whole fish serum has not previously been utilized as an immunogen for the development of monoclonal antibodies against fish IgM. The only partial attempt was reported by Al-Harbi et al. (2000), who immunized mice using semi-purified tilapia IgM obtained via ammonium sulfate precipitation. However, during the hybridoma screening phase, they relied on affinity-purified IgM to ensure the selection of IgM-specific hybridomas.

The rationale for the present approach was based on two key considerations. First, fish serum is the primary source of IgM, with its concentration in rainbow trout estimated to be approximately 100 to 1000 times higher than that of IgD and IgT, respectively (Salinas et al., 2021). Second, IgM is the predominant immunoglobulin produced in response to systemic immunization in fish. Accordingly, following mouse immunization with whole serum, hybridoma screening can be effectively conducted using an ELISA designed with an unrelated antigen (e.g., MBP) and sera collected from fish immunized with that antigen. Using this strategy, five hybridomas (1D4, 3D3, 3E3, 4B3, and 7F6) were identified that produced monoclonal antibodies reactive with rainbow trout antibodies—presumably of the IgM isotype—bound to MBP in the screening assay. The ability of these monoclonal antibodies to differentiate between sera from non-immunized rainbow trout and those systemically immunized with various antigens (IPN virus, *Lactococcus garvieae* bacterium, and sheep red blood cells) was further confirmed by ELISA, demonstrating the capacity of the mAbs to detect trout antibodies bound to the antigens.

The specificity of these monoclonal antibodies for rainbow trout IgM was validated through immunoblotting. Under reducing conditions, all five antibodies successfully detected a protein in the trout serum with an estimated molecular weight of approximately 75 kilodaltons, which corresponds closely to the expected size of the IgM heavy chain (Sanchez et al, 1993). Under non-reducing conditions, the antibodies recognized protein bands around 180 kDa and additional high-molecular-weight bands near the top of the electrophoresis lanes. The 180 kDa bands likely correspond to the IgM monomer, while the higher molecular weight bands are presumed to represent IgM tetramers (660–800 kDa) (Salinas et al, 2021), although precise molecular characterization was not possible due to the absence of suitable molecular weight markers. These findings are consistent with previous reports indicating that IgM exists in both monomeric and tetrameric forms in rainbow trout serum (Elcombe et al, 1985). Unlike IgM, serum IgT exists exclusively in a monomeric form with an approximate molecular weight of 180 kDa. In rainbow trout, secreted IgD is also present as two distinct monomeric variants of ~370 and ~400 kDa (Salinas et al, 2021), both of which exceed the upper limit of the molecular weight markers employed in this study. Therefore, based on the specific reactivity patterns observed in immunoblotting assays and successful performance of the mAbs in detecting systemic immune responses in rainbow trout against various antigens, it can be concluded that these antibodies are specific to trout IgM.

Considering the evidence presented by Zhang et al, (2010) that there is no cross-reactivity between IgT and IgM, it is reasonable to assume that the mAbs generated in the present study do not exhibit cross-reactivity with IgT. However, regarding IgD, it is noteworthy that the heavy chain of IgD contains the cμ1

domain, which is also present in IgM (Salinas et al., 2021). Therefore, a degree of cross-reactivity between IgD and IgM is theoretically plausible. Although the immunoblotting results in the current study did not reveal any detectable interaction between the produced mAbs and IgD, this absence of signal may be attributed to the relatively low concentration of IgD in serum compared to IgM (Salinas et al, 2021). Consequently, the possibility of cross-reactivity with IgD cannot be entirely ruled out and warrants further investigation using more sensitive detection methods or purified IgD preparations.

Collectively, the result of this study highlights the feasibility of using whole fish serum as an immunogen for monoclonal antibody production against IgM. Moreover, the incorporation of an unrelated antigen during hybridoma screening presents a practical approach for selecting antibodies capable of detecting antigen-bound IgM. This methodology may yield monoclonal antibodies with greater functional relevance than those selected solely based on reactivity with purified IgM.

Acknowledgment

This project was supported by research grants from Shahid Chamran University of Ahvaz, Ahvaz, Iran.

Conflict of Interest

The authors declare no conflict of interest.

Funding

Funding this work was supported by Shahid Chamran University of Ahvaz.

References

Al-Harbi, A.H., Truax, R., and Thune, R. L. (2000). Production and characterization of monoclonal antibodies against tilapia Oreochromis niloticus immunoglobulin. *Aquaculture*, *188*(3–4), 219-227.

Ausubel, F. M. (1992). Short protocols in molecular biology, Greene Pub. Associates, Wiley edition.

Coscia, M.R., and Oreste, U. (1998). Antarctic Fish Immunoglobulins: Preliminary Data on Structure and Antibody Specificity, In book: Fishes of Antarctica: A Biological Overview, Springer/Sci-Tech/Trade, pp.175-184.

Deluca, D., Wilson, M., and Warr, G. W. (1983). Lymphocyte heterogeneity in the trout, *Salmo gairdneri*, defined with monoclonal antibodies to IgM. *European Journal of Immunology*, *13*(7), 546-551.

Edholm, E.S., Bengtén, E., Stafford, J.L., Sahoo, M., Taylor, E.B., Miller, N.W., and Wilson, M. (2010) Identification of two IgD + B cell populations in channel catfish, *Ictalurus punctatus*. *Journal of Immunology*, *185*, 4082–4094.

Elcombe, B.M., Chang, R.J., Taves, C.J., and Winkelhake, J.L. (1985). Evolution of antibody structure and effector functions: comparative hemolytic activities of monomeric and tetrameric IgM from rainbow trout, *Salmo gairdnerii*. *Comparative Biochemistry and Physiology B*, *80*(4), 697-706.

Estevez, J., Leiro, J., Santamariana, M.T., Damainguez, J., and Ubeira, F.M. (1994). Monoclonal antibodies to turbot (*Scophthalmus maximus*) immunoglobulins: characterization and applicability in immunoassays. *Veterinary Immunology and Immunopathology*, *41*, 353–366.

Hikima, J., Jung, T.S., and Aoki, T. (2011). Immunoglobulin genes and their transcriptional control in teleosts. *Developmental and Comparative Immunology*, *35*, 924–936.

Huang, Y., Yuan, X., Mu, P., Li, Q., Ao, J., and Chen, X. (2019). Development of monoclonal antibody against IgM of large yellow croaker (*Larimichthys crocea*) and characterization of IgM+ B cells. *Fish and Shellfish Immunology*, *91*, 216-222.

Ji, J.F., Hu, C.B., Shao, T., Fan, D.D., Zhang, N., Lin, A.F., Xiang, L.X., and Shao, J.Z. (2020). Differential immune responses of immunoglobulin Z subclass members in antibacterial immunity in a zebrafish model. *Immunology*, *162*(1), 105-120.

Jingzhuang, Z., Liming, X., Miao, L., Yongsheng, C., Jiasheng, Y., Hongbai, Y., Hongbai, L., and Tongyan, L. (2014). Expression and rabbit antisera preparation of IgM heavy chain gene in rainbow trout (*Onchorhynchus mykiss*). *Journal of Fisheries of China*, *38*(8), 1175-1181.

Jones, E.M., Oliver, L.P., Ma, J., Leeuwis, R.H.J., Myrsell, V., Arkoosh, M.R., Dietrich, J.P., Schuster, C.M., Hawkyard, M., Kurt Gamperl, A., Kenneth, D., and Cain, K.D. (2022). Production of a monoclonal antibody specific to sablefish (*Anoplopoma fimbria*) IgM and its application in ELISA, western blotting, and immunofluorescent staining. *Fish and Shellfish Immunology*, *130*, 479-489.

Magnadottir, B. O., Kristjansdottir, H., and Gudmundsdottir, S. (1996). Characterisation of monoclonal antibodies to separate epitopes on salmon IgM heavy chain. *Fish and Shellfish Immunology*, *6*(3), 185-198.

Mahmoodi, P., Seyfi Abad Shapouri, M.R., Ghorbanpour, M., Haji Hajikolaei, M.R., Lotfi, M., Pourmahdi Boroujeni, M., and Daghari, M. (2015). Development of a simple indirect ELISA, based on prokaryotically expressed recombinant MBP-NS3 protein, for detection of antibodies against bovine viral diarrhea virus. *Jundishapur Journal of Microbiology*, *8*(3), e14311.https://doi.org/10.5812/jjm.14311.

Mashoof, S., Pohlenz, C., Chen, P.L., Deiss, T.C., Gatlin, D. 3rd., Buentello, A., and Criscitiello, M.F. (2014). Expressed IgH mu and tau transcripts share diversity segment in ranched *Thunnus orientalism*. *Developmental and Comparative Immunology*, *43*, 76–86.

Morrison, R.N., and Nowak, B.F. (2002). The antibody response of teleost fish. *Seminars in Avian and Exotic Pet Medicine*, *11*(1), 46-54.

Oliver, L.P., Bruce, T.J., Ma, J., Jones, E.M., and Cain, K.D. (2023). Development of a monoclonal antibody specific to burbot (*Lota lota*) IgM and optimization of an ELISA to measure anti-Aeromonas sp. antibody titers following pathogen challenge. *Fish and Shellfish Immunology*, *137*, doi: 10.1016/j.fsi.2023.108775.

Parra, D., Takizawa, F., and Oriol Sunyer, J. (2013). Evolution of B Cell Immunity. *Annual Review of Animal Biosciences*, *1*, 65-97.

Pettersen, E.F., Fyllingen, I., Kavlie, A., Maaseide, N.P., Glette, J., Endresen, C., and Wergeland, H.I. (1995). Monoclonal antibodies reactive with serum IgM and leukocytes from Atlantic Salmon (Salmo salar L). *Fish and Shellfish Immunology*, *5*, 275–287.

Rahnama, R., Seyfi Abad Shapouri, M.R., Peyghan, R., Rezaie, A., and Shahbazian, N. (2018). Cloning and expression of the constant region of rainbow trout (*Onchorhynchus mykiss*) μ immunoglobulin chain in *Escherichia coli*. *Iranian Journal of Fisheries Sciences*, *17*(3), 573-584.

Salinas, I., Fernandez-Montero, A., Ding, Y., and Oriol Sunyer, J. (2021). Mucosal immunoglobulins of teleost fish: A decade of advances. *Developmental and Comparative Immunology*, *121*, https://doi.org/10.1016/j.dci.2021.104079.

Sanchez, C., Coll, J., and Domínguez, J. (1991). One-step purification of the major rainbow trout immunoglobulin. *Veterinary Immunology and Immunopathology*, *27*(4), 383-391.

Sanchez, C., Lopez-Fierro, P., Zapata, A., and Dominguez, J. (1993). Characterization of monoclonal antibodies against heavy and light chains of trout immunoglobulin. *Fish and Shellfish Immunology*, *3*(4), 237-251.

Shin, G., Lee, H., Palaksha, K. J., Kim, Y., Lee, E., Shin, Y., Lee, E., Park, K., and Jung, T. (2006). Production of monoclonal antibodies against serum immunoglobulins of black rockfish (*Sebastes schlegeli Higendorf*). *Journal of Veterinary Sciences*, *7*(3), 293–295.

Thuvander, A., Fossum, C., and Lorenzen, N. (1990). Monoclonal antibodies to salmonid immunoglobulin: characterization and applicability in immunoassays. *Developmental and Comparative Immunology*, 14(4), 415-423.

Uchida, D., Hirose, H., Chang, P.K., Aranishi, F., Hirayabu, E., Mano, N., Mitsuya, T., Prayitno, S.B., and Natori, M. (2000). Characterization of Japanese eel immunoglobulin M and its level in serum. *Comparative Biochemestry and Physiology B*, *127*, 525–532.

Uchuwittayakul, A., Rodkhum, C., and Srisapoome, P. (2025). Production of a monoclonal antibody specific to the IgM heavy chain of Asian seabass (*Lates calcarifer* Bloch, 1790) and its application in assessing health status following vaccination and challenges with *Flavobacterium covae* and *Streptococcus iniae*. *Aquaculture*, *594*, https://doi.org/10.1016/j.aquaculture.2024.741445

Velázquez, J., Rodríguez, A., Aragón, H., Haidar, A., González, M., Valdés, R., Garay, H.E., Abreu, D.D., Ramos, Y., Cabrales, A., Morales, A., González, O., Herrera, F., Estrada, M.P., and Carpio Y. (2021). Monoclonal antibody against Nile tilapia (*Oreochromis niloticus*) IgM heavy chain: A valuable tool for detection and quantification of IgM and IgM+ cells. *Fish and Shellfish Immunology*, *110*, 44-54.

Vesely, T., Reschova, S., Pokorova, D., Hulova, J., and Nevorankova, Z. (2006). Production of monoclonal antibodies against immunoglobulin heavy chain in common carp (*Cyprinus carpio* L.). *Veterinární medicína*, *51*(5), 296-302.

Yang, S., Tang, X., Sheng, X., Xing, J., and Zhan, W. (2018). Development of monoclonal antibodies against IgM of sea bass (*Lateolabrax japonicus*) and analysis of phagocytosis by mIgM+ lymphocytes. *Fish and Shellfish Immunology*, *78*, 372-382.

Zhang, W., Tang, X.Q., Sheng, X.Z., Xing, J., and Zhan, W.B. (2017). Development and application of monoclonal antibodies against IgM of black rockfish (*Sebastes schlegeli*). *Journal of Fish Biology*, 90(4), 1668-1675.

Received: 18.02.2025
Accepted: 13.11.2025

DOI: 10.22055/ivj.2025.535366.2819

شناسایی پروتئین‌های آنتی ژنی *ستاریا لابیاتوپاپیلوزا* در گاو (*باس تورس*)

علیرضا البرزی[۱*]، پدرام حداد مولایان[۲]، مسعود قربانپور[۳] و محمدرضا تابنده[۴]

[۱] استاد گروه پاتوبیولوژی، دانشکده دامپزشکی، دانشگاه شهید چمران اهواز، اهواز، ایران
[۲] دانشجوی دکترای تخصصی انگل‌شناسی، دانشکده دامپزشکی، دانشگاه شهید چمران اهواز، اهواز، ایران
[۳] استاد گروه پاتوبیولوژی، دانشکده دامپزشکی، دانشگاه شهرکرد، شهرکرد، ایران
[۴] استاد گروه علوم پایه، دانشکده دامپزشکی، دانشگاه شهید چمران اهواز، اهواز، ایران

تاریخ دریافت: ۱۴۰۴/۴/۲۸ تاریخ پذیرش: ۱۴۰۴/۹/۲۳

چکیده

ستاریا لابیاتوپاپیلوزا یکی از نماتدهای انگلی موجود در گاو است که باعث آنسفالیت کرمی در میزبان‌های غیر اختصاصی می‌شود. پروتئین‌های آنتی‌ژنی می‌توانند برای توسعه آزمایش‌های تشخیصی و واکسن‌ها مورد استفاده قرار گیرند. این مطالعه با هدف تعیین پروفایل پروتئینی و آنتی‌ژنی *ستاریا لابیاتوپاپیلوزا* در گاو با استفاده از ایمونوبلاتینگ انجام شد. نمونه‌ها از گاوها در کشتارگاه اهواز گرفته شدند. عصاره‌های خام سوماتیک نماتد بالغ و میکروفیلاریا (به عنوان پروتئین‌ها یا آنتی‌ژن‌های S و MF به طور جداگانه با همگن‌سازی تهیه شدند. مواد دفعی ترشحی (ES) با انکوباسیون ۵ نماتد بالغ در محیط RPMI، (۳ میلی‌لیتر برای هر نماتد) حاوی پنی‌سیلین (۱۰۰ واحد در میلی‌لیتر) و استرپتومایسین (۱۰۰ میکروگرم در میلی‌لیتر) تهیه شدند. پروفایل پروتئینی و خواص آنتی‌ژنی نمونه‌های ES، S و MF نماتد *ستاریا لابیاتوپاپیلوزا* با الکتروفورز ژل پلی‌اکریل‌آمید سدیم دودسیل سولفات (SDS-PAGE) تعیین شد. خواص ایمنی‌زایی پروتئین‌ها با استفاده از ایمونوبلاتینگ و سرم‌های مثبت از گاوهای آلوده به نماتد بالغ تعیین شد. بیش از دو، ۸ و ۱۵ باند پروتئینی غالب در وزن مولکولی ۲۰۰ تا ۲۲ کیلو دالتون در ژل‌های SDS-PAGE نمونه‌های ES، MF و S نشان داده شد. در نتیجه، در ایمونوبلاتینگ ES، MF و S به ترتیب دو، ۱۴ و ۴ باند آنتی‌ژنی غالب مشاهده شد. نتایج ایمونوبلاتینگ ES، MF و S در *ستاریا لابیاتوپاپیلوزا* نشان داد که پروتئین‌های ۶۸ و ۶۴ کیلو دالتونی رایج‌ترین اجزای آنتی‌ژنی هستند که می‌توانند کاندیداهای بالقوه‌ای برای تحقیقات آینده در مورد تشخیص ایمونولوژیکی اختصاصی ستاریازیس گاوی باشند.

کلمات کلیدی: آنتی‌ژن‌ها، نمایه‌های آنتی‌ژنی، گاو، ایمونوبلاتینگ، *ستاریا لابیاتوپاپیلوزا*

* نویسنده مسئول: علیرضا البرزی، استاد گروه پاتوبیولوژی، دانشکده دامپزشکی، دانشگاه شهید چمران اهواز، اهواز، ایران
E-mail: a.alborzi@scu.ac.ir

DOI: 10.22055/ivj.2026.566326.2875

روش نوآورانه نیمه کمی Multiplex Single Primer Pair PCR برای تشخیص همزمان بعضی از پیروپلاسم‌های داخل سلولی اجباری

زهرا علیزاده سرابی[۱]، صدیقه نبیان[۲]، پرویز شایان[۲*]، سعید بکایی[۳] و حمیدرضا شکرانی[۴]

[۱] دانشجوی دکترای تخصصی انگل‌شناسی، دانشکده دامپزشکی، دانشگاه تهران، تهران، ایران
[۲] استاد گروه انگل‌شناسی، مرکز کنه و بیماری‌های منتقله، دانشکده دامپزشکی، دانشگاه تهران، تهران، ایران
[۳] استاد گروه بهداشت وکنترل مواد غذایی، دانشکده دامپزشکی، دانشگاه تهران، تهران، ایران
[۴] دانشیار گروه پاتوبیولوژی، دانشکده دامپزشکی، دانشگاه لرستان، خرم‌آباد، ایران

تاریخ دریافت: ۱۴۰۴/۹/۲۴ تاریخ پذیرش: ۱۴۰۵/۲/۳۰

چکیده

گونه‌های بابزیا و تیلریا از اجرام پیروپلاسمی هستند که نشخوارکنندگان را در صنعت دامپروری آلوده کرده و خسارات اقتصادی بالایی را در سراسر جهان موجب می‌شوند. تشخیص زود هنگام بیماری می‌تواند به مدیریت موفقیت‌آمیز درمان کمک کند. رنگ‌آمیزی گیمسا روشی رایج در سراسر جهان برای تشخیص پیروپلاسموز است که متأسفانه می‌تواند با برخی مشکلات جدی مانند تهیه‌ی لام‌های خونی مناسب و کیفیت رنگ‌آمیزی همراه باشد و گذشته از آن، آنالیز گسترش‌های تهیه شده نیز نیاز به تجربه‌ی بالایی دارد. روش‌های سرولوژیکی مانند ELISA یا IFAT نیز در برخی آزمایشگاه‌ها مورد استفاده قرار می‌گیرند. همچنین روش‌های مولکولی که مبتنی بر آنالیز DNA بوده و دقیق و قابل اعتماد هستند نیز ترجیحاً در بسیاری از آزمایشگاه‌ها مورد استفاده قرار می‌گیرند. هدف از مطالعه حاضر معرفی یک روش ساده و نوآورانه به نام semi-quantitative multiplex PCR بود که بتواند برای تشخیص همزمان گونه‌های بابزیا و تیلریا مفید واقع شود. برای این منظور، از آغازگرهای مشتق شده از ژن‌های 18S rRNA استفاده گردید که می‌توانند همزمان DNA را از میزبان‌ها (نشخوارکنندگان و کنه‌ها) و همچنین از گونه‌های بابزیا و تیلریا طوری تکثیر کنند که محصولات PCR آن‌ها در اندازه با یکدیگر متفاوت و قابل تشخیص تفریقی باشند. نتایج مطالعه حاضر همان طور که انتظار می‌رفت، نشان داد که طول متفاوت محصولات PCR از گونه‌های تیلریا و بابزیا، تمایز این انگل‌ها را از یکدیگر بر روی ژل آگارز ممکن می‌سازد. جالب توجه این است که این آغازگرها ناحیه‌ای از ژن 18S rRNA از سلول‌های میزبان را نیز به صورت همزمان تکثیر می‌کنند و محصول PCR حاصله بزرگتر از آمپلیکون‌های انگل‌ها می‌باشد. از آن جایی که جفت آغازگر معرفی شده به صورت همزمان DNA میزبان و انگل را تکثیر می‌کند، این ویژگی می‌تواند برای تجزیه و تحلیل نیمه کمی بار انگلی در نمونه‌ها مورد استفاده قرار گیرد. بنابراین می‌توان تاکید کرد که جفت آغازگر معرفی شده (VetUTPiro) می‌تواند به صورت همزمان برای تشخیص تفریقی بابزیوز و تیلریوز و همچنین برای تجزیه و تحلیل نیمه کمی بار انگلی برای مدیریت قابل کنترل درمان مورد استفاده قرار گیرد.

کلمات کلیدی: جنس تیلریا، جنس بابزیا، پی‌سی‌آر چندگانه نیمه کمی، مدیریت درمان، گوسفند

* نویسنده مسئول: پرویز شایان، استاد گروه انگل‌شناسی، مرکز کنه و بیماری‌های منتقله، دانشکده دامپزشکی، دانشگاه تهران، تهران، ایران
E-mail: **pshayan@ut.ac.ir**

DOI: 10.22055/ivj.2025.556919.2864

شناسایی بافتی و فراساختاری تلوسیت‌ها در بافت رحم سگ

حدیث امیریان[۱]، طیبه محمدی[۲*] و مهرداد پویان‌مهر[۲]

[۱] دانش‌آموخته دکترای حرفه‌ای دامپزشکی، دانشکده دامپزشکی، دانشگاه رازی، کرمانشاه، ایران
[۲] استادیار گروه علوم پایه و پاتوبیولوژی، دانشگاه رازی، کرمانشاه، ایران

تاریخ دریافت: ۱۴۰۴/۸/۱۱ تاریخ پذیرش: ۱۴۰۴/۹/۲۳

چکیده

تلوسیت‌ها، که با بدنه‌های سلولی باریک و زوائد سیتوپلاسمی کشیده معروف به تلوپود مشخص می‌شوند، سلول‌های بینابینی متمایزی هستند که در اندام‌های مختلف پستانداران، از جمله قلب، ریه، رحم، لوله‌های فالوپ و کلیه، شناسایی شده‌اند. این مطالعه به بررسی وجود، مورفولوژی، فراساختار و توزیع تلوسیت‌ها در بافت رحم سگ پرداخته است. نمونه‌هایی از شاخ رحم سگ‌های بالغ نژاد اشپیتز جمع‌آوری و برای بررسی‌های بافت‌شناسی، هیستوشیمی و میکروسکوپ الکترونی عبوری آماده شدند. تحت میکروسکوپ نوری، تلوسیت‌ها به صورت سلول‌های کشیده‌ای مشاهده شدند که دارای یک هسته باریک و زوائد سیتوپلاسمی نازک متعددی بودند که از بدنه سلول منشأ می‌گرفتند. در مجاورت نزدیک با واحدهای ترشحی غدد رحمی، عروق خونی، دسته‌های کلاژن بافت همبند و سلول‌های ماهیچه صاف در سراسر تمام لایه‌های دیواره رحم قرار داشتند. مورفولوژی کامل تلوسیت‌ها و تلوپودها، شامل ارتباطات نزدیک آن‌ها با سلول‌های غده‌ای، ماهیچه صاف و اندوتلیال، و همچنین فیبرهای کلاژن، به وضوح توسط میکروسکوپ الکترونی عبوری مشاهده شد. در مجموع، یافته‌های این مطالعه اولین شواهد مبنی بر حضور تلوسیت در رحم سگ را فراهم می‌کند و مورفولوژی و توزیع تقریبی آن‌ها را شرح می‌دهد.

کلمات کلیدی: تلوسیت، رحم، سگ، هیستولوژی، فراساختار

* نویسنده مسئول: طیبه محمدی، استادیار گروه علوم پایه و پاتوبیولوژی، دانشگاه رازی، کرمانشاه، ایران

E-mail: tymhd@razi.ac.ir

DOI: 10.22055/ivj.2026.556170.2862

تأثیر دی‌متیل‌ایتاکونات بر کاهش تغییرات بافتی و آپوپتوز تخمدان و بهبود تولید هورمون‌های جنسی در مدل تجربی سرطان پستان موش تحت درمان با دوکسوروبیسین

اعظم اسدسفتجانی[۱]، شیما حسینی‌فر[۲*] و محمدرضا تابنده[۳]

[۱] دانشجوی دکتری تخصصی بافت‌شناسی، دانشکده دامپزشکی، دانشگاه شهید چمران اهواز، اهواز، ایران
[۲] دانشیار گروه علوم پایه، دانشکده دامپزشکی، دانشگاه شهید چمران اهواز، اهواز، ایران
[۳] استاد گروه علوم پایه، دانشکده دامپزشکی، دانشگاه شهید چمران اهواز، اهواز، ایران

تاریخ دریافت: ۱۴۰۴/۸/۷ تاریخ پذیرش: ۱۴۰۴/۱۱/۲۷

چکیده

سمیت تخمدانی القاشده با دوکسوروبیسین (DOX) یکی از عوارض شایع شیمی‌درمانی در بیماران مبتلا به سرطان پستان است که اغلب با آسیب سلول‌های تخمدانی همراه بوده و منجر به آپوپتوز، اختلال در فولیکولوژنز و کاهش تولید هورمون‌های استروئیدی تخمدان می‌شود. دی‌متیل‌ایتاکونات (DMI)، یک متابولیت ایمنی با خواص ضدالتهابی و آنتی‌اکسیدانی است که می‌تواند اثرات محافظتی بالقوه‌ای داشته باشد، اما اطلاعات محدودی در مورد نقش محافظتی آن در برابر سمیت تخمدانی ناشی از شیمی‌درمانی وجود دارد. هدف از این مطالعه بررسی اثرات محافظتی احتمالی DMI بر تغییرات بافتی، آپوپتوز و تولید هورمون‌های جنسی در مدل موشی سرطان پستان 4T1 تحت درمان با DOX است. در این مطالعه تجربی، ۳۰ موش ماده بالغ نژاد BALB/c به صورت تصادفی به پنج گروه تقسیم شدند: کنترل سالم، کنترل سرطانی (القا سرطان با تزریق سلول‌های 4T1)، سرطان - DMI (50 mg/kg، تزریق داخل صفاقی، روزانه، ۲۸ روز)، سرطان - DOX (5 mg/kg، تزریق داخل صفاقی، هفته‌ای یک‌بار، ۴ هفته) و سرطان - DMI+DOX. سطوح سرمی استروژن و پروژسترون، بیان ژن‌های آپوپتوتیک تخمدان و تغییرات بافت تخمدان ارزیابی شد و با روش الایزا اندازه‌گیری شد. برای تحلیل آماری داده‌ها از نرم‌افزار GraphPad Prism نسخه ۱۰ استفاده شد و نتایج به صورت میانگین ± خطای معیار (Mean ± SEM) ارائه گردید. دوکسوروبیسین سطوح استرادیول (۳۷/۴+۲۳/۴۳ pg/ml) و پروژسترون (۳/۰+۴/۲ ng/ml) را به طور معنی‌داری کاهش داد و نیز موجب کاهش بیان Bcl2 (۰/۳۱ + ۰/۱)و افزایش بیان Bax (۴/۰+۰۴/۳۹) در بافت تخمدان، در مقایسه با گروه کنترل سرطانی شد (به ترتیب ۵۴/۲+۱۰/۸ pg/ml، ۵/۰+۱/۲ ng/ml، ۰/۰+۷۲/۰۹، ۱/۰+۸۱/۳۵). درمان همزمان **دی‌متیل‌ایتاکونات و دوکسوروبیسین** منجر به کاهش معنی‌دار Bax (۲/۵۹+۰/۴۵) و افزایش معنی‌دار Bcl-2 (۰/۶۱+۰/۰۳) نسبت به گروه دریافت‌کننده دوکسوروبیسین به تنهایی شد. همچنین، تغییرات بافتی قابل‌توجهی در بافت تخمدان از جمله افزایش آترزی فولیکولی، کاهش اندازه فولیکول‌ها و عدم وجود جسم زرد مشاهده شد. تجویز DMI سبب کاهش اختلالات بافتی و بهبود ساختار بافتی تخمدان، کاهش ضخامت اپی‌تلیوم سطحی و نرمال‌سازی سطوح هورمونی و بیان ژن‌های مرتبط با آپوپتوز گردید. درمان هم‌زمان با DMI و DOX بیش‌ترین اثر حفاظتی را در کاهش آسیب‌های بافتی ناشی از DOX نشان داد. نتایج این مطالعه نشان می‌دهد که DMI می‌تواند به عنوان ترکیبی محافظتی در کاهش سمیت تخمدانی در دوره شیمی درمانی مطرح باشد.

کلمات کلیدی: دی‌متیل‌ایتاکونات، دوکسوروبیسین، بافت‌شناسی تخمدان، آپوپتوز، سرطان سینه

* نویسنده مسئول: شیما حسینی‌فر، دانشیار گروه علوم پایه، دانشکده دامپزشکی، دانشگاه شهید چمران اهواز، اهواز، ایران
E-mail: sh.hosseinifar@suc.ac.ir

مقاله کامل
دوره بیست و دوم ـ شماره ۲ ـ تابستان ۱۴۰۵
DOI: 10.22055/ivj.2026.536372.2821

بررسی میزان آلودگی گوسفندان و بزهای ارومیه به انواع *کریپتوسپوریدیوم*

بهنام قربانی[۱]، وحید نجارنژاد[۲*] و فرناز ملکی‌فرد[۳]

[۱] دانش‌آموخته دکتری حرفه‌ای، دانشکده دامپزشکی دانشگاه ارومیه، ارومیه، ایران
[۲] دانشیار گروه بیماری‌های داخلی، دانشکده دامپزشکی دانشگاه ارومیه، ارومیه، ایران
[۳] دانشیار گروه پاتوبیولوژی، دانشکده دامپزشکی دانشگاه ارومیه، ارومیه، ایران

تاریخ دریافت: ۱۴۰۴/۴/۳۱ تاریخ پذیرش: ۱۴۰۵/۳/۱۲

چکیده

کریپتوسپوریدیوزیس، یک بیماری مشترک بین انسان و دام است که توسط گونه‌های *کریپتوسپوریدیوم* در انواع حیوانات و انسان ایجاد می‌شود. در نشخوارکنندگان تازه متولد شده، اغلب به صورت اسهال رخ داده و با ضررهای اقتصادی قابل توجهی همراه است. مطالعه حاضر با هدف تعیین میزان آلودگی نشخوارکنندگان کوچک در شهرستان ارومیه به انواع *کریپتوسپوریدیوم* انجام شد. در مجموع ۵۶۰ نشخوارکننده کوچک (۷۰ رأس گوسفند و ۷۰ رأس بز در هر فصل) از گله‌های اطراف ارومیه در چهار فصل سال مورد بررسی قرار گرفتند. به منظور جستجوی اووسیست‌های *کریپتوسپوریدیوم*، نمونه‌ها به روش فرمالین اتر تغلیظ و پس از تهیه گسترش روی لام به روش زیل نلسسون اصلاح شده رنگ‌آمیزی شدند. از ۵۶۰ حیوان مورد بررسی، ۶۷ مورد (۱۱/۹۶ درصد) به انواع گونه‌های *کریپتوسپوریدیوم* آلوده بودند. میزان آلودگی در گوسفندان (۱۸/۸۶ درصد) بیش‌تر از بزهای مورد بررسی (۶/۰۷ درصد) بود. تجزیه و تحلیل آماری داده‌ها همچنین وجود یک ارتباط معنی‌دار بین میزان آلودگی و عواملی مانند قوام مدفوع، سن، جنس و فصل را نشان داد. نتایج این مطالعه خطر زئونوتیک بالقوه انواع گونه‌های *کریپتوسپوریدیوم* را در منطقه تأکید کرده و نشان دهنده لزوم آگاهی بهداشت عمومی و استراتژی‌های مدیریت مؤثر در گله‌های نشخوارکننده کوچک منطقه است.

کلمات کلیدی: *کریپتوسپوریدیوم*، شیوع، نشخوارکنندگان کوچک، ارومیه، ایران

* نویسنده مسئول: وحید نجارنژاد، دانشیار گروه بیماری‌های داخلی، دانشکده دامپزشکی دانشگاه ارومیه، ارومیه، ایران
E-mail: v.najarnzhad@urmia.ac.ir

DOI: 10.22055/ivj.2026.579063.2889

شیوع مولکولی و عوامل خطر اپیدمیولوژیک عفونت ناشی از *بارتونلا هنسله*، در گربه‌های صاحب‌دار و بدون صاحب شهرستان اهواز، ایران

سارا حاجی‌زاده[۱]، بهمن مصلی‌نژاد[۲*]، داریوش غریبی[۳]، محمد راضی‌جلالی[۲] و مهدی پورمهدی‌بروجنی[۴]

[۱] دانشجوی دکتری تخصصی بیماری‌های داخلی حیوانات کوچک، دانشکده دامپزشکی، دانشگاه شهید چمران اهواز، اهواز، ایران

[۲] استاد گروه علوم درمانگاهی، دانشکده دامپزشکی، دانشگاه شهید چمران اهواز، اهواز، ایران

[۳] استاد گروه پاتوبیولوژی، دانشکده دامپزشکی، دانشگاه شهید چمران اهواز، اهواز، ایران

[۴] استاد گروه بهداشت مواد غذایی، دانشکده دامپزشکی، دانشگاه شهید چمران اهواز، اهواز، ایران

تاریخ دریافت: ۱۴۰۵/۱/۳۰ تاریخ پذیرش: ۱۴۰۵/۳/۲۵

چکیده

بارتونلا هنسله، یک باکتری زئونوز است که گربه‌های خانگی به عنوان مخزن اصلی آن عمل می‌کنند و با ایجاد باکتریمی پایدار، انتقال عامل بیماری را عمدتاً از طریق کک گربه (*کتنوسفالیدس فلیس*) تسهیل می‌کنند. با توجه به اهمیت بهداشت عمومی عفونت در گربه‌ها و محدود بودن داده‌های مولکولی از جنوب غربی ایران، این مطالعه با هدف تعیین شیوع مولکولی و شناسایی عوامل خطر اپیدمیولوژیک مستقل مرتبط با عفونت *بارتونلا هنسله*، در گربه‌های صاحب‌دار و بدون صاحب در اهواز، ایران انجام شد. در این مطالعه مقطعی، ۱۶۰ گربه مورد بررسی قرار گرفتند که به طور مساوی بین دو گروه صاحب‌دار و بدون صاحب توزیع شده بودند. گربه‌های بالغ ۶۵ درصد از جمعیت مورد مطالعه را تشکیل می‌دادند، در حالی که ۳۵ درصد نابالغ بودند؛ همچنین ۵۵ درصد نر و ۴۵ درصد ماده بودند. گربه‌های نژاد مو کوتاه اهلی، شایع‌ترین تیپ نژادی را تشکیل می‌دادند (۵۱/۹ درصد). از هر حیوان نمونه‌های خون کامل، سواب دهانی و ناخن جمع‌آوری شد و با استفاده از واکنش زنجیره‌ای پلیمراز متداول با هدف تکثیر قطعه‌ای به طول ۴۱۴ جفت باز از ناحیه فاصله‌انداز رونویسی داخلی htrA مورد بررسی قرار گرفتند و سپس برای برخی آمپلیکون‌های نماینده توالی‌یابی جهت تأیید انجام شد. ارتباط بین عوامل خطر بالقوه و عفونت با استفاده از رگرسیون لجستیک تک متغیره و چند متغیره ارزیابی و همچنین کسر منتسب به جمعیت محاسبه شد. DNA مربوط به *بارتونلا هنسله* در ۱۶/۹ درصد از گربه‌ها (فاصله اطمینان ۹۵ درصد: ۱۱/۴ تا ۲۳/۷) شناسایی شد. شیوع عفونت در گربه‌های بدون صاحب (۲۶/۳ درصد) به طور معنی‌داری بیش‌تر از گربه‌های صاحب‌دار (۷/۵ درصد) بود (OR=4.39؛ فاصله اطمینان ۹۵ درصد: ۱٫۶۶–۱۱٫۵۸؛ p=۰٫۰۰۲). تحلیل کسر منتسب به جمعیت نشان داد که به ترتیب ۶۷ درصد و ۳۶ درصد از موارد عفونت به دسترسی به محیط خارج از منزل و آلودگی به کک نسبت داده می‌شوند. این یافته‌ها نشان می‌دهد که مواجهه محیطی و آلودگی به ناقل‌ها از عوامل تعیین‌کننده اصلی عفونت هستند و اهمیت کنترل کک و محدود کردن دسترسی کنترل نشده به محیط بیرون را برای کاهش بار عفونت و خطر زئونوز برجسته می‌سازند.

کلمات کلیدی: *بارتونلا هنسله*، گربه، شیوع مولکولی، اپیدمیولوژی، زئونوز

* نویسنده مسئول: بهمن مصلی‌نژاد، استاد گروه علوم درمانگاهی، دانشکده دامپزشکی، دانشگاه شهید چمران اهواز، اهواز، ایران

E-mail: bmosallanejad@scu.ac.ir

DOI: 10.22055/ivj.2025.536829.2823

شناسایی و بررسی فیلوژنتیک یک cDNA کدکننده پروتئین کالومنین حاوی دامنه EF-hand در *Strongyloides ratti*

عباس جلودار[1*]

[1] دانشیار گروه علوم پایه، دانشکده دامپزشکی، دانشگاه شهید چمران اهواز، اهواز، ایران

تاریخ دریافت: ۱۴۰۴/۵/۲ تاریخ پذیرش: ۱۴۰۴/۷/۳۰

چکیده

Strongyloides ratti به عنوان یک مدل تجربی برای تشخیص استرونژیلوئیداز در انسان عمل می‌کند. در این مطالعه پروتئین ترشحی کالومنین حاوی دامنه EF-hand از رت که به عنوان یک مولکول سیگنالینگ کلسیم عمل می‌کند، توالی یابی و شناسایی گردید. یک قطعه ژن به طول ۸۴۸ نوکلئوتید با RT-PCR افزوده سازی شد. در جستجوی بانک ژن نشان داده شد که این محصول ۹۸/۵۴ درصد با یک توالی mRNA ناکامل از *Strongyloides ratti* مشابهت داشت. با استفاده از این قطعه ژن به عنوان جستجوگر، پایگاه داده ژنی Expressed Sequence Tags (EST) مورد جستجو قرار گرفت که متعاقب آن، یک قطعه ژن ۹۹۸ نوکلئوتیدی از طریق مناطق همپوشان شناسایی شد که *Sr*CAL نامگذاری گردید. این ژن یک پروتئین شامل ۳۱۴ اسید آمینه را کد می‌کند که وزن مولکولی آن ۳۶/۷۴ کیلو دالتون و نقطه ایزوالکتریک (pI) آن ۴/۶۱ است. این پروتئین حاوی یک پپتید سیگنال با محل برش بین اسیدهای آمینه ۲۱-۲۲ می‌باشد. جستجوی در پایگاه داده‌های ژنی نشان داد که این پروتئین دارای پنج دامنه EF-hand (cd16226) به منظور اتصال به کلسیم است که بسیار حفاظت شده می‌باشند. نتایج نشان داد که *Sr*CAL بر اساس تشابه اسید آمینه‌های بین ۲۹ تا ۲۹۶ در ابرخانواده پروتئین‌های Efh_CREC_Calumenin طبقه‌بندی می‌شود. پیش‌بینی ساختار ثانویه پروتئینی نشان داد که *Sr*CAL از ۳۹/۱۸ درصد مارپیچ آلفا، ۲۱/۱۸ درصد رشته‌های بتا و ۴۲/۶۱ درصد لوپ تشکیل شده است. مدل‌سازی ساختار سه‌بعدی که با استفاده از ۲۳۲ اسید آمینه که ۷۴ درصد از کل توالی ناحیه کدگذاری شده را شامل می‌شود، نشان داد که این پروتئین با ۹۹/۸ درصد اطمینان مشابهت با ساختار کریستالی یک پروتئین حاوی دامنه EF-hand از *Danio rerio* می‌باشد. بررسی فیلوژنتیک *Sr*CAL کم‌ترین فاصله ژنتیکی (۰/۱۹ درصد) را با تنها توالی پروتئینی موجود جدا شده از *S. ratti* (XP_024499492.1) دارد. *Sr*CAL می‌تواند نقش مهمی در سیگنالینگ کلسیم ایفا کند که ممکن است به عنوان یک ژن خانه‌دار با پتانسیل قوی به عنوان یک هدف دارویی اختصاصی نماتودی عمل کند.

کلمات کلیدی: نماتود، دامنه EF-hand، *Strongyloides ratti*، RT-PCR، کالومنین

* نویسنده مسئول: عباس جلودار، دانشیار گروه علوم پایه، دانشکده دامپزشکی، دانشگاه شهید چمران اهواز، اهواز، ایران

E-mail: jolodara@scu.ac.ir

DOI: 10.22055/ivj.2026.557381.2866

ارزیابی برون‌تنی هم‌افزایی فعالیت‌های ضدباکتریایی و ضدبیوفیلمی عصاره پاریتاریا مورالیس (گلسنگ) و نانوذرات کیتوزان

افشین صالحی[۱]، مسعود قربانپور[۲*]، علی نظری‌عالم[۳] و امین نعمت‌الهی[۴]

[۱] دانشجوی دکتری تخصصی باکتری‌شناسی، دانشکده دامپزشکی، دانشگاه شهرکرد، شهرکرد، ایران
[۲] استاد گروه پاتوبیولوژی، دانشکده دامپزشکی، دانشگاه شهرکرد، شهرکرد، ایران
[۳] دانشیارگروه میکروب‌شناسی و ایمنی‌شناسی، دانشکده پزشکی، دانشگاه علوم پزشکی کاشان، کاشان، ایران
[۴] دانشیارگروه بهداشت و کنترل کیفی مواد غذایی، دانشکده دامپزشکی، دانشگاه شهرکرد، شهرکرد، ایران

تاریخ دریافت: ۱۴۰۴/۸/۱۳ تاریخ پذیرش: ۱۴۰۵/۴/۴

چکیده

داروهای گیاهی ترکیب شده با مواد نانو نگاه‌های قابل توجهی را در حوزه پزشکی زیستی به خود جلب کرده‌اند؛ با این حال، توان ضدباکتریایی ترکیب کیتوزان با عصاره گلسنگ *پروتوپارملیوپسیس مورالیس* (*Protoparmeliopsis muralis*) تاکنون مورد بررسی قرار نگرفته است. هدف از پژوهش حاضر، ارزیابی اثر هم‌افزای عصاره *پروتوپارملیوپسیس مورالیس* و نانوذرات کیتوزان (CS/NPs) بر روی باکتری‌های بیماری‌زای منتخب بود. فعالیت ضدباکتریایی با استفاده از آزمون حداقل غلظت مهارکنندگی (MIC) مورد ارزیابی قرار گرفت و اثرات ضدبیوفیلمی آن نیز با آزمون **کریستال** ویوله سنجیده شد. مخلوطی حاوی ۱۰ درصد عصاره *پروتوپارملیوپسیس مورالیس* و ۰/۰۵ درصد نانوذرات کیتوزان تهیه گردید و تعامل هم‌افزا از طریق روش **چکربورد** مورد بررسی بیش‌تر قرار گرفت. CS/NPs فعالیت ضدباکتریایی قوی‌تری نسبت به عصاره *پروتوپارملیوپسیس مورالیس* از خود نشان داد. علاوه بر این، آزمون چکربورد تأیید کرد که میان *پروتوپارملیوپسیس مورالیس* و CS/NPs اثر هم‌افزایی وجود دارد. ترکیب آن‌ها فعالیت ضدبیوفیلمی را نیز به طور قابل توجهی افزایش داد که پتانسیل آن را به عنوان رویکردی نویدبخش برای کنترل رشد باکتری‌ها و عفونت‌های مرتبط با بیوفیلم برجسته می‌سازد. در مجموع، یافته‌های این مطالعه نشان می‌دهد که ترکیب عصاره **گل‌سنگ** و نانوذرات کیتوزان می‌تواند به عنوان یک گزینه امیدوارکننده برای مطالعات آتی با هدف شناسایی و توسعه ترکیبات جدید ضدمیکروبی و ضدبیوفیلم مطرح شود. با این حال، انجام پژوهش‌های بیش‌تر، از جمله بررسی‌های مکانیسم اثر و ارزیابی‌های درون‌تنی، برای درک بهتر و تأیید اثرات مشاهده‌شده ضروری است.

کلمات کلیدی: کیتوزان، گلسنگ، ضد باکتریایی، ضد بیوفیلمی

* نویسنده مسئول: مسعود قربانپور، استاد گروه پاتوبیولوژی، دانشکده دامپزشکی، دانشگاه شهرکرد، شهرکرد، ایران
E-mail: ghorbanpoor-m@sku.ac.ir

DOI: 10.22055/ivj.2025.505300.2775

روشی ساده برای تولید آنتی‌بادی‌های مونوکلونال ضد IgM ماهی

مسعودرضا صیفی‌آباد شاپوری[1*]، رویا رهنما[2]، رحیم پیغان[3]، آناهیتا رضائی[1] و نسترن شهبازیان[4]

[1] استاد گروه پاتوبیولوژی، دانشکده دامپزشکی، دانشگاه شهید چمران اهواز، اهواز، ایران

[2] دانش‌آموخته دوره دکتری بهداشت و بیماری های آبزیان، دانشکده دامپزشکی، دانشگاه شهید چمران اهواز، اهواز، ایران

[3] استاد گروه بهداشت دام، طیور و آبزیان، دانشکده دامپزشکی، دانشگاه شهید چمران اهواز، اهواز، ایران و عضو قطب بهداشت و بیماری‌های ماهیان گرمابی، دانشگاه شهید چمران اهواز، اهواز، ایران

[4] استادیار بخش آبزیان، سازمان دامپزشکی ایران، تهران، ایران

تاریخ دریافت: ۱۴۰۴/۱۱/۳۰ تاریخ پذیرش: ۱۴۰۴/۸/۲۲

چکیده

ایمونولوگوبولین M (IgM) ایزوتیپ آنتی‌بادی غالب در سرم ماهی‌های استخوانی است و نقش مرکزی در پاسخ‌های ایمنی سیستمیک ماهیان دارد. آنتی‌بادی‌های مونوکلونال (mAbs) برعلیه IgM ماهی‌ها ابزارهای ارزشمندی برای تحقیقات ایمنی‌شناسی و مدیریت بیماری‌ها در آبزی‌پروری می‌باشند. پروتکل‌های سنتی تولید این نوع mAb نیازمند IgM خالص هستند که تهیه آن به دلیل پیچیدگی روش‌های خالص‌سازی در گونه‌های ماهیان استخوانی با چالش همراه است. در این مطالعه، ما یک روش ساده برای تولید آنتی‌بادی‌های مونوکلونال ضد IgM با ایمن‌سازی موش‌ها با سرم کامل قزل‌آلای رنگین‌کمان (Oncorhynchus mykiss) ارائه می‌دهیم که به خالص-سازی IgM نیاز ندارد. در این روش هیبریدوماها با استفاده از یک ELISA غیرمستقیم بر اساس یک آنتی‌ژن غیرمرتبط (مانند پروتئین متصل شونده به مالتوز) و سرم‌های قزل‌آلای حاوی آنتی‌بادی ضد این آنتی‌ژن غربالگری شدند. این شیوه منجر به شناسایی پنج کلون هیبریدومای پایدار (D4۱، D3۳، E3۳، B3۴ و F6۷) گردید. آنتی‌بادی های منوکلونال تولید شده به طور مؤثر آنتی‌بادی‌های قزل‌آلا بر علیه ویروس نکروز پانکراس عفونی، باکتری لاکتوکوکوس گارویه و گلبول‌های قرمز خون گوسفند را نیز شناسایی کردند. ایمونوبلاتینگ تحت شرایط احیا کننده و غیر احیا کننده ویژگی این آنتی‌بادی‌های منوکلونال را برای IgM ماهی قزل‌آلا تأیید کرد. بنابراین این روش یک شیوه جایگزین عملی و کارآمد برای تولید آنتی‌بادی های منوکلونال کاربردی بر ضد IgM ماهی فراهم می‌کند.

کلمات کلیدی: آنتی‌بادی منوکلونال، ماهی قزل‌آلا، IgM، ELISA، ایمونوبلاتینگ

* نویسنده مسئول: مسعودرضا صیفی‌آباد شاپوری، استاد گروه پاتوبیولوژی، دانشکده دامپزشکی، دانشگاه شهید چمران اهواز، اهواز، ایران

E-mail: masoudrs@scu.ac.ir

Iranian Veterinary Journal

Mailing Address of the Editor
Dr. Mohammad Razi Jalali, DVM, PhD
Editor in chief of Iranian Veterinary Journal
Ahvaz, Postal Code: 61355 P.O. Box : 145, Iran
Tel / Fax : +98 61 33336312
http://ivj.ir
E-mail: ivj@scu.ac.ir

This Journal has been granted the rating of **Scientific – Research** by the Commission for Evaluation of Iranian Scientific Journals, the Ministry of Science, Research and Technology, through the letter numbered 3.2910.545 dated 30.7.2006
This journal is indexed by Iran and Islamic World Scientific Citation Center (**ISC**)

Published by
Regional Information Center for Science and Technology and Islamic World Science Citation Center

IRANIAN VETERINARY JOURNAL

SCIENTIFIC – RESEARCH

Contents